ABSTRACT

Title of Document: BUILDING BLOCK SYNTHESIS AND RECOGNITION PROPERTIES OF CUCURBIT[N]URIL (N = 7,8) DERIVATIVES.

Brittany Vinciguerra, Doctor of Philosophy, 2015

Directed By: Professor Lyle Isaacs, Department of Chemistry & Biochemistry

Molecular containers have been a topic of interest for chemists since the discovery of crown ethers and their molecular recognition properties in the late 1960's. Since then, the field of molecular containers has expanded rapidly to include many high affinity and highly selective host molecules. Chapter 1 introduces common molecular containers and goes on to discuss the CB[n] family of molecular containers. The CB[n] family are an exemplary group of hosts because they exhibit extremely high affinities (K_a values up to 10^{17} M^{-1}) and high selectivity towards their guests which make them excellent candidates for many supramolecular applications. In order to maximize the use of CB[n], it became important to access specialized and functionalized derivatives to cater to various applications and chemistry. Early functionalization routes were limited by a lack of mechanistic understanding, but the

mechanistic work of the Isaacs, Kim, and Day groups led to more successful syntheses.

Chapter 2 discusses a building block synthesis towards water-soluble CB[7] derivatives Me_2CB[7] and CyCB[7]. The recognition properties of Me_2CB[7] are investigated as well as its use in drug solubilization. It is found that Me_2CB[7], though 10 times more water soluble than CB[7], is able to solubilize drugs only as well as CB[7]. Additionally, a route towards a monofunctionalized CB[7] derivative, Cl-CB[7], bearing a primary chloride which is able to undergo further functionalization to a clickable azide by S_N2 chemistry is presented. A click reaction with a small alkyne is performed resulting in a self-associating host whose self-assembly process is further investigated.

Chapter 3 discusses a building block synthesis towards the first water-soluble CB[8] hosts Me_4CB[8] and Cy_2CB[8]. Mechanistic details of the CB[8] formation are elucidated from contrasting experiments and the recognition properties of the CB[8] derivatives are investigated by ^{1}H NMR spectroscopy and X-ray crystallography. The CB[8] derivatives are investigated as potential drug solubilizing agents and it is found that they are able to solubilize several larger pharmaceutical molecules whereas CB[8] is water insoluble.

BUILDING BLOCK SYNTHESIS AND RECOGNITION PROPERTIES OF CUCURBIT[N]URIL (N = 7,8) DERIVATIVES.

By

Brittany Marie Vinciguerra

Dissertation submitted to the Faculty of the Graduate School of the
University of Maryland, College Park, in partial fulfillment
of the requirements for the degree of
Doctor of Philosophy
2015

Advisory Committee:
Professor Lyle Isaacs, Chair
Professor Jeffrey Davis
Professor Daniel Falvey
Associate Professor Yu-Huang Wang
Associate Professor Volker Briken, Dean's Representative

Dedication

To my parents, Susie Richards and Chris Wheeler, and my husband, Tim Vinciguerra.

Acknowledgements

I would like to thank my Ph.D. advisor, Professor Lyle Isaacs, for his guidance and encouragement over the last five years. I am thankful for every hard lesson, every failed project, and especially for every joyful success. I have learned so much about thinking like an organic chemist from him and appreciate the time and effort he put towards my graduate education.

I would also like to thank my undergraduate professors, especially Professors Bill Davis, David Wasmund, and John McClusky, for their early encouragement. Learning from you changed everything about what I dreamed for my entire career. You showed me what it meant to be an educator and a scientist and encouraged me to pursue my Ph.D.

I would like to thank the former Isaacs group members for their support and mentorship. Thank you for teaching me proper laboratory techniques, ingenious engineering, and many other necessary lessons. I would especially like to thank Drs. Jimmy Wittenberg, Ben Zhang, and Liping Cao for their extra encouragement and friendship. Thank you to Liz Robinson for endless scientific discussions and support. I would also like to thank my first undergraduate researcher Kristin Benke for being a great mentee and friend.

I would also like to thank the current Isaacs group members. Thank you for your scientific input and your advice, both research and life-related. I am very grateful to have had your expertise to guide me and your friendship to support me. I would especially like to thank our postdoctoral researchers for allowing me to contribute to their projects and expand my field of knowledge by working with them. I would also like to thank my current undergraduate researcher Chris Knocke for being a willing mentee.

Lastly, I would like to thank my family and friends back home. Thank you for supporting my decision to move across the country and pursue my Ph.D. Without your constant love and support, this would have been impossible for me.

Table of Contents

List of Tables

Chapter 3

List of Figures

Chapter 1

Chapter 2

Chapter 3

List of Schemes

Chapter 1

Chapter 2

Chapter 3

Chapter 4

List of Abbreviations

Å	angstrom
br	broad
CB[n]	cucurbit[n]uril
$CHCl_3$	chloroform
CH_3CN	acetonitrile
D	diffusion coefficient
d	doublet
D_2O	deuterium oxide
CH_2Cl_2	dichloromethane
DMF	dimethylformamide
DMSO	dimethylsulfoxide
DOSY	diffusion-ordered spectroscopy
ESI-MS	electrospray ionization-mass spectrometry
g	gram
h	hour
HCl	hydrochloric acid
H_2SO_4	sulfuric acid
Hz	hertz
IR	infrared
J	coupling constant
KBr	potassium bromide

KOH	potassium hydroxide
$K_2S_2O_8$	potassium persulfate
m	multiplet
M	molar
M^+	molecular ion
Me	methyl
MeOH	methanol
MHz	megahertz
min	minute
μM	micromolar
mM	millimolar
M.p.	melting point
MW	molecular weight
m/z	mass to charge ratio
NaOH	sodium hydroxide
$(NH_4)_2S_2O_8$	ammonium persulfate
NMR	nuclear magnetic resonance
Ph	phenyl
ppm	parts per million
PSD	phase solubility diagram
PXDA	*para*-xylylene diammonium ion
RB	round-bottom
RT	room temperature

s	singlet
t	triplet
THF	tetrahydrofuran
VT	variable temperature

Chapter 1: Introduction to Molecular Containers

1.1 Introduction.

The field of supramolecular chemistry studies the non-covalent interactions between molecules and the resulting effects on the properties of supramolecular systems. Nature provides many excellent examples of supramolecular systems such as the streptavidin-biotin complex, a high affinity protein complex (K_d = 10^{14}).[1] The high affinity of streptavidin for biotin comes from two important features[2]: 1) The high shape-complementarity of the binding pocket for biotin and 2) the eight hydrogen bonds made between biotin and the surrounding protein residues. Researchers in the supramolecular field have long tried to design molecules that could mimic the essential elements of avidin and other natural receptors in synthetic host-guest systems with the hope of achieving similarly impressive high affinity interactions.

Of major interest in supramolecular chemistry is the design and use of molecular containers for a wide variety of applications such as drug solubilization[3] and delivery,[4] catalysis,[5] signaling,[6] protein folding,[7] and many others. This chapter discusses commonly used molecular containers and their applications, the cucurbit[n]uril family of molecular containers and their properties, and the synthesis of cucurbit[n]uril derivatives.

1.2 Commonly Used Molecular Containers.

Molecular containers are a wide class of macrocylic molecules which are able to bind smaller molecules through non-covalent interactions thereby creating a host-guest complex. The formation of these complexes can impart new properties such as improved solubility or stability to the guest and/or host molecules. This non-covalent approach to modification of compounds has led to exciting advances in catalysis, molecular switches,[8] chemical sensors,[9] and drug delivery. Some common molecular containers include calixarenes, crown ethers, pillararenes, and cyclodextrins (Figure I-1).

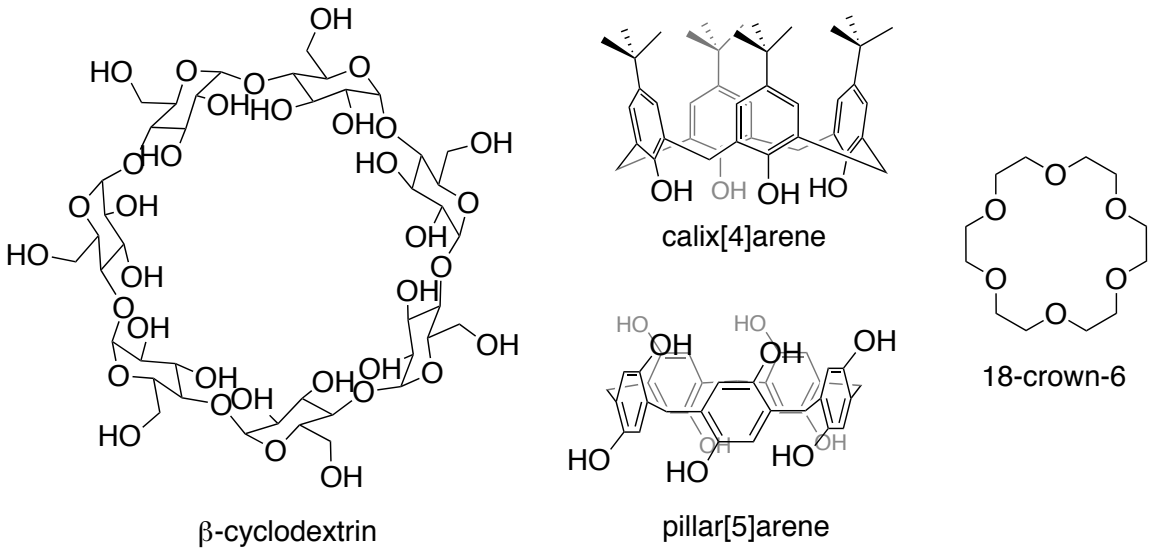

Figure I-1. Structures of β-cyclodextrin, calix[4]arene, pillar[5]arene, and 18-crown-6.

Crown ethers have the distinction of being one of the first examples of a synthetic host molecule. First published by Pedersen in 1967,[10] their ability to sequester metal cations led to their study and use in catalysis. The use of these early host molecules, along with others, was so impactful that the work earned Pederson, Cram, and Lehn the

Nobel Prize in Chemistry in 1987 and helped to establish the field of synthetic supramolecular chemistry. Since then, molecular containers have become more specialized and synthetically complex. For example, calixarenes are composed of *meta* methylene-linked phenols with bulky alkyl groups in the *para* position, creating a bowl-shaped cavity that is able to bind hydrophobic guests and alkyl ammonium ions. Pillararenes, first synthesized in 2008 by Ogoshi and co-workers,[11] are structurally similar to calixarenes, but their *para*-linked hydroquinone groups create a highly symmetrical pillar-shaped molecule. Interestingly, pillararenes display planar chirality based on the direction of the hydroquinone functionality, allowing for optically active containers. Pillararenes featuring small hydroquinone functionalities can racemize between enantiomers while pillararenes featuring bulky groups, such as cyclohexyl, can be isolated as individual enantiomers.[12]

Cyclodextrins are one of the most commercially available molecular containers (in everyday life and in the laboratory setting) due to their low-cost synthesis. They are composed of linked dextrose units and can also bind hydrophobic molecules and alkyl ammonium ions. In addition to being cost effective, cyclodextrins are also easily functionalized and are soluble in many solvents which makes them prime candidates for various applications from household products such as Febreze™ and sensors[13] in chemical research to pharmaceutical products such as Sugammadex and Captisol.[14] Cyclodextrins have served as a trail blazing example of achievement for molecular containers. However, a big drawback to the use of cyclodextrins is their lack of specificity and modest binding affinities towards guests. These limitations have inspired the search for higher affinity and higher selectivity molecular containers. In the past

decade alone, there has been an increase in the synthesis of new families of molecular containers with incredible recognition properties.

1.3 The Cucurbit[n]uril Family of Molecular Containers.

In 1905, Behrend et. al. reported the synthesis of a polymeric material from the condensation of one equivalent of glycoluril (**I-1**) with two equivalents of formaldehyde in concentrated hydrochloric acid (Scheme I-1).[15] The material, which was eventually named "Behrend's Polymer," was then recrystallized from sulfuric acid, giving a white crystalline product. The crystalline compound was not characterized at the time, but was found to form complexes with various metal salts in solution, a process that was discovered by the observation of a change in color upon addition of the crystalline material to the salt solution. In 1981, Mock et. al. repeated Behrend's original experiment and were able to obtain crystals suitable for X-ray crystallography.[16] Mock found that the compound was a highly symmetrical pumpkin-shaped macrocycle consisting of six glycoluril units bridged together by twelve methylene groups. The compound was named "cucurbituril" after the Latin name for the gourd family, *cucurbitaceae*.

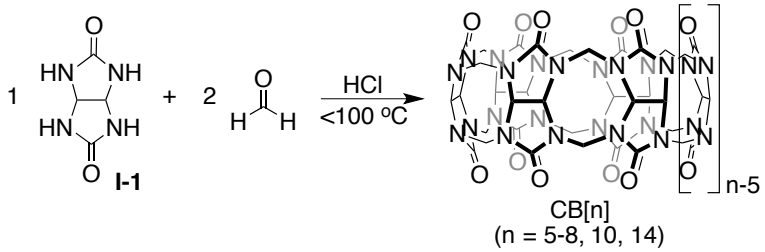

Scheme I-1. Synthesis and structure of CB[n].

Since Mock's determination of the structure of cucurbituril, now known as cucurbit[6]uril (CB[6]) where 6 represents the number of glycoluril units included in the macrocycle, several research groups have worked towards the synthesis and isolation of other members of the cucurbit[n]uril (CB[n], n = number of glycoluril units) family and elucidation of their recognition properties. The work of Mock,[17] Day,[18] Buschmann,[19] Kim,[20] Zhu[21], and Isaacs[22] has led to the synthesis and isolation of CB[5], CB[6], CB[7], CB[8], CB[10], and, more recently, CB[14] and the study of many interesting CB[n]-guest complexes. Today, there are procedures for the isolation of various CB[n] congeners and studies which describe the effects of variables such as type and concentration of acid and presence of metal cations on the outcome of CB[n]-forming reactions.[23]

Cucurbit[n]urils have several unique structural characteristics which contribute to their interesting properties. There are two main features that stabilize and strengthen the non-covalent interactions with guests: 1) the highly polar carbonyl-lined portal which promotes ion-dipole interactions with electrostatically positive groups and 2) a hydrophobic cavity which is well suited to hold the alkyl or aryl bodies of these guests. In fact, one of the main driving forces for a CB[n] binding event is the enthalpically favorable displacement of high energy water molecules from within the hydrophobic cavity by a guest.[24] Additionally, the glycoluril backbone is rigid which leads to a high selectivity for guests based on the volume and electrostatic properties of the guest. These unique features contribute to the high binding affinities that CB[n] display for their guests (up to 10^{18} M^{-1}).[25] Typical high affinity guests for CB[n] include alkyl and aryl

ammonium or diammonium ions (Figure I-2), while some lower affinity guests include metal cations and a variety of neutral organic molecules.

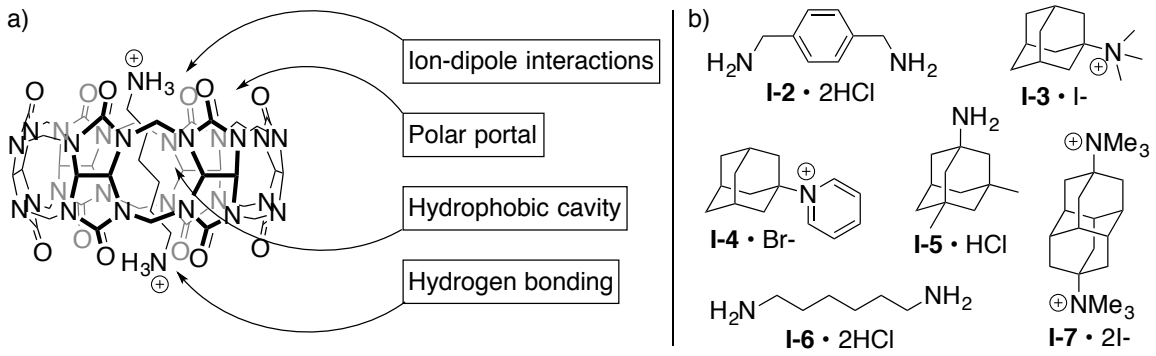

Figure I-2. a) Recognition properties of CB[n]. b) Typical alkyl ammonium guests for CB[n].

The wide range of cavity volumes and portal diameters displayed the CB[n] family allow them to be highly selective for very different guests. CB[5], being considerably smaller than the rest of the CB[n] family, cannot bind many organic molecules due to its too small portal but interestingly has been known to bind to gas molecules such as Kr, CO_2, CO, O_2, and N_2, and organic solvents such as methanol and acetonitrile. CB[6] is able to bind a wider variety of guests than CB[5], but still is limited by the small cavity and portal size. For example, CB[6] binds well to smaller alkyl ammonium ions such as hexanediammonium (**I-6**) (K_a = (4.49 ±0.84) × 10^8 M^{-1})[26], but a slightly larger guest such as *p*-xylylenediammonium ion (**I-2**) requires the addition of heat in order to be fit into CB[6] and the even larger **I-3** cannot fit inside CB[6] at all. Because of this size limitation, research interests tend to focus on the larger CB[n] congeners CB[7] and CB[8]. CB[7] in particular is known to make impressively high

affinity complexes with adamantane ammonium guests (**I-3**, **I-4**, and **I-5**) and other bulky compounds and has been the recent focus of binding studies on high-affinity host-guest complexes. In 2014, the Isaacs group published a CB[7]-diamantane guest (**I-7**) complex with an attomolar dissociation constant (K_a = 7.2 x 10^{17} in pure D_2O)[25], an unheard of value in the world of synthetic receptors and which surpasses the binding affinity of avidin for biotin ($K_a \approx 10^{15}$).[1] CB[8] is also capable of binding these larger guests, and even more interestingly CB[8] is large enough to form ternary complexes with two identical or different guests.[27]

One of the disadvantages of working with CB[n] is that they are poorly water soluble with CB[7] being the most soluble (20 mM) and CB[6] and CB[8] the least soluble (< 50 μM)[28], which can make their use in biological applications, a very important area for molecular containers, difficult. CB[n] are insoluble in organic solvents as well, though several CB[n] derivatives have modest solubility in solvents such as DMSO.[29]

1.4 Early Synthesis of Cucurbit[n]uril Derivatives.

Some of the first attempts towards functionalized CB[n] were performed by the groups of Stoddart and Zhu. These groups synthesized functionalized CB[n] from functionalized glycoluril units which mostly produced CB[5] and CB[6] derivatives. For example, in 1992 Stoddart and coworkers published the synthesis of Me_{10}CB[5] from the homomeric cyclization of dimethyl glycoluril (**I-1$_{Me}$**)and formaldehyde in HCl in low yield, a process which was later improved by Day and coworkers (Scheme I-2).[30] Interestingly, Me_{10}CB[5] and the related cyclohexano derivative are water soluble.

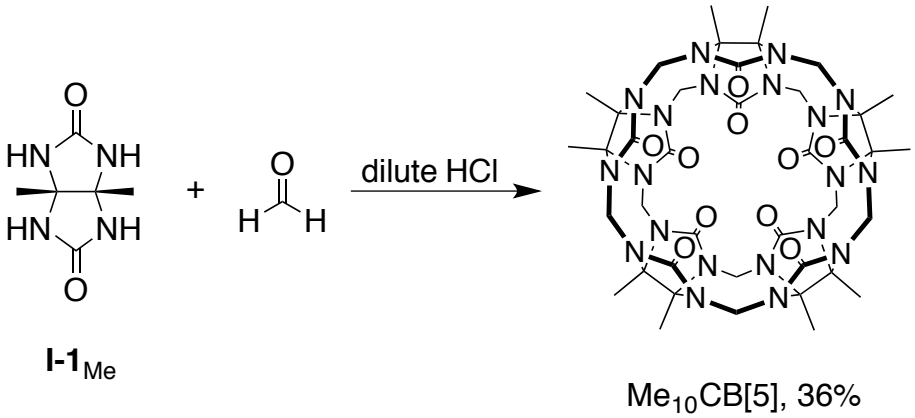

Scheme I-2. Synthesis of $Me_5CB[10]$ from **I-1$_{Me}$** and formaldehyde.

One of the limitations to this synthetic approach is that the products are preferentially CB[5]-sized. The small cavity and even smaller portal of CB[5] limits the guest interactions which can occur and also limits the possible applications for these compounds. This preference for the formation of smaller products has been attributed to the 1,5-diaxial interactions between the substituents on neighboring glycoluril units across the 8-membered methylene-bridged rings. These interactions become more severe as the size of the CB[n] increases, limiting the formation of larger products.

This limitation inspired researchers to investigate the macrocyclization of functionalized glycoluril with regular glycoluril to give partially functionalized CB[n]. Day and coworkers published the synthesis of $Me_6CB[6]$ with alternating functionalized and unfunctionalized glycoluril units and $Me_4CB[6]$ which features two functionalized glycoluril units on opposite sides of an ellipsoidal cavity (Scheme I-3).[31] Additionally, Day published an extensive synthesis of cyclopentano CB[n] (n = 5-7) derivatives based on the hypothesis that the slightly strained cyclopentano ring might affect the bond angles across the N–C–N plane and allow for the formation of larger CB[n] derivatives.[32]

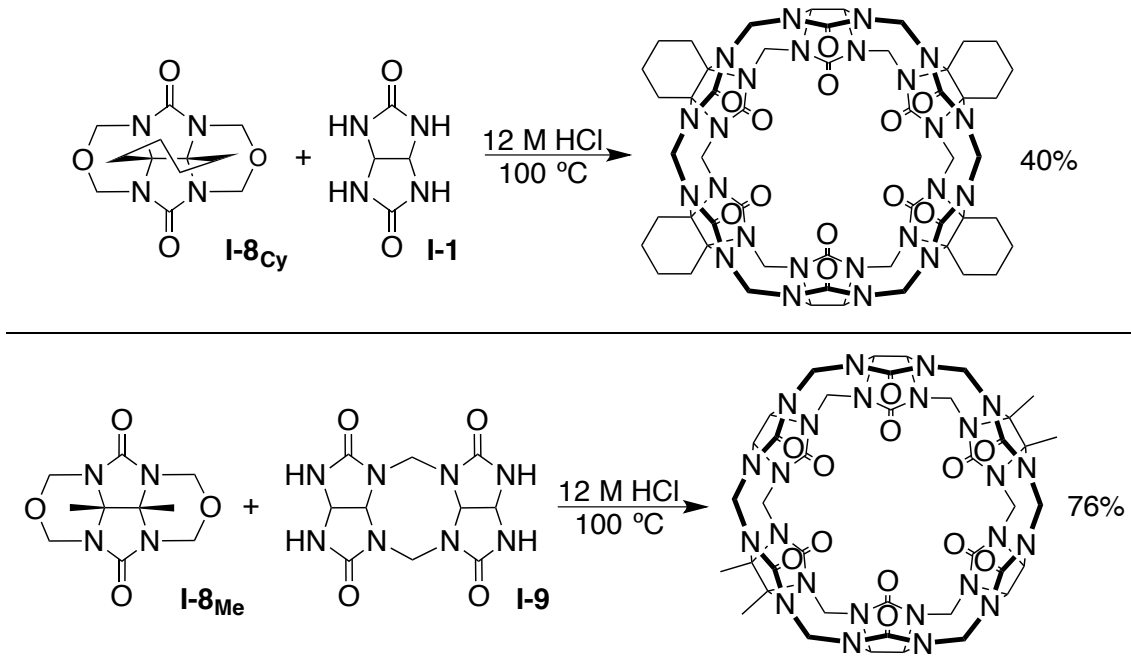

Scheme I-3. Synthesis of heteromeric CB[6] derivatives.

In 2003 Kimoon Kim and coworkers published the synthesis of perhydroxy-CB[n] ($(HO)_{2n}$CB[n]) from preformed CB[n].[29b] This approach sidesteps the complication of separating CB[n] of different sizes from one another by starting out with a single size of preformed CB[n]. A radical oxidation reaction is then performed in water with potassium persulfate ($K_2S_2O_8$) which replaces the hydrogen atoms on the equatorial methine carbon atoms of the CB[n] with hydroxyl groups to give $(HO)_{2n}$CB[n] in 40-45% yield for CB[5] and CB[6], but < 5% for CB[7] and CB[8] (Scheme I-4). One of the main contributing factors to the medium yield of this procedure is the limited solubility of the CB[n] (especially CB[6] and CB[8]) and $K_2S_2O_8$ in water. For CB[7] and CB[8], it is believed the very low yields are a result of the instability of the perhydroxylated products. $(HO)_{12}$CB[6] is soluble in DMSO and DMF allowing Kim and coworkers to

further elaborate on these compounds using well-known chemistry to give allyloxy and acetyloxy derivatives as pictured in Scheme I-4. The Kim group has been able to use these perhydroxy-CB[n] to do incredible chemistry – such as the covalent attachment of CB[6] to glass slides[33] and the formation of nanospheres – but the all-over functionalization of the perhydroxy-CB[n] limits the control researchers can have over subsequent covalent attachments.

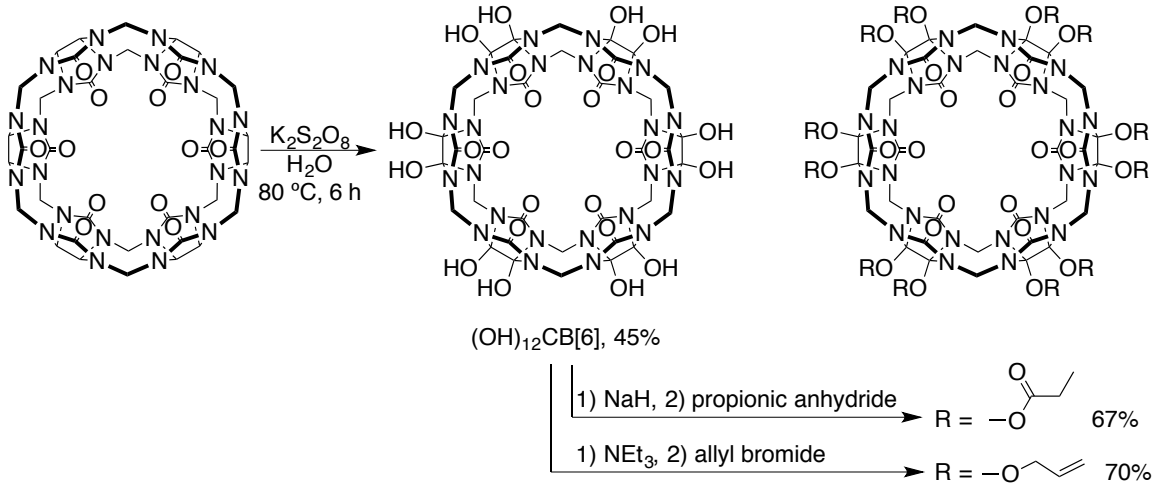

Scheme I-4. Synthesis of $(HO)_{12}$CB[6] from CB[6] and subsequent syntheses of perfunctionalized CB[6] derivatives.

After the publication of $(HO)_{2n}$CB[n], researchers sought to tame the perhydroxylation reaction to give $(HO)_1$CB[n]. In 2012 Scherman and coworkers used an imidizolium guest and a variation on Kim's conditions to synthesize $(HO)_1$CB[6].[34] This approach addressed one of the big problems with the perhydroxy synthesis- the low solubility of each reactant. The presence of the imidazolium guest increases the solubility of CB[6] and Scherman also replaced the poorly soluble $K_2S_2O_8$ with the much

more water soluble ammonium persulfate ($(NH_4)_2S_2O_8$). One of the interesting features of this synthesis is that by limiting the equivalents of $(NH_4)_2S_2O_8$, they were able to achieve a mixture of $(HO)_1$CB[6] and CB[6] so that the unreacted CB[6] can be isolated and recycled into a new reaction. However, due to the oxidant being the limiting reagent and the chromatographic purification the yield of this process is only 12%. Additionally, the success of this synthesis requires the use of a specialized guest which limits this process to CB[6].

1.5 Mechanism of Cucurbit[n]uril Formation.

Before the recent advances in post-functionalization of CB[n], synthetic efforts towards CB[n] derivatives and analogues were largely focused on the macrocylization of glycoluril units and glycoluril analogues. However, until the mechanism of CB[n] formation was elucidated by the separate and joint efforts of the Isaacs and Day groups during the early 2000's, this approach was incredibly difficult. Without an understanding of the mechanism of CB[n] formation, it was impossible to rationally predict and control the outcome of reactions.

Early mechanistic studies by Isaacs and Day indicated that when glycoluril and formaldehyde are heated in acid, they first form the glycoluril dimers **I-9S** and **I-9C**. The C-shaped **I-9C** is the more stable of the two and **I-9S** can isomerize to **I-9C** (Scheme I-5). It was then hypothesized that the oligomerization continues, forming the compound known as Behrend's polymer. The polymer, which contains many diastereotopic methine C-H bonds, is composed of C-shaped and S-shaped subunits that can isomerize. It was

hypothesized that this compound could then undergo end-to-end cyclization, yielding CB[6] as the major product with other CB[n] homologues as side products.

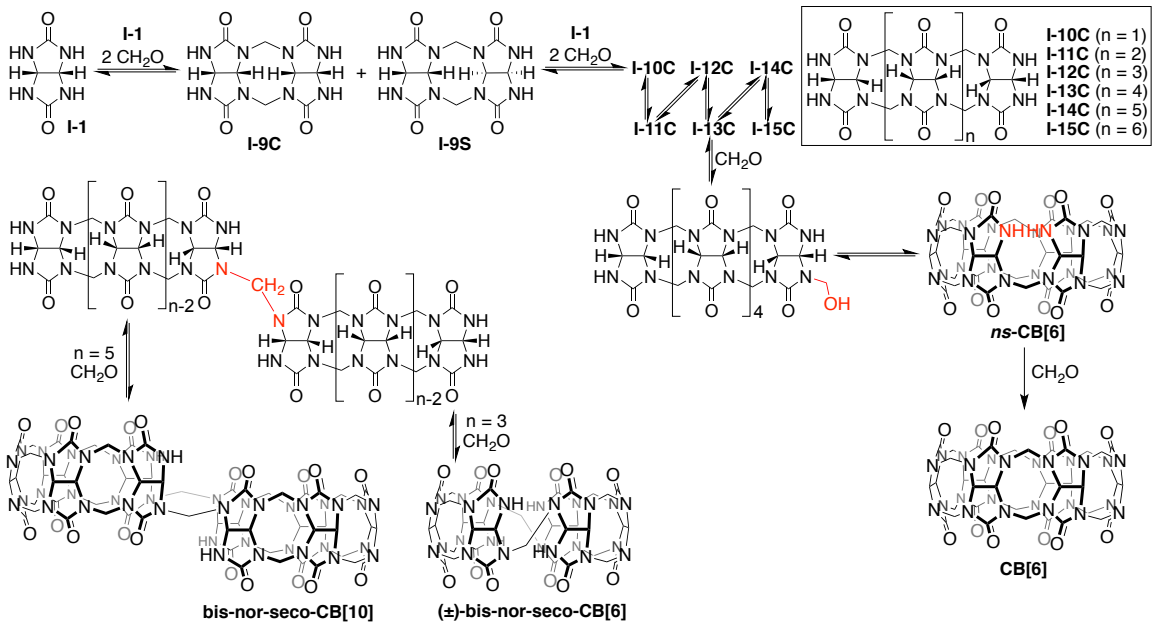

Scheme I-5. Chain-growth cyclo-oligomerization mechanism of CB[n] formation.

Follow-up studies by Isaacs, Kim, and Day uncovered more details of this mechanism.[35] Day and coworkers resubmitted CB[n] to reaction conditions and found that CB[5], CB[6], and CB[7] are stable in reaction conditions and therefore are thermodynamic products of the CB[n]-forming reaction while CB[8] decomposes under the reaction conditions to give smaller CB[n] products, indicating that CB[8] is a kinetically-controlled product. In particular, the isolation of various lengths of glycoluril oligomers **I-10C** – **I-15C** and inverted CB[n] homologues by Isaacs, Kim, and coworkers suggested that a chain-growth cyclo-oligomerization process may be occurring. These compounds were isolated from a reaction mixture of one equivalent of **I-1** and one equivalent of formaldehyde by Dowex chromatography and recrystallization. The

isolation of these products supported the idea that a chain-growth mechanism is operating in this reaction where one equivalent of **I-1** and two equivalents of formaldehyde can add stepwise to each oligomer, forming longer oligomers. These C-shaped oligomers (**I-12C** – **I-15C**) then cyclize with two equivalents of formaldehyde as the ureidyl nitrogen end groups are brought closer together by each new glycoluril unit added. This mechanistic theory also accounts for the formation of the isolable nor-seco and inverted CB[n] products, as demonstrated in Scheme I-5.

The Isaacs group has a long history of synthesizing CB[n] derivatives from glycoluril building blocks. For example, compound **I-16** is an acyclic CB[n] derivative synthesized by electrophilic aromatic substitution between hydroquinone derivatives and a partially substituted glycoluril tetramer bis (cyclic ether) (Scheme I-6).[36] The multiple steps leading to the motor compounds have been performed on multi-gram scales in high yield. The acyclic compound is able to accommodate varieties of larger guests using similar binding motifs as classic CB[n], with the addition of aromatic walls which facilitate π-π interactions and the water-solubilizing sulfonate arms. These properties make **I-16** an excellent drug solubilizing agent, a topic which has been reported on frequently by the Isaacs group in collaboration with the group of Prof. Volker Briken.[37] Additionally, the naphthalene-functionalized relative of compound **I-16** has been investigated as a reversal agent for neuromuscular blockade during anesthesia. It was found that the naphthalene relative effectively reverses neuromuscular blockade in mice similarly to the cyclodextrins-based product Sugammadex.[38] These acyclic derivatives have been an outstanding example of the impact CB[n] chemistry could have on the field

of supramolecular chemistry; an example that has inspired increased efforts towards functionalized CB[n] derivatives.

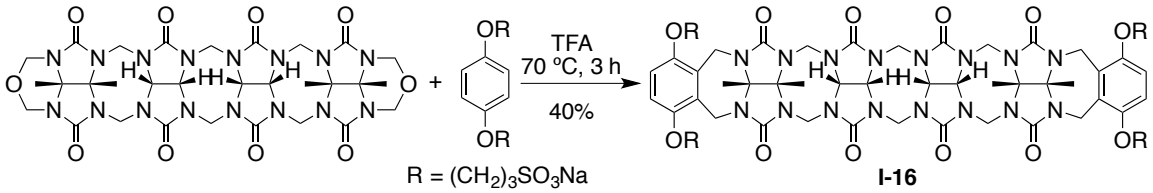

Scheme I-6. Building block synthesis of acyclic CB[n] congener **I-16**.

Isaacs and coworkers demonstrated the synthesis of CB[6] derivatives from the reaction of *nor-seco*-CB[6] (*ns*-CB[6]), a CB[6]-like host missing a single methylene bridge, and phthaldialdehyde which yielded a C_s-symmetric CB[6] derivative **I-17** with a xylene moiety as pictured in Scheme I-7.[39] The destruction of the top-bottom symmetry of CB[6] created differences in the two carbonyl-lined portals. Interestingly, single diastereomers of host-guest complexes were observed by ^{1}H NMR, indicating that one portal was capable of more favorable ion-dipole interactions with a guest than the other.

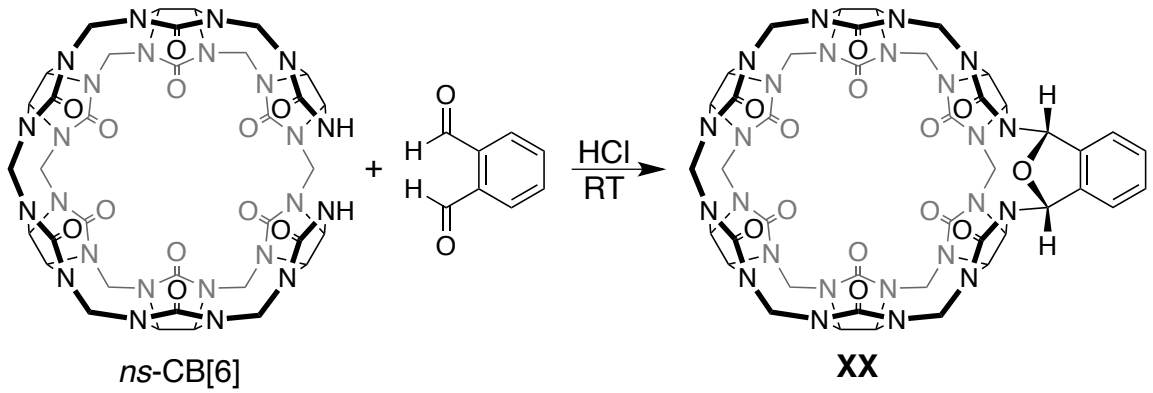

Scheme I-7. Synthesis of asymmetric CB[6] host **I-17** from *ns*-CB[6].

In 2011, Isaacs and coworkers published the gram-scale templated synthesis of an acyclic glycoluril hexamer **I-13C** from **I-1**, paraformaldehyde, and **I-2** as template in HCl (Scheme I-8).[40] Compound **I-13C** precipitates from the reaction mixture as the complex with **I-2**, which is easily removed by subsequent washes with aqueous NaOH and NaOH in methanol. The bulk synthesis of this oligomer was an exciting discovery for the CB[n] field as it signified an ability to control reaction outcomes and isolate kinetic products on a large scale. Additionally, glycoluril hexamer **I-13C** has four reactive ureidyl nitrogens that make it a great building block for the synthesis of larger CB[n] derivatives.

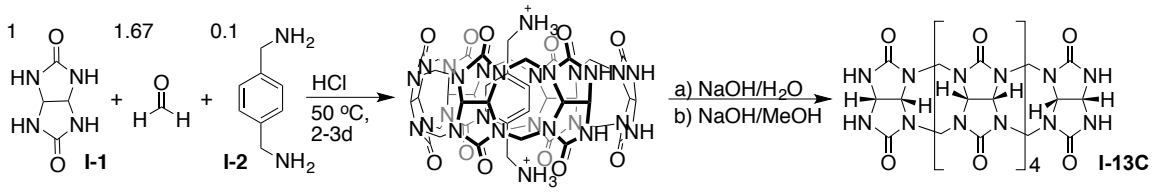

Scheme I-8. Templated synthesis of glycoluril hexamer **I-13C**.

In the same publication, **I-13C** was reacted with functionalized phthaldialdehyde derivatives to give CB[6] derivatives with an external functional group (Scheme I-9). The same reaction was also performed between **I-13C** and 2,3-napthalenedicarboxaldehyde to give a fluorescent CB[6] derivative which was later used in collaboration with Prof. Pavel Anzenbacher and co-workers for the sensing of nitrosamines in aqueous solution.[9]

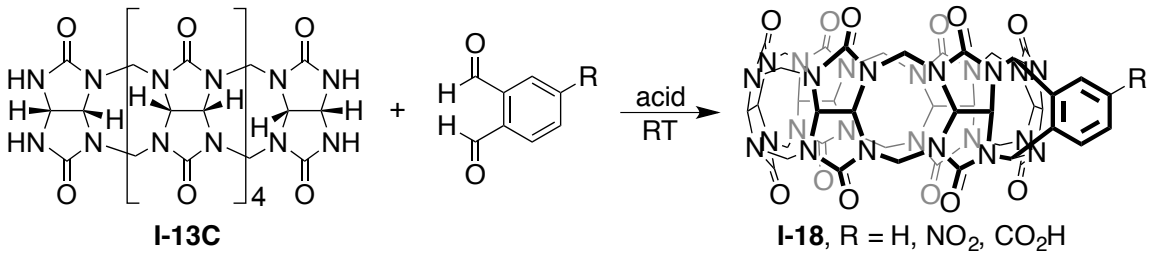

Scheme I-9. Synthesis of monofunctionalized CB[6] **I-18** from **I-13C** and a functionalized phthaldialdehyde.

1.6 Conclusion.

The synthesis of functionalized cucurbit[n]urils has become so important over the past few years, that many of these more recent developments overlap with the synthetic work presented in the following chapters. In fact, many of the synthetic methods presented all aim to supply a solution to the same problems: 1) How can we selectively synthesize functionalized CB[n] derivatives? 2) Can we access derivatives of the larger CB[n] congeners? 3) Can we improve the solubility properties of CB[n]? 4) Can we do all of this and maintain or improve the recognition properties of CB[n]? Fortunately, many of these problems have been thoroughly addressed in recent years. The next two chapters will address a method to access larger, water-soluble CB[n] derivatives.

Chapter 2: Synthesis and Self-Assembly Processes of Monofunctionalized Cucurbit[7]uril Derivatives

2.1 Introduction.

In 2012, we published the first example of a mono-functionalized CB[7] derivative. On the tail of various functionalized CB[6] derivatives synthesized by the Isaacs and Scherman groups, interest in functional CB[n] derivatives increased and the lack of CB[7] derivatives left a huge gap in CB[n] research. CB[7] is a more desirable molecular container for many applications because it is the most water soluble member of the CB[n] family, exhibits unsurpassed binding affinities for its guests, and possesses a larger cavity than the more accessible CB[6] which is able to bind a wider variety of biologically and chemically relevant guests.

This results and discussion section is organized as follows. First, we discuss the preparation of CB[7] derivatives Me_2CB[7], CyCB[7], and MePhCB[7] by a building block approach using glycoluril hexamer **II-1** and glycoluril bis(cyclic ethers) **II-2**. Then, we describe their basic properties (e.g. x-ray crystallography, host-guest binding, aqueous solubility, and drug solubilization). Next, we synthesize monofunctionalized CB[7] derivatives that contain reactive alkylchloride and azide functional groups. Finally, we describe the self-assembly of a CB[7] derivative to yield a cyclic tetrameric assembly in water.

2.2 Synthesis of Me_2CB[7] and CyCB[7].

Given the ready access to gram scale quantities of glycoluril hexamer **II-1** and glycoluril bis (cyclic ethers) **II-2** we decided to investigate their transformation into CB[7] derivatives (Scheme II-1). After much experimentation, we performed the reaction between **II-1** and **II-2**$_{Me}$ with added KI in 9 M H_2SO_4 at 110 ˚C for 30 minutes.[41] Analysis of the crude reaction mixture using *p*-xylylenediammonium ion (**II-3**) as ^{1}H NMR probe[42] showed the presence of a 55:45 ratio of CB[6] and Me_2CB[7]. As expected, the major competing reaction in this hexamer plus monomer building block approach to CB[7] derivatives is the unimolecular cyclization of hexamer to give CB[6]. Purification of the mixture was achieved by the addition of aqueous KI to an aqueous solution of the crude reaction mixture which results in precipitation of most of the CB[6] byproduct followed by final purification by treatment with activated carbon to yield Me_2CB[7] (380 mg) in 31% yield. A similar reaction was performed between **II-1** and **II-2**$_{Cy}$ which delivered CyCB[7] in 18% yield. We find that Me_2CB[7] (≥ 264 mM) and CyCB[7] (≥ 181 mM) are significantly more soluble in water than CB[7] itself (20-30 mM)[43] which suggests that they might find utility in applications where highly soluble compounds are needed (e.g. supramolecular polymers or drug solubilization).[44] When we performed related reactions with **II-2**$_{Ph}$ or **II-2**$_{CO2Et}$ we did not observe the formation of any CB[7] derivatives but rather observed the formation of CB[6] by unimolecular cyclization of **II-1**. From our previous work[45] we know that **II-2**$_{Ph}$ and **II-2**$_{CO2Et}$ are less reactive than alkylated glycolurils **II-2**$_{Me}$ or **II-2**$_{Cy}$ which makes them less able to undergo bimolecular reaction with **II-1** to give CB[7] derivatives. In contrast, however, a similar reaction between **II-1** and **II-2**$_{MePh}$ resulted in a mixture of CB[6] and

MePhCB[7] in a 61:30 ratio based on analysis of the crude ^{1}H NMR in the presence of **3**. Pure MePhCB[7] could only be obtained in a meager 3% yield after Dowex™ ion exchange chromatography.

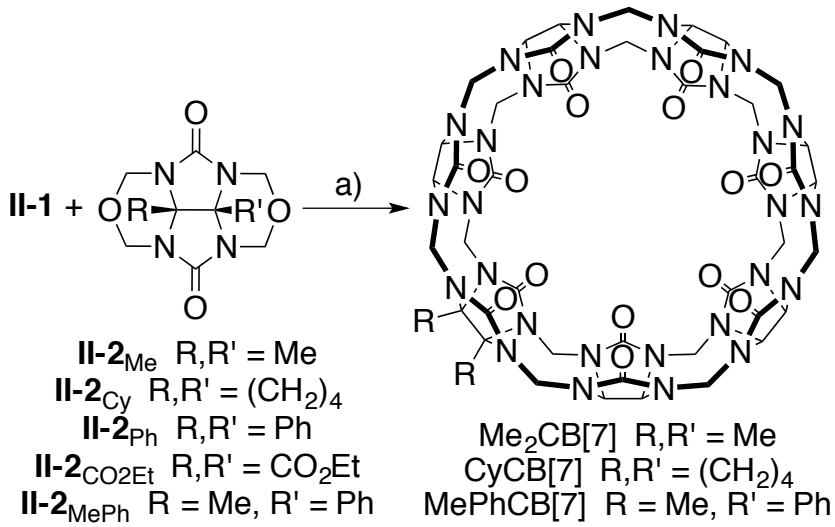

Scheme II-1. Synthesis of Me_2CB[7], CyCB[7], and MePhCB[7]. Conditions: a) 9 M H_2SO_4, 110 ˚C, KI, 30 min.

2.3 Properties of Me_2CB[7] Studied by X-ray Crystallography.

We were fortunate to obtain single crystals of Me_2CB[7] as its Me_2CB[7]•**II-3** complex and to solve its structure by X-ray crystallography. Figure II-1a shows a cross-eyed stereoview of the structure of one of the Me_2CB[7]•**II-3** complexes in the crystal. In contrast to CB[6] derivatives which display an ellipsoidal deformation through their equator upon functionalization,[42, 46] the CB[7] derivative Me_2CB[7] appears structurally similar to CB[7] itself.[20] For example, the distance between the ureidyl C=O O-atoms of a single glycoluril unit average 6.05 Å (range 5.87 – 6.154 Å) which is comparable to that observed for CB[7] (6.05 Å; range 5.913 – 6.114) itself. Similarly, the dimensions along the equator of Me_2CB[7] are comparable to that of CB[7] as well. For example, the

distance between the opposing methine C-atoms on each fourth glycoluril on Me_2CB[7] averages 11.398 Å (range 11.247 – 11.516 Å) whereas CB[7] averages 11.404 Å (range 11.173 – 11.591 Å). One structural parameter that is rather different for CB[7] and Me_2CB[7] is the average distance between ureidyl C=O oxygen atoms on every fourth glycoluril at one portal. For Me_2CB[7] the distances average 8.188 Å (range 7.197 – 9.026 Å; standard deviation = 0.644 Å) whereas for CB[7] the distances average 8.139 Å (range 7.553 – 8.718 Å, standard deviation = 0.364 Å). The glycolurils appear to pivot such that one oxygen atom moves inward and one moves outward which results in the ureidyl C=O portals undergoing an ellipsoidal deformation. Overall, the molecular structures of CB[7] and Me_2CB[7] are similar. Figure II-1b shows a cross-eyed stereoview of the basic packing of individual complexes of Me_2CB[7]•**II-3** into a square array parallel to the *xy*-plane within the crystal. The Me groups of two adjacent Me_2CB[7]•**II-3** complexes orient themselves toward each others ureidyl C=O portals. The iodide counterions (not depicted) are found at the corners of the square array and extend in columns along the *z*-axis.

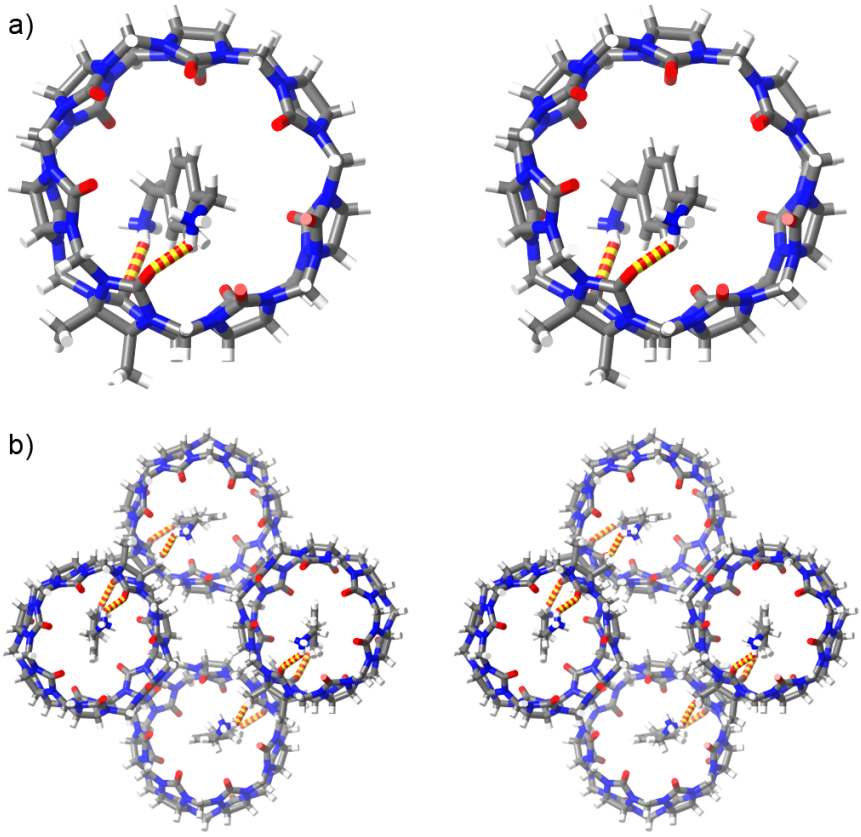

Figure II-1. Cross-eyed stereoviews of: a) the x-ray crystal structure of $Me_2CB[7]$•**II-3**, and b) a portion of the crystal lattice showing the three dimensional packing motif. Color code: C, gray; H, white; N, blue; O, red; H-bonds, red-yellow striped.

2.4 Recognition Properties of $Me_2CB[7]$ and CyCB[7].

After establishing the basic structural features of $Me_2CB[7]$ we decided to investigate its molecular recognition properties. For this purpose, we used guests (**II-3** – **II-11**) shown in Figure II-2 which increase in size from hexanediamine **II-4** to adamantane derivatives **II-9** – **II-11**. Guests **II-3** – **II-11** are well known to form complexes with unsubstituted CB[7] with binding constants up to 4.2×10^{12} M^{-1} for CB[7]• **II-9**.[47] Figure II-3 shows the ^1H NMR spectra recorded for $Me_2CB[7]$• **II-3**,

Me_2CB[7]• **II-4**, Me_2CB[7]• **II-7**, and Me_2CB[7]• **II-10**. The guest resonances observed in ^{1}H NMR spectra are nearly identical in chemical shift to those measured for the corresponding CB[7] complexes (Appendix 1) which indicates that the magnetic environment inside the cavity of CB[7] and Me_2CB[7] are quite similar. The resonances observed in the ^{1}H NMR spectra that correspond to the H-atoms of C_{2v}-symmetric Me_2CB[7] reflect its lower symmetry. For example, three doublets of relative integral two and one doublet of relative integral one are observed for the upfield shifted H-atoms of the diastereotopic CH_2-groups of the Me_2CB[7]•**II-3** complex (Figure II-3a). The main reason for synthesizing CB[7] derivatives is to be able to incorporate them into more complex systems while maintaining their recognition properties. Therefore, we viewed it as critical to verify that the high binding constants observed for CB[7] are maintained for CB[7] derivatives like Me_2CB[7]. For this purpose, we used the complexes CB[7]•**II-11** and Me_2CB[7]•**II-11** because the H-atoms adjacent to the pyridinium N-atom are located at the ureidyl C=O portal in the complexes. Given that the presence of the two Me groups induce a change in the O•••O distance in the substituted glycoluril (*vide supra*) we thought that these protons might exhibit different chemical shifts in the CB[7]•**II-11** and Me_2CB[7]•**II-11** complexes. Experimentally, we find that H_n resonates at 8.95 ppm for CB[7]•**II-11** and 8.96 ppm for Me_2CB[7]•**II-11** (Appendix 1). We used ^{1}H NMR competition experiments (Appendix 1) to determine that the K_a value for Me_2CB[7]•**II-11** is 3.2×10^{12} M^{-1} relative to the known K_a value for CB[7]•**II-11** (1.98×10^{12} M^{-1}).[47] Accordingly, it seems reasonable to expect that CB[7] derivatives like Me_2CB[7] will function well as CB[7] surrogates in more complicated systems.

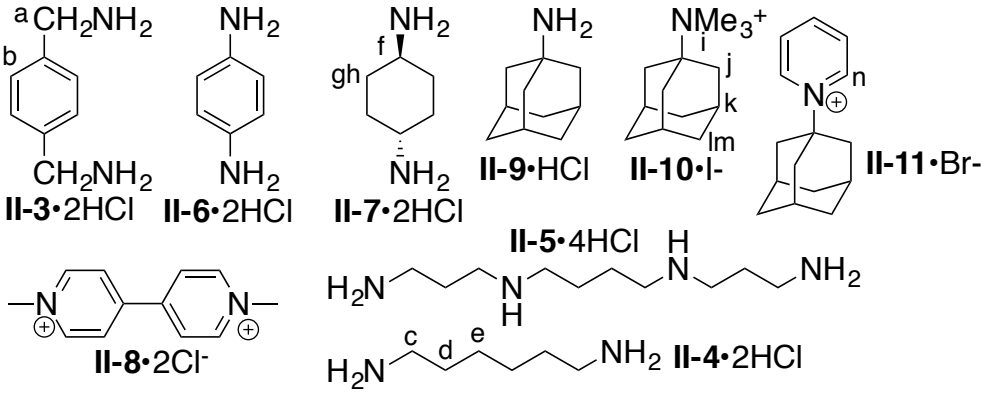

Figure II-2. Structure of guests used in this study.

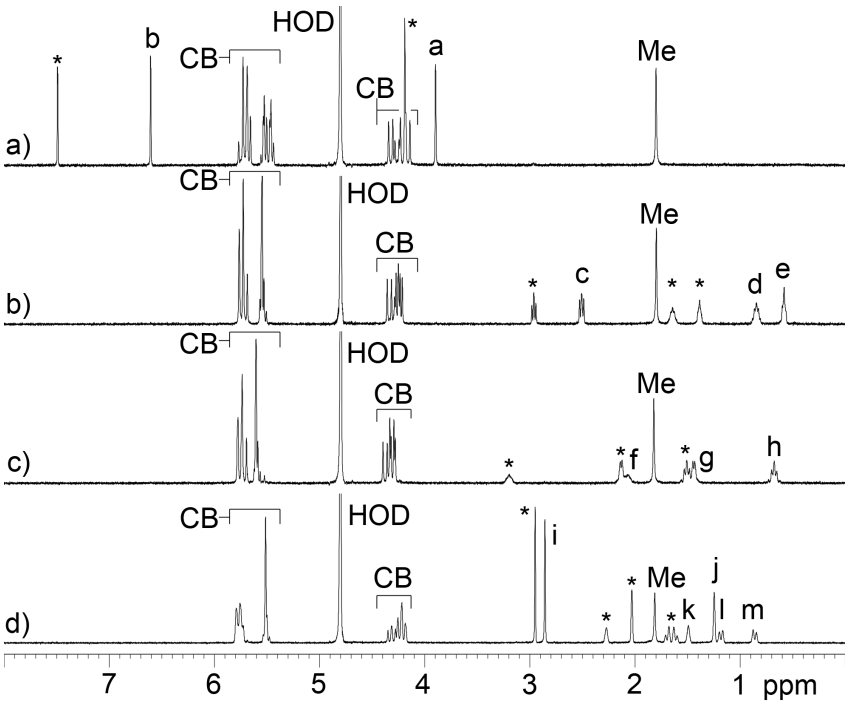

Figure II-3. ^{1}H NMR spectra (400 MHz, D_2O, RT) recorded for mixtures of: a) Me_2CB[7] and **II-3** (2 equiv.), b) Me_2CB[7] and **II-4** (2 equiv.), c) Me_2CB[7] and **II-7** (2 equiv.), d) Me_2CB[7] and **II-10** (2 equiv.). Resonances marked with * arise from free guest.

2.5 Stability of $Me_2CB[7]$.

Experiments performed by Day and co-workers established that CB[5], CB[6], and CB[7] are quite stable under the hot acidic conditions (conc. HCl, 100 ˚C, 24 h) used in their formation.[48] Accordingly, we wondered whether the Me substituents on the convex face of $Me_2CB[7]$ might stabilize cationic intermediates accessible under acidic conditions and thereby accelerate decomposition reactions of $Me_2CB[7]$. Figure II-4 shows a plot of the mole fraction of $Me_2CB[7]$ versus time for a solution of $Me_2CB[7]$ heated at 110 ºC in 9M H_2SO_4. Over the course of 6 days, $Me_2CB[7]$ completely decomposes. The ^1H NMR spectrum of the crude reaction mixture using **II-3** as probe after 6 days shows the presence of macrocycles with CB[6] sized cavities (≈ 24% of the crude mixture). Electrospray mass spectrometry of the crude reaction mixture allows us to identify the presence of comparable amounts of CB[6] and $Me_2CB[6]$. Given that few applications require such highly acidic and high temperature conditions, we believe that dialkylated CB[7] derivatives will be sufficiently stable in most situations.

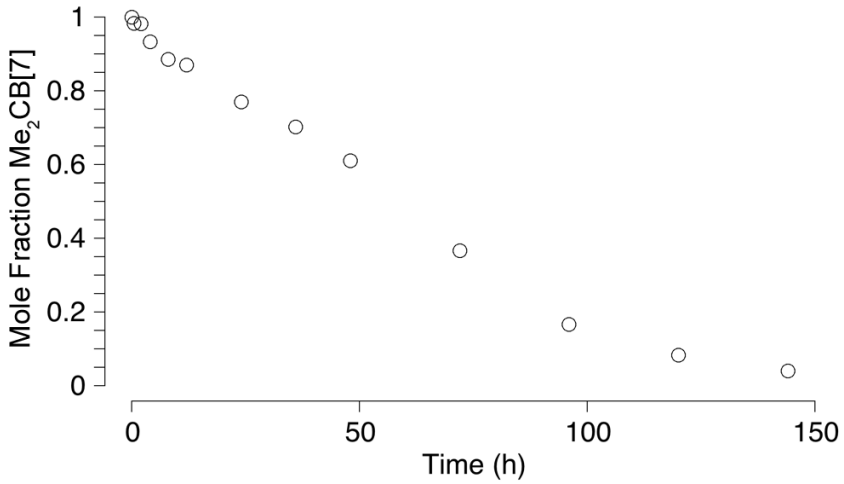

Figure II-4. Plot of the mole fraction of $Me_2CB[7]$ upon heating at 110 ºC in 9M H_2SO_4 as a function of time.

2.6 Drug Solubilization using Me_2CB[7].

One of the emerging areas for application of CB[n] molecular containers involves their use as solubilizing excipients for insoluble pharmaceutical agents. Given the high solubility of Me_2CB[7] in water, we decided to test its ability to solubilize albendazole and camptothecin, which have previously been solubilized by unsubstituted CB[7]. Figure 4 shows the phase solubility diagrams constructed for albendazole with either Me_2CB[7] or CB[7]. To construct the phase solubility diagrams, we stirred a solution of a known concentration of host with an excess of insoluble drug overnight, filtered the solution to remove excess insoluble drug, and measured the concentration of soluble drug by 1 H NMR using $CH_3SO_3^-$ as a nonbinding internal standard of known concentration. The phase solubility diagrams for albendazole and Me_2CB[7] or CB[7] are quite similar at low concentrations of container (up to 10 mM). This result can be explained by the fact that the linear region of phase solubility diagrams for 1:1 host:guest complexes obeys eq 1, where K_a is the host· guest binding constant (M^{-1}) and s_0 is the intrinsic solubility of guest (drug). Given that s_0 for albendazole is the same regardless of which host is used and that the K_a values for the CB[7]•albendazole and Me_2CB[7]• albendazole are expected to be very similar, then the initial slopes should also be very similar, according to eq 1. Somewhat surprisingly, at higher concentrations of Me_2CB[7] (e.g., 25− 50 mM), the concentration of albendazole in solution reaches a plateau of 5.8 mM, which is lower than that achieved with 15 mM CB[7] (8.1 mM). The plateau in the phase solubility diagram for Me_2CB[7]•albendazole indicates that the complex possesses only moderate solubility in water (~ 5.8 mM). Why does Me_2CB[7], which is far more water soluble CB[7], perform less well in the solubilization of albendazole? We believe that the

introduction of the Me groups on the convex face of uncomplexed Me_2CB[7] dramatically increases its solubility relative to that of CB[7] because they prevent the CH•••O interactions between the methine C−H groups on the convex face of one container with the ureidyl C=O portals of another container in the solid state, which has been implicated as a controlling factor in the solubility trends of CB[n] compounds.37 Within the Me_2CB[7]•albendazole and CB[7]•albendazole complexes, the drug fills the cavity and protrudes through the ureidyl C=O portals. Accordingly, the Me groups cannot enhance the solubility of Me_2CB[7]•albendazole in the same way as they do Me_2CB[7]. On the contrary, the presence of the hydrophobic Me groups decreases the solubility of Me_2CB[7]•albendazole relative to that of CB[7]•albendazole. A similar trend was noted for the solubilization of camptothecin by CB[7] and Me_2CB[7] (Appendix 1). These results suggest that a major consideration in the design of CB[n] derivatives for use as solubilizing excipients is the incorporation of groups designed to enhance the solubility of both the container and its container•drug complexes.

$$K_{\mathrm{a}} = \frac{\mathrm{slope}}{s_0(1-\mathrm{slope})} \qquad (1)$$

2.7 Synthesis of Functionalized Derivatives II-18 – II-20.

The following work was performed in collaboration with Dr. Liping Cao. The preparation of glycoluril derivative **II-12** bearing a primary alkyl chloride is shown in Scheme II-2. First, we react butanedione **II-13** with isopropylamine **II-14** in Et_2O with $TiCl_4$ to deliver the known diimine **II-15**.[49] Next, we deprotonated **II-15** with LDA in THF followed by subsequent alkylation with 3-iodo-1-chloropropane to yield **II-16** in

69% yield after hydrolytic workup.[50] Compound **II-16** was transformed into glycoluril **II-17** by reaction with urea in HCl at room temperature in 35% yield. Finally, treatment of **II-16** with formalin in HCl gives **II-12** in 68% yield.

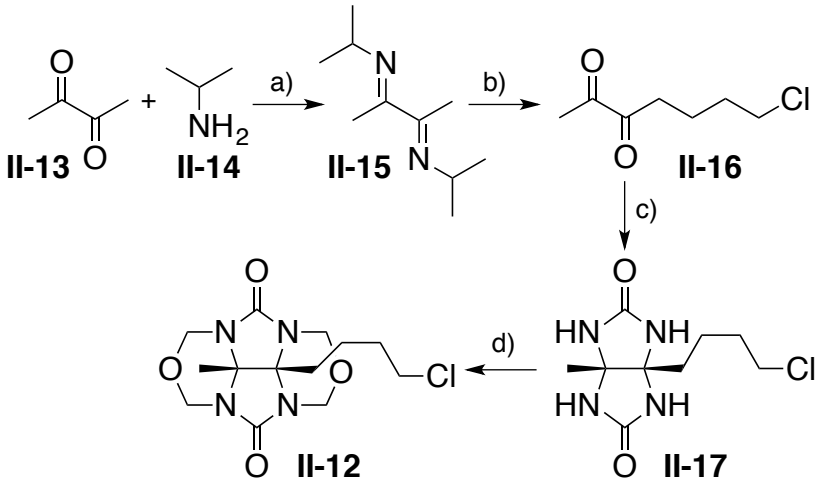

Scheme II-2. Synthesis of glycoluril derivative **II-12**. Conditions: a) Et_2O, $TiCl_4$, b) LDA, THF, $Cl(CH_2)_3I$, 69%, c) HCl, urea, 35%, d) HCl, formalin, 68%.

With access to gram scale quantities of **II-12** we decided to synthesize monofunctionalized CB[7] derivative **II-18** (Scheme II-3). The reaction between **II-1** and **II-12** was conducted in 9M H_2SO_4 at 110 ˚C in the presence of KI as developed for the synthesis of Me_2CB[7], CyCB[7], and MePhCB[7] described above. The ^{1}H NMR spectrum of the crude reaction mixture obtained using **II-3** as probe allowed us to estimate that **II-18** comprised 66% of the crude material. Purification by Dowex™ ion exchange chromatography allowed us to isolate 210 mg **II-18** in pure form in 16% yield. Clearly, the purification process is far from ideal and we are working to improve the process. We found that **II-18** can be transformed into monofunctionalized CB[7] derivative **II-19** which contains a reactive azide functional group in 81% yield by simply

heating with NaN_3 in H_2O at 80 ºC for 2 days. Azide **II-19** reacts with propargyl ammonium chloride (**II-21**) in the presence of Pericas' catalyst[51] in H_2O at 50 ºC to give **II-20** in 95% yield. The ^1H NMR spectrum of the purified sample of **II-20** in the presence of **II-3** – which is a strong binder for CB[7] sized cavities[47] and thereby disrupts any potential self-assembly processes of **II-20** – is shown in Figure II-5a.

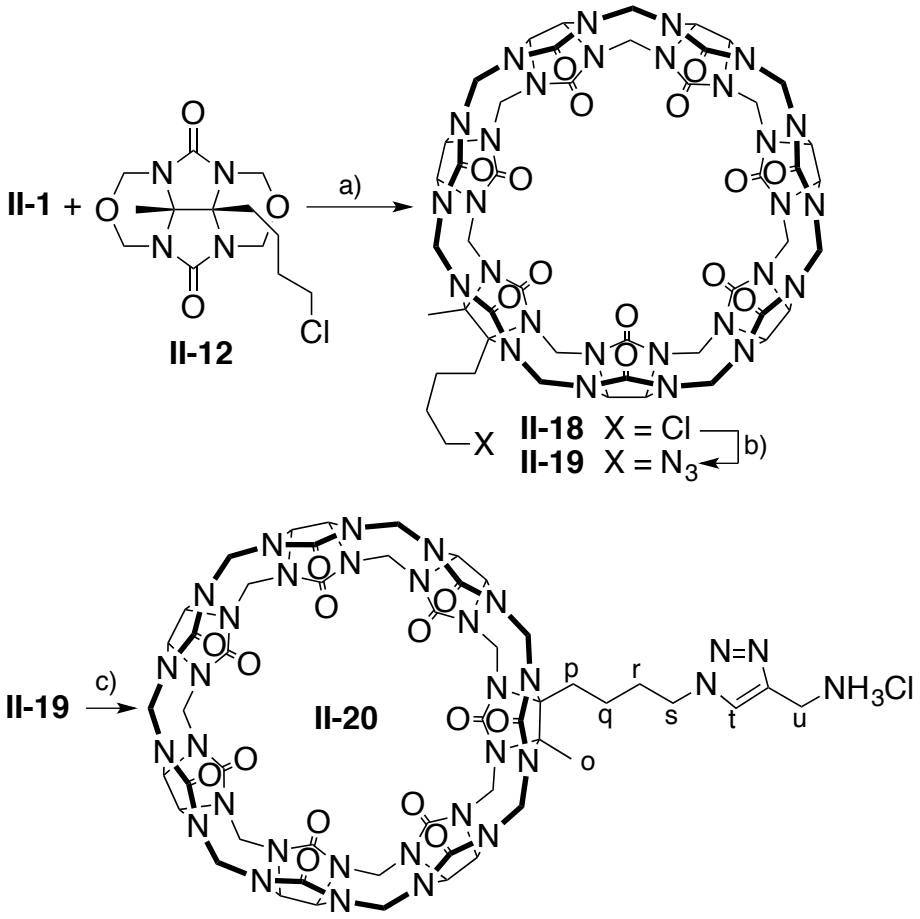

Scheme II-3. Synthesis of CB[7] derivatives. Conditions: a) 9M H_2SO_4, KI, 110 ºC, 16%, b) NaN_3, 80 ºC, 81%, c) **II-21**, Pericas' catalyst, H_2O, 50 ºC, 95%.

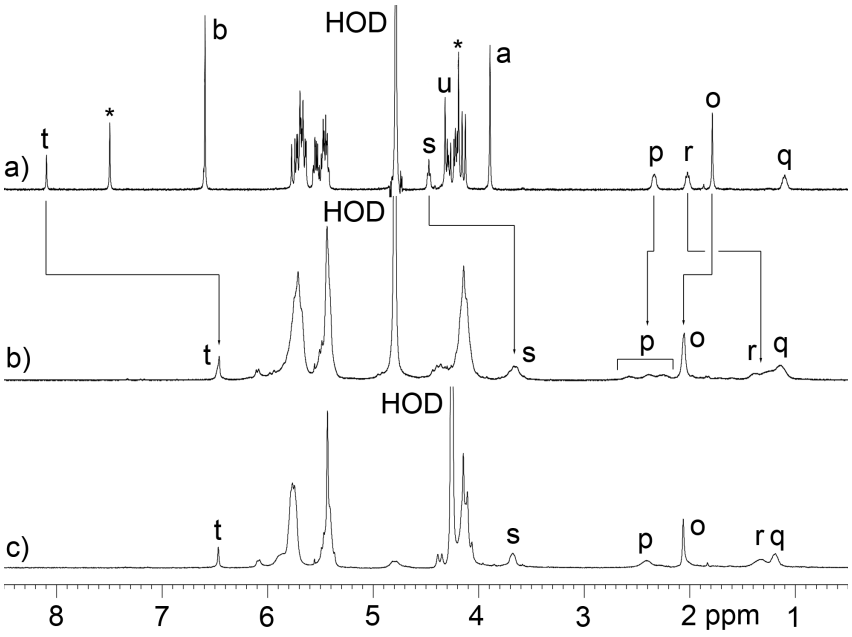

Figure II-5. ^{1}H NMR spectra (400 MHz, D_2O) recorded for mixtures of: a) **II-20** and **II-3** (1.4 equiv.), b) **II-20** (3.3 mM) at 20 ºC, and c) **II-20** (3.3 mM) at 80 ºC.

2.8 Self-Assembly of II-20 to Yield Cyclic Tetramer II-20$_4$.

We anticipated that **II-20** which contains both a CB[7] sized cavity and a covalently attached triazolyl ammonium ion – which is a good guest for CB[7] sized cavities – would undergo self assembly processes in water. A priori it was hard to predict whether supramolecular polymerization processes or formation of discrete cyclic assemblies would predominate.[52] Figure II-5b shows the ^{1}H NMR spectrum recorded for a 3.3 mM solution of **II-20** in D_2O at room temperature. A single relatively sharp triazole C-H resonance is observed at 6.45 ppm which suggested the formation of a well defined assembly. On the other hand, the upfield region of the spectrum between 2.70 and 1.00 ppm corresponding to the $(CH_2)_4$ linker between the CB[7] moiety and the triazole binding unit are broadened and the presence of several groups of resonances suggested

the presence of several different assemblies. Figure II-5c shows the ^{1}H NMR spectrum recorded at 80 ºC which shows that these different groups of resonances coalesce and sharpen into four distinct resonances corresponding to each of the four CH_2-groups of the linking chain. The fact that the resonances for H_t and H_u are still strongly upfield shifted in the ^{1}H NMR spectrum recorded at 80 ºC (Figure II-5b versus II-5c) suggests that the assembly **II-20**$_n$ persists at high temperature. To gain insight into the degree of oligomerization (n) of the self-assembled species (**II-20**$_n$) formed in D_2O we performed diffusion ordered spectroscopy (DOSY)[53] for the monomeric complex **II-20•II-3** and for the self-assembled species **II-20**$_n$ as shown in Figure II-6. The diffusion coefficients measured using four different resonances for **II-20•II-3** and **II-20**$_n$ averaged 2.646 ± 0.026 × 10^{-10} m^2 s^{-1} and 1.638 ± 0.045 × 10^{-10} m^2 s^{-1}, respectively (Figure II-6). The ratio of diffusion constants for **II-20•II-3** and **II-20**$_n$ is 1.616. The Stokes-Einstein equation (eq. 2) shows the relationship between the diffusion coefficient (D) and the hydrodynamic radius (r_s) in a medium of viscosity η where k_B is Boltzmann's constant and T is temperature.[53] If we assume that **II-20•II-3** and **II-20**$_n$ are roughly spherical then the ratio of the measured diffusion coefficients can be converted into a ratio of molecular weights which gives the oligomerization number. For a trimeric, tetrameric, or pentameric assembly theory predicts the ratio D(**II-20•II-3**) / D(**II-20**$_n$) = 1.442 (n = 3), 1.587 (n = 4), and 1.709 (n = 5). In this manner, the measured ratio of diffusion coefficients of 1.616 strongly suggests the formation of cyclic tetramer assembly **II-20**$_4$.

$$D = k_B T / 6 \eta r_s \qquad (2)$$

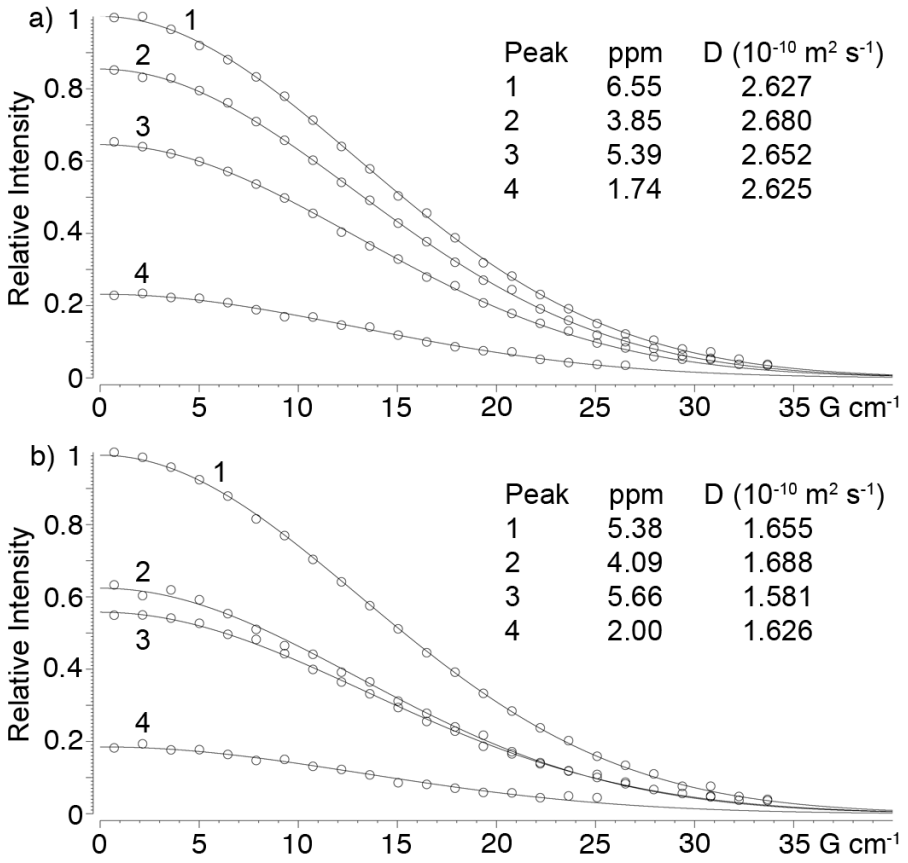

Figure II-6. DOSY spectra recorded (600 MHz, D_2O, RT) for: a) **II-20•II-3**, and b) cyclic tetramer **II-20$_4$**.

To provide additional evidence for the formation of the cyclic tetrameric assembly **II-20$_4$** we performed electrospray ionization mass spectrometry of 100 μM solutions in H_2O and 100,000 resolution on an LTQ-Orbitrap instrument (ThermoFisher, San Jose, CA). Figure II-7a shows the mass spectrum obtained which shows a 4^+ ion at *m/z* = 1329.97, a 5^+ ion at *m/z* = 1068.68, and a 6^+ at *m/z* = 894.31. The 4^+ ion corresponds to the **II-20**$_4^{4+}$ assembly. Figure II-7b shows the expansion of the region of the **II-20**$_4^{4+}$ ion and Figure II-7c shows the theoretical ion distribution for molecular formula $C_{200}H_{228}N_{128}O_{56}$. The excellent match between Figure II-7b and II-7c provides strong evidence for the description of this structure as the cyclic tetramer **II-20**$_4^{4+}$. Other ions of

significant intensity in Figure II-7a were observed at *m/z* = 1068.68 which corresponds to [**II-20**$_4$•Na]$^{5+}$ and *m/z* = 894.31 which corresponds corresponds to [**II-20**$_4$•Na$_2$]$^{6+}$. To gain further insight into this system, we isolated ion **II-20**$_4^{4+}$ and performed collisional induced dissociation experiments (Figure II-7d). We observed the cleavage of covalent bonds rather than the expected dissociation of non-covalent aggregate **II-20**$_4^{4+}$ into smaller non-covalent aggregate ions (e.g. monomers, dimers, or trimers). Overall, the electrospray mass spectrometric investigations strongly support that **II-20** self-assembles to give the highly stable cyclic tetrameric aggregate **II-20**$_4^{4+}$.

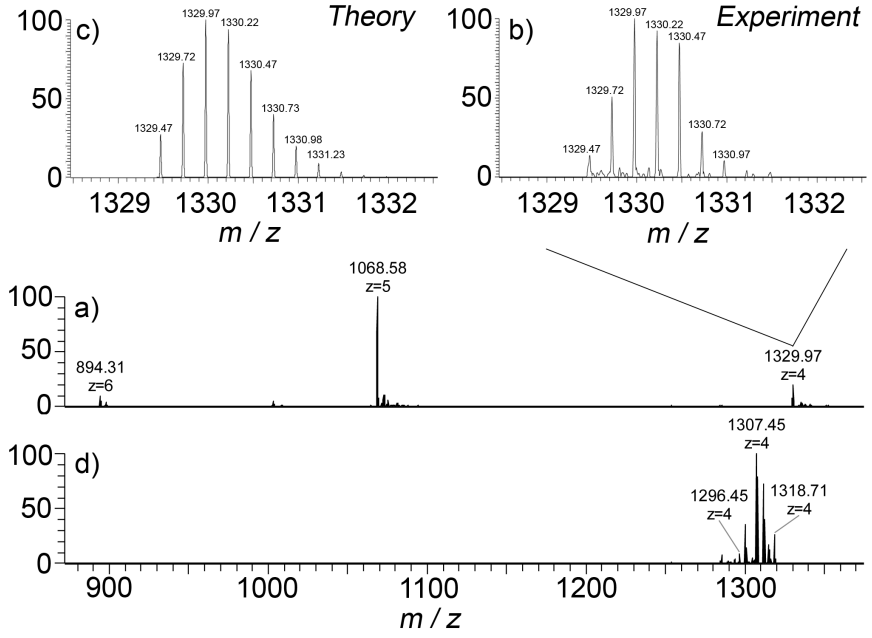

Figure II-7. Electrospray ionization mass spectra recorded for: a) a solution of **II-20**$_4$ (100 μM, H_2O), b) expansion of the **II-20**$_4^{4+}$ ion region, and c) theoretical distribution obtained for the molecular formula $C_{200}H_{228}N_{128}O_{56}$, and d) mass spectrum obtained upon collisional induced dissociation.

2.9 Enumeration of the Different Diastereomers of II-20$_4$.

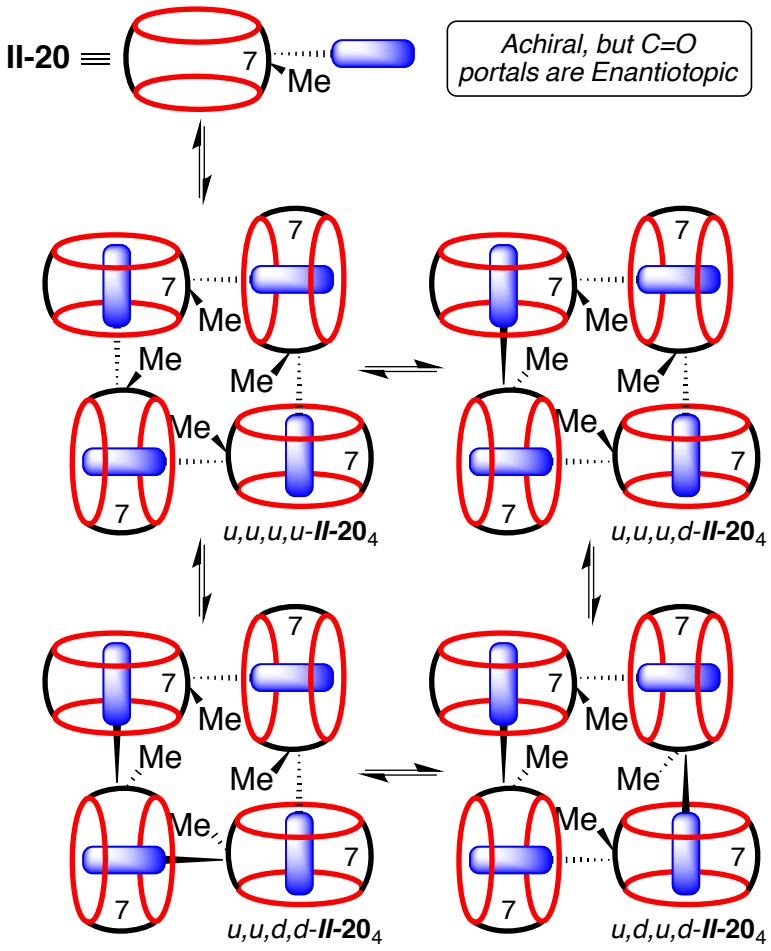

Scheme II-4. Self-assembly of CB[7] derivative **II-20** to give the cyclic tetramer **II-20**$_4$ as a mixture of diastereomers.

Although compound **II-20** is achiral due to the presence of a mirror plane that runs through the equator of the molecule, complexation events that desymmetrize the cavity result in the formation of complexes that are enantiomers and the two C=O portals can be described as enantiotopic. Accordingly, when four molecules of **II-20** self-assemble to form **II-20**$_4$, there are several diastereomers that can form (Scheme II-4). For

example, all four Me groups can be pointing up (u,u,u,u-**II-20**$_4$), three up and one down (u,u,u,d-**II-20**$_4$), and two different combinations of two up and 2 down (u,u,d,d-**II-20**$_4$ and u,d,u,d-**II-20**$_4$).[54] The various diastereomers are able to interconvert with one another by a sequence of dissociation of one of the CB[7]•triazolyl ammonium complexes to give a linear tetramer, followed by rotation of the CB[7] group and recomplexation of the triazolyl ammonium through the opposite ureidyl C=O portal of the CB[7] moiety. In this way, the averaging of the signals observed in the high temperature ^{1}H NMR spectrum shown in Figure II-5c is readily understandable.

2.10 Summary.

In summary, we have shown that CB[7] derivatives are accessible by a building block approach that involves the condensation of glycoluril hexamer **II-1** with glycoluril bis(cyclic ethers) **II-2**$_{Me}$, **II-2**$_{Cy}$, **II-2**$_{MePh}$, and **II-12**. Compounds Me_2CB[7] and CyCB[7] possess superior solubility in water which makes them well suited as a solubilization agent for poorly soluble pharmaceutical agents. Compound **II-18** which bears a reactive primary alkylchloride group is the first monofunctionalized CB[7] derivative to be reported. Compound **II-18** undergoes further functionalization reactions to yield **II-19** and subsequently **II-20** by click chemistry. We find that **II-20** undergoes a self-assembly process in water to yield cyclic tetramer **II-14** as established by NMR (VT and DOSY) and mass spectrometric measurements.

We believe that the implications of this research go well beyond the system specific details described above. For example, unfunctionalized CB[7] has been the most

widely applied CB[n] compound because of its good solubility in water and its exceptional binding affinity and selectivity toward its guests in water. This paper provides two water soluble monofunctionalized CB[7] derivatives that are amenable to further functionalization reactions by S_N2 and click chemistry which promises to allow the homogenous covalent attachment of CB[7] to solid phases, macromolecules like proteins and polymers, and incorporation into other complex and functional (bio)molecular systems. When that occurs, the continued impact of the CB[n] family of molecular containers on the chemical sciences will be significant.

Chapter 3: Synthesis and Recognition Properties of Cucurbit[8]uril Derivatives

3.1 Introduction

In the wake of the synthesis of functionalized CB[7], we began to pursue similar CB[8] derivatives with the goal of creating water-soluble CB[8] hosts with the same recognition properties of CB[8]. Other researchers also continued to look for methods to synthesize large CB[n] derivatives bearing functional groups. Most recently, in 2015, Bardelang and coworkers published a gram-scale synthesis of $(HO)_1$CB[n] (n = 6, 7, 8) which is performed in hydrogen peroxide and acid and irradiated by a light source, achieving nearly quantitative conversion (95-98%).[55] The ready access to large CB[n] derivatives in large quantities is a hopeful sign for the future of CB[n] applications. The following research details a building block process towards the first water-soluble CB[8] derivatives, the investigation of their recognition properties, and their use as drug solubilizing agents.

3.2 Synthesis and Characterization of CB[8] Derivatives.

The successful synthesis of monofunctionalized CB[7] derivatives by reaction of **III-1** with glycoluril bis(cyclic ethers) **III-2**$_{Me}$ and **III-2**$_{Cy}$ encouraged us to adapt this chemistry toward CB[8]. Accordingly, we performed the reaction between **III-1** and **III-2**$_{Me}$ (2.5 equiv.) in the presence of KI in 6 M HCl at 110 ˚C for 30 min (Scheme III-1).

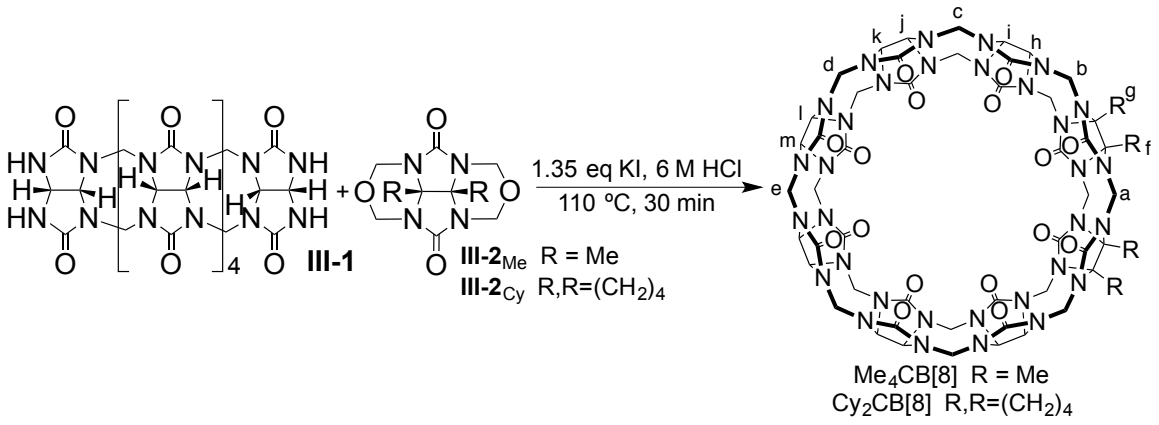

Scheme III-1. Building block synthesis of CB[8] derivatives.

The crude reaction mixture was analyzed by ^{1}H NMR using *p*-xylylenediammonium ion (**III-3**) as probe[40] which revealed the presence of CB[6], Me_2CB[7], and Me_4CB[8] in a 5:32:52 ratio. The purification was challenging and a multistep procedure was required. Initially, the crude reaction mixture was treated with disulfonated guest **III-4** to form the tight and very slowly dissociating Me_2CB[7]•**III-4** complex. This mixture which contains CB[6], Me_2CB[7]•**III-4**, and Me_4CB[8] possibly in complex with **III-4** was loaded onto a Dowex 50WX2-400 ion exchange column that was eluted with formic acid/HCl mixtures. Complex Me_2CB[7]•**III-4** which is a neutral zwitterion but which bears two external SO_3^- groups elutes rapidly from the sulfonated Dowex resin followed by an admixture of CB[6] and Me_4CB[8]. To further enrich the Me_4CB[8] content of the refined solid, the solid was washed with a mixture of formic acid, acetic acid, and acetone. The refined solid was subsequently treated with activated carbon and heated at reflux to yield Me_4CB[8] in a pure form (320 mg, 11% yield). Me_4CB[8] was fully characterized by the standard methods which are fully in accord with

the depicted structure. For example, the electrospray ionization spectrum established the molecular formula $C_{60}H_{60}N_{34}O_{16}$ corresponding to $[Me_4CB[8]\bullet\mathbf{III\text{-}3}]^{2+}$ (Appendix 2) Figure III-3a and b shows the ^1H NMR spectrum recorded for $Me_4CB[8]$ on its own and as the $Me_4CB[8]\bullet\mathbf{III\text{-}3}_2$ complex. The presence of two Me resonances (f and g) indicates that $Me_4CB[8]$ is overall C_{2v} symmetric and the observation of five doublets (H_a – H_e; 1:2:2:2:1 intensity ratio) in the 4-5 ppm region for the diastereotopic CH_2 groups is consistent with the depicted structure of $Me_4CB[8]$. The ^{13}C NMR spectrum of $Me_4CB[8]$ (Appendix 2) displays four C=O resonances which is consistent with the depicted structure. To differentiate spectroscopically between $Me_4CB[8]$ and an isomer with an identical pattern of ^1H and ^{13}C NMR resonances (Appendix 2), we performed nuclear Overhauser effect (NOE) measurements which showed enhancement of the half-intensity resonance for H_a upon irradiation of the methyl (H_f, H_g) resonances which is diagnostic for the depicted structure of $Me_4CB[8]$. $Cy_2CB[8]$ was prepared and purified in an analogous manner and was fully characterized (Appendix 2). Both CB[8] derivatives possess enhanced solubility in water relative to CB[8] itself ($Me_4CB[8]$ = 3.1 mM, $Cy_2CB[8]$ = 0.9 mM, CB[8] ≤ 10 μM).

3.3 Mechanism of Guest-Assisted Dowex™ Ion Exchange Chromatography

The separation of Me_4CB[8] from the other reaction products proved to be much more challenging than expected for several reasons. First, the reaction conditions only yield approximately 50% of the CB[8] product and several varied CB[n] congeners as side products Second, due to the fact that an alkylated CB[8] had never been synthesized before, the solubility properties of Me_4CB[8] in organic or aqueous media were unknown which made recrystallization and other solubility-dependent separation methods, such as extractions, difficult. Third, possibly due to the interference of the alkyl groups, Dowex™ ion exchange chromatography was unable to efficiently separate Me_4CB[8] from the smaller methylated CB[n] congeners. The result was a slightly improved mixture enriched with Me_4CB[8], yet still containing other methylated CB[n] congeners. Given that Dowex™ ion exchange chromatography is regularly a highly effective method for the separation of CB[n] congeners, we decided to investigate this issue and design a method which would allow for the isolation of any CB[n] derivative by Dowex™ ion exchange chromatography. The separation of sulfonate containing compounds by Dowex™ ion exchange chromatography had previously been documented by the Isaacs group.[56] It had been shown that the presence of sulfonate moieties caused these compounds to elute quickly from Dowex™ ion exchange resin, so we decided to introduce guests bearing sulfonate moieties to non-covalently modify the elution speed of the alkylated CB[n] congeners.

The rapid elution of the Me_2CB[7]•**III-4** complex from the Dowex™ ion exchange resin made us wonder if this process could be expanded to purify other CB[n] derivatives. The Me_2CB[7]•**III-4** complex elutes much more rapidly than any other

organic byproduct that large quantities (500-700 mg) of pure Me_2CB[7]•**III-4** complex were obtained in the first 400 mL of eluent. Because of these large quantities, we attempted to remove **III-4** from Me_2CB[7] with the aim of using this process to purify other CB[n] in the future (for example, improving the purification of Cl-CB[7]). However, we found that the formation of the Me_2CB[7]•**III-4** complex is nearly irreversible. A usual method for removal of an alkyl or aryl ammonium guest from a CB[n] cavity is to add base to deprotonate the ammonium creating the weaker binding amine guest which is easily washed away. However, guest **III-4** does not have ammonium protons and is not susceptible to base removal. Additionally, the sterically large and negatively charged sulfonate groups which make the formation of the Me_2CB[7]•**III-4** complex slow also prevent the dissociation of the complex by creating an energy barrier to the removal of guest. This energy barrier is so high that in aqueous solution with a 10 equivalent excess of adamantane ammonium ion **III-5**, an extremely strong binder for CB[7] ($K_a = 4.23 \pm 1.00 \times 10^{12}$),[26] we saw no exchange of guest after 2 d at reflux. The same solution was placed in a microwave reactor for 6 h at 150 ºC and less than 50% of guest was exchanged. Additionally, guest **III-4** was added to Me_2CB[7]•**III-5** complex in solution and no exchange occurred at room temperature. Under microwave conditions for 1 hour, there was approximately 10% exchange and after 3 hours approxiamately 50% of the guest had exchanged. This indicates that the K_a of Me_2CB[7] for guest **III-4** is less than that of Me_2CB[7] for **III-5**, but that the K_d is in fact very low which allows for Me_2CB[7]•**III-4** complex to accumulate in the presence of **III-5**.

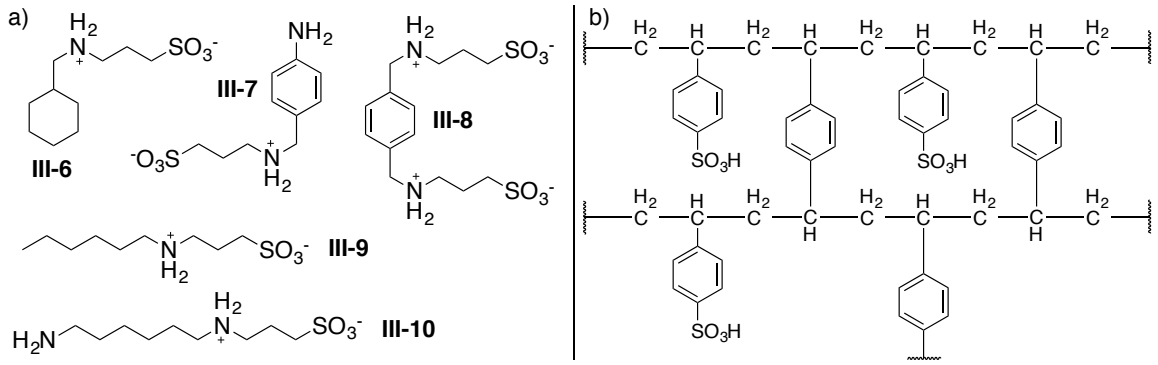

Figure III-1. a) Structures of sulfonate guests designed for guest-assisted Dowex chromatography and b) structure of Dowex™ resin.

The fast elution of the Me_2CB[7]•**III-4** complex can be attributed to two factors: 1) the sulfonate moieties are repelled by the sulfonate residues on the Dowex ion exchange resin and 2) the occupation of the CB[n] portal by the guest prevents proton exchange between the carbonyls and the sulfonic acid residues to give CB[n]•H^+ and sulfonate. Guest **III-4** has two sulfonate arms which may contribute to the high energetic penalty of removing the guest from the cavity and also prevents **III-4** from complexing with CB[6]. We decided to design a series of guests (Figure III-1a) that would test these factors by asking these questions: 1) if two sulfonate arms are necessary, 2) whether the dimethyl ammonium moiety is necessary, 3) whether the volume of the guest has an effect, and 4) if both carbonyl portals need to be occupied. It was found that guests with only one sulfonate arm and/or only one electrostatically positive binding site (**III-6**, **III-7**, **III-9**, **III-10)** would dissociate on the column and have no noticeable effect on the elution speed of the CB[n]. Additionally, deletion of the dimethyl ammonium moiety (**III-8**) did not significantly increase the K_d of the sulfonated **III-3** derivatives.

3.4 Discerning the Mechanism of Me_4CB[8] Formation.

In an effort to better understand the Me_4CB[8] forming reaction and thereby improve the scope and yield of this reaction we performed some control experiments. A priori, one can postulate two pathways (Scheme III-2): 1) two equivalents of **III-2**$_{Me}$ undergo dimerization to yield tetramethyl glycoluril dimer **III-11** which then reacts with **III-1** to give Me_4CB[8], or 2) the two pairs of NH groups of **III-1** reacts with two equivalents of **III-2**$_{Me}$ to give a linear glycoluril octamer bis(cyclic ether) which then undergoes unimolecular cyclization to give Me_4CB[8]. Experimentally, we reacted **III-1** with **III-11**[57] under our standard reaction conditions and observed mainly CB[6], traces of Me_2CB[7], but no Me_4CB[8]. Accordingly, we believe that Me_4CB[8] formation predominately follows pathway 2.

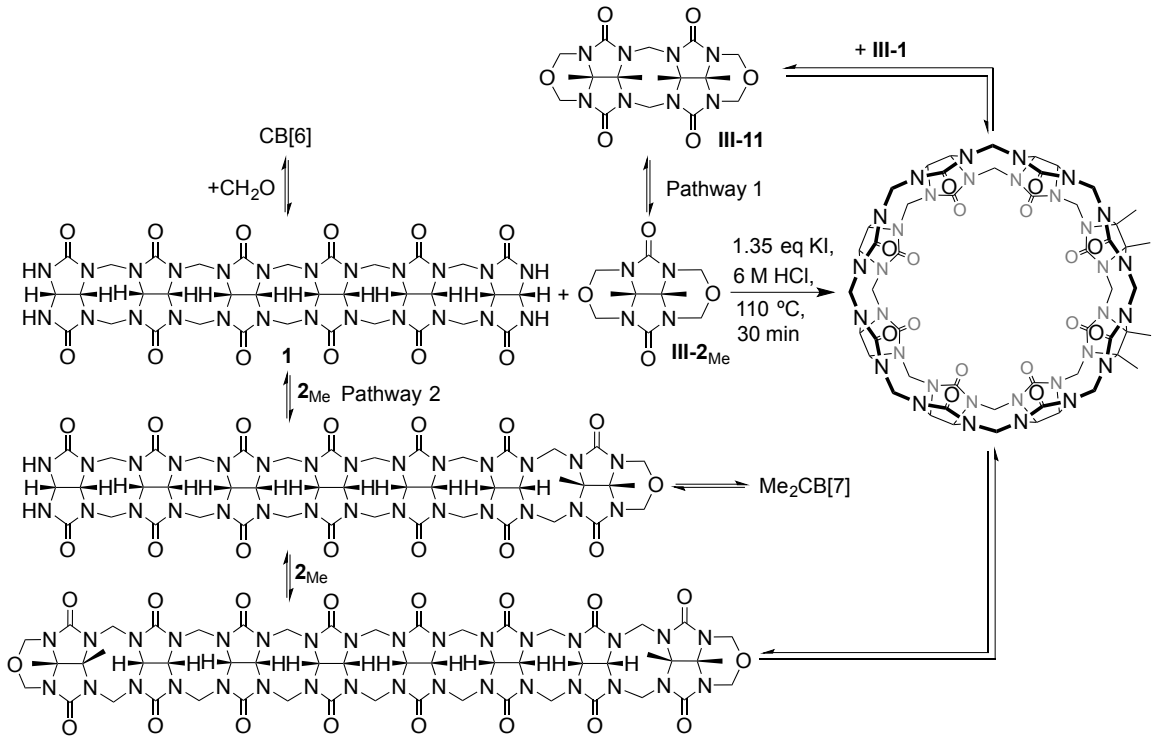

Scheme III-2. The two potential mechanistic pathways for the formation of Me_4CB[8].

3.5 Properties of $Me_4CB[8]$ and $Cy_2CB[8]$ Studied by X-ray Crystallography.

We were fortunate to obtain single crystals of $Me_4CB[8]$•**III-3**$_2$, $Cy_2CB[8]$•**III-3**$_2$, and $Me_4CB[8]$•**III-12** and determine their structures by x-ray crystallography which corroborates the structural assignments made by NMR spectroscopy and symmetry arguments. There are several noteworthy aspects of the crystal structures. For example, the complexes exhibit substantial ellipsoidal deformations as measured between opposing CH_2 groups ($Cy_2CB[8]$•**III-3**$_2$: long axis = 14.00 Å and short axis = 10.95 Å; $Me_4CB[8]$•**III-12**: long axis = 14.37 Å and short axis = 11.21 Å) which can be attributed in part to the steric demands of the substituted glycolurils; related deformations have previously been noted for $Me_4CB[6]$ and its complexes.[46] The cyclohexyl rings of $Cy_2CB[8]$ exist in the boat conformation because of the conformational restraints of the bicyclic glycoluril framework enforcing a syn-periplanar dihedral angle (0.51° in the crystal). The two aromatic rings of guest **III-3** in the $Cy_2CB[8]$•**III-3**$_2$ complex are

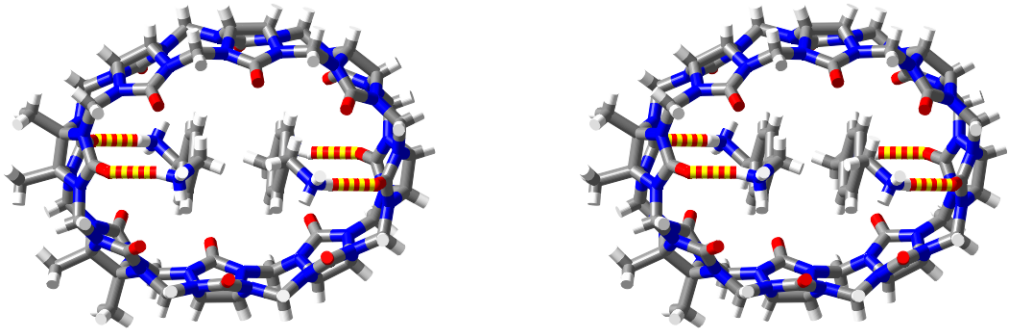

Figure III-2. Stereoview of the x-ray crystal structure of $Me_4CB[8]$•**III-3**$_2$. Color code: C, gray; H, white; N, blue; O, red; H-bonds, red-yellow striped.

arranged in an offset geometry with a mean interplanar separation of 3.71 Å which is ≈ 0.3 Å longer than that typically ascribed to π•••π interactions. In the structure of Me_4CB[8]•**III-12**, guest **III-12** adopts a U-shaped conformation as previously observed for CB[8]•**III-12**.[47] The three dimensional packing of the complexes in the crystal feature the I^- counterions in the interstitial sites between complexes presumably benefitting from glycoluril CH•••I^- interactions on the convex face of the CB[8] derivatives.

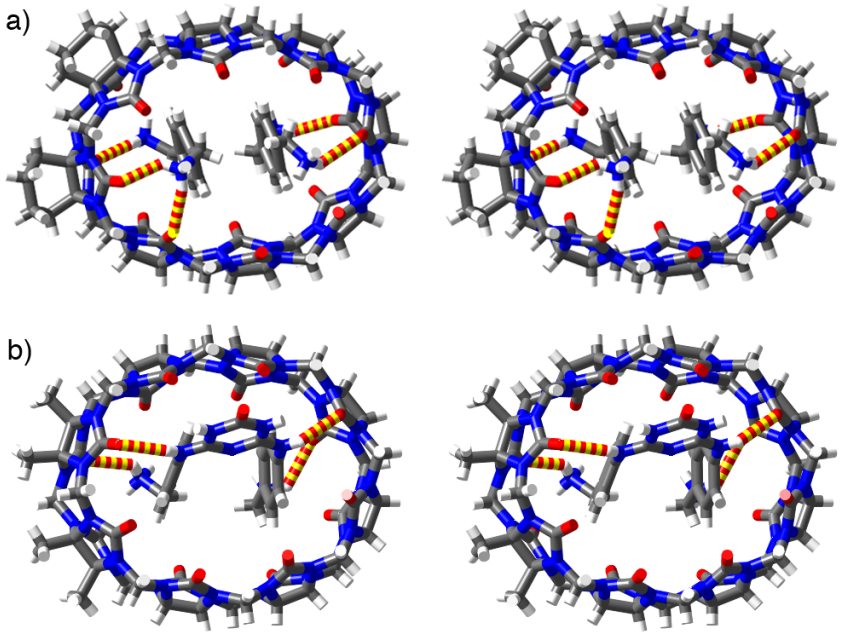

Figure III-3. Stereoviews of the x-ray crystal structures of: a) Cy_2CB[8]•**III-3**$_2$, and b) Me_4CB[8]•**III-12**. Color code: C, gray; H, white; N, blue; O, red; H-bonds, red-yellow striped.

3.6 Recognition Properties of Me_4CB[8].

After having qualitatively determined that the CB[8] derivatives share the recognition abilities of unsubstituted CB[8] we decided to compare the binding constants of Me_4CB[8] with those of CB[8] in a quantitative manner. We hypothesized that the ellipsoidal deformation observed in the x-ray crystal structure of Me_4CB[8]•**III-12** might translate into a higher affinity of Me_4CB[8] toward ellipsoidal guests compared to unsubstituted CB[8]. For this purpose, we allowed Me_4CB[8] and CB[8] to compete for a limited quantity of guest according to equation 1 and 2.[58] We identify resonances for Me_4CB[8]•guest and CB[8]•guest that can be separately integrated which allows a determination of the relative concentrations of Me_4CB[8]•guest and CB[8]•guest and by use of mass balance expressions we can determine the concentrations of free Me_4CB[8] and CB[8] (Appendix 2).

$$\begin{matrix} \text{CB[8]•}\mathbf{G} \\ + \\ \text{Me}_4\text{CB[8]} \end{matrix} \underset{}{\overset{K_{rel}}{\rightleftharpoons}} \begin{matrix} \text{Me}_4\text{CB[8]•}\mathbf{G} \\ + \\ \text{CB[8]} \end{matrix} \quad (1)$$

$$K_{rel} = \frac{[\text{Me}_4\text{CB[8]•}\mathbf{G}]\,[\text{CB[8]}]}{[\text{CB[8]•}\mathbf{G}]\,[\text{Me}_4\text{CB[8]}]} \quad (2)$$

$$K_{a,Me4CB[8]} = K_{rel} \bullet K_{a,CB[8]} \quad (3)$$

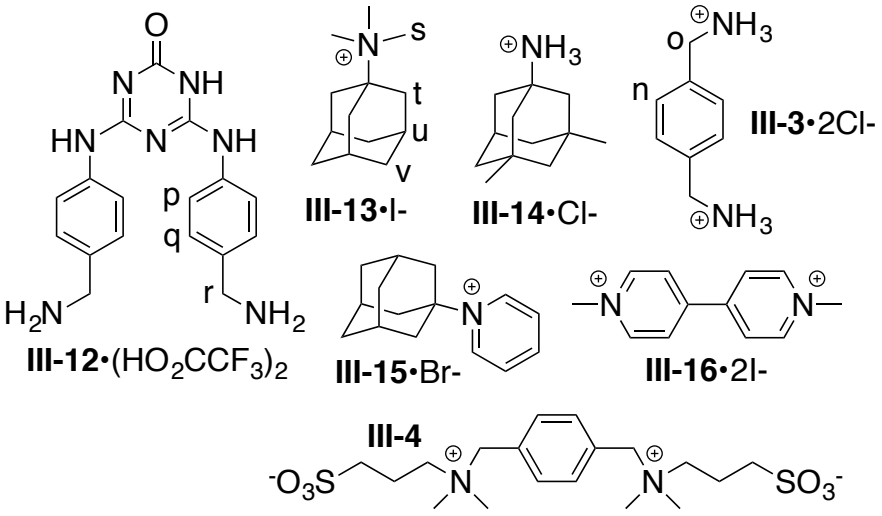

Figure III-4. Structures of guests used in the binding studies.

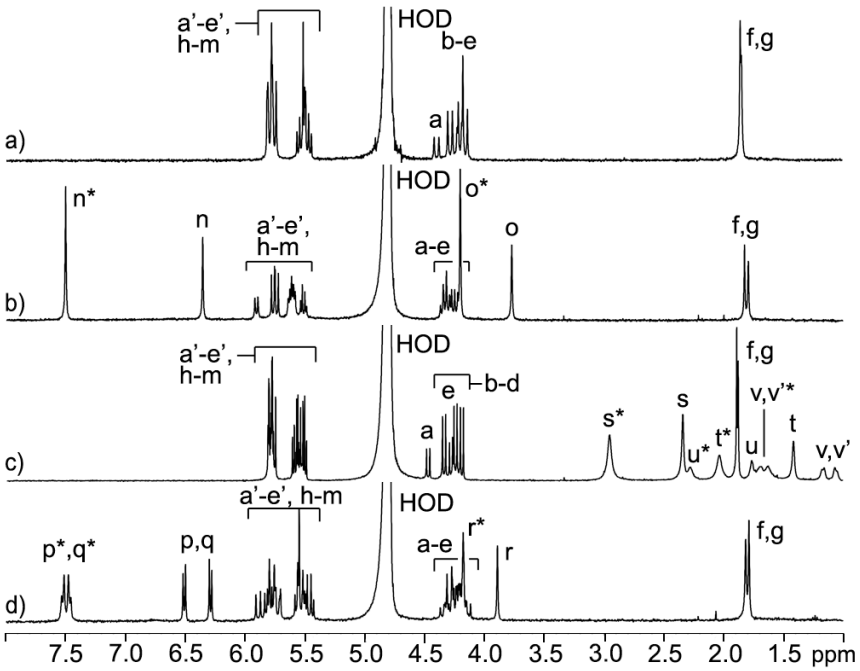

Figure III-5. ^{1}H NMR spectra (D_2O, 600 MHz, rt) of: a) Me_4CB[8], b) Me_4CB[8]•**III-3**$_2$ and excess **III-3**, c) Me_4CB[8]•**III-13** and excess **III-13**, d) Me_4CB[8]•**III-12** and excess **III-12**. Resonances marked with asterisks (*) arise from unbound guest**.**

For example, Figure III-6 shows the ^{1}H NMR spectra recorded at 800 MHz for a 1:1:1 mixture of CB[8], Me_4CB[8], and **III-13**. We use the ^{1}H NMR resonances for H_s in the CB[8]•**III-13** and Me_4CB[8]•**III-13** complexes which appear at 2.39 and 2.37 ppm respectively to determine the complex concentrations. Substitutions of the concentration values into equation 2 allows us to determine K_{rel} (Table III-1). In this manner, we determined that Me_4CB[8] binds tighter to guests **III-12** (2.52-fold), **III-13** (1.16 fold), **III-15** (2.43 fold) than CB[8] does; in contrast Me_4CB[8] binds weaker than CB[8] to **III-14** (K_{rel} = 0.26). Finally, we can use equation 3 and the previously determined K_a values with unsubstituted CB[8][47] to determine K_a for the Me_4CB[8]•guest complexes as given in Table III-1. Unfortunately, the trends in K_{rel} values are not sufficiently clear to allow us to make any conclusions regarding the influence of host ellipsoidal deformation on K_{rel}.

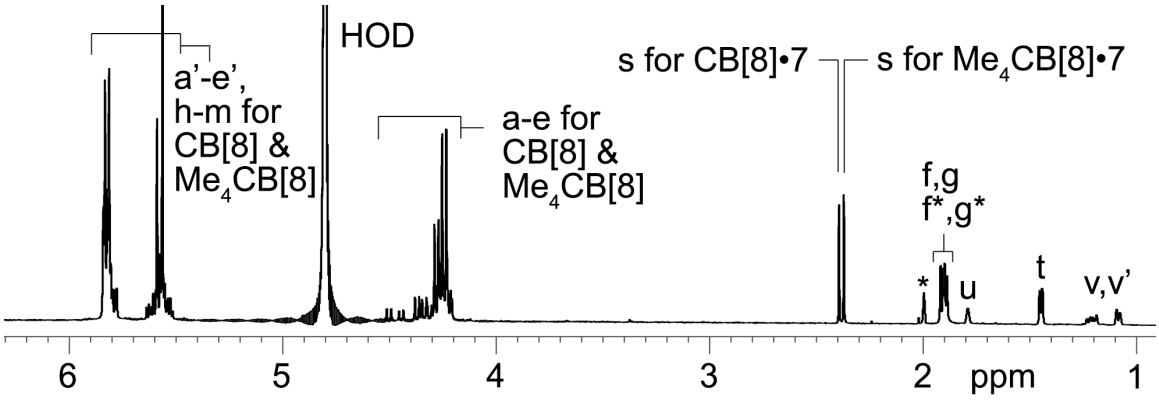

Figure III-6. ^{1}H NMR spectra (50 mM NaO_2CCD_3 buffered D_2O, pH 4.74, 800 MHz, RT) for an equimolar (50 μM) mixture of Me_4CB[8], CB[8], and **III-13**.

Table III-1. Values of K_{rel} and K_a for Me_4CB[8]•guest complexes.

Guest	K_{rel}	K_a (M^{-1})
III-12	2.52	1.45×10^{11}
III-14	0.26	1.13×10^{11}
III-13	1.16	1.12×10^{11}
III-15	2.43	4.87×10^{9}

3.7 Using Me_4CB[8] as a Drug Solubilizing Agent.

Finally, we sought to take advantage of the higher solubility of Me_4CB[8] compared to CB[8] in a relevant application area. Accordingly, we decided to investigate the ability of Me_4CB[8] to act as a solubilizing agent for four insoluble drugs (amiodarone, estradiol, tamoxifen, albendazole, Figure III-7).[59] Experimentally, we stir a solution of a known concentration of Me_4CB[8] (or CB[8]) with an excess of insoluble drug until equilibrium is reached, filter off the insoluble material, and then measure the concentration of drug in solution by ^{1}H NMR integration of drug resonances relative to an internal standard of known concentration. Multiple measurements at different host concentrations are then used to construct a phase solubility diagram. Figure III-8 shows the phase solubility diagrams (PSDs) constructed for Me_4CB[8] or CB[8] with amiodarone.

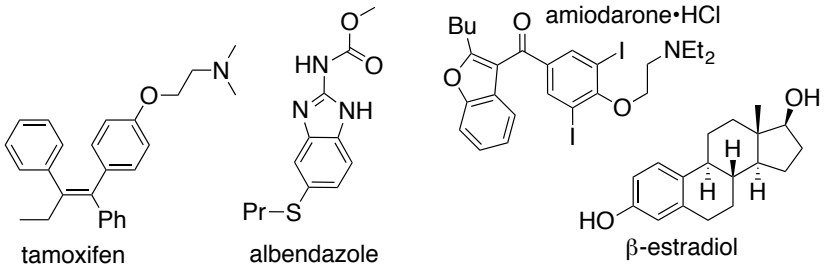

Figure III-7. Structures of drugs used in this study.

Linear PSDs are generally indicative of the formation of soluble, well-defined 1:1 host-guest complexes. The slope of linear phase solubility diagrams (PSD) is related to the inherent solubility of the drug (s_0) and the binding constant (K_a, M^{-1}) for the host-drug complex according to equation 4. The slope of the PSD for Me_4CB[8] with amiodarone is 0.44 whereas it is too small to measure for CB[8]. Given that the K_a values for Me_4CB[8] and CB[8] complexes are very similar for soluble guests as shown above it is somewhat counterintuitive that Me_4CB[8] is the superior solubilizing agent. In this case, the CB[8]•amiodarone complex is formed but is insoluble, hence it is the enhanced solubility of Me_4CB[8] and its Me_4CB[8]•drug complexes relative to CB[8] that is crucial for its function as a solubilizing agent. Similar PSD measurements were done with tamoxifen, albendazole, and estradiol (Table III-2). In all cases, Me_4CB[8] was a good solubilizing agent with slope values in the 0.08 – 0.44 range.

Table III-2. Values of slope and K_a (M^{-1}) derived from the PSDs for solubilization of four drugs with Me_4CB[8] or CB[8].

Drug	***Me_4CB[8]***		***CB[8]***	
	Slope	***K_a (M^{-1})***	***Slope***	***K_a (M^{-1})***
Amiodarone	0.44	12100	0	-
Tamoxifen	0.36	46700	0.36	46700
β-Estradiol	0.086	10700	0	-
Albendazole	0.37	221000	0	-

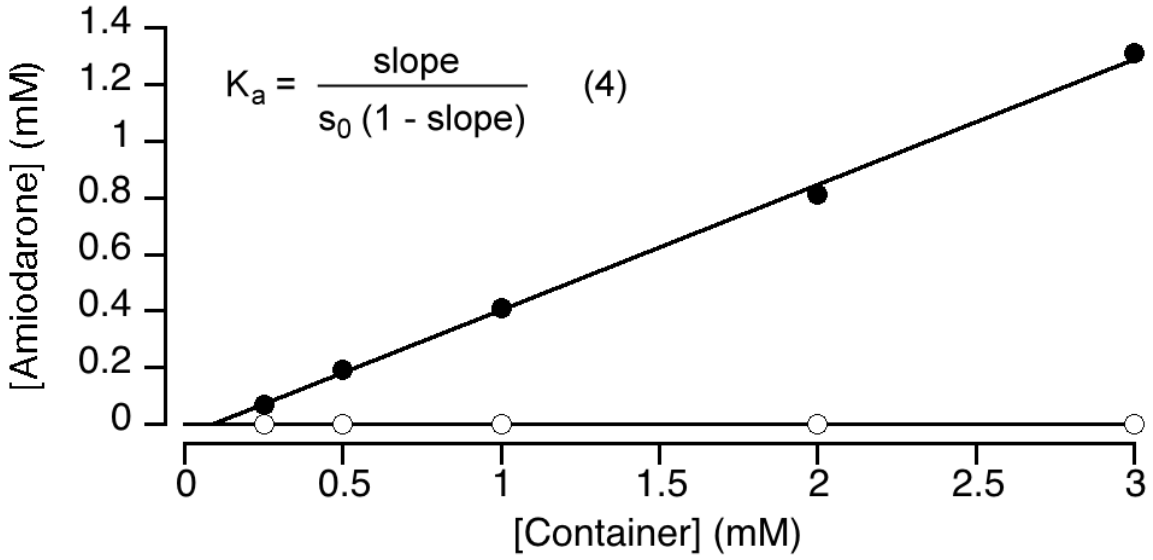

Figure III-8. Phase solubility diagrams constructed for amiodarone with Me_4CB[8] (•) and CB[8] (o). Conditions: 20 mM sodium phosphate buffered D_2O (pH = 7.4, rt).

3.8 Summary.

In summary, we have demonstrated that Me_4CB[8] and Cy_2CB[8] can be formed by the condensation of glycoluril hexamer **III-1** with bis (cyclic ethers) **III-2** under well defined conditions. The CB[8] derivatives maintain the essential binding features of unfunctionalized CB[8] in that they also bind to guests **III-3 – III-5** and **III-12** – **III-16** and display comparable complexation induced changes in chemical shift. ^{1}H NMR competition experiments between Me_4CB[8] and CB[8] for a limited quantity of guest established that Me_4CB[8] displays quite similar binding constants (K_a) compared to CB[8]. Finally, Me_4CB[8] is a better solubilizing agent than CB[8] for four insoluble drugs which can be traced to the enhanced solubility of the Me_4CB[8]•drug complexes. In conclusion, we present the first building block strategy that allows the synthesis of CB[8] derivatives. The work, especially in light of the recent report of $(HO)_1$CB[8],[55] suggests a bright future for CB[8] derivatives in the basic science of CB[n] chemistry and advanced applications.

Chapter 4: Summary and Future Work

4.1 Summary.

The science of molecular containers has advanced rapidly in recent years. The recent synthetic advances in CB[n] derivative chemistry has opened up opportunities for CB[n] hosts to rival the long-reigning cyclodextrins. The newly available hosts benefit from superior binding properties to cyclodextrins, enhanced solubility over unfunctionalized CB[n], and/or cheap large-scale synthetic schemes, making them excellent hosts for a variety of applications. This body of work described new synthetic approaches towards functionalized CB[7] and CB[8], an area which had previously been largely unexplored.

Chapter 2 described the building block synthesis of monofunctionalized CB[7] derivatives and their physical and recognition properties. It was found that though Me_2CB[7] and CyCB[7] are highly water soluble and share many of the same highly selective recognition properties as CB[7], the functionalized CB[7] derivatives did not make effective drug solubilizing agents. This chapter also described the synthesis and applications of Cl-CB[7]. In chapter 3 we discussed the synthesis of two water-soluble CB[8] derivatives, Me_4CB[8] and Cy_2CB[8], and the mechanism of their formation. After investigating their recognition properties by both ^{1}H NMR and x-ray crystallography, we demonstrated that the CB[8] derivatives also were capable of solubilizing insoluble pharmaceuticals.

4.2 Future Work.

We were able to synthesize larger CB[n] derivatives (n = 7, 8) using a building block approach from glycoluril hexamer **IV-1** and functionalized glycoluril bis (cyclic ethers) **IV-2**. Using a similar approach, possibly in combination with a large alkyl ammonium guest as template, we may be able to access larger, previously unknown CB[n] such as CB[9].

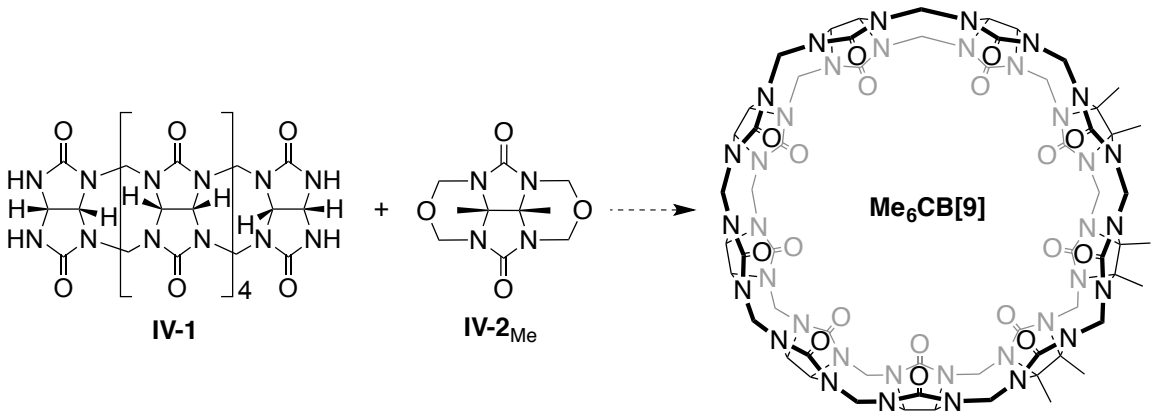

Scheme IV-XX. Proposed synthesis of CB[9] derivatives.

A concern for this synthesis is the stability of the macrocycle, a problem which was noted in the synthesis of CB[10]. CB[10] is able to form in reaction mixtures as a complex with CB[5] as the guest which both templates the formation of CB[10] and stabilizes the product in reaction conditions until it can be isolated. Using a similar approach, an alkyl or aryl ammonium guest which can fill the cavity of CB[9] may be able to template the reaction and stabilize the large macrocycle.

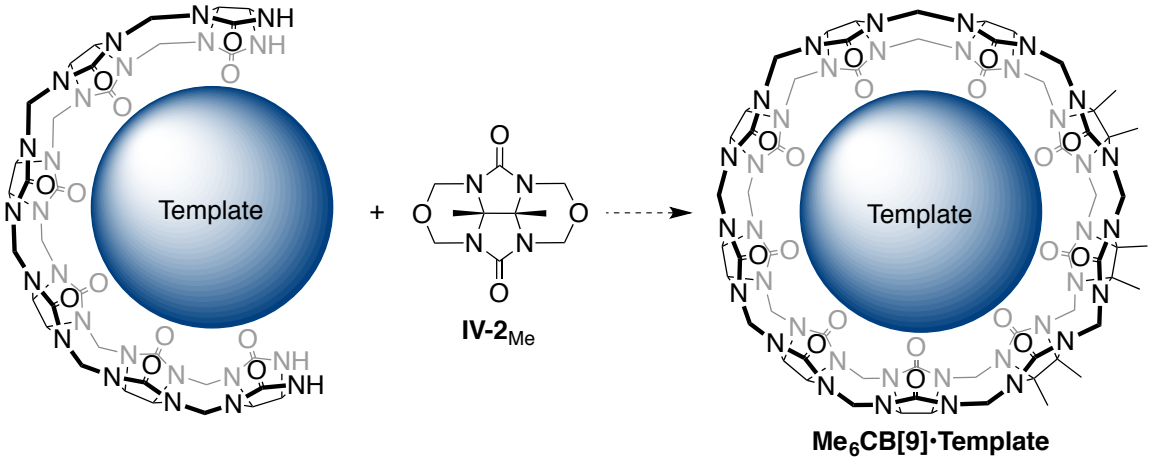

Scheme IV-XX. Proposed templated synthesis of $Me_6CB[9]$.

CB[9] would be an important host as its larger cavity may allow for binding larger pharmaceutical agents or the formation of interesting ternary complexes, as can be seen with CB[8]. Furthermore, based on the well documented trends of CB[n] solubility, we could expect that CB[9] may have solubility properties similar to CB[7] and could be soluble up to 20 mM.

Appendix 1

Synthesis and Self-Assembly Processes of Monofunctionalized Cucurbit[7]uril

Supporting Information

*by Brittany Vinciguerra, Liping Cao, Joe R. Cannon, Peter Y. Zavalij, Catherine Fenselau, and Lyle Isaacs**

Department of Chemistry and Biochemistry, University of Maryland, College Park, MD 20742

Table of Contents

General Experimental Details. Starting materials were purchased from commercial suppliers were used without further purification. Compounds **SI1**, **II-14**, **II-15**, and **II-18** were prepared according to the literature procedures.[1-4] Melting points were measured on a Meltemp apparatus in open capillary tubes and are uncorrected. TLC analysis was performed using pre-coated plastic plates from Merck. IR spectra were recorded on a JASCO FT/IR 4100 spectrometer and are reported in cm^{-1}. NMR spectra were measured on a spectrometers operating at 400, 500, or 600 MHz for ^{1}H and 100, 125, and 150 MHz for ^{13}C NMR spectra. Routine mass spectrometry was performed using a JEOL AccuTOF electrospray instrument (ESI). The mass spectrometric investigations of $\mathbf{20}_4$ were performed using an LTQ-Orbitrap XL (ThermoFisher, San Jose, CA).

Synthetic Procedures and Characterization Data

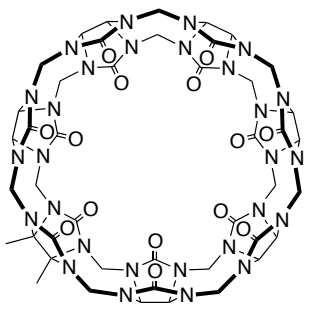

Compound $Me_2CB[7]$. A mixture of hexamer **II-1** (1.000 g, 1.03 mmol) and KI (0.230 g, 1.35 mmol) were dissolved in 9 M aqueous H_2SO_4 (5 mL) and then treated with dimethyl glycoluril bis (cyclic ether) $\mathbf{II\text{-}2}_{Me}$ (0.260 g, 1.03 mmol). The flask was then sealed with a rubber septum and heated at 110 °C for 30 min. The homogenous clear orange mixture was poured into a 50 mL centrifuge tube and methanol (43 mL) was added, causing a white precipitate to appear. The mixture was sonicated for 5 min and then centrifuged at 7200 rpm for 8 min. The supernatant was discarded and acetone (45 mL) was added to the centrifuge tube. The mixture was sonicated until the solid was resuspended and then centrifuged at 7200 rpm for 8 min. The supernatant was discarded and the precipitate was dried under high vacuum overnight. The crude white powder (1.23 g) was analyzed by ^{1}H NMR in the presence of

p-xylylene diamine and determined to be a mixture of approximately 50:50 CB[6]:Me_2CB[7]. The crude white powder was dissolved in H_2O (30 mL) and sonicated for 5 min, yielding an orange solution. To this solution, 1 M aqueous KI solution (1.8 mL) was added. The mixture was shaken thoroughly and allowed to sit at RT for 10 min, causing a yellow-white precipitate to form. The mixture was centrifuged at 7200 rpm for 8 min. The supernatant was poured into methanol (100 mL) and centrifuged at 7200 rpm for 8 min. The supernatant was discarded and the solid was dried under high vacuum (0.69 g). The solid was redissolved in ultrapure water (30 mL). The solution was treated with activated carbon (Fisher Chemical, Norit* Netural, C170-500, 4.00 g). The mixture was stirred for 24 h and then filtered. The solution was dried under high vacuum, yielding a white solid. After ^{1}H NMR analysis in the presence of **II-3**, the solid was determined to be pure dimethyl-CB[7] (0.380 g, 0.321 mmol, 31% yield). M.p. > 350 °C. IR (KBr, cm^{-1}): 1733s, 1473m, 1321m, 1235m, 1193m, 1117m, 806m. ^{1}H NMR (400 MHz, D_2O, as Me_2CB[7]•**3**, RT): 6.61 (s, 4H), 5.75-5.65 (m, 14H), 5.60-5.40 (m, 12H), 4.32 (d, J = 15.6, 4H), 4.26 (d, J = 15.6, 2H), 4.21 (d, J = 15.6, 4H), 4.16 (d, J = 15.6, 4H), 3.90 (s, 4H), 1.80 (s, 6H). ^{13}C NMR (125 MHz, D_2O, RT, 1,4-dioxane as internal standard): δ 157.3, 157.1, 157.0, 156.1, 78.9, 72.0, 71.9, 71.9, 71.8, 71.7, 71.6, 53.4, 53.0, 52.9, 49.2, 16.2. ESI-MS (**II-3** as guest): *m/z* 664 ([M• **II-3** + 2H]$^{2+}$). HR ESI-MS (**II-3** as guest): *m/z* 664.24531 ([Me_2CB[7]• **II-3** + 2H]$^{2+}$, $C_{52}H_{60}N_{30}O_{14}^{2+}$, calcd, for 664.24526). X-ray crystal structure.

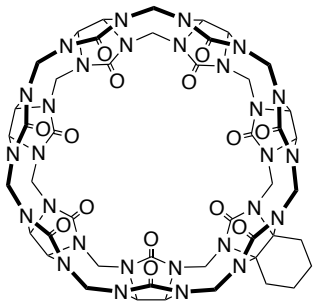

Compound CyCB[7]. A mixture of hexamer (1.000 g, 1.03 mmol) and KI (0.230 g, 1.35 mmol) were dissolved in 9 M aqueous H_2SO_4 (5 mL) and then treated with cyclohexyl glycoluril bis (cyclic ether) (0.288 g, 1.03 mmol). The flask was then sealed with a rubber septum and heated at 110 ˚C for 30 min. The homogenous clear orange mixture was poured into a 50 mL centrifuge tube and methanol (43 mL) was added, causing a white precipitate to appear. The mixture was sonicated for 5 min and then centrifuged at 7200 rpm for 8 min. The supernatant was discarded and acetone (45 mL) was added to the centrifuge tube. The mixture was sonicated until the solid was resuspended and then centrifuged at 7200 rpm for 8 min. The supernatant was discarded and the precipitate was dried under high vacuum overnight. The crude white powder (1.17 g) was analyzed by ^{1}H NMR in the presence of *p*-xylylene diamine and determined to be a mixture of approximately 66:33 CB[6]: CyCB[7]. The crude white powder was dissolved in H_2O (40 mL) and sonicated for 5 min, yielding an orange solution. To this solution, 1M aqueous KI solution (3.0 mL) was added. The mixture was shaken thoroughly and allowed to sit at RT for 10 min, causing a yellow-white precipitate to form. The mixture was centrifuged at 7200 rpm for 8 min. The supernatant was poured into methanol (100 mL) and centrifuged at 7200 rpm for 8 min. The supernatant was discarded and the solid was dried under high vacuum (0.45 g). The solid was redissolved in ultrapure water (30 mL). The solution was treated with activated carbon (Fisher Chemical, Norit* Netural, C170-500, 4.00 g). The mixture was stirred for 24 h and then filtered. The solution was dried under high vacuum, yielding a white solid. After ^{1}H NMR analysis in the presence of *p*-xylyene diamine, the solid was

determined to be pure CyCB[7] (0.23 g, 0.188 mmol, 18% yield). M.p. > 350 °C. IR (KBr, cm^{-1}): 1728s, 1476s, 1323m, 1236m, 1193m, 1100w, 806m. ^{1}H NMR (400 MHz, D_2O, as CyCB[7]• **II-3**, RT): 6.65 (s, 4H), 5.79 (d, *J* = 15.6, 2H), 5.75 (d, *J* = 16.20, 8H) 5.72 (d, *J* = 16.2, 4H), 5.59 (d, *J* = 8.1, 2H), 5.56 (d, *J* = 8.1, 2H), 5.55-5.45 (m, 8H), 4.30 (d, *J* = 15.6, 2H), 4.28 (d, *J* = 16.2, 4H), 4.26 (d, *J* = 16.2, 4H), 4.21 (d, *J* = 16.2, 4H), 3.94 (m, 4H), 2.31 (m, 4H), 1.52 (s, 4H). ^{13}C NMR (125 MHz, D_2O, RT, 1,4-dioxane as internal standard): δ 156.4, 156.2, 156.2, 155.9, 76.5, 71.0, 70.9, 70.8, 70.8, 70.7, 70.6, 52.4, 52.0, 51.9, 48.0, 21.4, 12.8. ESI-MS (**II-3** as guest): *m/z* 677 ([CyCB[7]• **II-3** + 2H]$^{2+}$). HR ESI-MS (**II-3** as guest): *m/z* 677.25205 ([CyCB[7] **II-•3** + 2H]$^{2+}$, $C_{54}H_{62}N_{30}O_{14}^{2+}$, calcd, for 677.2521).

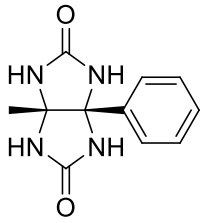

Compound SI1. To 1-phenylpropane-1,2-dione (4.84 g, 32.7 mmol) was added a solution of urea (7.85 g, 130.8 mmol) in HCl (250 mL, 0.30 M), and the reaction mixture was capped. The reaction was then stirred at RT for 2 days. The precipitates were filtered, washed with H_2O (200 mL) and Et_2O (200 mL) sequentially, and then dried under high vacuum to yield **SI1** as a white solid (6.74 g, 29.1 mmol, 89 %). The ^{1}H NMR matches that reported in the literature.[4]

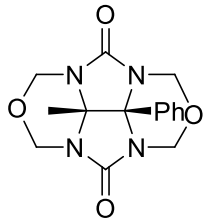

Compound II-2$_{MePh}$. To a 50 mL flask was added a mixture of **SI1** (812 mg, 3.49 mmol), paraformaldehyde (504 mg, 16.8 mmol) in 9 M HCl (20 mL), and the flask was capped with a septum. The reaction was then stirred at RT for 24 h upon which time additional H_2O (20

mL) was added into the reaction mixture, and stirred for an additional 12 h. The precipitates were filtered, washed with H_2O (20 mL) and EtOH (10 mL) sequentially, dried under high vacuum to yield compound $\mathbf{2}_{MePh}$ as a white solid (635 mg, 2.01 mmol, 58 %). M.p. 289-291 ˚C. IR (KBr, cm^{-1}): 3442w, 1740s, 1726s, 1469s, 1448m, 1413s, 1394m, 1385s, 1269m, 1206w, 1176s, 1127w, 1107w, 1079w, 1020s, 992w, 974w, 945m, 924w, 859m. ^{1}H NMR (400 MHz, DMSO-d_6): 7.60-7.50 (m, 3H), 7.50-7.40 (m, 2H) 5.36 (d, J = 11.2, 2H), 5.31 (d, J = 11.2, 2H), 5.01 (d, J = 11.2, 2H), 4.56 (d, J = 11.2, 2H), 1.19 (s, 3H). ^{13}C NMR (100 MHz, DMSO-d_6): 157.7, 132.8, 129.8, 129.3, 127.7, 78.1, 73.9, 71.3, 70.5, 19.1 HR-MS: *m/z* 317.1235 ($[M + H]^+$, calcd. for $C_{15}H_{17}N_4O_4^+$, 317.1250).

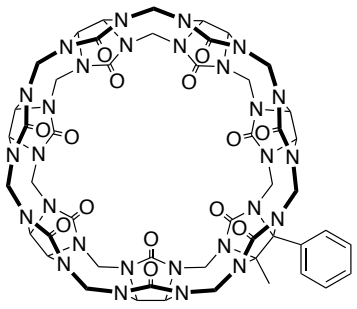

Compound MePhCB[7]. A mixture of **1** (973 mg, 1.0 mmol) and KI (224 mg, 1.35 mmol) were dissolved in 9M aqueous H_2SO_4 (5 mL) and then treated with $\mathbf{2}_{MePh}$ (380 mg, 1.2 mmol). The flask was then sealed with a rubber septum and heated at 110 ˚C for 30 min. The reaction solution was then poured into MeOH (40 mL) which resulted in a gray precipitate. The mixture was centrifuged at 7200 rpm for 5 min. The supernatant was decanted and the precipitate was washed with MeOH (40 mL × 3) and centrifuged at 7200 rpm for 5 min. The precipitate was dried under high vacuum to give crude, gray powder (1.32 g, including includes 30% of MePh CB[7], 61% of CB[6] and 9% of unidentified products). The crude solid was dissolved in a solution of 88% formic acid/0.4 M HCl (1:1, v:v) (10 mL). The solution containing the crude solid was loaded onto a column (3 cm diameter)

containing 20 cm Dowex 50WX2 ion-exchange resin pretreated with 88% formic acid/0.4 M HCl (1:1, v:v). The column was eluted with 88% formic acid/0.4 M HCl (1:1, v:v, 400 mL), and then 88% formic acid/0.6 M HCl (1:1, v:v, 400 mL), and then 88% formic acid/0.8 M HCl (1:1, v:v, 400 mL). The fraction purity was assessed by ^{1}H NMR using **3** as a probe. The appropriate factions were combined and solvent was removed by rotary evaporation and dried under high vacuum. The yellow solid was then washed with MeOH (40 mL) and centrifuged at 7200 rpm for 5 min. The supernatant was decanted and the precipitate was dried under high vacuum to give crude compound MePhCB[7] as a white powder (36 mg, 0.029 mmol, 2.9%). M.p. > 300 ˚C. IR (KBr, cm^{-1}): 3455s, 3001w, 2923w, 1730s, 1637m, 1472s, 1421m, 1337m, 1321s, 1235s, 1193s, 1101w, 1024w, 968m, 940w, 892w. ^{1}H NMR (500 MHz, D_2O, >1 equiv. **3**): 7.70-7.60 (m, 3H), 7.57 (s, unbound **3**), 7.30 (d, *J* = 6.9, 2H), 6.73 (s, 4H), 5.98 (d, *J* = 15.9, 2H), 5.90-5.70 (m, 12H), 5.70-5.45 (m, 10H), 5.41 (d, *J* = 9.1, 1H), 5.17 (d, *J* = 9.1, 1H), 4.45-4.10 (m, 14H), 4.27 (s, unbound **3**), 4.02 (s, 4H), 1.20 (s, 3H). ^{13}C NMR (125 MHz, D_2O, dioxane as internal reference, >1 equiv. **3**): 156.9, 156.6, 156.6, 156.5, 156.5, 133.8, 133.7, 130.7, 130.1, 130.0, 129.6, 129.0, 128.0, 85.0, 80.2, 71.8, 71.7, 71.6, 71.5, 71.3, 71.2, 71.1, 71.1, 71.0, 53.5, 53.3, 52.8, 52.6, 52.3, 50.7, 49.5, 42.8, 42.3, 18.2 (only 34 of the 39 resonances expected were observed). HR-MS: *m/z* 695.2515 ([M•**3**+2H]$^{2+}$, calcd. for $C_{49}H_{48}N_{28}O_{14}$•$C_8H_{14}N_2^{2+}$, 695.2531).

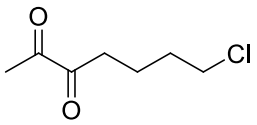

7-Chloroheptane-2,3-dione. To a solution of N,N'-diisopropyl 1,2-butanediimine[1] (10 g, 64.4 mmol) in 150 mL of THF maintained at 0 ˚C was added LDA (38.8 mL, 77.6 mmol) slowly for 1 h. The solution was stirred at 0

˚C for another 6 h, followed by addition of a solution of 1-chloro-3-iodopropane (15.6 g, 76.4 mmol) in THF (20 mL). The reaction was stirred at 0 ˚C for 10 h upon which time 1 N HCl (320 mL) was added into the reaction mixture, and stirred for an additional 5 h at RT. The THF was removed by rotary evaporation, and the remaining aqueous layer was extracted with dichloromethane (300 mL × 3). The combined organic extracts were washed with 1 N HCl (200 mL), water (200 mL), and sat. $NaHCO_3$ (200 mL) sequentially, and then dried over Na_2SO_4. The organic extracts were evaporated to afford almost pure compound **II-16**,[2] which was distilled (56-58 ˚C/0.05 mm Hg) to give the pure product (7.30 g, 44.9 mmol, 69 %) as yellow oil. IR (KBr, cm^{-1}): 2952w, 1715s, 1353w. ^1H NMR (400 MHz, $CDCl_3$): 3.54 (t, J = 6.2, 2H), 2.78 (t, J = 6.9, 2H), 2.33 (s, 3H), 1.85-1.70 (m, 4H). ^{13}C NMR (100 MHz, $CDCl_3$): 198.6, 197.3, 44.4, 34.8, 31.7, 23.6, 20.3.

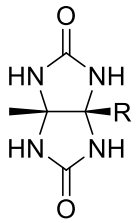

R = $CH_2CH_2CH_2CH_2Cl$

***Compound* II-*17*.** To compound **II-16** (9.4 g, 57.8 mmol) was added a solution of urea (10.4 g, 173.4 mmol) in HCl (50 mL, 0.3 M), and was capped. The reaction was then stirred at RT for 1 day. The precipitates were filtered, washed with H_2O (30 mL × 2) and acetone (30 mL × 2) sequentially, dried under high vacuum to yield **II-17** as a white solid (5.0 g, 20.3 mmol, 35 %). M.p. > 194 ˚C (dec.). IR (KBr, cm^{-1}): 2952w, 1723s, 1677s, 1502m, 1174m, 1139w, 1046w. ^1H NMR (500 MHz, DMSO-d_6): 7.19 (s, 2H), 7.09 (s, 2H), 3.62 (t, J = 6.5, 2H), 1.75-1.65 (m, 2H), 1.65-1.60 (m, 2H), 1.55-1.45 (m, 2H), 1.34 (s, 3H), ppm. ^{13}C NMR (125 MHz, DMSO-d_6): 159.6, 77.2, 75.5, 45.1, 34.5, 32.3, 21.5, 20.3 ppm. ESI-MS: *m/z* 247.1 ($[M+H]^+$).

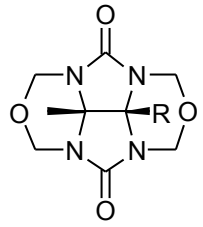

R = $CH_2CH_2CH_2CH_2Cl$

Compound II-18. To a flask was added a mixture of **II-17** (5.00 g, 20.3 mmol), formaldehyde (37% in H_2O, 7.9 mL), H_2O (4.5 mL), and conc. HCl (15 mL), and was capped. The reaction was then stirred at RT for 23 h upon which time additional H_2O (60 mL) was added into the reaction mixture, and stirred for an additional 5 h. The precipitates were filtered, washed with H_2O (200 mL) and EtOH (50 mL) sequentially, dried under high vacuum to yield compound **II-18** as a white solid (4.6 g, 13.9 mmol, 68 %). M.p. > 165 ˚C (dec.). IR (KBr, cm^{-1}): 3434m, 3013w, 2952w, 2882w, 1721s, 1475s, 1421s, 1388m, 1305m, 1245m, 1180m, 1146w, 1108w, 1063w, 1019m, 985w, 947w, 875w. ^1H NMR (500 MHz, $CDCl_3$): 5.53 (d, *J* = 11.1, 2H), 5.51 (d, *J* = 11.1, 2H), 4.82 (d, *J* = 11.1, 2H), 4.76 (d, *J* = 11.1, 2H), 3.61 (t, *J* = 6.2, 2H), 2.30-2.20 (m, 2H), 1.95-1.85 (m, 2H), 1.86 (s, 3H), 1.60-1.50 (m, 2H) ppm. ^{13}C NMR (125 MHz, $CDCl_3$): 157.6, 75.3, 73.5, 71.1, 70.8, 44.2, 31.9, 28.9, 21.4, 17.2 ppm. ESI-MS: *m/z* 331.1 ($[M+H]^+$).

Unsuccessful Reaction Between Hexamer II-1 and II-2$_{Ph}$. A mixture of **II-1** (9.7 mg, 0.01 mmol) and KI (0.22 mg, 1.35 mmol) were dissolved in 9 M aqueous H_2SO_4 (0.2 mL) and then treated with **II-2**$_{Ph}$ (4.6 mg, 0.012 mmol). The flask was then sealed with a rubber septum and heated at 110 ˚C for 30 min. The reaction solution was then poured into MeOH (3 mL) which resulted in a gray precipitate. The mixture was centrifuged at 7200 rpm for 5 min. The supernatant was decanted and the precipitate was washed with MeOH (3 mL × 3) and centrifuged at 7200 rpm for 5 min. The precipitate was dried under high vacuum to give crude, gray powder (10.9 mg). The precipitate was assessed

by ^{1}H NMR using **II-3** as a probe which showed that presence of CB[6] (94%) and unidentified products (6%).

Unsuccessful Reaction Between Hexamer II-1 and II-2$_{CO2Et}$. A mixture of **II-1** (9.7 mg, 0.01 mmol) and KI (0.22 mg, 1.35 mmol) were dissolved in 9 M aqueous H_2SO_4 (0.2 mL) and then treated with **II-2**$_{CO2Et}$ (4.5 mg, 0.012 mmol). The flask was then sealed with a rubber septum and heated at 110 ˚C for 30 min. The reaction solution was then poured into MeOH (3 mL) which resulted in a gray precipitate. The mixture was centrifuged at 7200 rpm for 5 min. The supernatant was decanted and the precipitate was washed with MeOH (3 mL × 3) and centrifuged at 7200 rpm for 5 min. The precipitate was dried under high vacuum to give crude, gray powder (11.1 mg). The precipitate was assessed by ^{1}H NMR using **3** as a probe which showed the presence of CB[6] (96%) and unidentified products (4%).

Details of the Mass Spectrometric Investigations of II-20$_4$. Aqueous CB7 solution was diluted to 100μM and infused directly into an LTQ-Orbitrap XL (ThermoFisher, San Jose, CA). Precursor and product ion spectra following collisional induced dissociation at varying normalized collision energies (NCE) were acquired at maximum resolution. Theoretical spectra and neutral masses were produced using the incorporated Xcalibur 2.0 software suite.

References:

1. Kimpe, N. D.; D'Hondt, L.; Stanoeva, E. *Tetrahedron Lett.* **1991**, *32*, 3879-3882.

2. Kimpe, N. D.; Stevens, C. *Tetrahedron* **1995**, *51*, 2387-2402.

3. Özçubukçu, S.; Ozkal, E.; Jimeno, C.; Pericàs, M. *Org. Lett.* **2009** *11*, 6480-6483.

4. Butler, A. R.; Leitch, E. *J. Chem. Soc., Perkin Trans. 2* **1980**, *1*, 103-105.

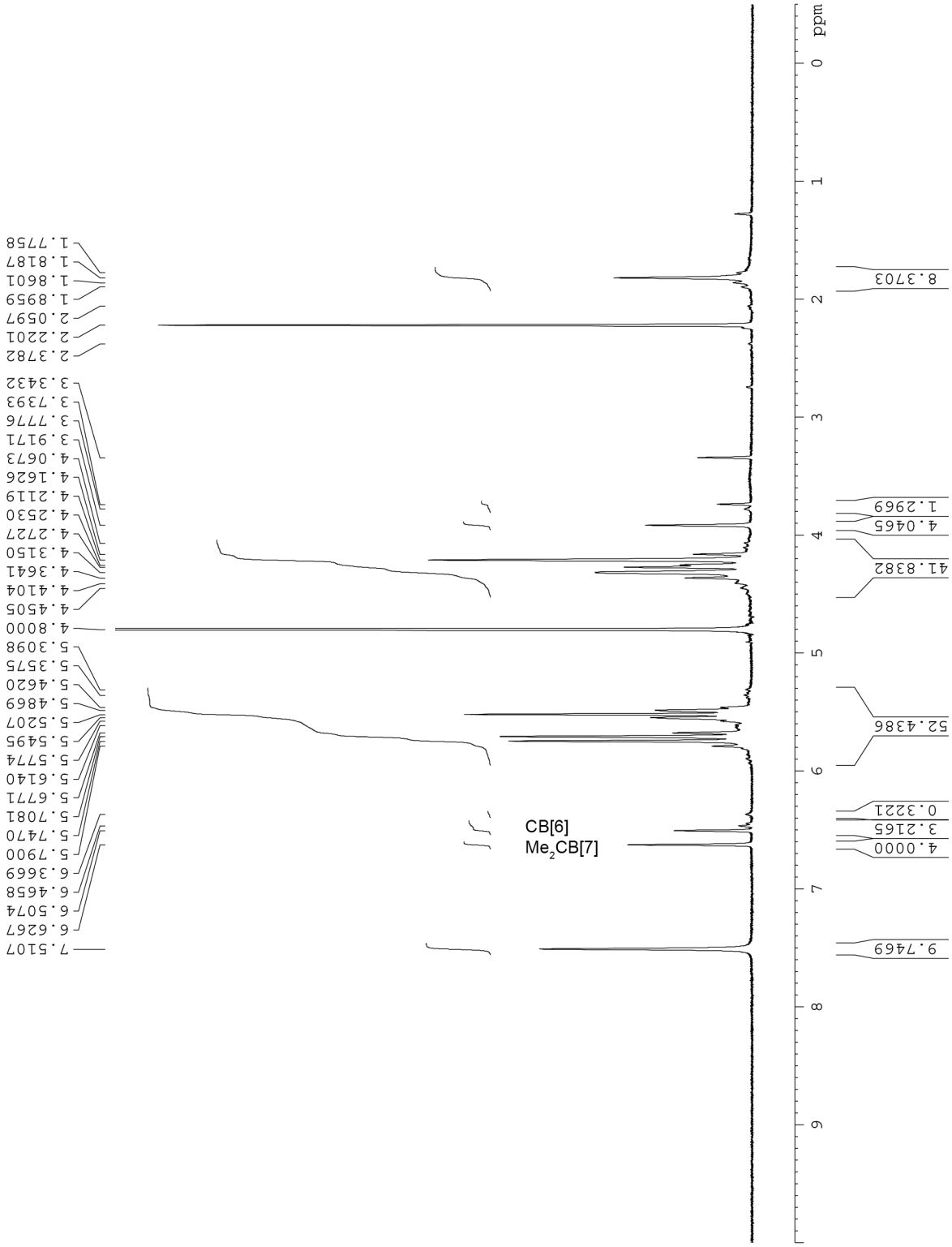

Figure II-S1. ^{1}H NMR spectrum recorded (400 MHz, D_2O, RT) for the crude reaction mixture from the reaction between **II-1** and **II-2**$_{Me}$ in the presence of **II-3** as a probe. ^{1}H NMR integration of the **II-3** binding region (6-7 ppm) allows us to determine the contents of the crude mixture (53% Me_2CB[7], 43% CB[6], and 4% unidentified).

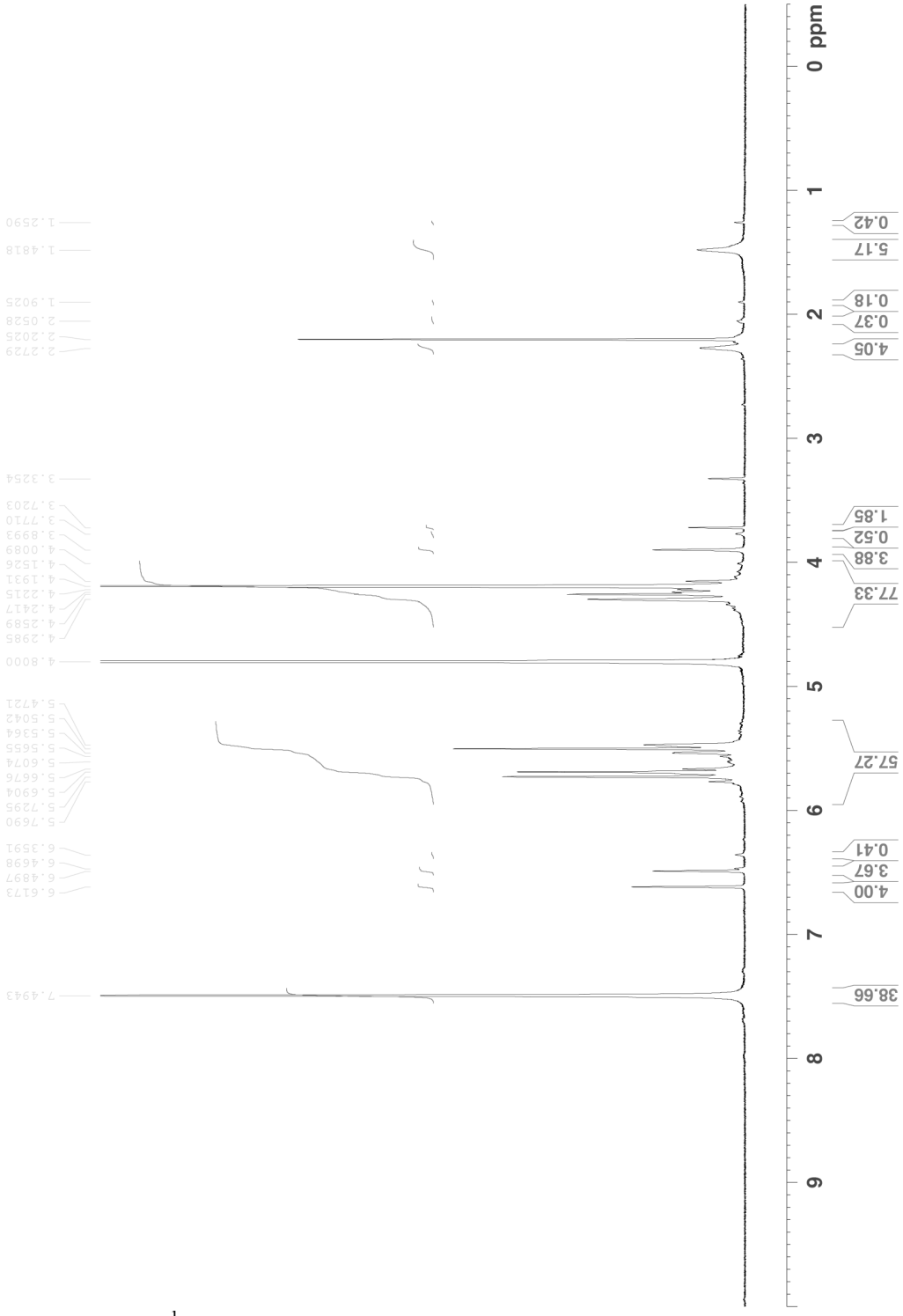

Figure II-S2. ^{1}H NMR spectrum recorded (400 MHz, D_2O, RT) for the crude reaction mixture from the reaction between **II-1** and **II-2**$_{Cy}$ in the presence of **II-3** as a probe. ^{1}H NMR integration of the **II-3** binding region (6-7 ppm) allows us to determine the contents of the crude mixture (50% CyCB[7], 45% CB[6], and 5% unidentified).

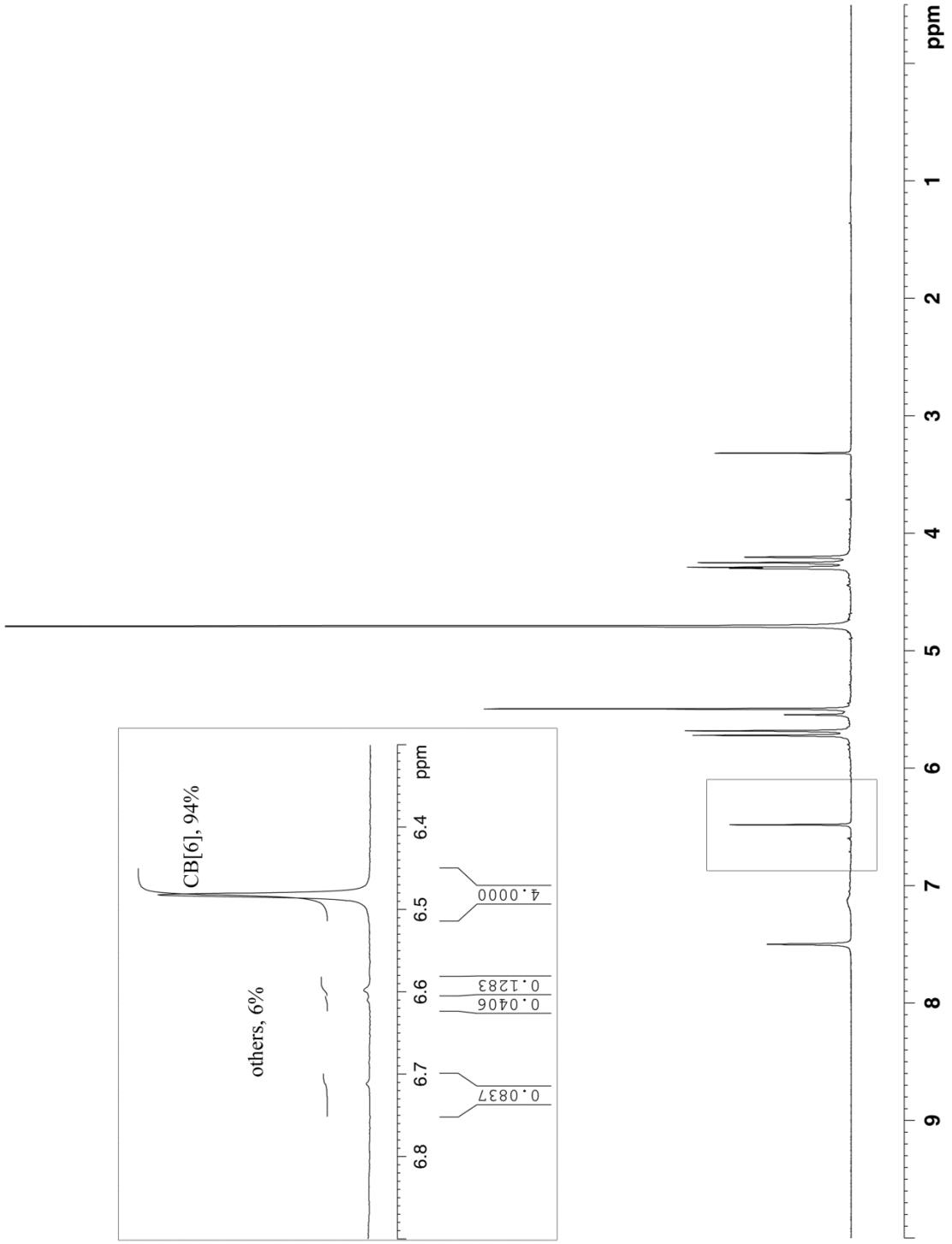

Figure II-S3. ^{1}H NMR spectrum recorded (400 MHz, D_2O, RT) for the crude reaction mixture from the attempted cyclization of **II-1** and **II-2**$_{Ph}$ in the presence of an excess of **II-3** as a probe.

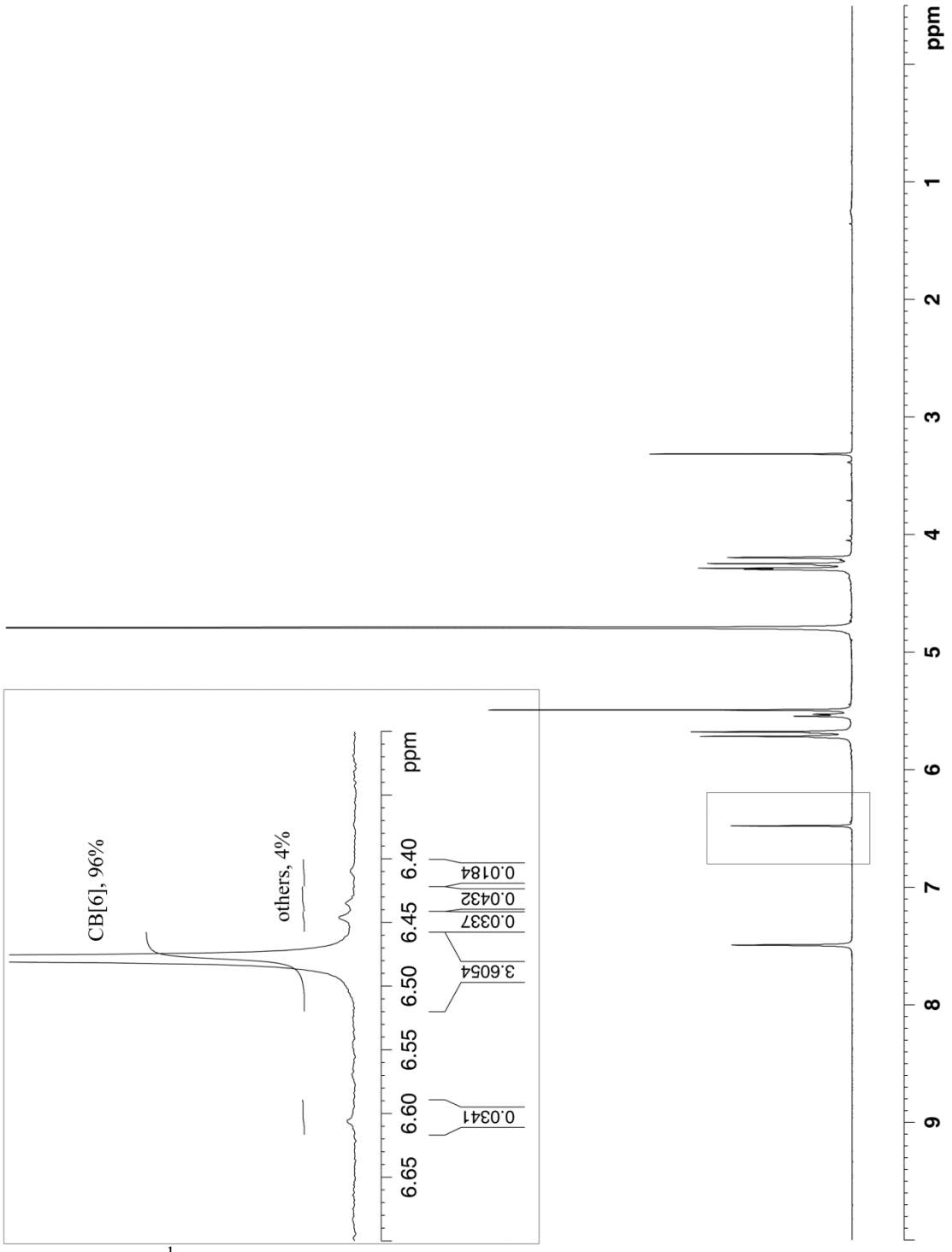

Figure II-S4. ^{1}H NMR spectrum recorded (400 MHz, D_2O, RT) for the crude reaction mixture from the attempted cyclization of **II-1** and **II- 2**$_{CO2Et}$ in the presence of an excess of **II-3** as a probe.

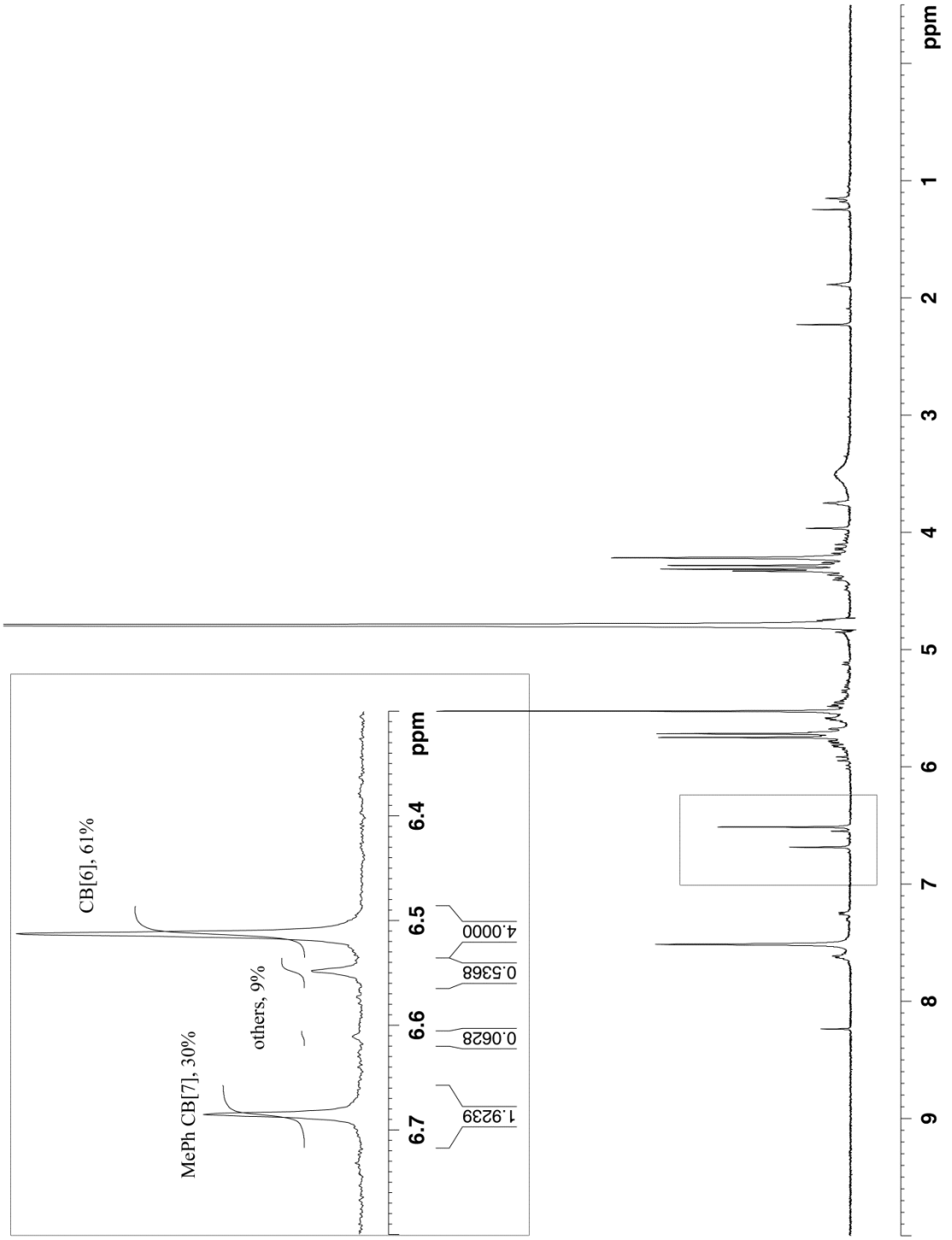

Figure II-S5. ^{1}H NMR spectrum recorded (400 MHz, D_2O, RT) for the crude reaction mixture from the reaction between **II-1** and **II-2**$_{MePh}$ in the presence of **II-3** as a probe. ^{1}H NMR integration of the **II-3** binding region (6-7 ppm) allows us to determine the contents of the crude mixture (30% MePhCB[7], 61% CB[6], and 9% unidentified).

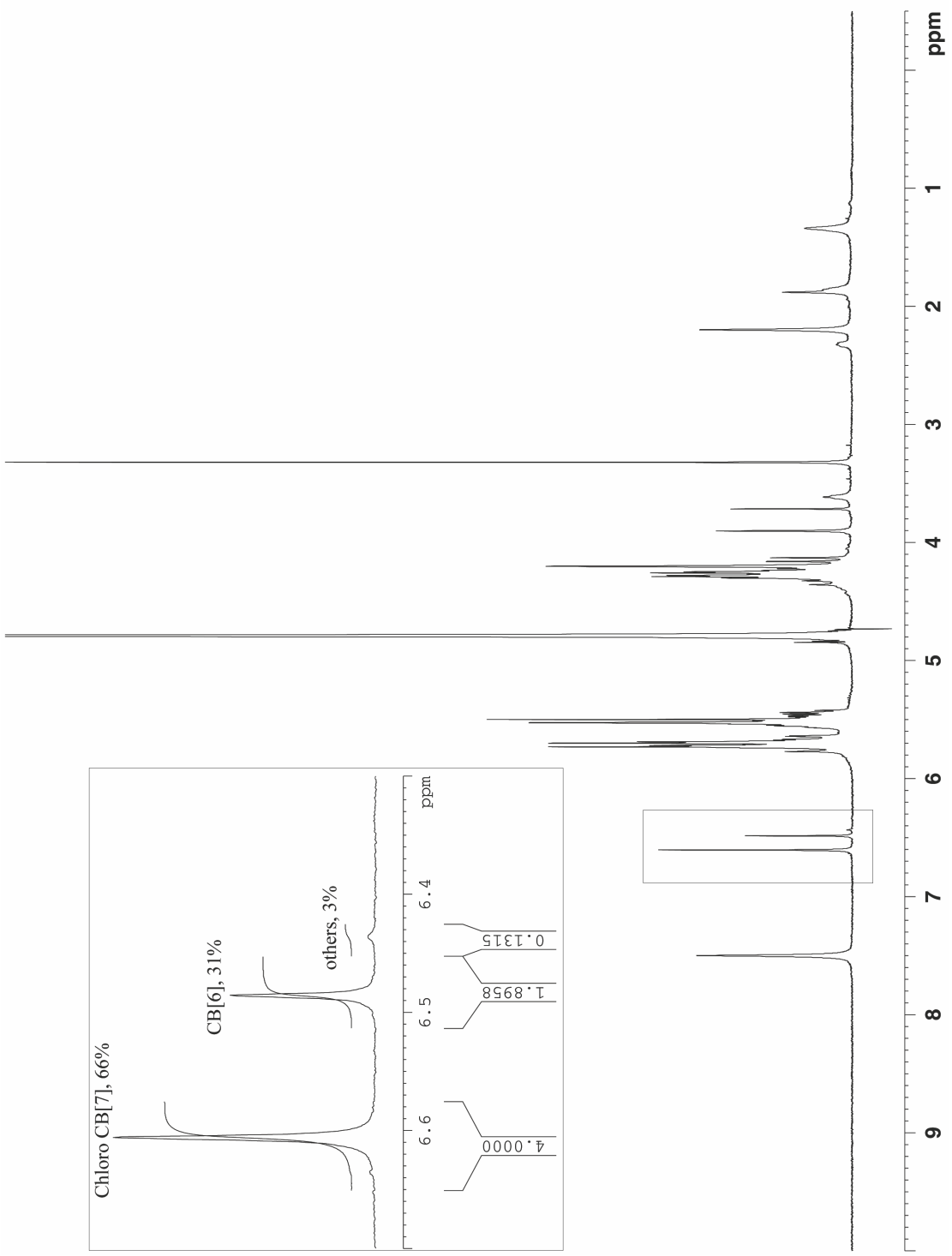

Figure II-S6. ^{1}H NMR spectrum recorded (400 MHz, D_2O, RT) for the crude reaction mixture from the reaction between **II-1** and **II-12** in the presence of **II-3** as a probe. ^{1}H NMR integration of the **II-3** binding region (6-7 ppm) allows us to determine the contents of the crude mixture (66% **II-18**, 31% CB[6], and 3% unidentified).

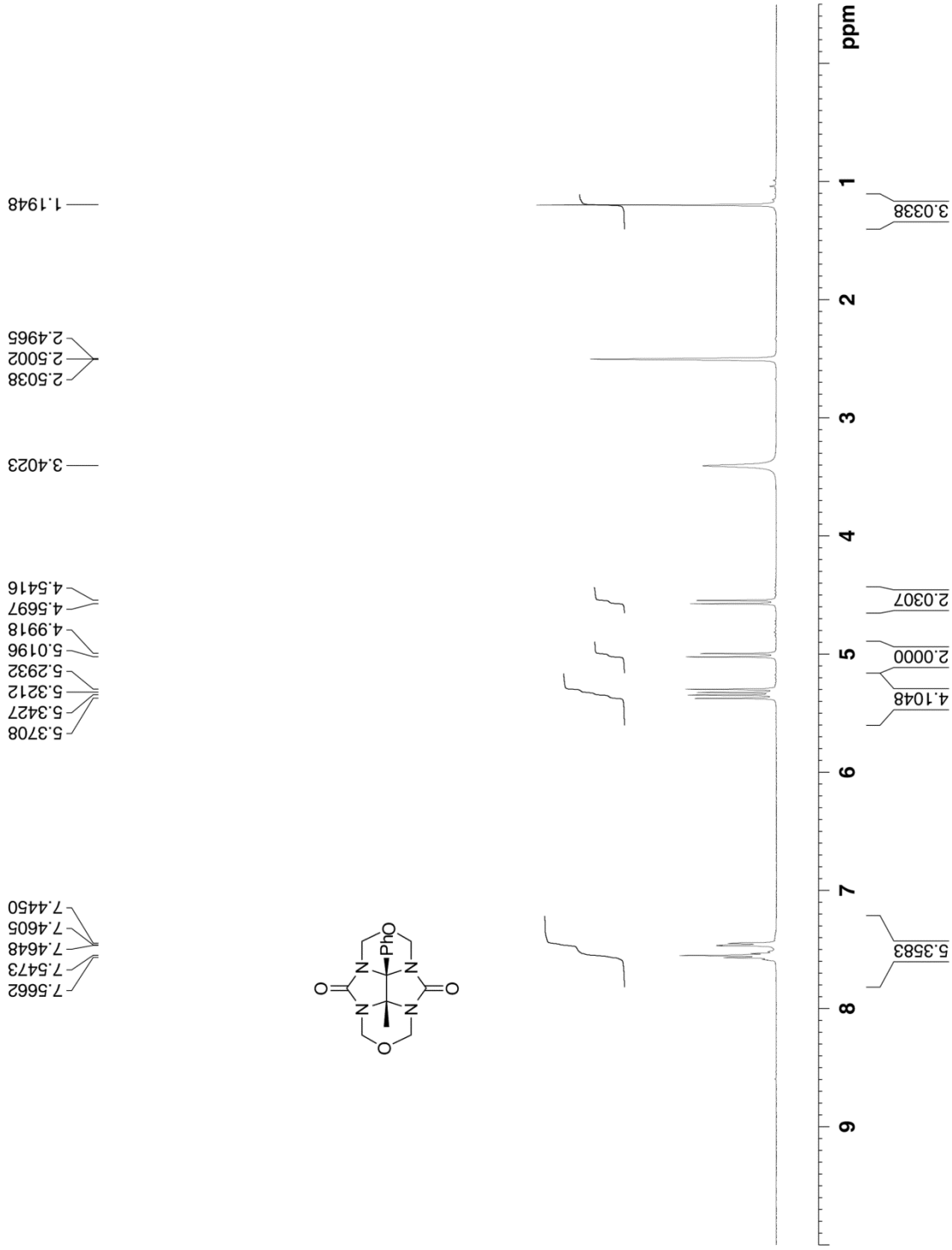

Figure II-S7. ^{1}H NMR spectra recorded (400 MHz, DMSO-d_6, RT) for compound **II-2$_{MePh\bullet}$**.

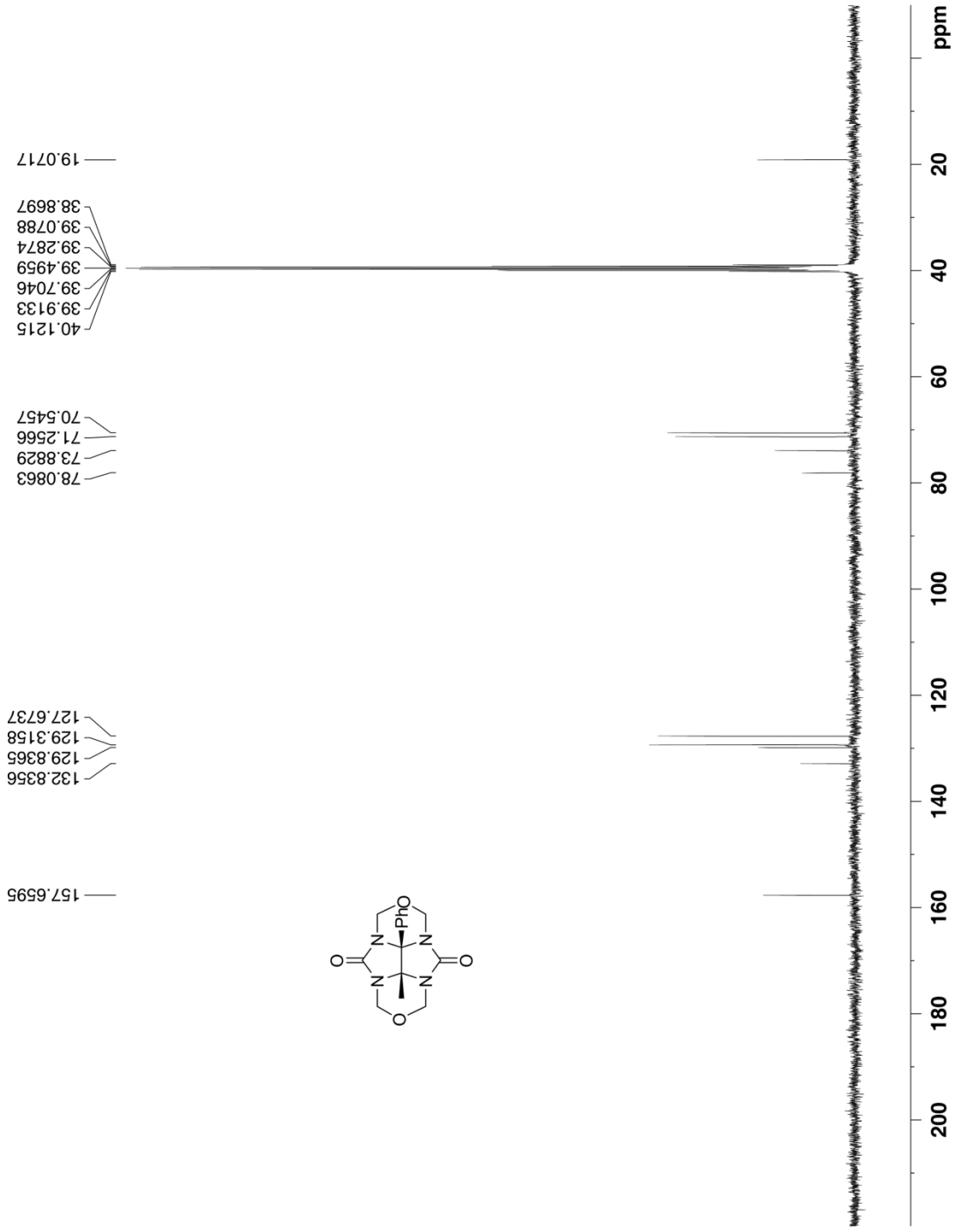

Figure II-S8. ^{13}C NMR spectra recorded (100 MHz, DMSO-d_6, RT) for compound **II-2**$_{MePh}$.

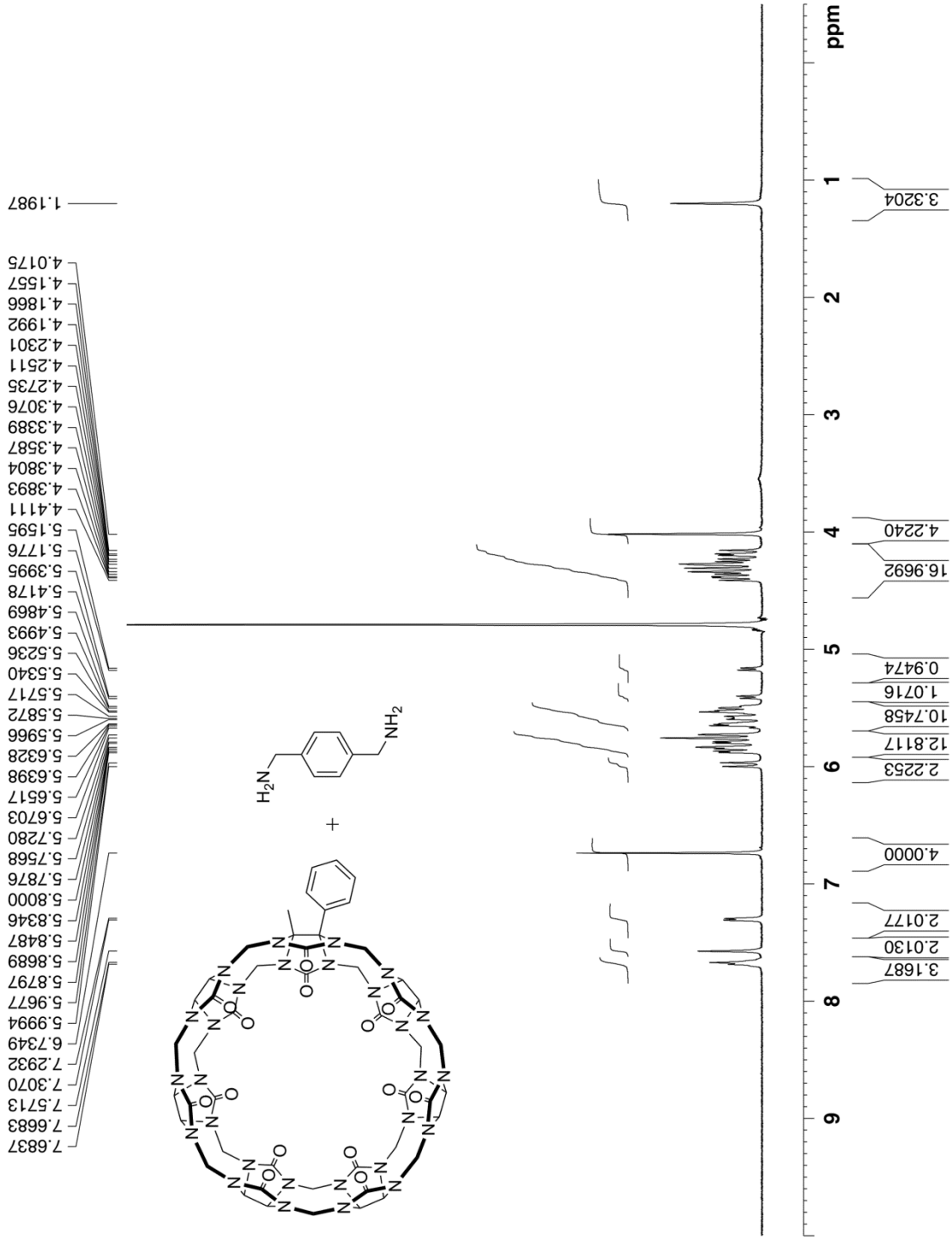

Figure II-S9. ^{1}H NMR spectra recorded (500 MHz, D_2O, RT) for MePhCB[7] and excess **II-3.**

Figure II-S10. ^{13}C NMR spectrum recorded (125 MHz, D_2O, dioxane as internal reference, RT) for a mixture of MePhCB[7] and **II-3**.

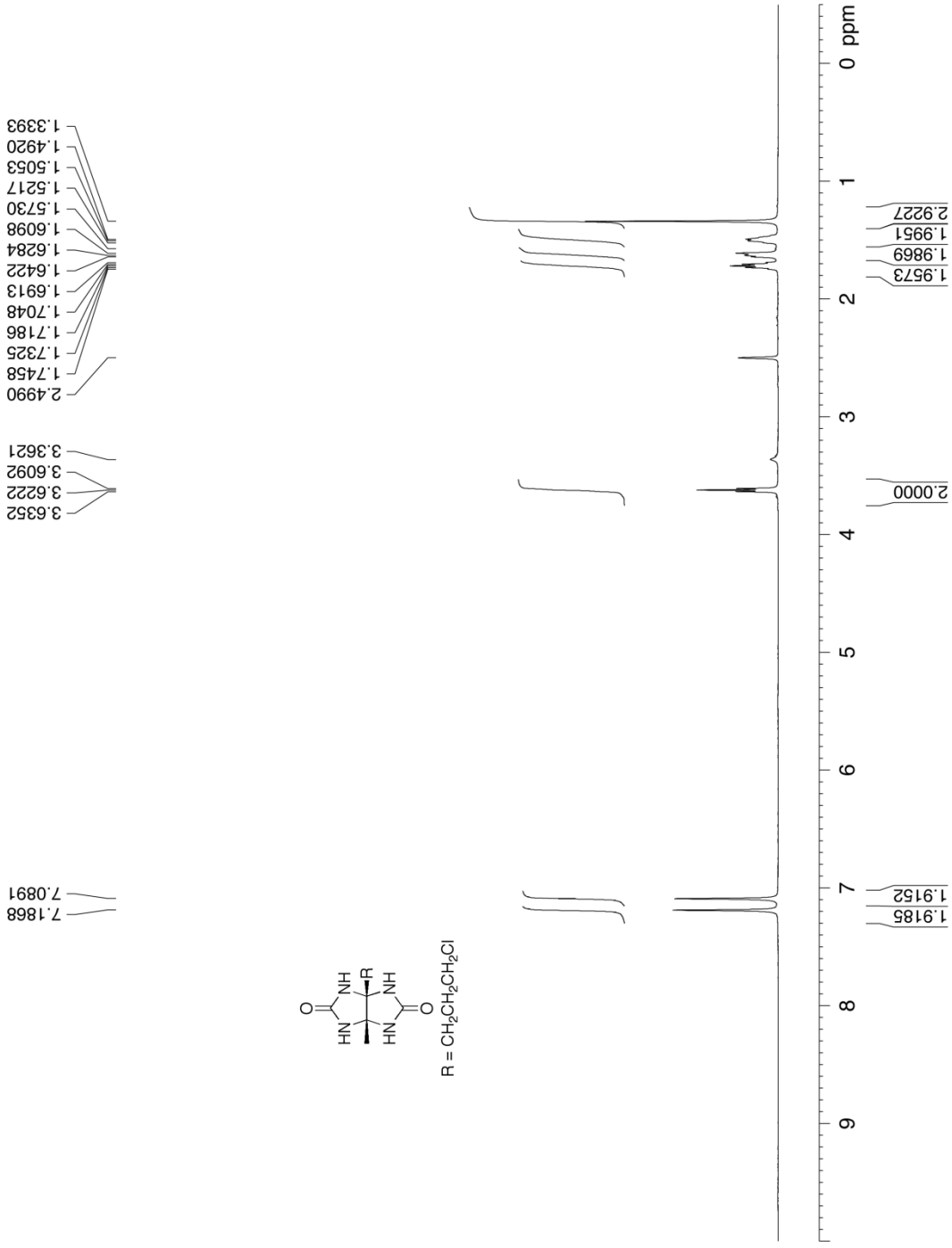

Figure II-S11. ^{1}H NMR spectra recorded (500 MHz, DMSO-d_6, RT) for compound **II-17**.

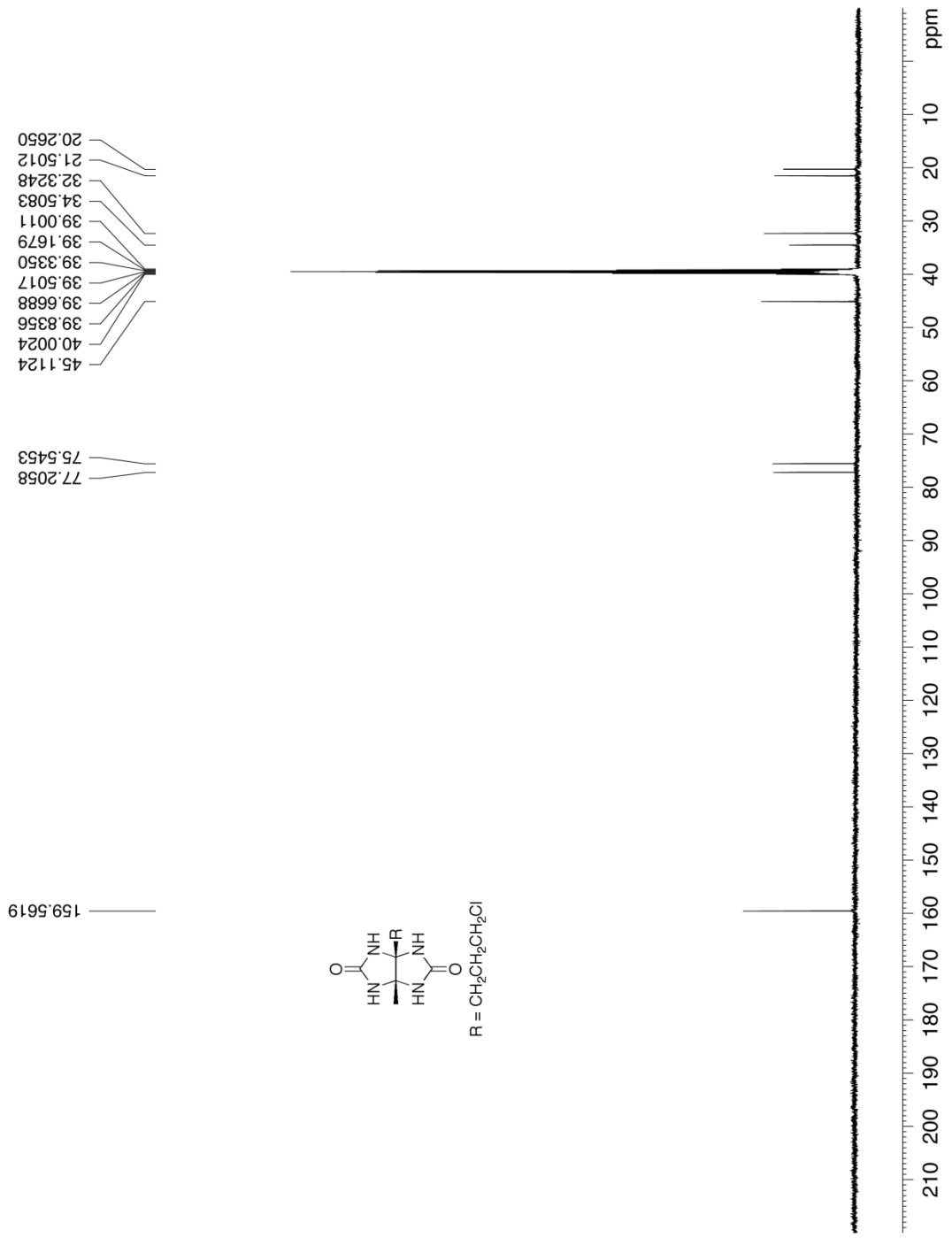

Figure II-S12. ^{13}C NMR spectra recorded (125 MHz, DMSO-d_6, RT) for compound **II-17.**

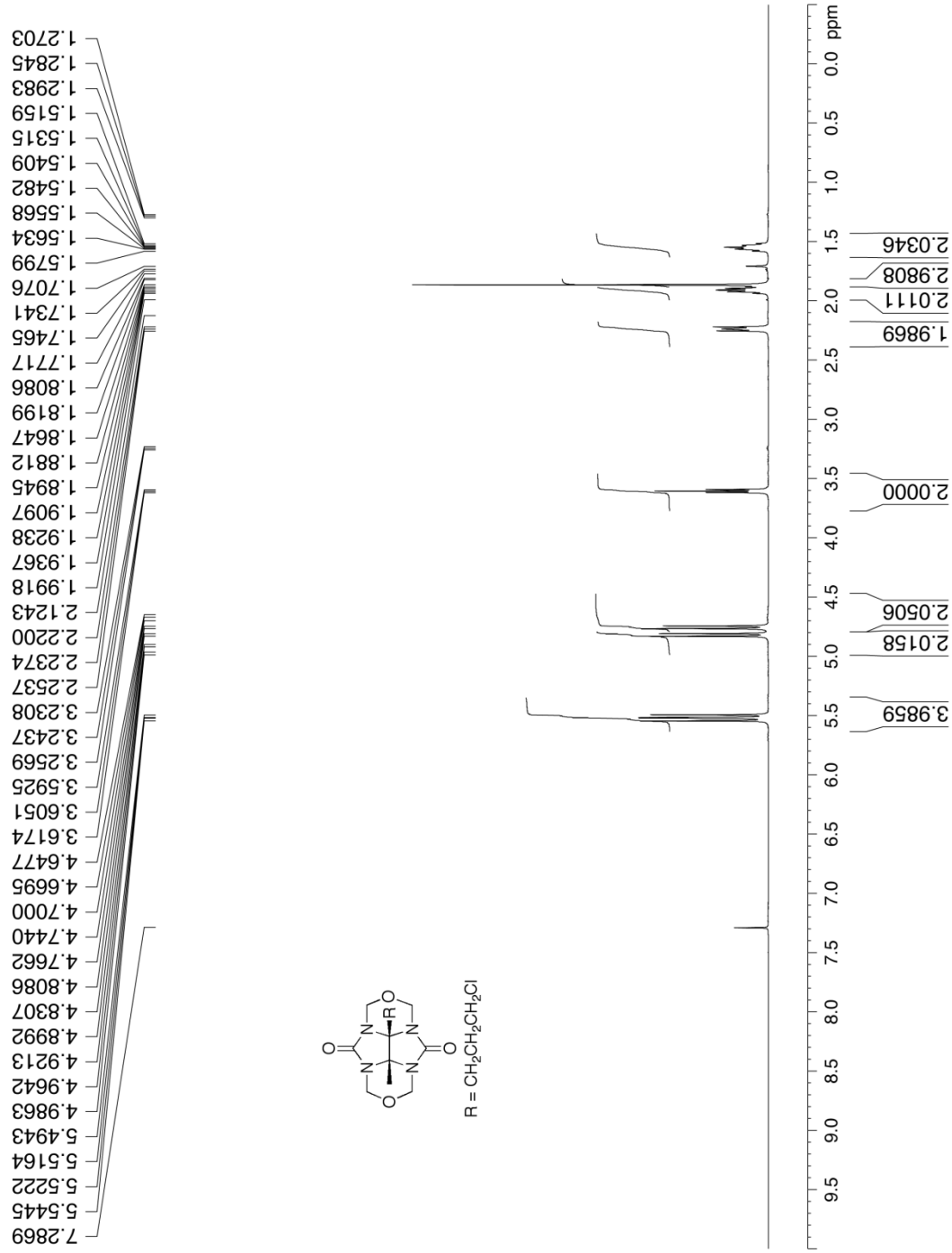

Figure II-S13. ^{1}H NMR spectra recorded (500 MHz, $CDCl_3$, RT) for compound **II-12.**

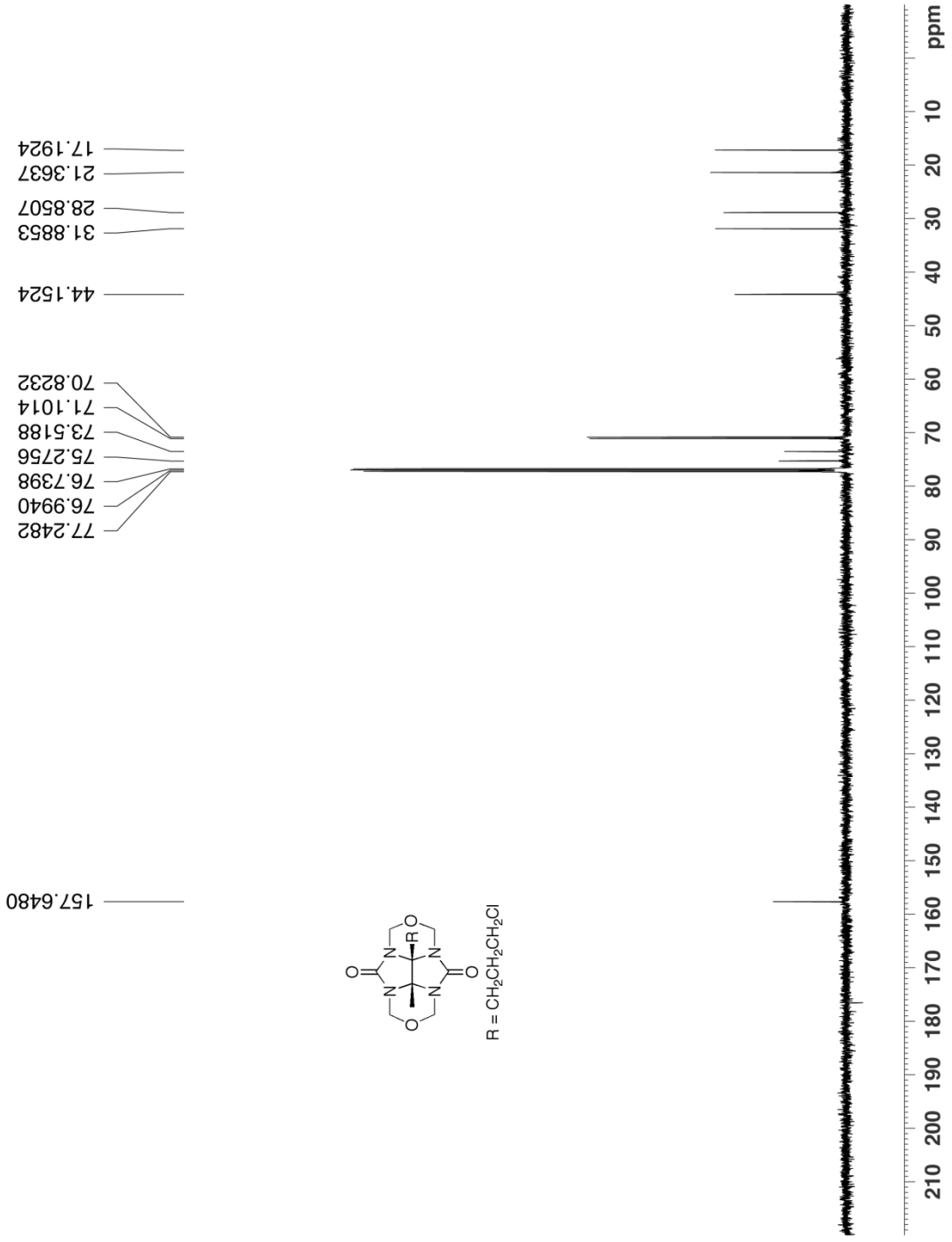

Figure II-S14. ^{13}C NMR spectra recorded (125 MHz, $CDCl_3$, RT) for compound **II-12.**

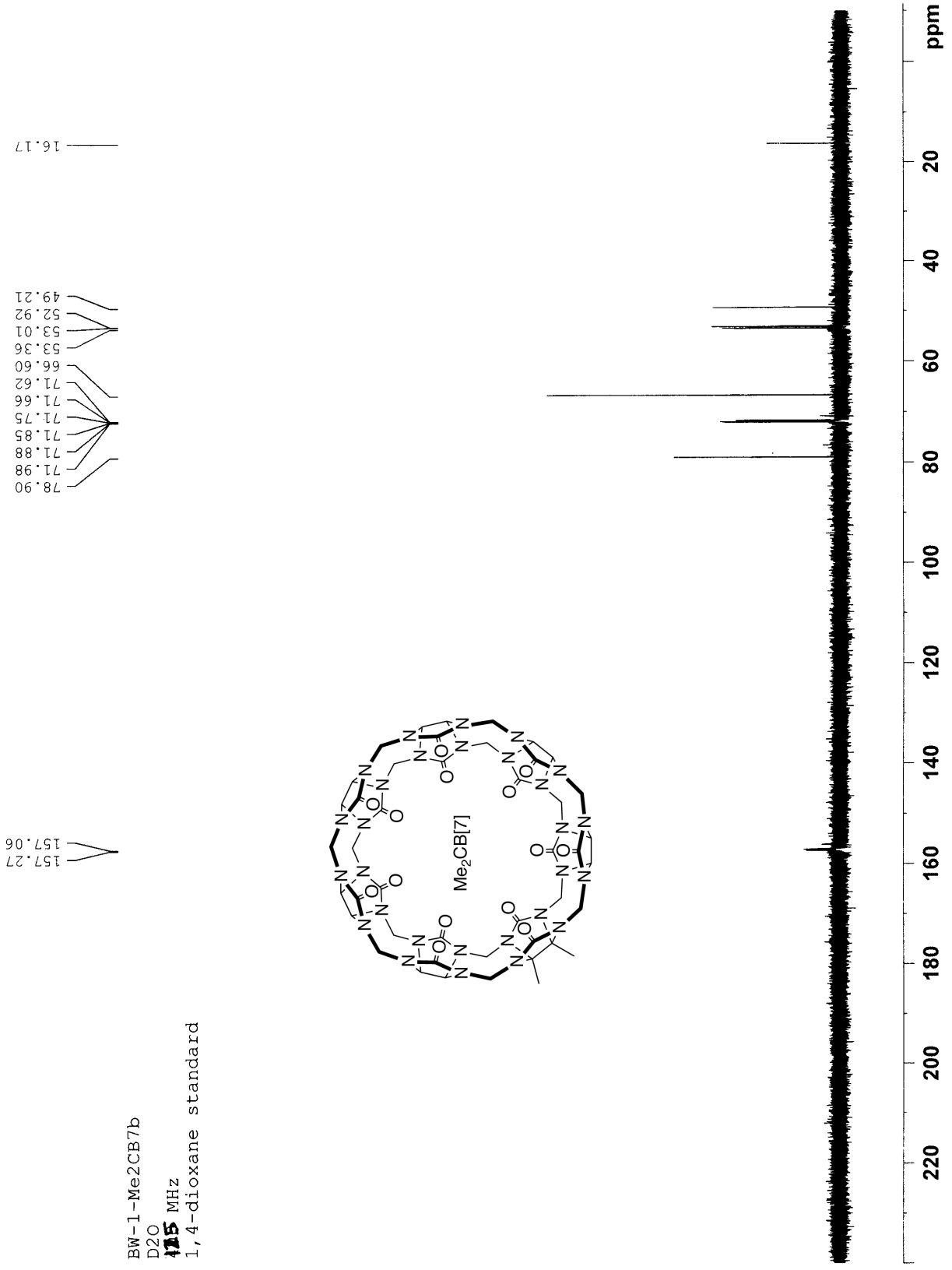

Figure II-S15. ^{13}C NMR spectra recorded (100 MHz, D_2O, RT) for $Me_2CB[7]$.

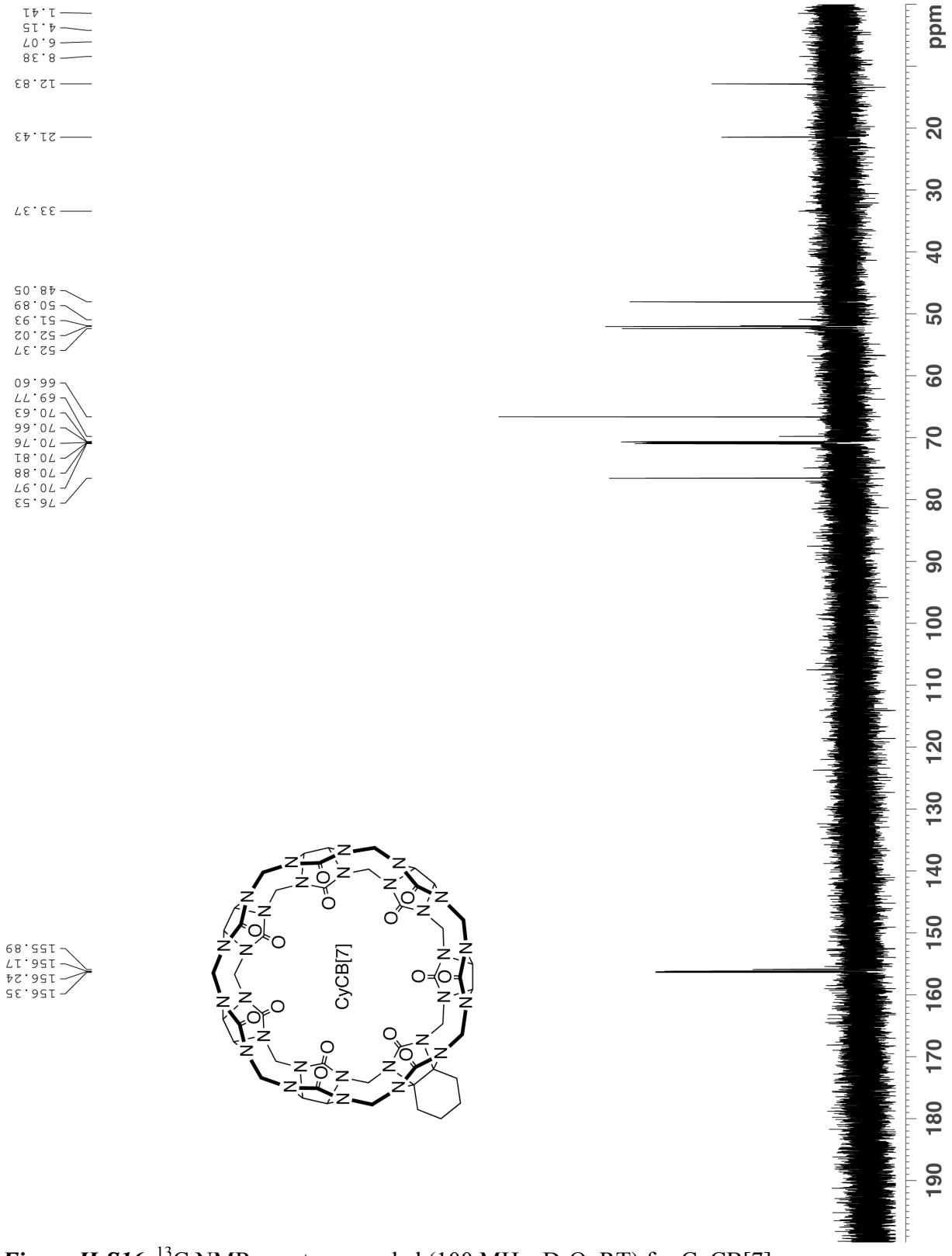

Figure II-S16. ^{13}C NMR spectra recorded (100 MHz, D_2O, RT) for CyCB[7].

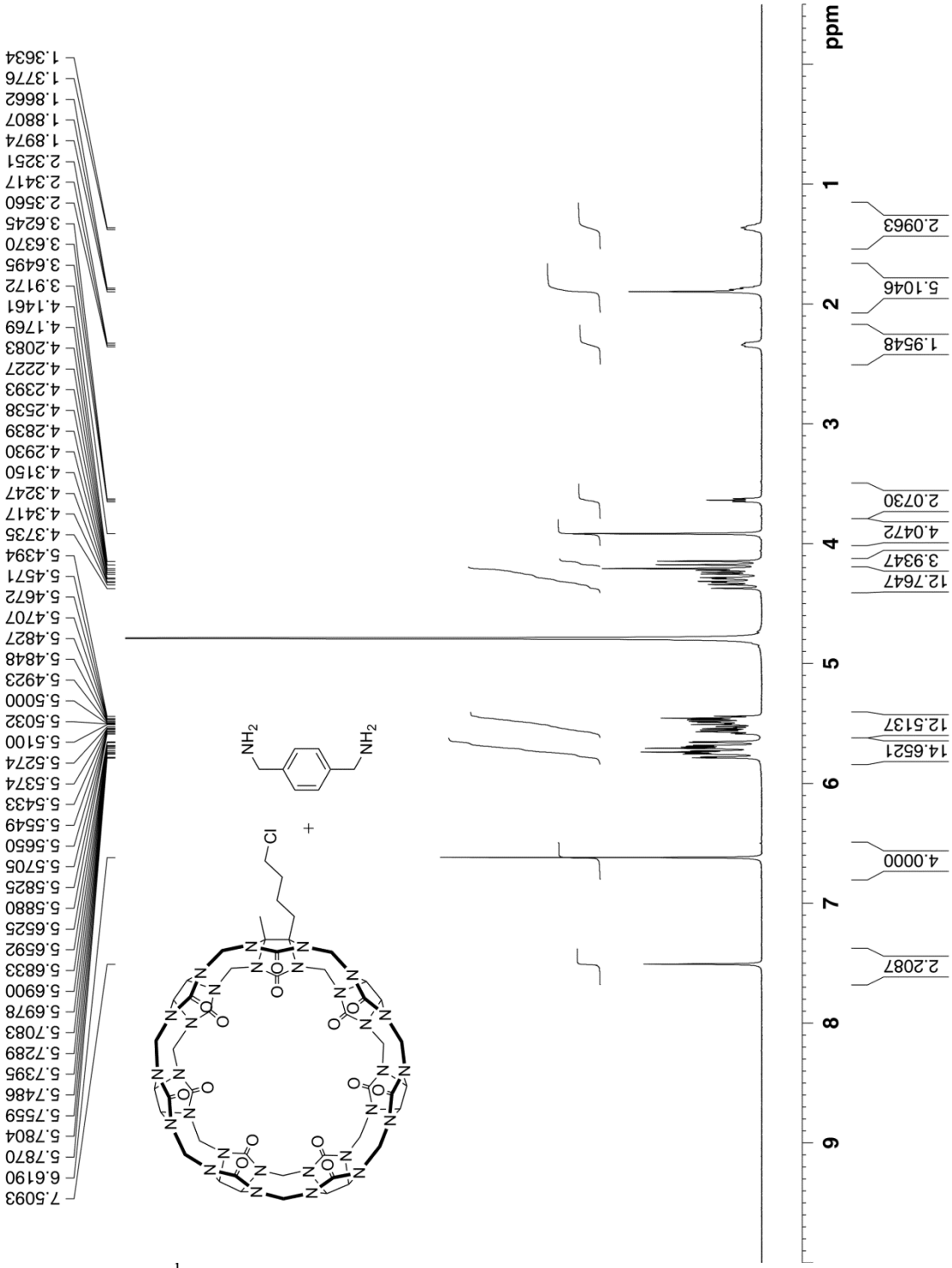

Figure II-S17. ^{1}H NMR spectra recorded (500 MHz, D_2O, RT) for **II-18** and excess **II-3.**

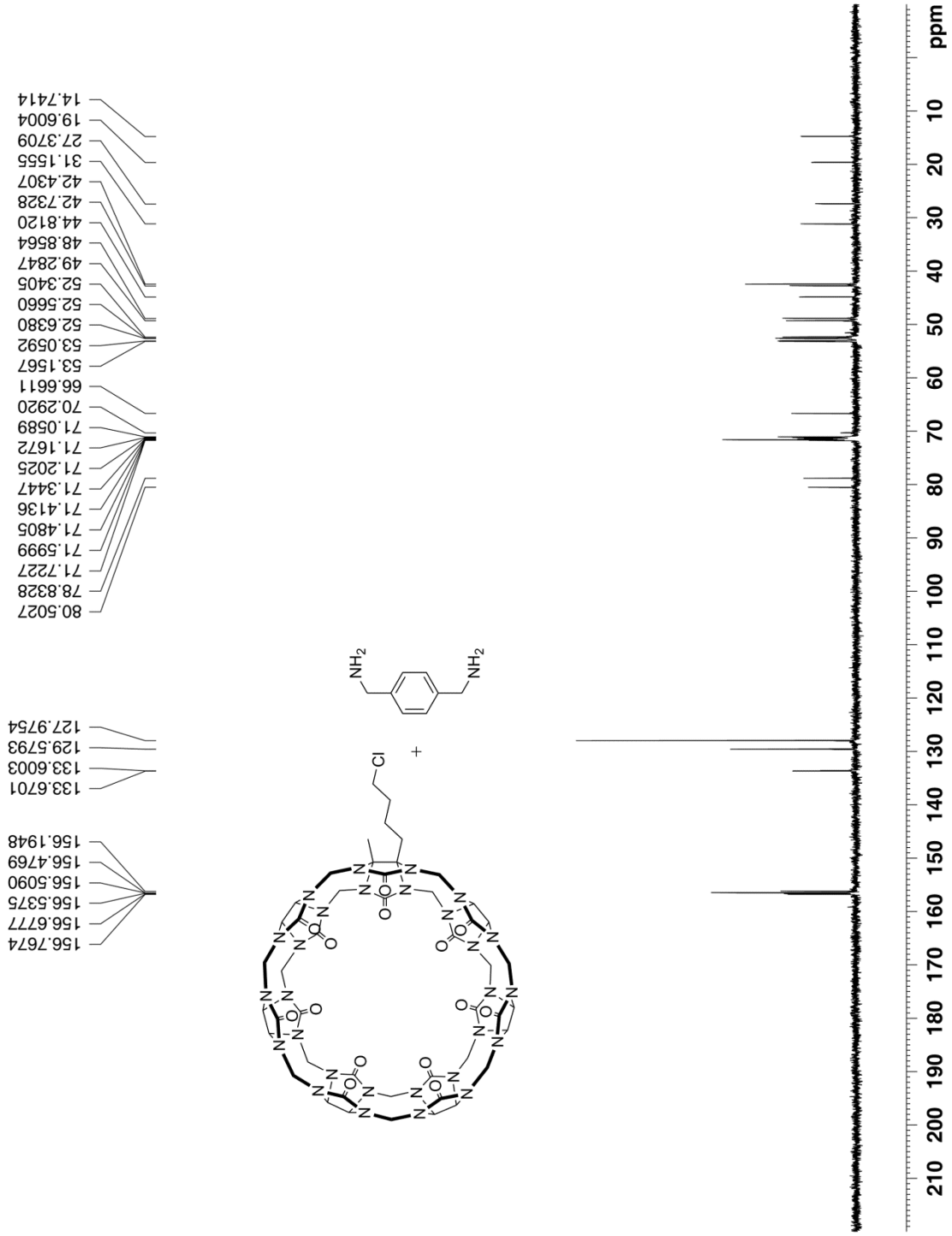

Figure II-S18. ^{13}C NMR spectra recorded (125 MHz, D_2O, RT) for **II-18•II-3.**

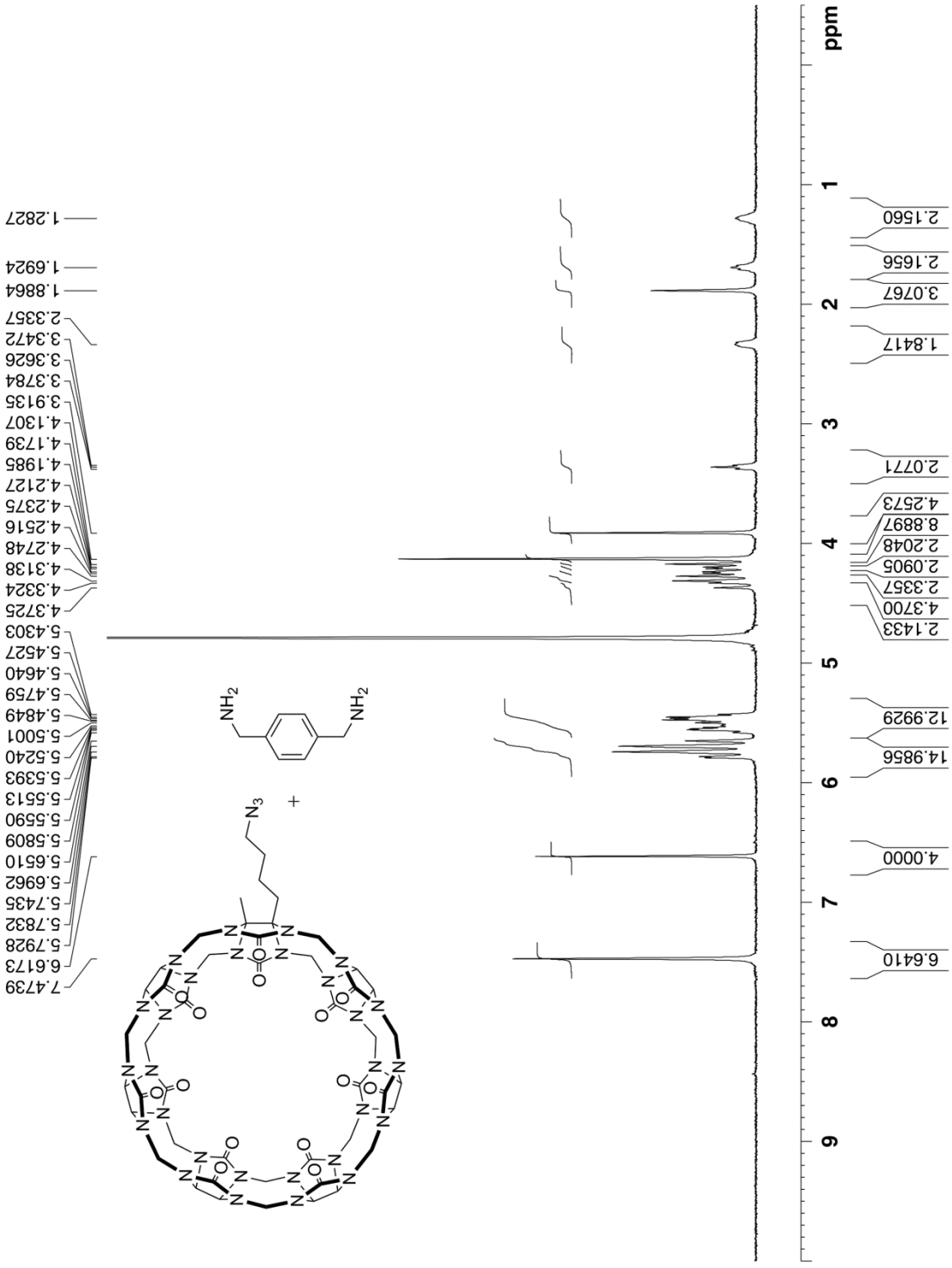

Figure II-S19. ^{1}H NMR spectrum recorded (400 MHz, D_2O, RT) for a mixture of **II-19** and excess **II-3**.

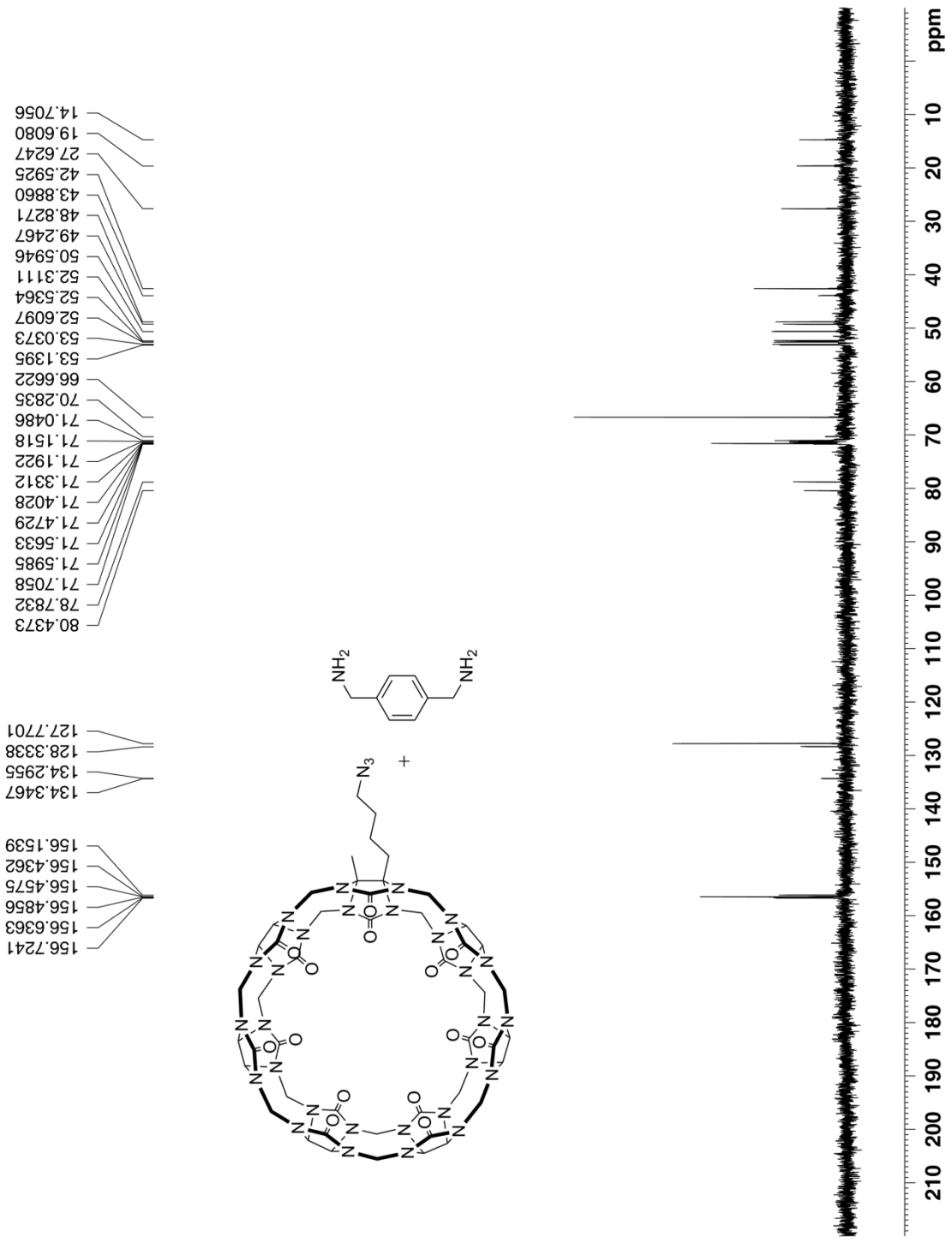

Figure II-S20. ^{13}C NMR spectrum recorded (125 MHz, D_2O, dioxane as internal reference, RT) for a mixture of **II-19** and **II-3**.

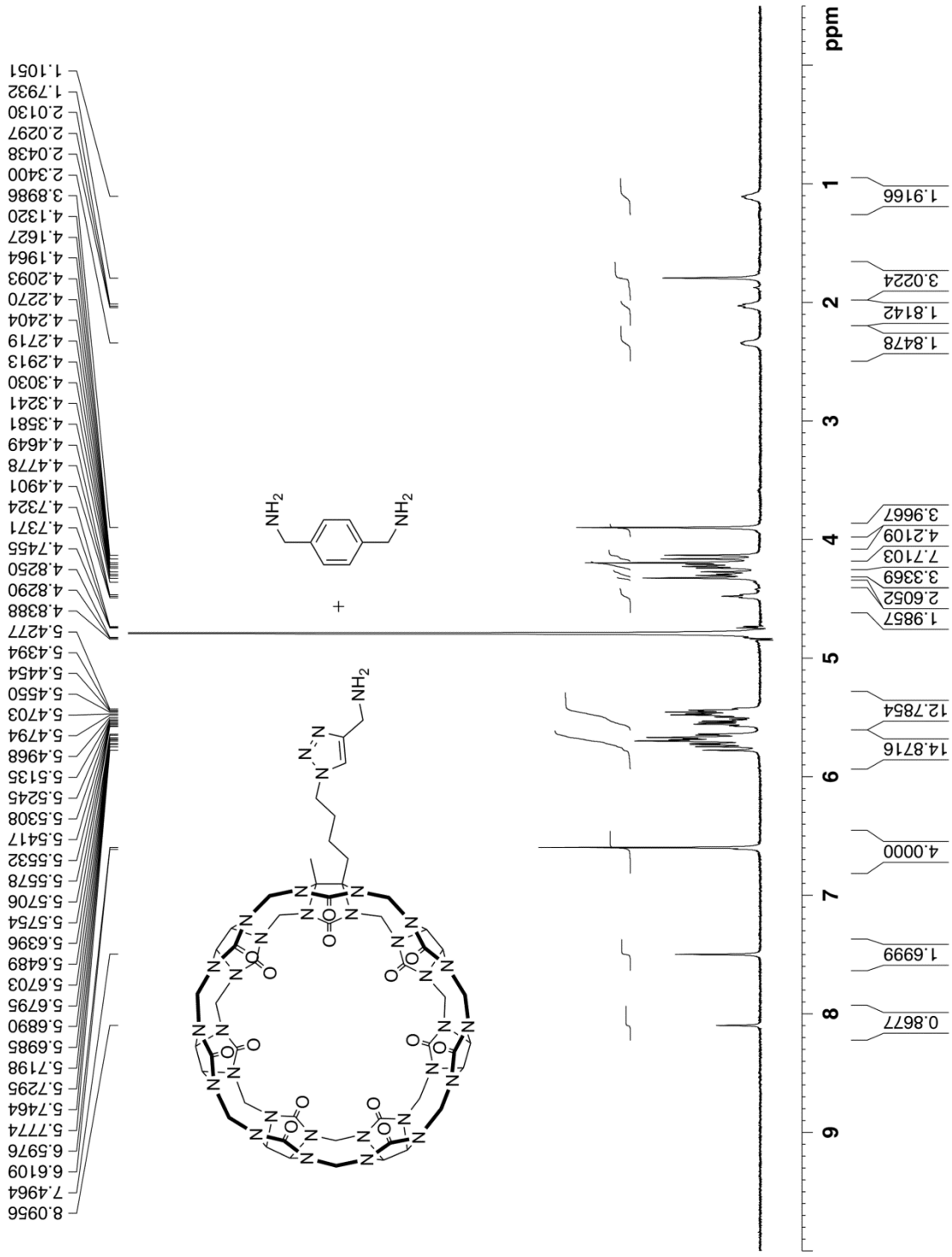

Figure II-S21. ^{1}H NMR spectrum recorded (500 MHz, D_2O, RT) for a mixture of **II-20** and excess **II-3**.

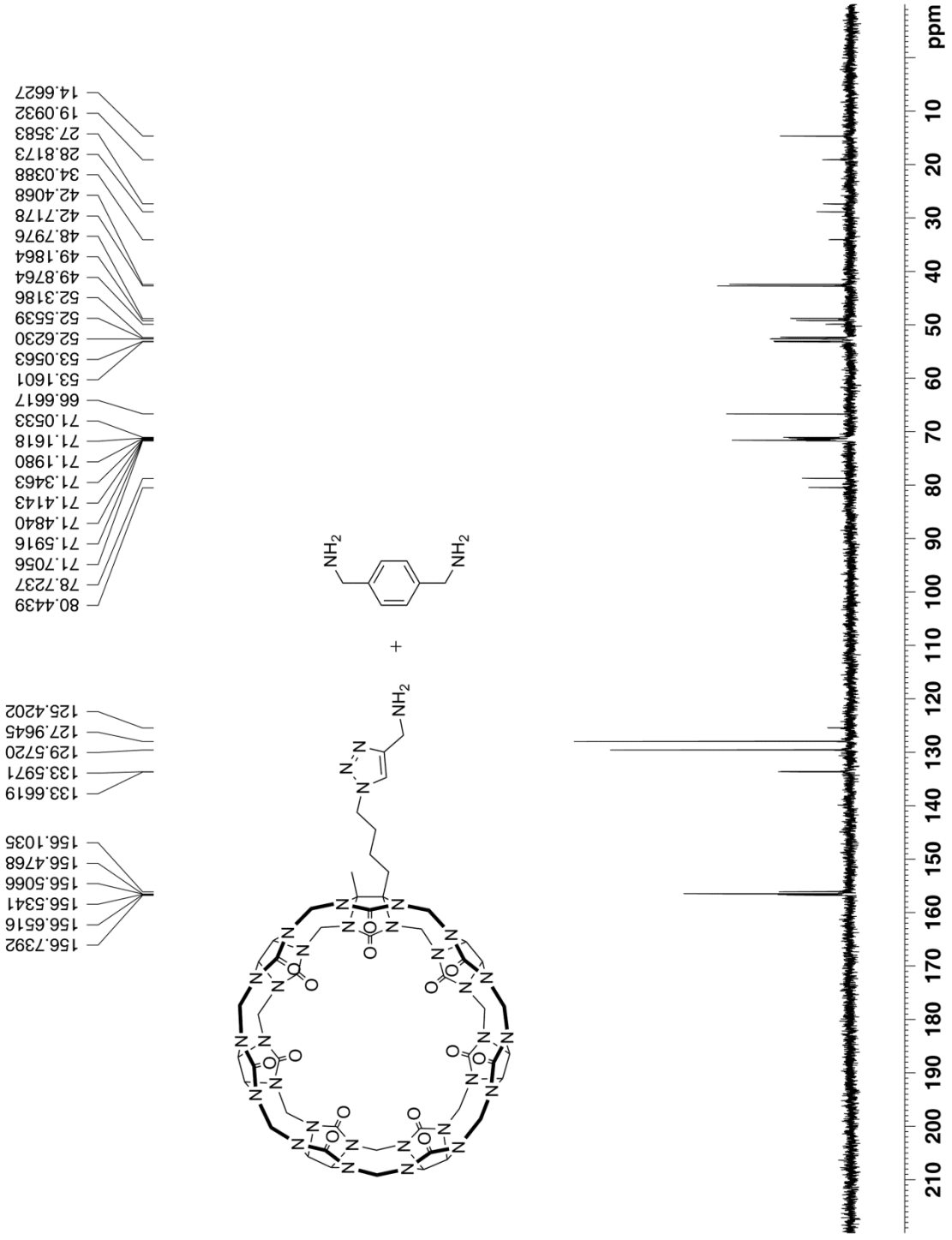

Figure II-S22. ^{13}C NMR spectrum recorded (125 MHz, D_2O, dioxane as internal reference, RT) for a mixture of **II-20** and **II-3**.

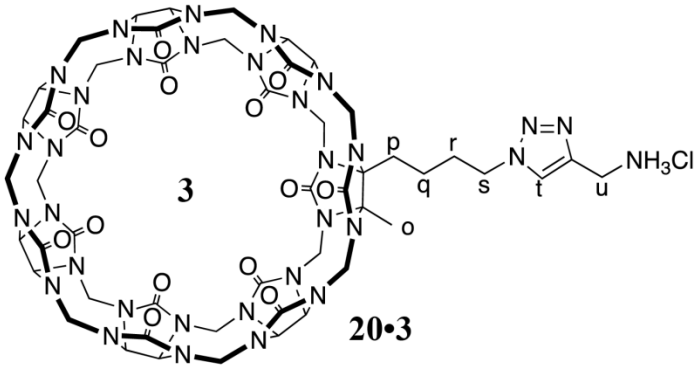

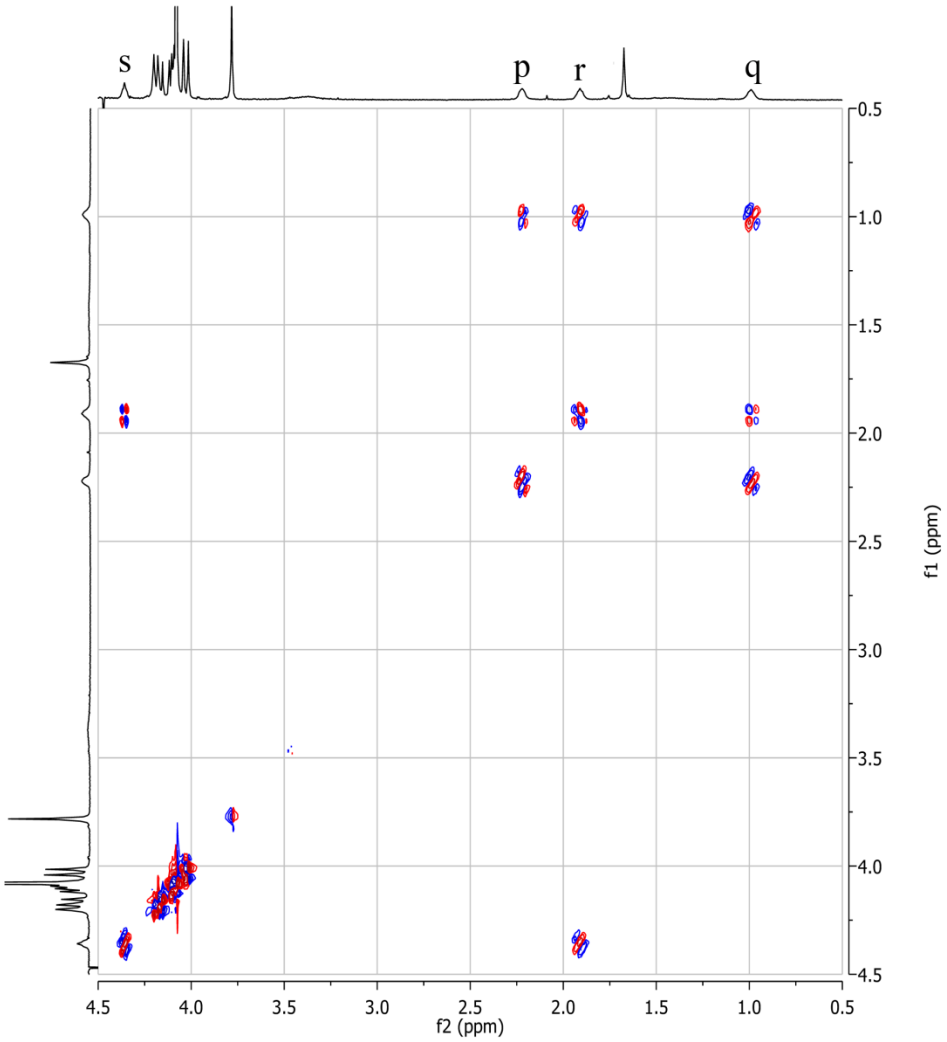

Figure II-S23. Partial DQCOSY ^{1}H NMR spectrum recorded (600 MHz, D_2O, RT) for the monomeric complex **II-20• II-3**.

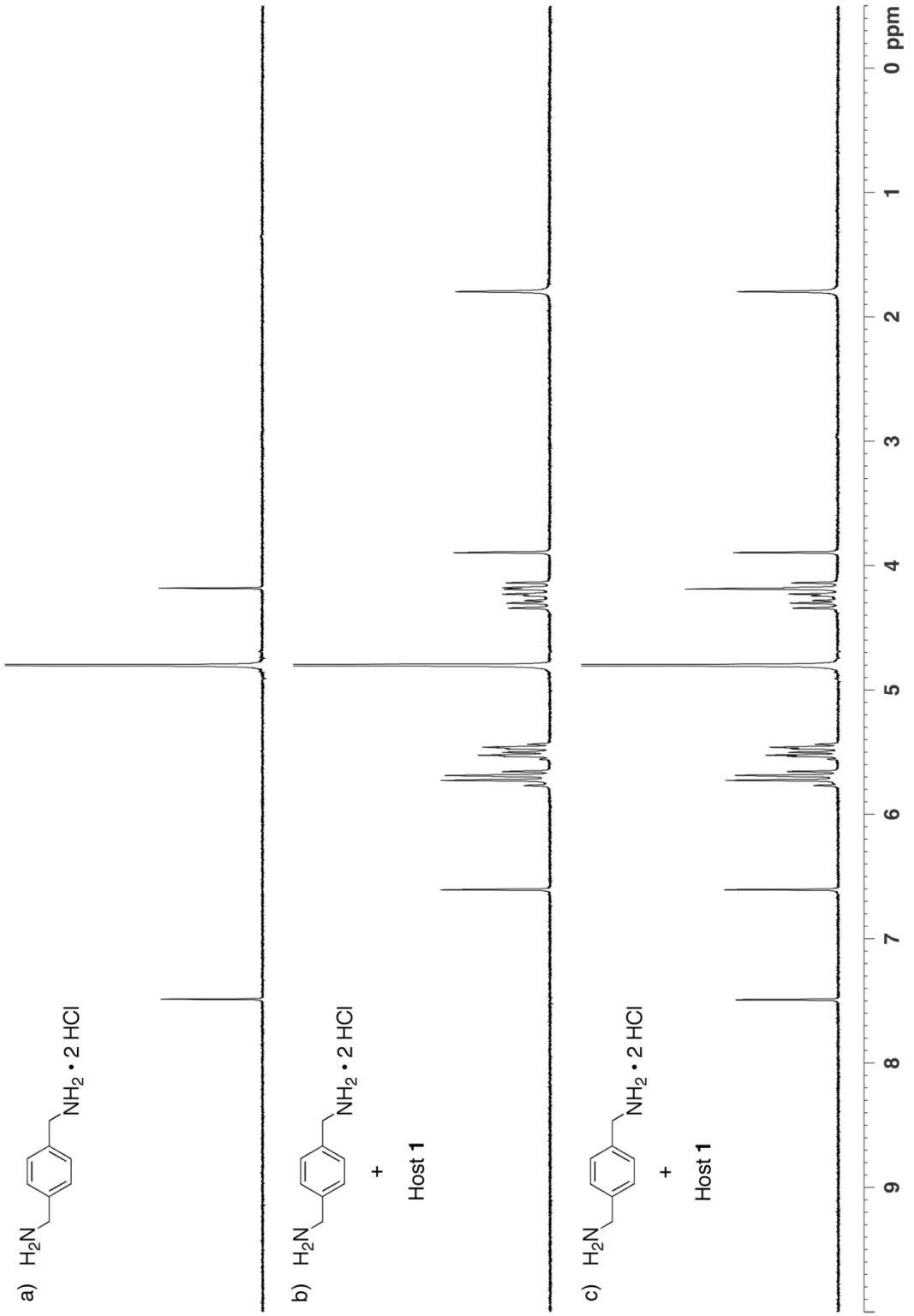

Figure II-S24. ^{1}H NMR spectra recorded (D_2O, 400 MHz, RT) for : a) **II-3** (0.5 mM), b) a 1:1 mixture of Me_2CB[7] (0.5 mM) and **3 II-** (0.5 mM), and c) a 1:2 mixture of Me_2CB[7] (0.5 mM) and **II-3** (1 mM).

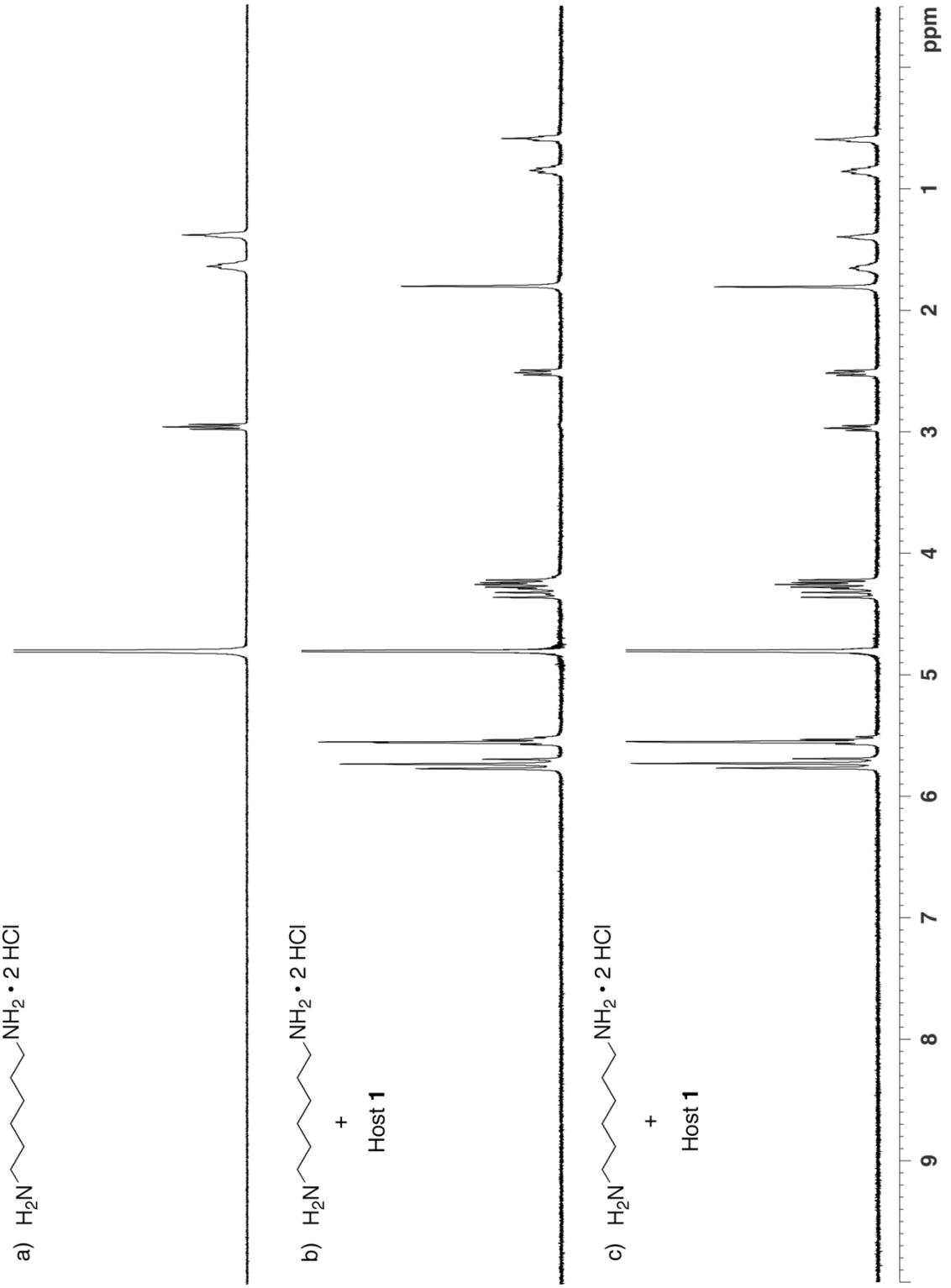

Figure II-S25. ^{1}H NMR spectra recorded (D_2O, 400 MHz, RT) for : a) **II-4** (0.5 mM), b) a 1:1 mixture of Me_2CB[7] (0.5 mM) and **II-4** (0.5 mM), and c) a 1:2 mixture of Me_2CB[7] (0.5 mM) and **II-4** (1 mM).

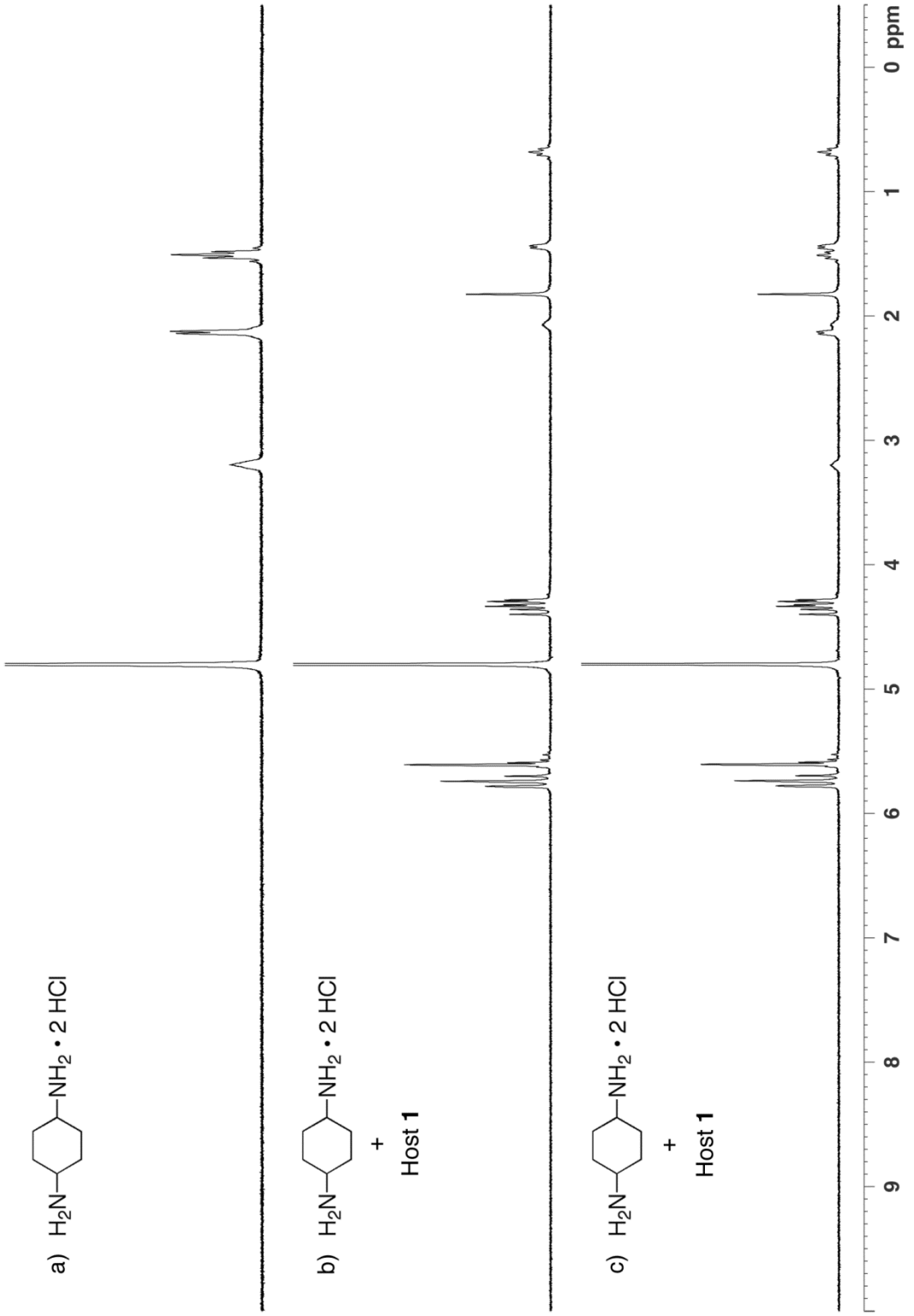

Figure II-S26. ^{1}H NMR spectra recorded (D_2O, 400 MHz, RT) for : a) **II-7** (0.5 mM), b) a 1:1 mixture of Me_2CB[7] (0.5 mM) and **II-7** (0.5 mM), and c) a 1:2 mixture of Me_2CB[7] (0.5 mM) and **II-7** (1 mM).

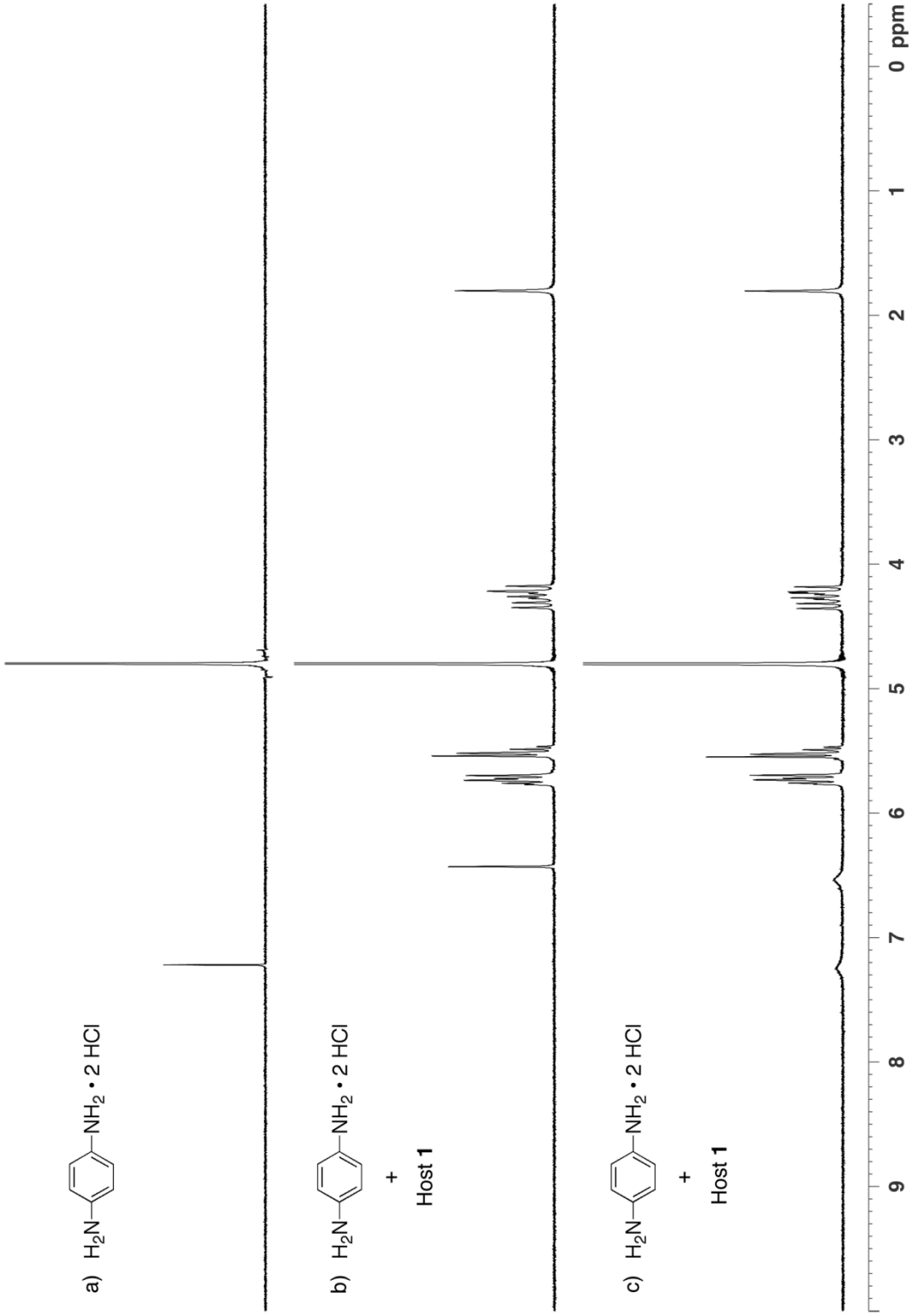

Figure II-S27. ^{1}H NMR spectra recorded (D_2O, 400 MHz, RT) for : a) **II-6** (0.5 mM), b) a 1:1 mixture of Me_2CB[7] (0.5 mM) and **II-6** (0.5 mM), and c) a 1:2 mixture of Me_2CB[7] (0.5 mM) and **II-6** (1 mM).

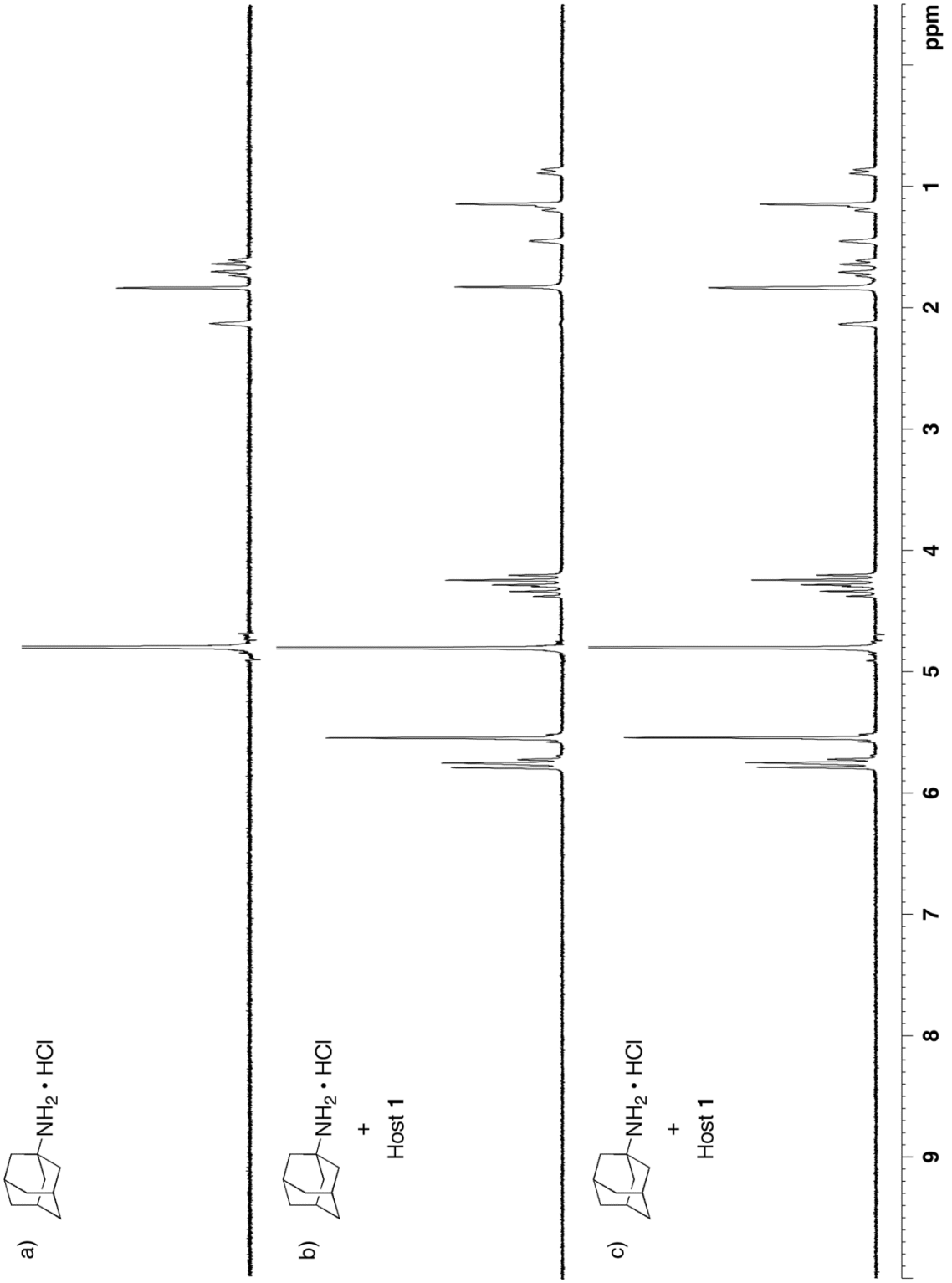

Figure II-S28. ^{1}H NMR spectra recorded (D_2O, 400 MHz, RT) for : a) **II-9** (0.5 mM), b) a 1:1 mixture of Me_2CB[7] (0.5 mM) and **II-9** (0.5 mM), and c) a 1:2 mixture of Me_2CB[7] (0.5 mM) and **II-9** (1 mM).

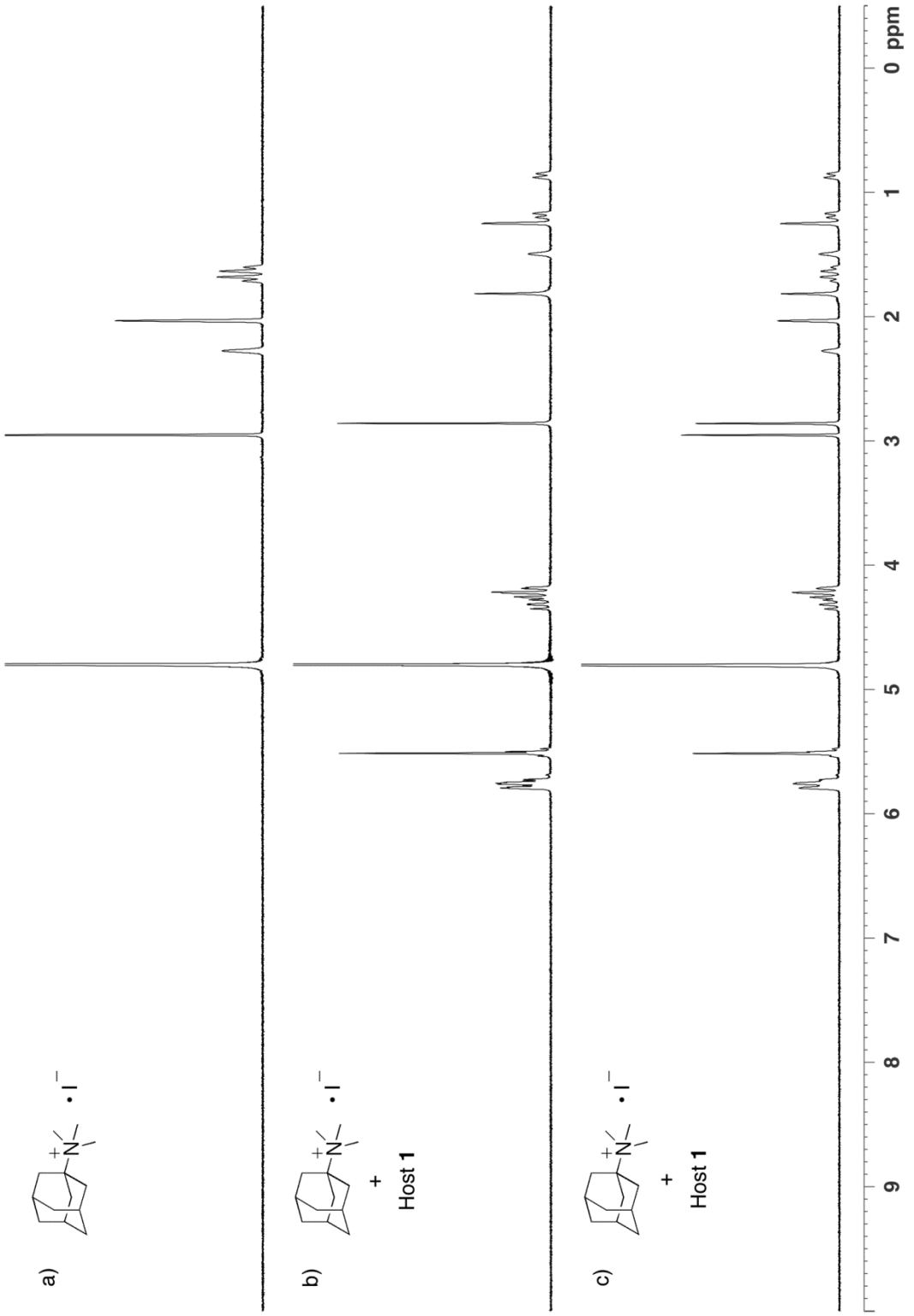

Figure II-S29. ^{1}H NMR spectra recorded (D_2O, 400 MHz, RT) for : a) **II-10** (0.5 mM), b) a 1:1 mixture of Me_2CB[7] (0.5 mM) and **II-10** (0.5 mM), and c) a 1:2 mixture of Me_2CB[7] (0.5 mM) and **II-10** (1 mM).

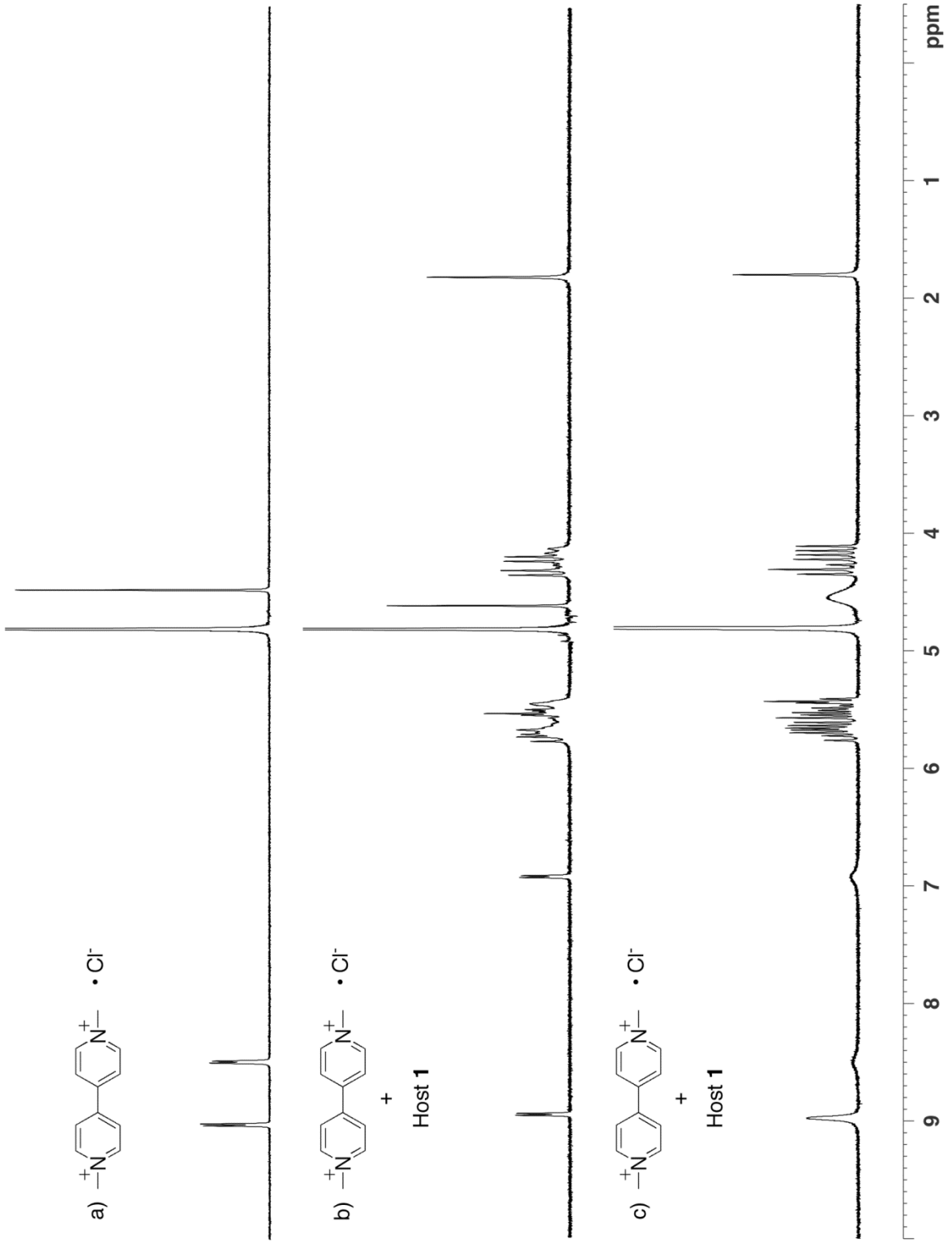

Figure II-S30. ^{1}H NMR spectra recorded (D_2O, 400 MHz, RT) for : a) **II-8** (0.5 mM), b) a 1:1 mixture of $Me_2CB[7]$ (0.5 mM) and **II-8** (0.5 mM), and c) a 1:2 mixture of $Me_2CB[7]$ (0.5 mM) and **II-8** (1 mM).

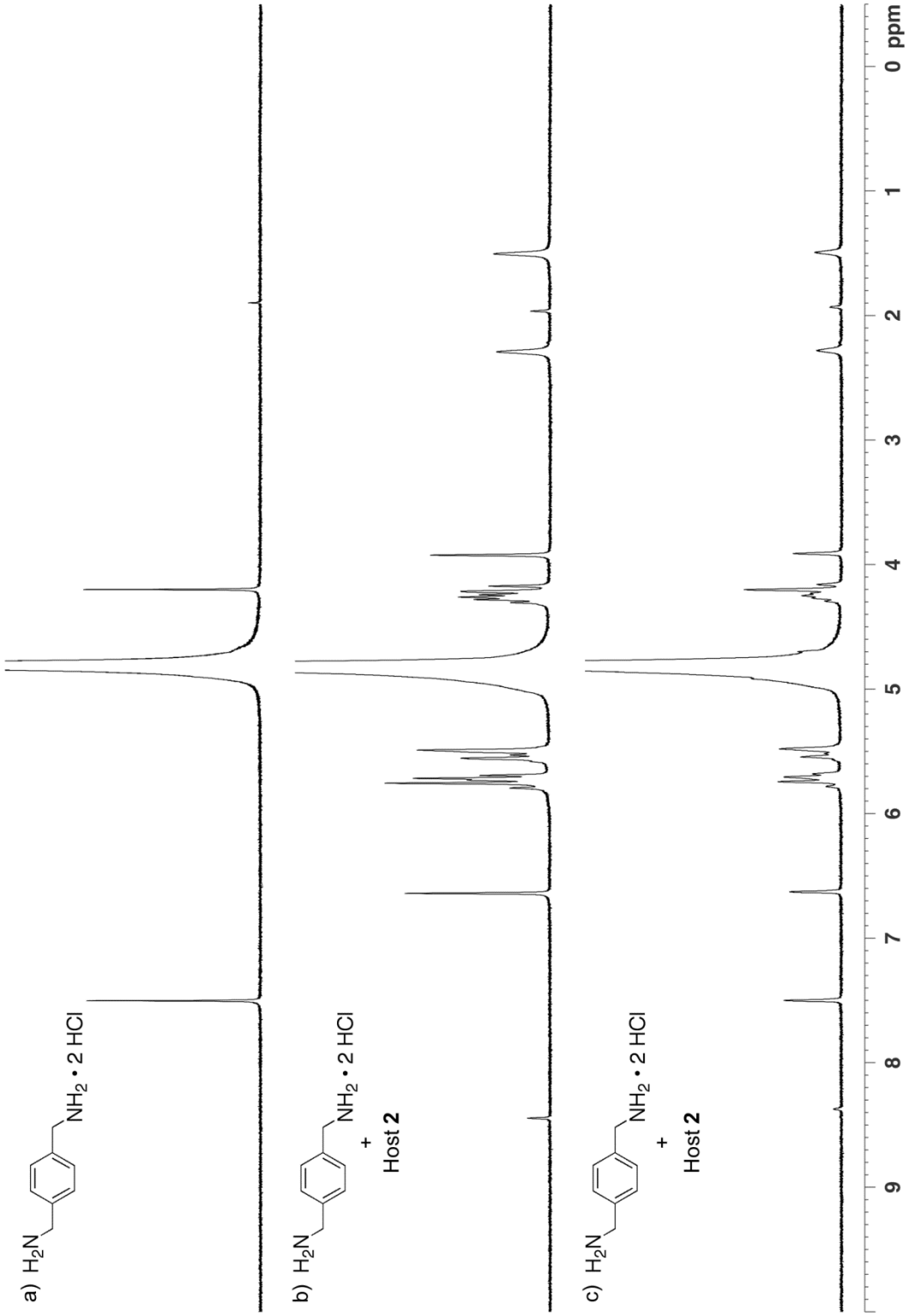

Figure II-S31. ^{1}H NMR spectra recorded (D_2O, 400 MHz, RT) for : a) **II-3** (0.5 mM), b) a 1:1 mixture of CyCB[7] (0.5 mM) and **II-3** (0.5 mM), and c) a 1:2 mixture of CyCB[7] (0.5 mM) and **II-3** (1 mM).

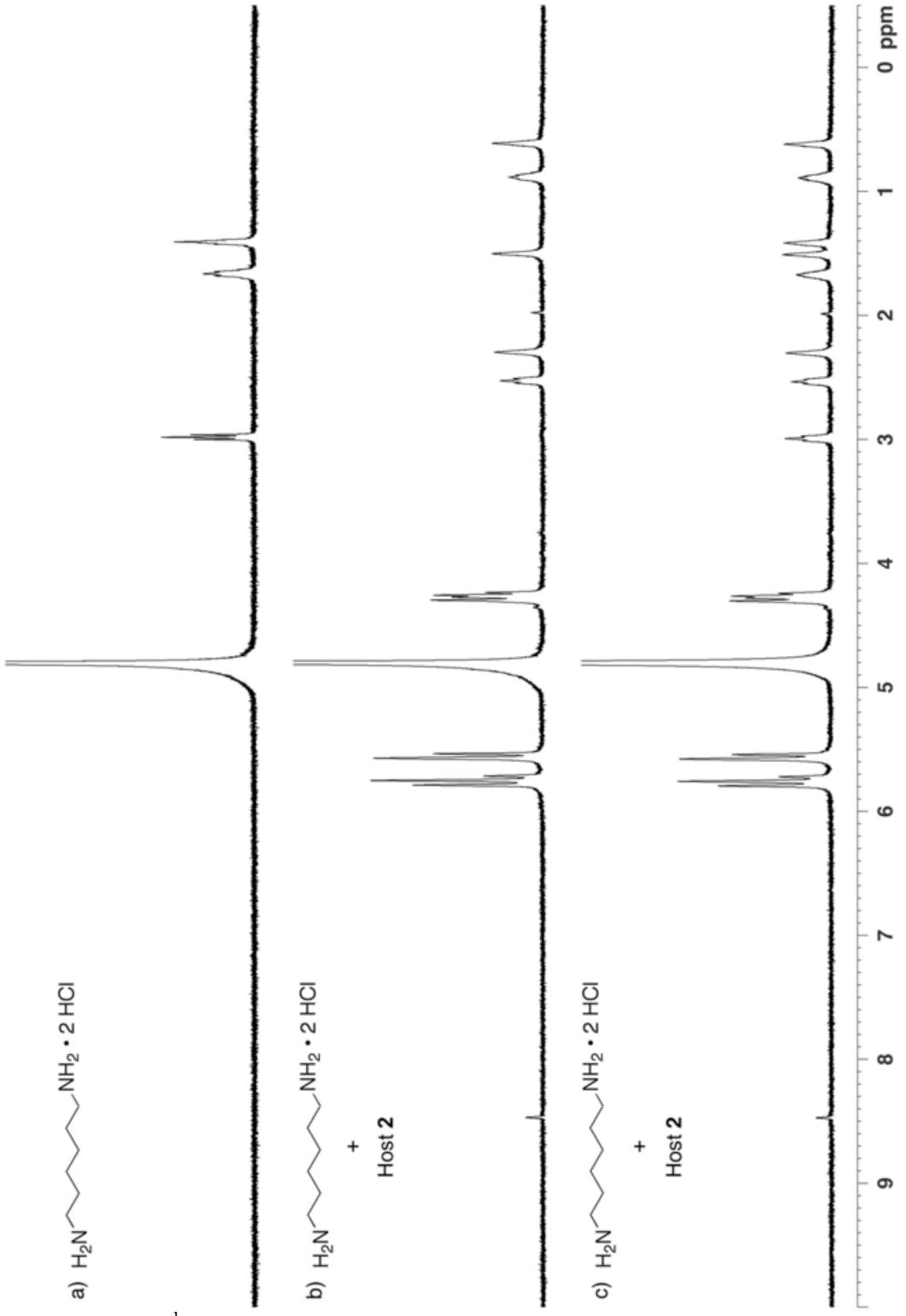

Figure II-S32. ^{1}H NMR spectra recorded (D_2O, 400 MHz, RT) for : a) **II-4** (0.5 mM), b) a 1:1 mixture of CyCB[7] (0.5 mM) and **II-4** (0.5 mM), and c) a 1:2 mixture of CyCB[7] (0.5 mM) and **II-4** (1 mM).

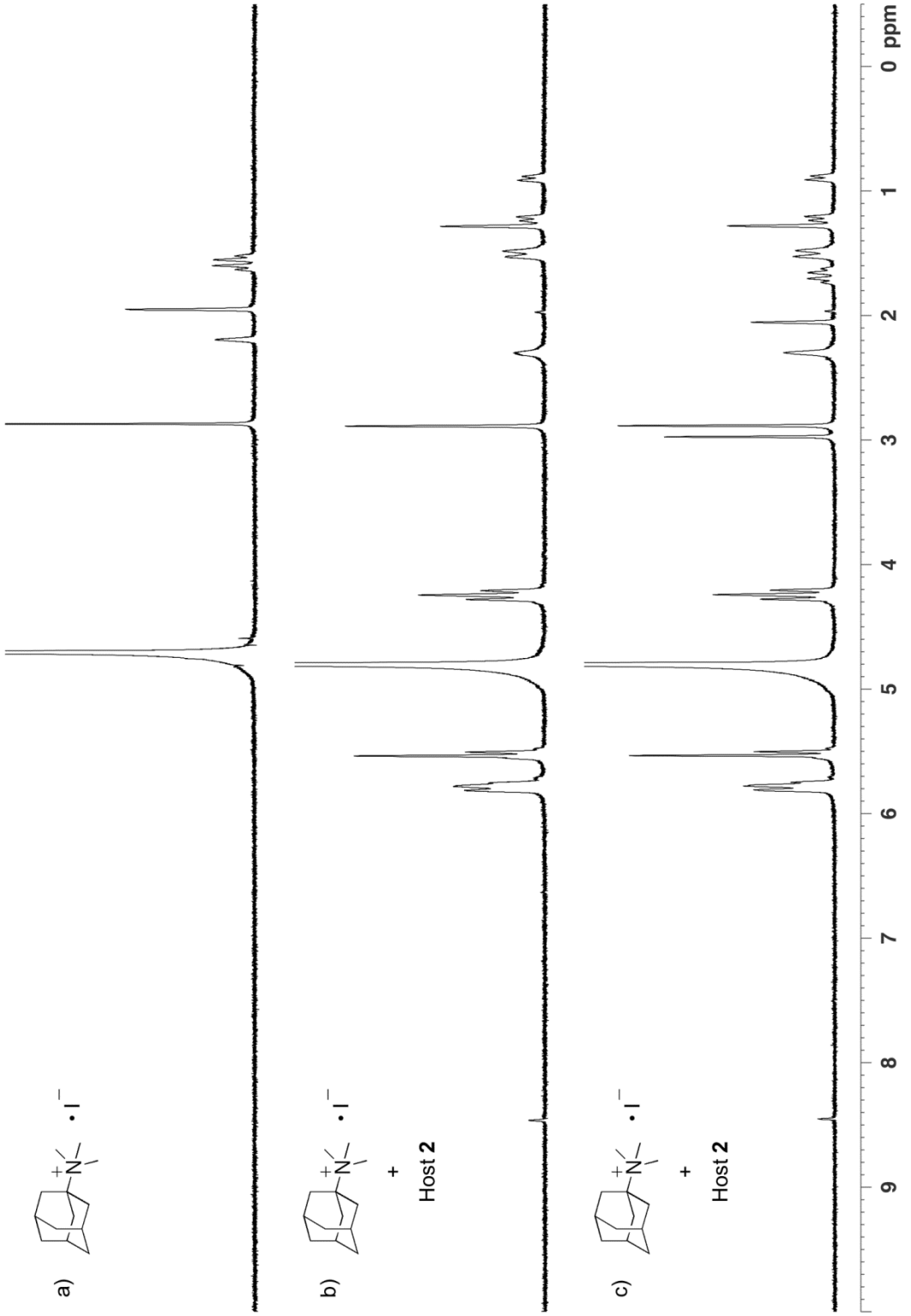

Figure II-S33. ^{1}H NMR spectra recorded (D_2O, 400 MHz, RT) for : a) **II-10** (0.5 mM), b) a 1:1 mixture of CyCB[7] (0.5 mM) and **II-10** (0.5 mM), and c) a 1:2 mixture of CyCB[7] (0.5 mM) and **II-10** (1 mM).

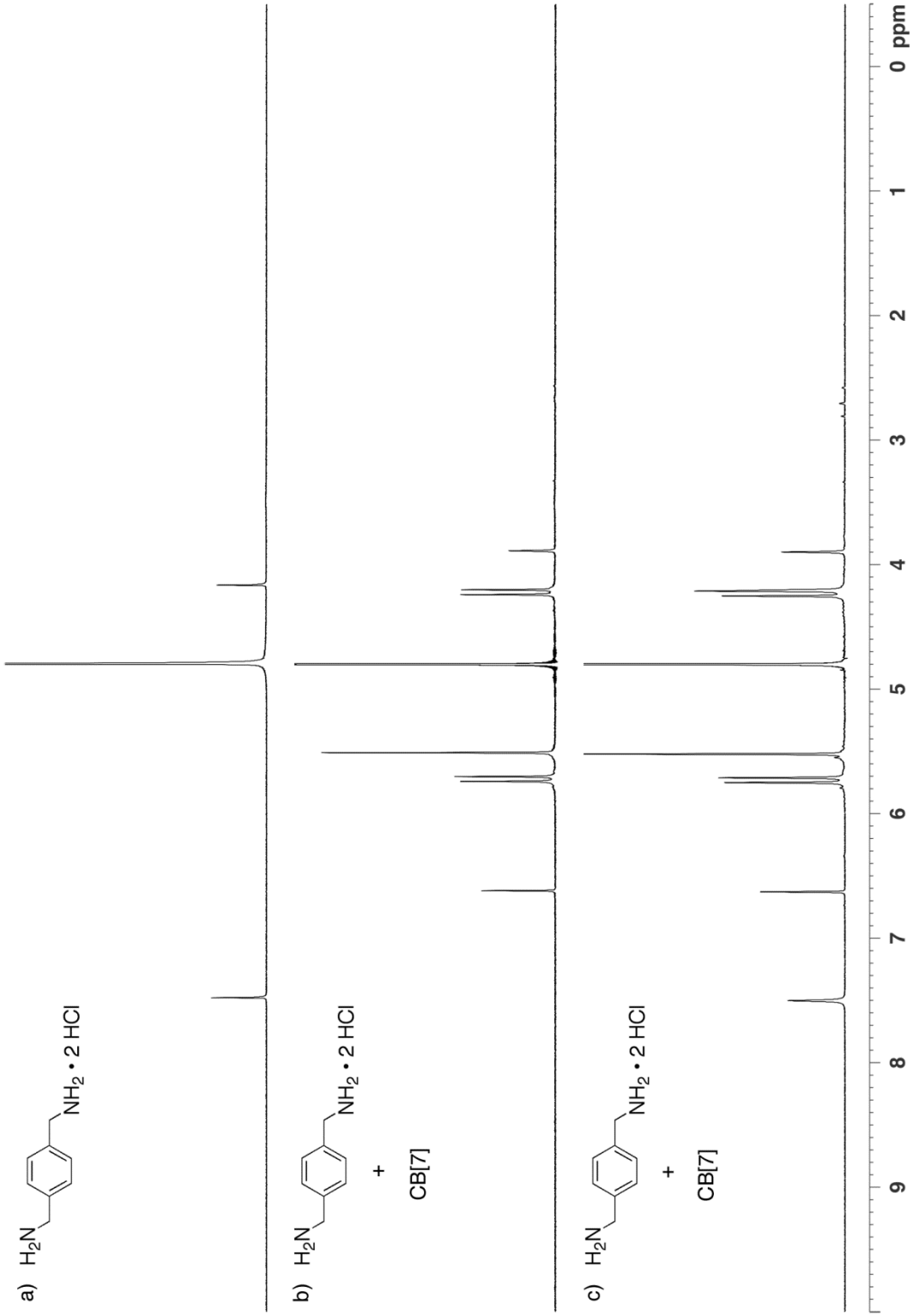

Figure II-S34. ^{1}H NMR spectra recorded (D_2O, 400 MHz, RT) for : a) **II-3** (0.5 mM), b) a 1:1 mixture of CB[7] (0.5 mM) and **II-3** (0.5 mM), and c) a 1:2 mixture of CB[7] (0.5 mM) and **II-3** (1 mM).

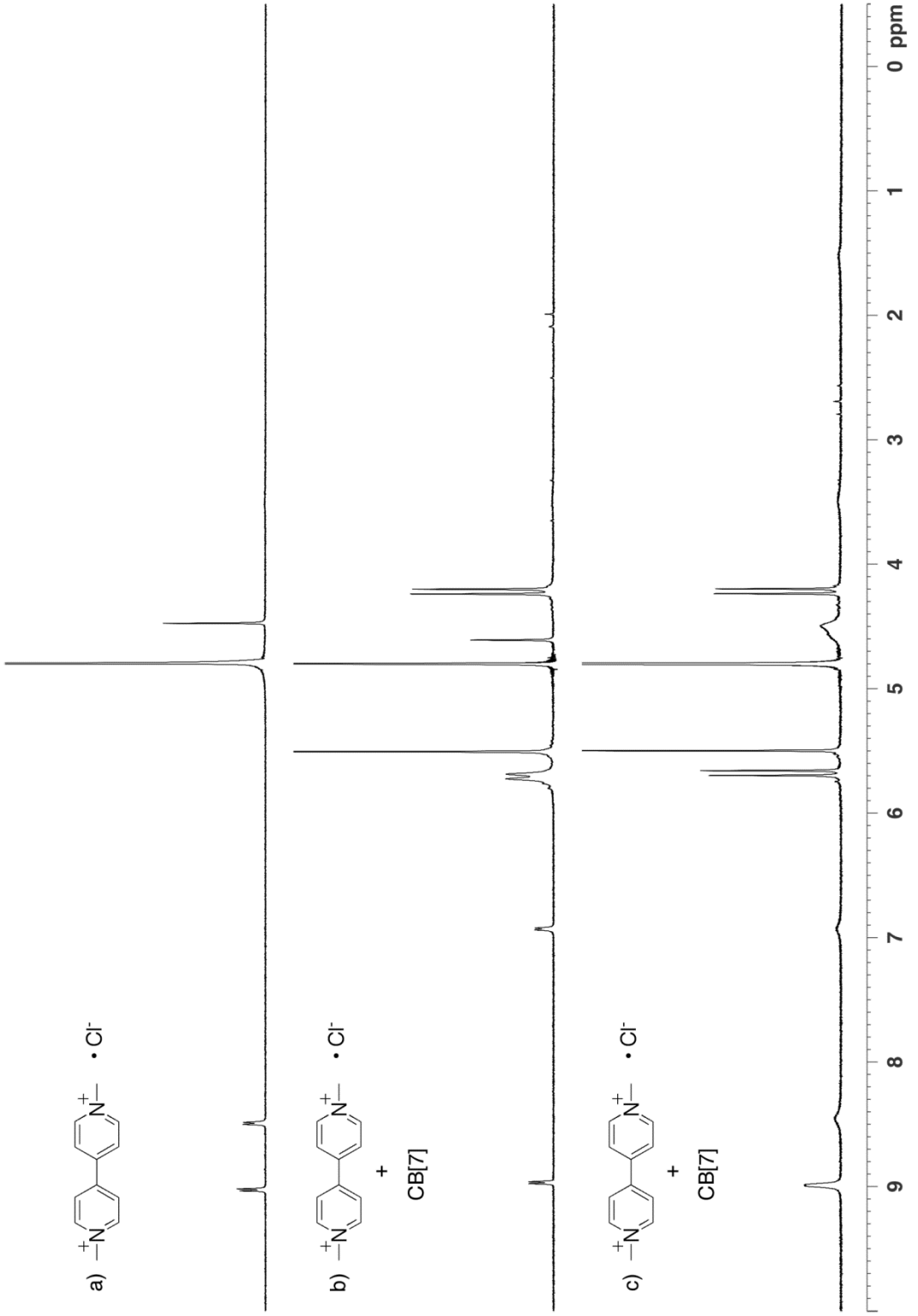

Figure II-S35. ^{1}H NMR spectra recorded (D_2O, 400 MHz, RT) for : a) **II-8** (0.5 mM), b) a 1:1 mixture of CB[7] (0.5 mM) and **II-8** (0.5 mM), and c) a 1:2 mixture of CB[7] (0.5 mM) and **II-8** (1 mM).

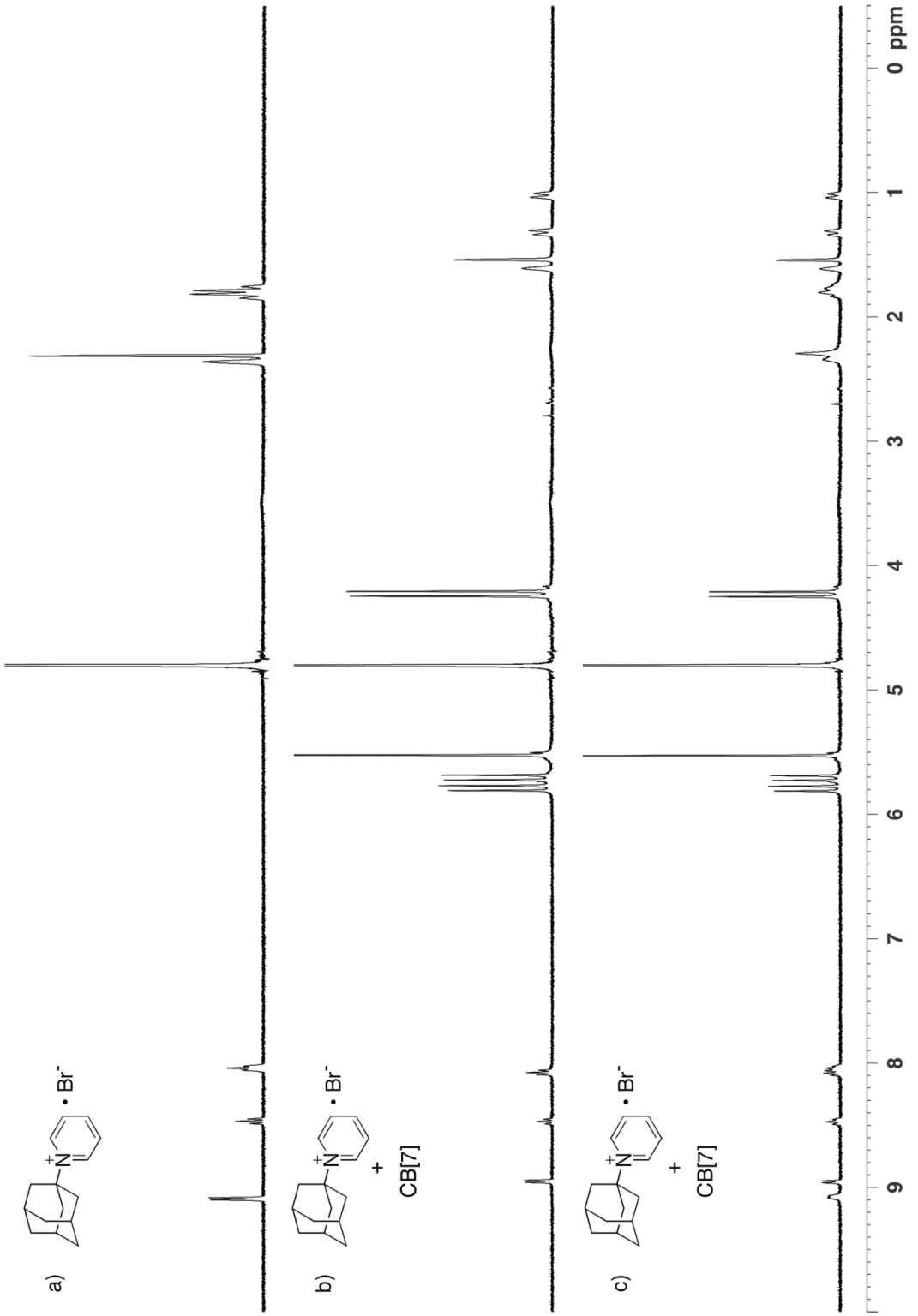

Figure II-S36. ^{1}H NMR spectra recorded (D_2O, 400 MHz, RT) for : a) **II-11** (0.5 mM), b) a 1:1 mixture of CB[7] (0.5 mM) and **II-11** (0.5 mM), and c) a 1:2 mixture of CB[7] (0.5 mM) and **II-11** (1 mM).

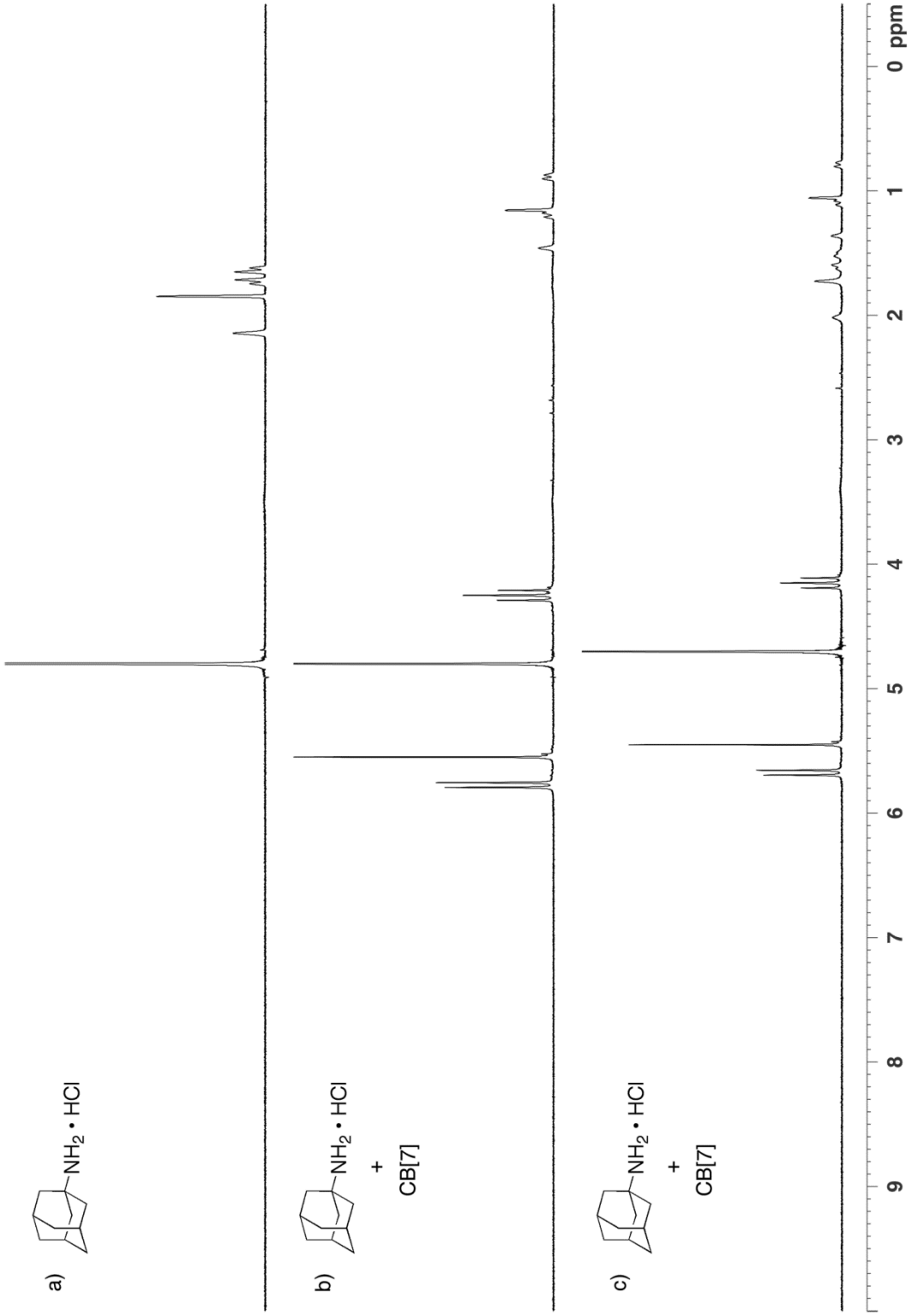

Figure II-S37. ^{1}H NMR spectra recorded (D_2O, 400 MHz, RT) for : a) **II-9** (0.5 mM), b) a 1:1 mixture of CB[7] (0.5 mM) and **II-9** (0.5 mM), and c) a 1:2 mixture of CB[7] (0.5 mM) and **II-9** (1 mM).

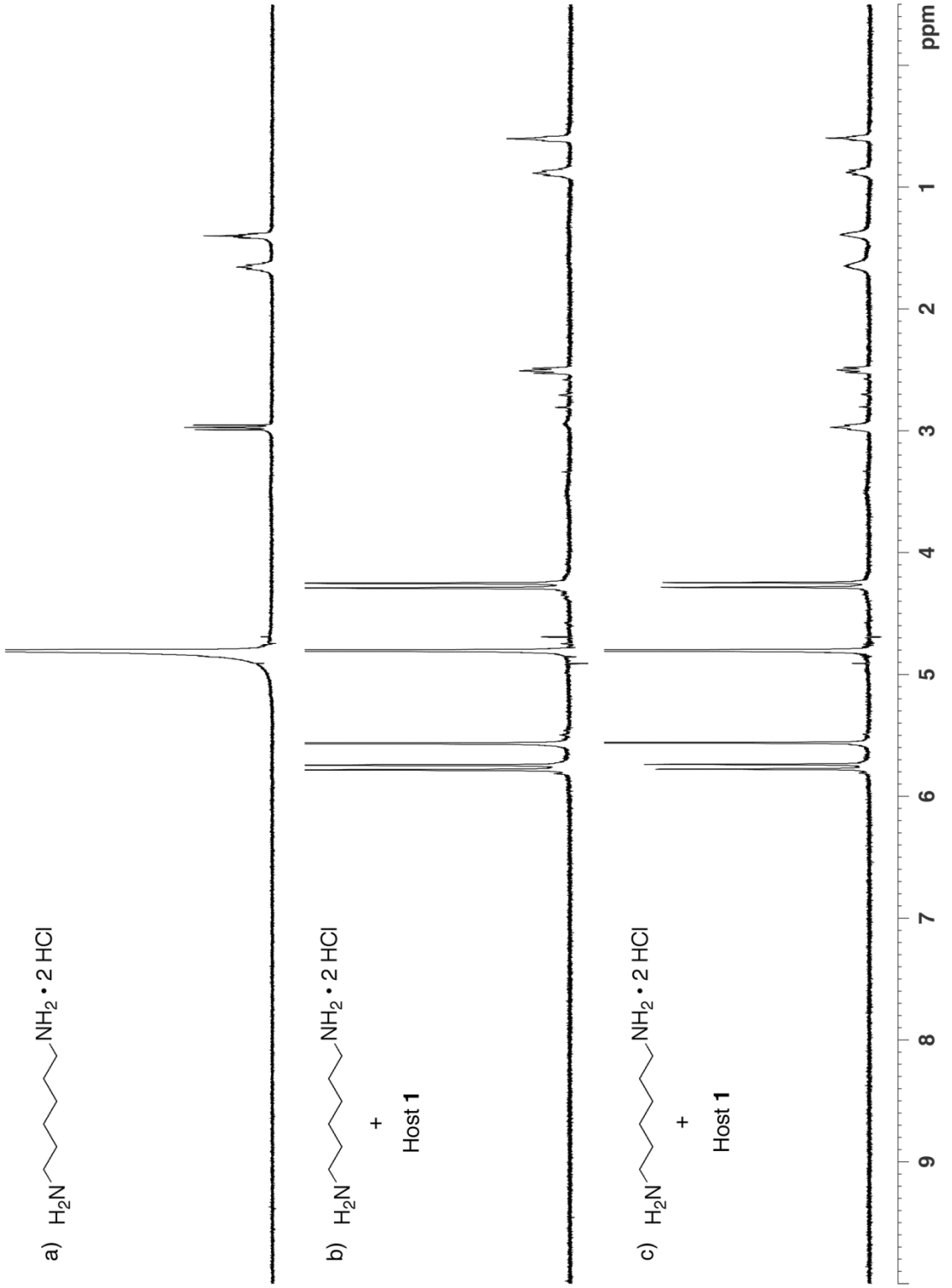

Figure II-S38. ^{1}H NMR spectra recorded (D_2O, 400 MHz, RT) for : a) **II-4** (0.5 mM), b) a 1:1 mixture of CB[7] (0.5 mM) and **II-4** (0.5 mM), and c) a 1:2 mixture of CB[7] (0.5 mM) and **II-4** (1 mM).

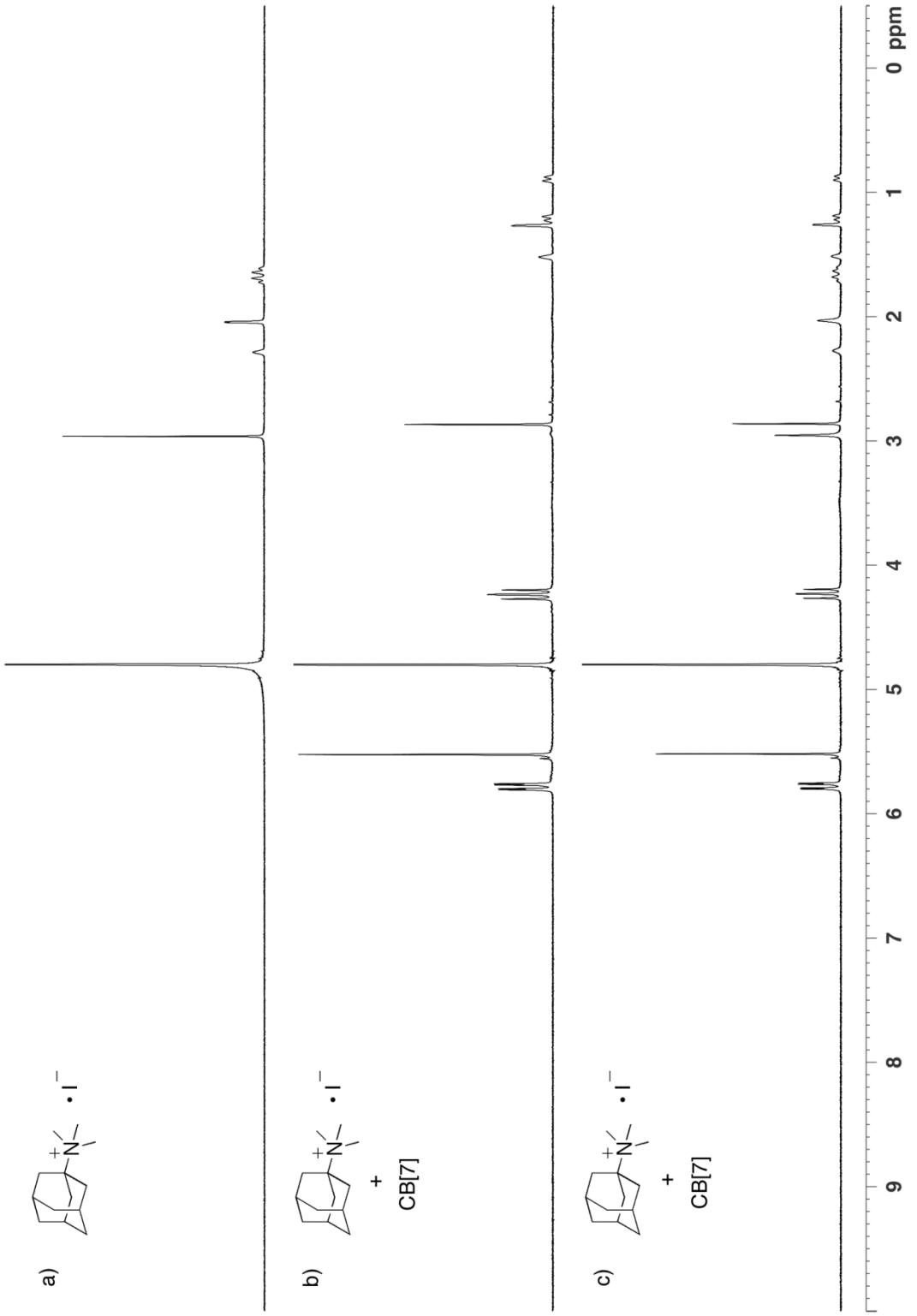

Figure II-S39. ^{1}H NMR spectra recorded (D_2O, 400 MHz, RT) for : a) **II-10** (0.5 mM), b) a 1:1 mixture of CB[7] (0.5 mM) and **II-10** (0.5 mM), and c) a 1:2 mixture of CB[7] (0.5 mM) and **II-10** (1 mM).

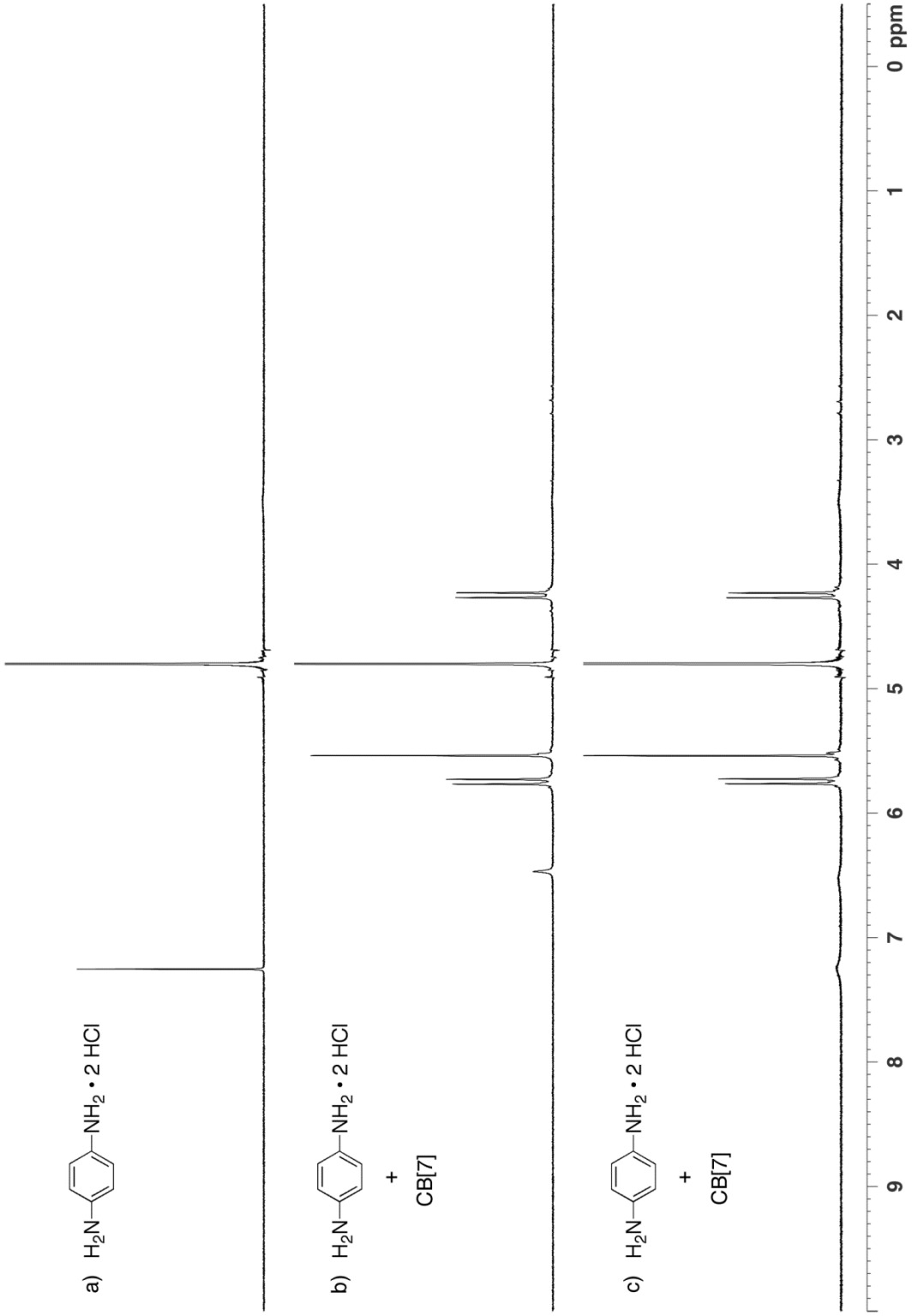

Figure II-S40. ^{1}H NMR spectra recorded (D_2O, 400 MHz, RT) for : a) **II-6** (0.5 mM), b) a 1:1 mixture of CB[7] (0.5 mM) and **II-6** (0.5 mM), and c) a 1:2 mixture of CB[7] (0.5 mM) and **II-6** (1 mM).

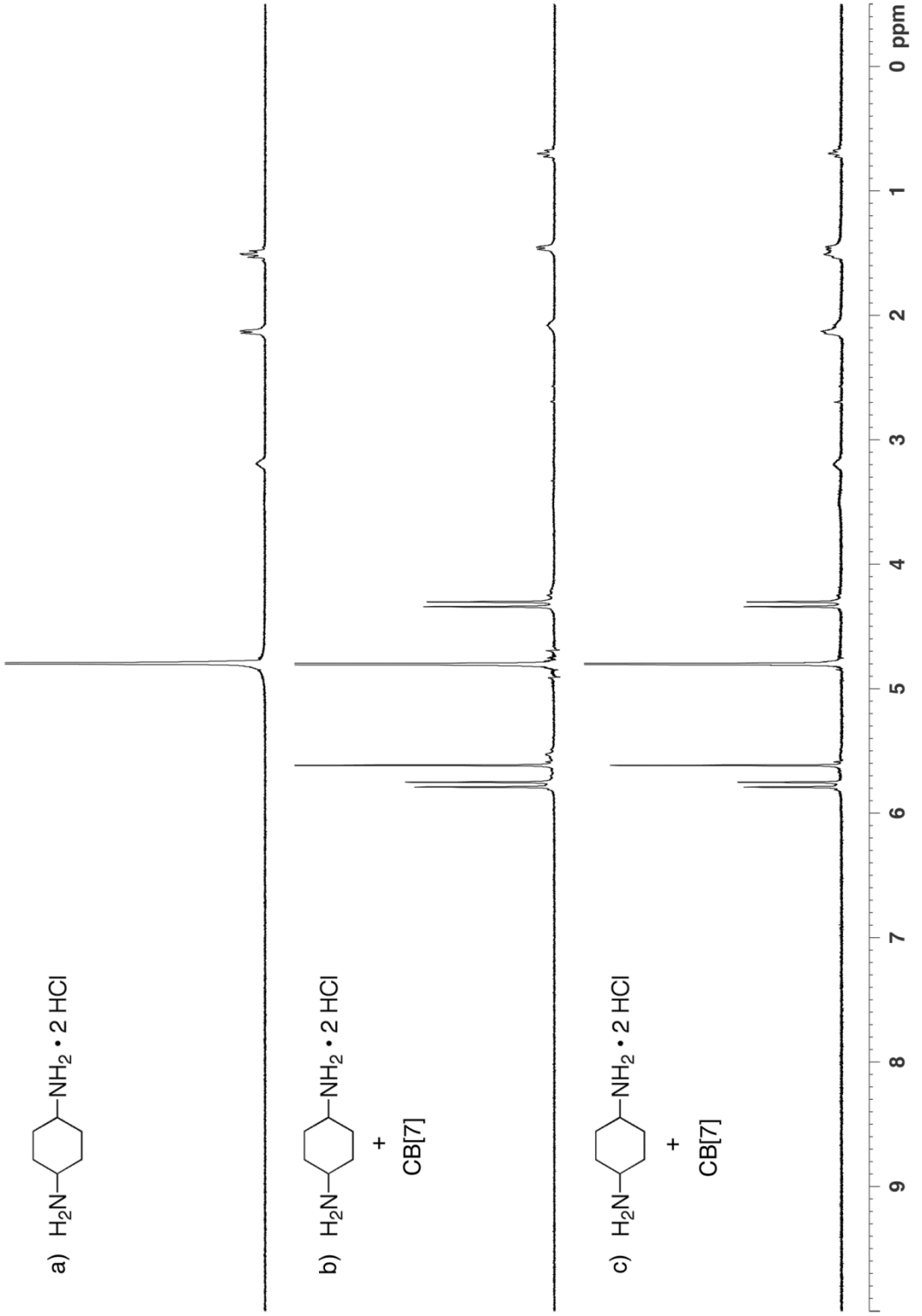

Figure II-S41. ^{1}H NMR spectra recorded (D_2O, 400 MHz, RT) for : a) **II-7** (0.5 mM), b) a 1:1 mixture of CB[7] (0.5 mM) and **II-7** (0.5 mM), and c) a 1:2 mixture of CB[7] (0.5 mM) and **II-7** (1 mM).

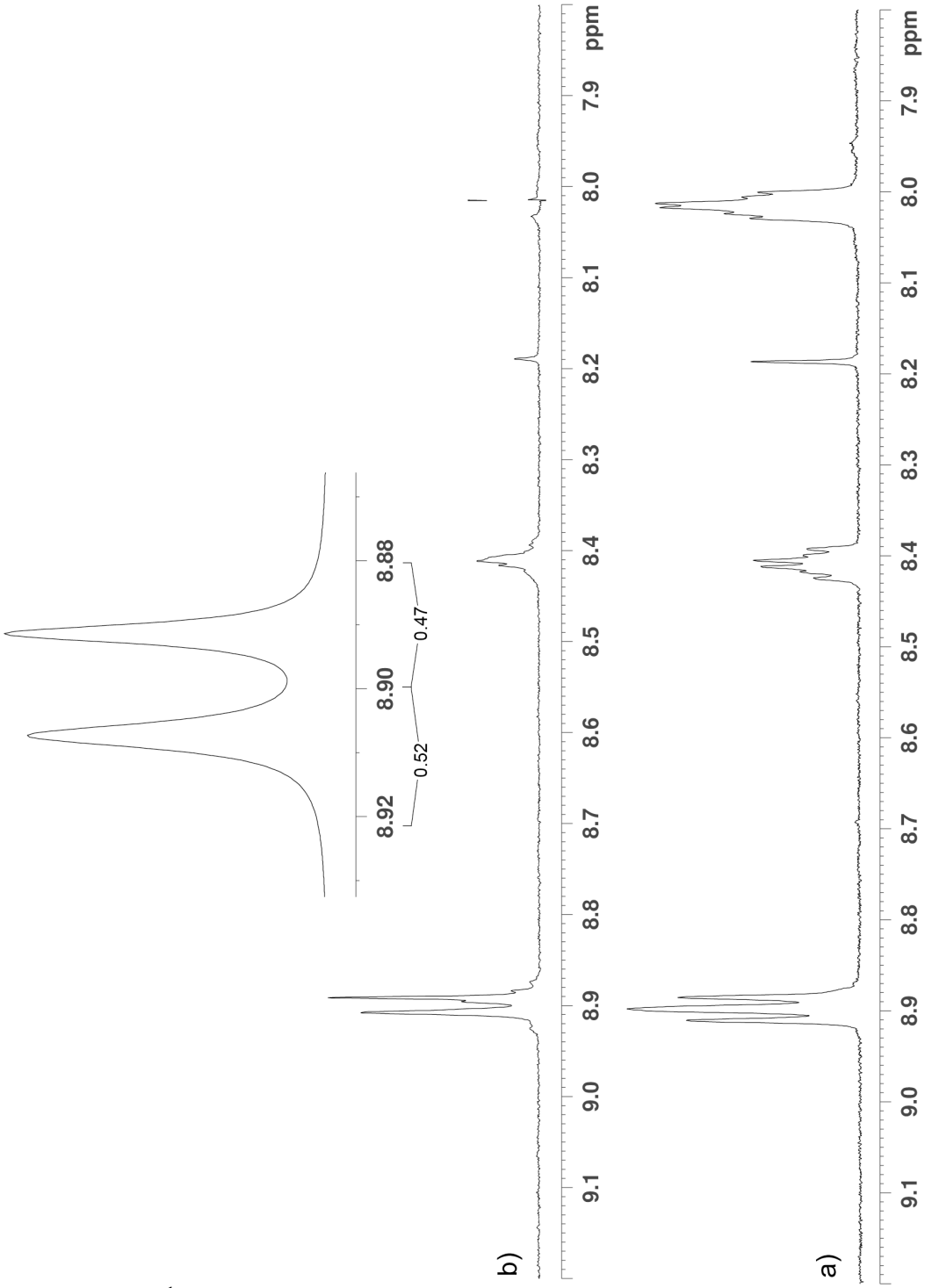

Figure II-S42. ^{1}H NMR spectra recorded (600 MHz, 50 mM buffer, RT) for: a) a mixture of CB[7] (0.77 mM), Me_2CB[7] (0.77 mM), and **II-11** (0.7 mM) b) the same sample as part a, but with homodecoupling by irradiation of the signal at 8.02 ppm. The inset shows the integration of the expansion of the deconvoluted spectrum used to determine the K_{rel} value.

Details of the Crystal Structure of $Me_2CB[7]$. A colorless prism-like specimen of $C_{52}H_{80}I_2N_{30}O_{25}$, approximate dimensions 0.34 mm × 0.43 mm × 0.44 mm, was used for the X-ray crystallographic analysis. The X-ray intensity data were measured on a Bruker APEX-II CCD system equipped with a graphite monochromator and a MoKα sealed tube (λ = 0.71073 Å). Data collection temperature was 200 K.

The total exposure time was 22.73 hours. The frames were integrated with the Bruker SAINT software package using a narrow-frame algorithm. The integration of the data using an orthorhombic unit cell yielded a total of 104851 reflections to a maximum θ angle of 25.00° (0.84 Å resolution), of which 13325 were independent (average redundancy 7.869, completeness = 99.8%, R_{int} = 3.85%, R_{sig} = 2.87%) and 10588 (79.46%) were greater than $2\sigma(F^2)$. The final cell constants of *a* = 23.750(4) Å, *b* = 49.017(8) Å, *c* = 13.018(2) Å, *V* = 15155.(4) $Å^3$, are based upon the refinement of the XYZ-centroids of 9437 reflections above 20 σ(I) with 4.580° < 2θ < 54.07°. Data were corrected for absorption effects using the multi-scan method (SADABS). The calculated minimum and maximum transmission coefficients (based on crystal size) are 0.6300 and 0.7300.

The structure was solved and refined using the Bruker SHELXTL Software Package, using the space group P c c n, with Z = 8 for the formula unit, $C_{52}H_{80}I_2N_{30}O_{25}$. The final anisotropic full-matrix least-squares refinement on F^2 with 1028 variables converged at R_1 = 7.62%, for the observed data and wR_2 = 17.67% for all data. The goodness-of-fit was 1.000. The largest peak in the final difference electron density synthesis was 1.436 $e^-/Å^3$ and the largest hole was -1.601 $e^-/Å^3$ with an RMS deviation of 0.078 $e^-/Å^3$. On the basis of the final model, the calculated density was 1.560 g/cm^3 and F(000), 7264 e^-.

Crystallographic References: APEX2 Version 2010.11-3 (Bruker AXS Inc.) SAINT Version 7.68A (Bruker AXS Inc., 2009) SADABS Version 2008/1 (G. M. Sheldrick, Bruker AXS Inc.) XPREP Version 2008/2 (G. M. Sheldrick, Bruker AXS Inc.) XS Version 2008/1 (G. M. Sheldrick, *Acta Cryst.* (2008). A**64**, 112-122) XL Version 2008/4 (G. M. Sheldrick, *Acta Cryst.* (2008). A**64**, 112-122) Platon (A. L. Spek, *Acta Cryst.* (1990). A**46**, C-34)

Table II-S1. Sample and crystal data for UM2261.

Identification code	2261	
Chemical formula	$C_{52}H_{80}I_2N_{30}O_{25}$	
Formula weight	1779.26	
Temperature	200(2) K	
Wavelength	0.71073 Å	
Crystal size	0.34 × 0.43 × 0.44 mm	
Crystal habit	colorless prism	
Crystal system	orthorhombic	
Space group	P c c n	
Unit cell dimensions	a = 23.750(4) Å	α = 90°
	b = 49.017(8) Å	β = 90°
	c = 13.018(2) Å	γ = 90°

Volume	15155.(4) $Å^3$
Z	8
Density (calculated)	1.560 Mg/cm^3
Absorption coefficient	0.924 mm^{-1}
F(000)	7264

Table II-S2. Data collection and structure refinement for UM2261.

Diffractometer	Bruker APEX-II CCD
Radiation source	sealed tube, MoKα
Theta range for data collection	2.18 to 25.00°
Index ranges	$-28 \le h \le 28$, $-57 \le k \le 58$, $-15 \le l \le 15$
Reflections collected	104851
Independent reflections	13325 [R(int) = 0.0385]
Coverage of independent reflections	99.8%
Absorption correction	multi-scan
Max. and min. transmission	0.7300 and 0.6300
Structure solution technique	direct methods
Structure solution program	SHELXS-97 (Sheldrick, 2008)
Refinement method	Full-matrix least-squares on F^2
Refinement program	SHELXL-97 (Sheldrick, 2008)
Function minimized	$\Sigma\, w(F_o^2 - F_c^2)^2$
Data / restraints / parameters	13325 / 374 / 1028
Goodness-of-fit on F^2	1.000
Final R indices	10588 data; $I>2\sigma(I)$ $R_1 = 0.0762$, $wR_2 = 0.1708$
	all data $R_1 = 0.0890$, $wR_2 = 0.1767$
Weighting scheme	$w=1/[\sigma^2(F_o^2)+(0.05P)^2+49.67P]$, $P=(\max(F_o^2,0)+2F_c^2)/3$
Largest diff. peak and hole	1.436 and -1.601 $eÅ^{-3}$
R.M.S. deviation from mean	0.078 $eÅ^{-3}$

$R_{int} = \Sigma|F_o^2 - F_o^2(\text{mean})| / \Sigma[F_o^2]$
$R_1 = \Sigma||F_o| - |F_c|| / \Sigma|F_o|$
$\text{GOOF} = S = \{\Sigma[w(F_o^2 - F_c^2)^2] / (n - p)\}^{1/2}$
$wR_2 = \{\Sigma[w(F_o^2 - F_c^2)^2] / \Sigma[w(F_o^2)^2]\}^{1/2}$

Crystallographic information file for Me_2CB[7]•**II-3** is available free of charge on ACS publication website at DOI: 10.1021/ja3058502.

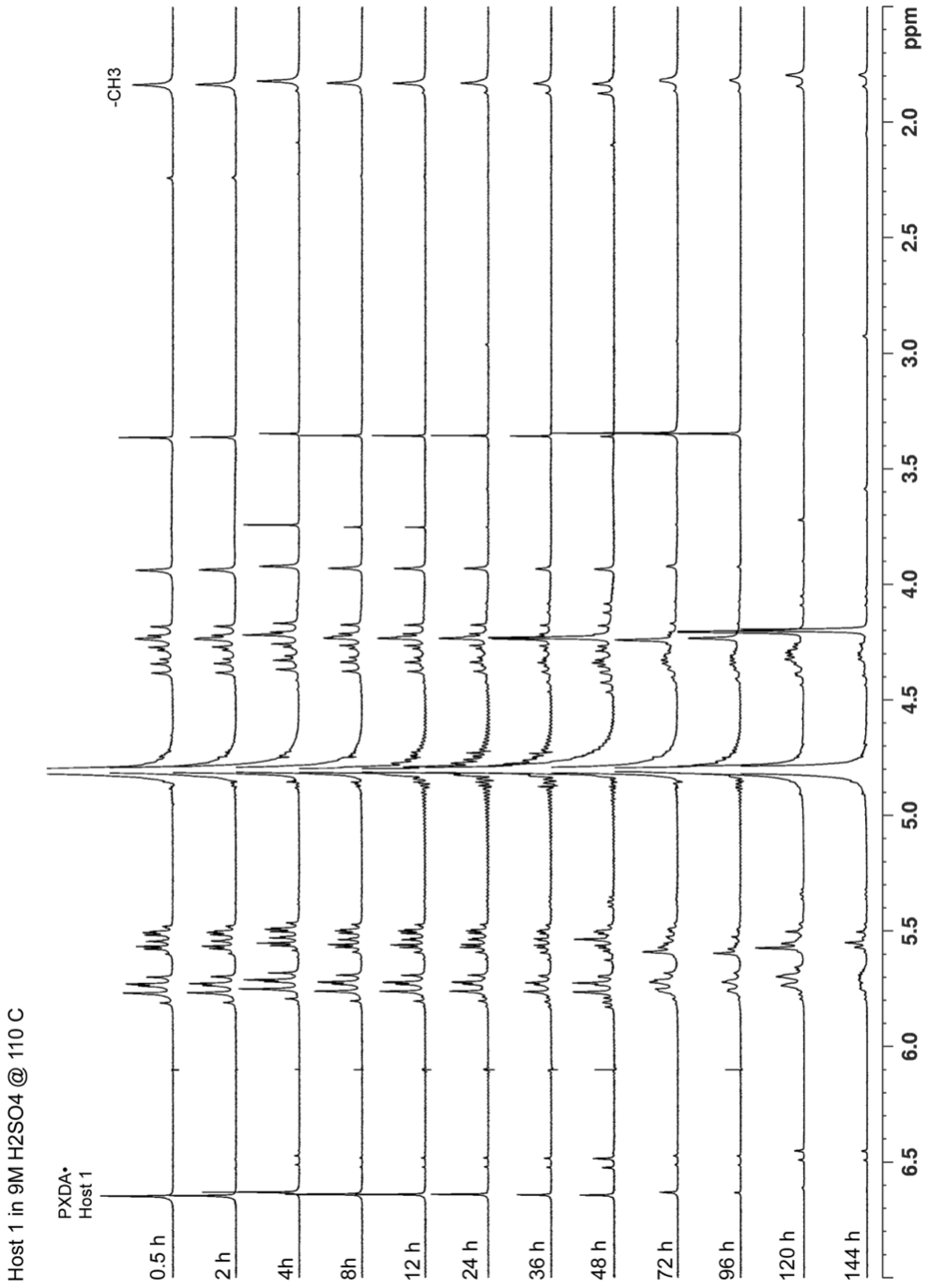

Figure II-S43. Decomposition of $Me_2CB[7]$ in 9M H_2SO_4 at 110 ˚C. ^1H NMR spectra recorded (400 MHz, D_2O, RT) for aliquots of the reaction mixture in the presence of excess guest **II-3** as a function of time.

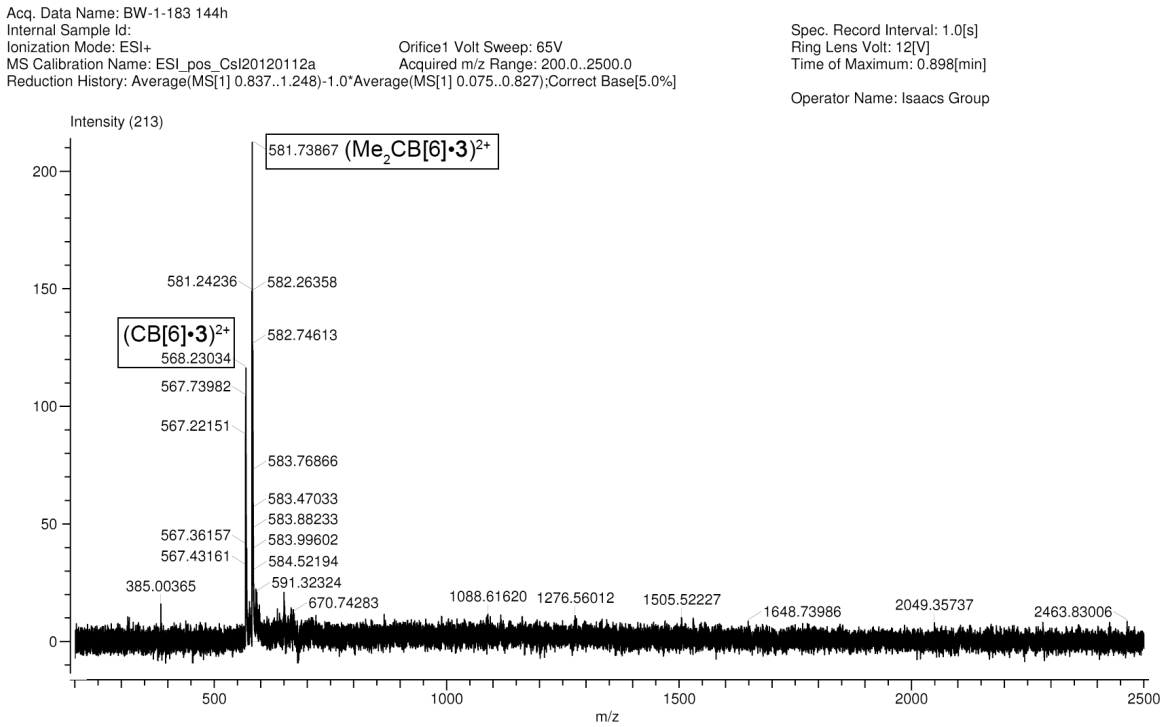

Figure II-S44. Electrospray mass spectrum recorded for the sample from Figure II-S43 at time = 144h.

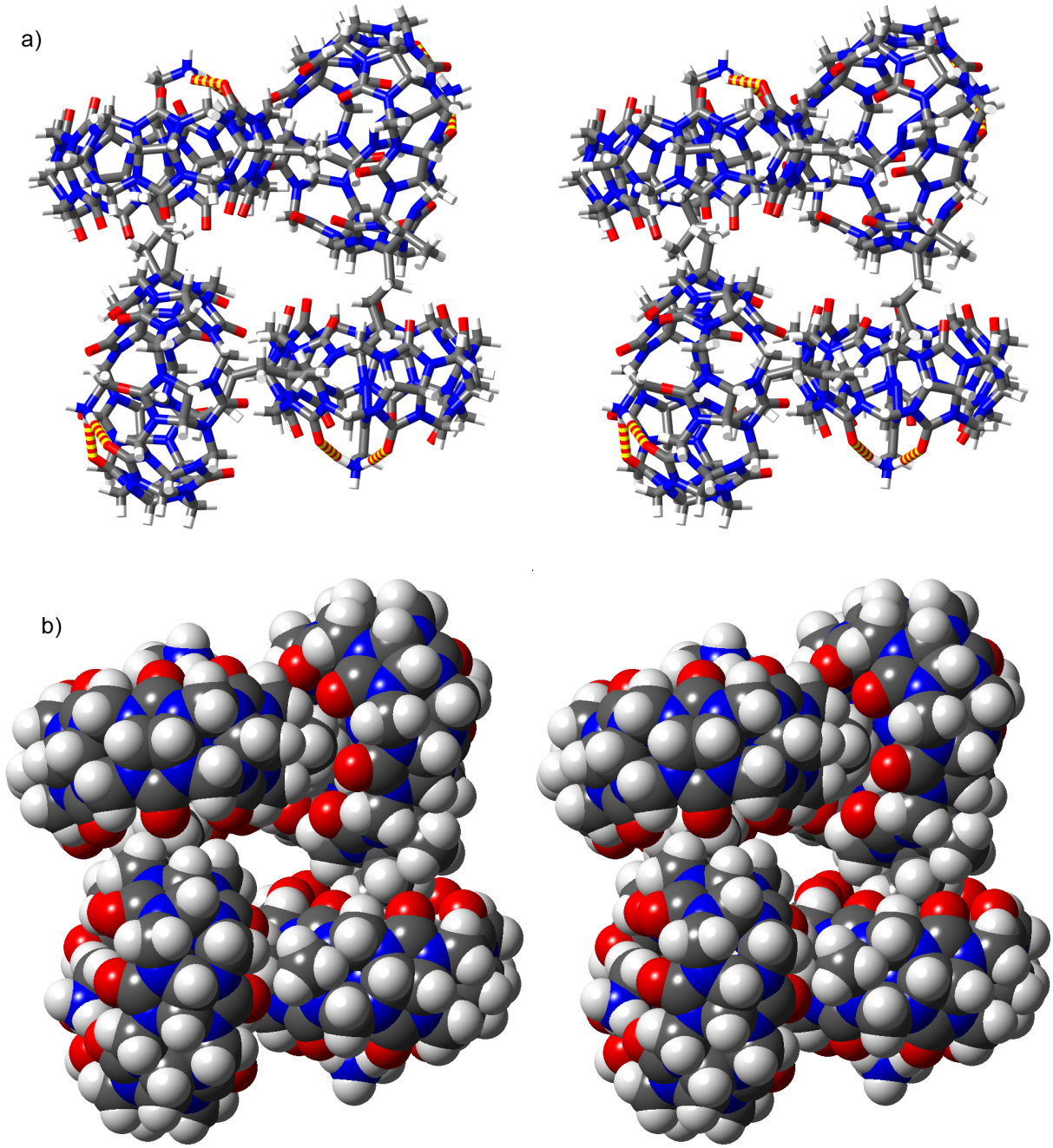

Figure II-S45. Cross-eyed stereoviews of MMFF minimized models of u,u,u,u- **II-20**$_4$: a) line bond structure, and b) space filling. Color-code: C, gray; H, white; N, blue; O, red; H-bonds, red-yellow striped.

Appendix 2

Synthesis and Recognition Properties of Cucurbit[8]uril Derivatives

Supporting Information

*by Brittany Vinciguerra, Peter Y. Zavalij, and Lyle Isaacs**

Department of Chemistry and Biochemistry, University of Maryland, College Park, MD 20742

Table of Contents **Pages**

General Experimental Details. Starting materials were purchased from commercial suppliers were used without further purification. Melting points were measured on a Meltemp apparatus in open capillary tubes and are uncorrected. IR spectra were recorded on a JASCO FT/IR 4100 spectrometer and are reported in cm^{-1}. NMR spectra were measured on spectrometers operating at 400, 600, or 800 MHz for ^{1}H and 125 MHz for ^{13}C NMR spectra. Routine mass spectrometry was performed using a JEOL AccuTOF electrospray instrument (ESI). Guest molecules **III-6 – III-10** were prepared according to literature procedures and characterization data matched the reported values.

References:

1. Yu, Y.; Li, J.; Zhang, M.; Cao, L.; Isaacs, L. *Chem. Comm.* **2015**, *51*, 3762-3765.
2. Kong, X.; Migneault, D.; Valade, I.; Xinfu, W.; Gervais, F. (Lahive & Cockfield, LLP) Methods and compositions for treating amyloid-related diseases. US Patent 20,070,010,573, January 11, 2007.
3. Fujisawa, K.; Humbert-Droz, M.; Letrun, R.; Vauthey, E.; Wesolowski, T. A.; Sakai, N.; Matile, S. *J. Am. Chem. Soc.* **2015**, *137*, 11047-11056.
4. Bodesheim, F.; Gieβler, W.; Nischk, G. (Farbinfabriken Bayer Aktiengesellchaft) Verfahren zer Herstellung von N-(ω-Aminoalkyl)-aminoalkansulfonsäuren. German Patent 1,200,318, September 9, 1965.

Synthetic Procedures and Characterization Data

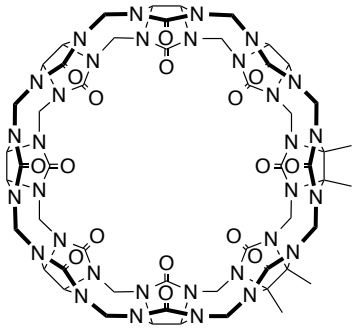

Compound $Me_4CB[8]$. Compound **III-1** (2.000 g, 2.06 mmol) was combined with KI (0.460 g, 2.78 mmol) in a 25 mL round-bottom flask and then 6 M aqueous HCl (10 mL) was added and the white heterogeneous mixture was stirred and sonicated until all clumps disappeared, about 2 minutes. Next, **III-2**$_{Me}$ (1.309 g, 5.15 mmol) was added to the mixture and the flask was sealed with a rubber septum and secured with steel wire. The reaction was stirred at 110 ºC for 30 minutes. After 30 minutes, the dark purple reaction mixture was uncapped and poured into a 125 mL Erlenmeyer flask. Methanol (80 mL) was added to the flask causing an orange precipitate to appear and then the mixture was stirred for ten minutes at room temperature. The mixture was centrifuged (8 minutes at 7500 rpm) in portions in 50 mL centrifuge tubes. The supernatant was decanted and disposed of. The crude orange solid was washed, by the addition of methanol (40 mL) followed by mixing on the vortexer to break up the solid and sonication for 10 minutes. The mixture was then centrifuged for 8 minutes at 7500 rpm. This washing procedure was repeated once more with methanol (50 mL) and then a third time with acetone (50 mL). The solid was dried under vacuum for at least 6 hours to give a yellowish crude material (3.410 g). The crude material was analyzed by ^{1}H NMR and found to contain 52% Me_4CB[8], 32% Me_2CB[7], 5% CB[6], and the rest was unidentified oligomers and methylated CB[6] derivatives. This crude mixture was combined with **III-4** (1.425 g) and dissolved in 0.6 M HCl:66% formic acid (1:1 v:v; 20 mL). This mixture was loaded onto a column containing Dowex 50WX2-400 (Acros# 203045000) Ion Exchange resin. The column was eluted with 1:1

0.6 M HCl:66% formic acid (2 L), followed by 1:1 0.8 M HCl:66% formic acid (2 L), and finally 1:1 1.0 M HCl:66% formic acid (1 L, or until material stops eluting). We monitored the composition of the column fractions by ^{1}H NMR spectroscopy by adding **III-3** as a probe guest and observing the resonances in the 6-7 ppm region of the spectrum as described previously (*J. Am. Chem. Soc.* **2011**, *133*, 17966). The fractions containing Me_4CB[8] were collected and the solvent was removed by rotary evaporation. The resulting solid contained largely Me_4CB[8] with small amounts of CB[6] and methylated CB[6] derivatives. The resulting solid (0.950 g) was stirred in 3:1:0.25 acetic acid:formic acid:acetone (20 mL) for 2 d at 40 ºC, causing a precipitate to form. The solid was collected by centrifugation, rinsed with acetone, and dried under vacuum. This material was found to be nearly pure Me_4CB[8] by ^{1}H NMR analysis and was further purified by refluxing with activated carbon (1 g, Fisher C170-500) in water (250 mL) for 1 d. The carbon was filtered and the material was collected by rotary evaporation giving pure Me_4CB[8] as an off white solid (0.320 g, 0.231 mmol, 11% yield). M.p. > 350 $^\circ$C. IR (KBr, cm^{-1}): 1728s, 1466s, 1317m, 1230s, 1191m, 971m, 829m, 805m. ^{1}H NMR (400 MHz, D_2O, as Me_4CB[8]• **III-3**$_2$, RT): 5.80-5.74 (m, 16H), 5.59-5.50 (m, 12H), 4.41 (d, *J* = 16.3, 2H), 4.30 (d, *J* = 15.6, 4H), 4.24 (d, *J* = 15.5, 4H), 4.19 (d, *J* = 15.2, 4H), 1.86 (s, 6H), 1.85 (s, 6H). ^{13}C NMR (125 MHz, D_2O, RT, 1,4-dioxane as internal standard, **3** as guest): δ 157.8, 157.4, 156.7, 155.8, 132.9, 127.0, 78.5, 78.0, 73.3, 73.0, 72.4, 71.4, 70.9, 55.6, 53.5, 52.1, 49.9, 44.6, 42.8, 16.5, 15.7. ESI-MS (**III-3** as guest): *m/z* 761 ([M• **III-3** + 2H]$^{2+}$). HR ESI-MS (**III-3** as guest): *m/z* 761.28520 ([Me_4CB[8]• **III-3** + 2H]$^{2+}$, $C_{60}H_{70}N_{34}O_{16}^{2+}$, calcd, for 761.28545). X-ray crystal structure.

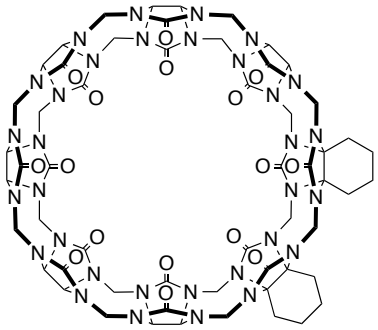

Compound $Cy_2CB[8]$. Compound **III-1** (2.000 grams, 2.06 mmol) and KI (0.460 g, 2.78 mmol) were combined in a 25 mL round-bottom flask with 6M aqueous HCl (10 mL). The mixture was stirred and sonicated until all clumps disappeared, approximately 2 minutes. To this mixture **III-2**$_{Cy}$ (1.442 g, 5.15 mmol) was added and the reaction was sealed with a rubber septum and secured with steel wire. The reaction mixture was stirred at 110 ºC for 30 minutes. After 30 minutes, the reaction was uncapped and the resulting dark purple mixture was poured into a 125 mL Erlenmeyer flask. Methanol (80 mL) was added, causing a light orange precipitate to appear, and the mixture stirred at room temperature for 10 minutes. The mixture was centrifuged (8 minutes at 7500 rpm) in portions in 50 mL centrifuge tubes. The supernatant was decanted and disposed of. The remaining orange solid was washed, by the addition of methanol (40 mL) followed by mixing on the vortexer to break up the solid and sonication for 10 minutes. The mixture was then centrifuged for 8 minutes at 7500 rpm. This washing procedure was repeated once more with methanol (50 mL) and then a third time with acetone (50 mL). The solid was dried under vacuum for at least 6 hours to give a yellowish crude material (3.974 g). The crude material was analyzed by ^{1}H NMR and found to contain 31% $Cy_2CB[8]$, 26% CyCB[7], and 42% CB[6] and CB[6] derivatives. The crude solid was combined with **III-4** (1.424 g, 3.27 mmol) and dissolved in 1:1 0.6 M HCl:66% formic acid (15 mL) by sonicating for 5 minutes and then gently heating until a clear brown solution was obtained. This solution was loaded onto a column containing Dowex 50WX2-400 resin. The compound was eluted by increasing HCl concentration: first 1:1 0.6 M HCl:66% formic acid (1 L),

then 1:1 0.8 M HCl:66% formic acid (1 L), and finally 1:1 1.0 M HCl:66% formic acid (1.5 L). We monitored the composition of the column fractions by 1H NMR spectroscopy by adding **III-3** as a probe guest and observing the resonances in the 6-7 ppm region of the spectrum as described previously (*J. Am. Chem. Soc.* **2011**, *133*, 17966). Each eluent was collected in 250 mL fractions and selected fractions were combined and concentrated by rotary evaporation together. The improved material (325 mg) was stirred in 3:1:0.25 acetic acid:formic acid:acetone (9.3 mL) for 2 d at 40 ºC, causing a precipitate to form. The solid was collected by centrifugation, rinsed with acetone (20 mL), and dried under vacuum. This material was found to be approximately 98% Cy_2CB[8] and was further purified by refluxing with activated carbon (0.5 g) in water (200 mL) for 1 d. The carbon was removed by filtration and the filtrate was concentrated by rotary evaporation to give Cy_2CB[8] as an off-white solid (123 mg, 0.086 mmol, 4% yield). M.p. > 350 °C. IR (KBr, cm^{-1}): 1711s, 1455m, 1312m, 1225s, 1187s, 969m, 800s. ^{1}H NMR (400 MHz, D_2O, as Cy_2CB[8]• **III-3**$_2$, RT): 6.35 (s, 4H), 5.93 (d, *J* = 15.2, 4H), 5.79 (d, *J* = 15.4, 4H), 5.77 (d, *J* = 15.7, 4H), 5.65-5.58 (m, 12H), 5.53 (d, *J* = 8.88, 2H), 5.48 (d, *J* = 8.88, 2H), 4.33 (d, *J* = 15.3, 4H), 4.27 (d, *J* = 15.5, 4H), 4.25 (d, *J* = 15.7, 4H), 4.18 (s, excess **III-3**, 4H), 3.74 (s, 4H), 2.31 (s, 4H), 2.20 (s, 4H), 1.47 (s, 8H). ^{13}C NMR (125 MHz, D_2O, RT, 1,4-dioxane as internal standard, **III-3** as guest): δ 157.8, 157.4, 156.8, 156.4, 133.5, 129.5, 127.0, 77.4, 76.8, 73.3, 72.5, 71.5, 70.9, 55.7, 53.6, 49.9, 42.7, 42.2, 22.7, 21.6, 13.5, 13.1. ESI-MS (**III-3** as guest): *m/z* 788 ([M• **III-3** + 2H]$^{2+}$). HR ESI-MS (**III-3** as guest): *m/z* 787.80160 ([Cy_2CB[8]• **III-3** + 2H]$^{2+}$, $C_{64}H_{74}N_{34}O_{16}^{2+}$, calcd, for 787.80232). X-ray crystal structure.

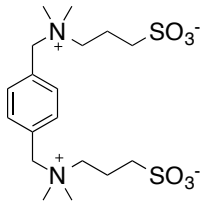

***Compound* III-*4*.** N, N, N, N-tetramethyl-1,4-benzenedimethanamine (14.700 g, 0.076 mol) was dissolved in methanol (120 mL) in a 500 mL round bottom flask and stirred at 0 ºC for 15 min. Propane sultone (28.009 g, 0.229 mol) was dissolved in methanol (120 mL) and this solution was slowly added to the flask over 30 minutes. The reaction was removed from the ice bath and stirred at RT for 24 h. The resulting precipitate was collected by vacuum filtration and the solid was washed with methanol (100 mL) and dried under high vacuum to give **III-4** as a white solid (25.163 g, 0.058 mol, 76% yield). M.p. = 300-302 ºC. IR (ATR, cm^{-1}): 1486w, 1208m, 1180s, 1037s, 884w, 877w, 750w, 738w. ^{1}H NMR (400 MHz, D_2O) 7.70 (s, 4H), 4.61 (s, 4H), 3.52-3.48 (m, 4H), 3.10 (s, 12H), 2.99 (t, 4H), 2.37-2.29 (m, 4H). ^{13}C NMR (125 MHz, D_2O, RT, 1,4-dioxane as internal standard) δ 133.0, 129.0, 66.9, 62.0, 49.2, 46.7, 17.7. ESI-MS: *m/z* 437 ($[M + H]^+$). HR ESI-MS: *m/z* 437.1765 ($[M + H]^+$, $C_{18}H_{33}N_2O_6S_2^+$, calcd. for 437.1780).

Attempted reactions between III-1 and III-11 in various acids. Compound **III-1** (75 mg, 0.077 mmol) and KI (17 mg, 0.104 mmol) were placed in a glass vial. Acid (2 M, 4 M, 6 M HCl; 3 M, 6 M, 9 M H_2SO_4, 0.38 mL) was added and the mixture stirred until hexamer either dissolved or became a smooth heterogeneous mixture. Compound **III-11** (42 mg, 0.093 mmol) was added and the mixture stirred at 80 ºC for 30 min. The reaction mixture was precipitated by the addition of 2 mL methanol and centrifuged. The collected solids were dried by vacuum. Each mixture was analyzed by ^{1}H NMR using **III-3** as probe to determine the composition of the mixture.

Attempted reactions between III-1 and increasing equivalents of III-10. Compound **III-1** (75 mg, 0.077 mmol) and KI (17 mg, 0.104 mmol) were placed in a glass vial. H_2SO_4

(9M, 0.38 mL) was added and the mixture stirred until **III-1** either dissolved or became a smooth heterogeneous mixture. Compound **III-11** (1.2, 2, or 5 equivalents) was added and the mixture stirred at 80 ºC for 30 min. The mixture was precipitated by the addition of 2 mL methanol and centrifuged. The collected solids were dried under high vacuum. Each mixture was analyzed by ^{1}H NMR using **III-3** as a probe to determine the composition of the mixture.

Procedure for binding competition experiments between Me$_4$CB[8], CB[8], and guests. Stock solutions of Me$_4$CB[8], CB[8], and guests in 50 mM sodium acetate buffer (pH = 4.74) were prepared and calibrated by ^{1}H NMR spectroscopy using an internal standard of known concentration. Using the calculated concentrations, equimolar amounts of Me$_4$CB[8] and CB[8] were combined in an NMR tube. To this mixture, 1 equivalent of guest solution was added so that each of the three components was present at a 50 μM concentration. The mixture was shaken for a minute and then allowed to sit at room temperature for an hour. The mixture was analyzed by ^{1}H NMR spectroscopy (800 MHz). Integrals for the relevant ^{1}H NMR resonances were obtained using MestReNova deconvolution software.

Procedure for constructing phase solubility diagrams for drugs with CB[8] or Me$_4$CB[8]. To a solution of a known concentration of Me$_4$CB[8] or CB[8] in either 50 mM sodium phosphate buffer (pH = 7.40) or 50 mM sodium acetate buffer (pH = 4.74) an excess (3 eq.) of solid drug was added. The heterogeneous mixtures were stirred at room temperature for 2d. Each solution was then filtered through a sterile syringe filter with a 0.2 μm polyethersulfone membrane into a clean vial. Each solution was analyzed by ^{1}H NMR spectroscopy (600 MHz) using either methane sulfonic acid or 1,4-dioxane

as an internal standard. The concentration of solubilized drug was calculated by comparison of the integrals for selected ^{1}H NMR resonances of drug to the internal standard.

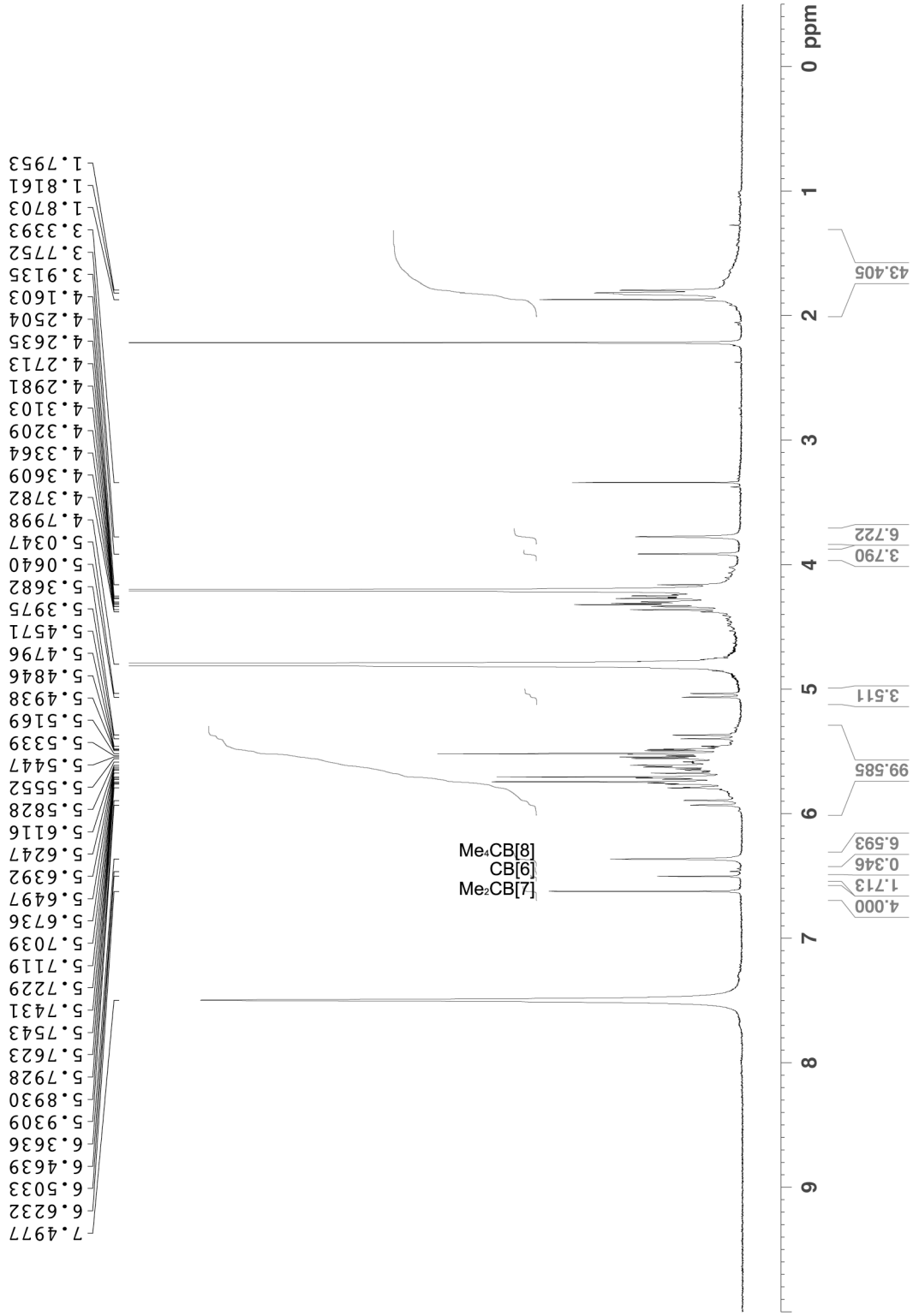

Figure III-S1. ^{1}H NMR spectrum recorded (400 MHz, D2O, RT) for the crude reaction mixture from the reaction between **III-1** and **III-2**$_{Me}$ in the presence of **III-3** as a probe. ^{1}H NMR integration of the **III-3** binding region (6-7 ppm) allows us to determine the contents of the crude mixture (32% Me_2CB[7], 5% CB[6], 52% Me_4CB[8] and 11% unidentified).

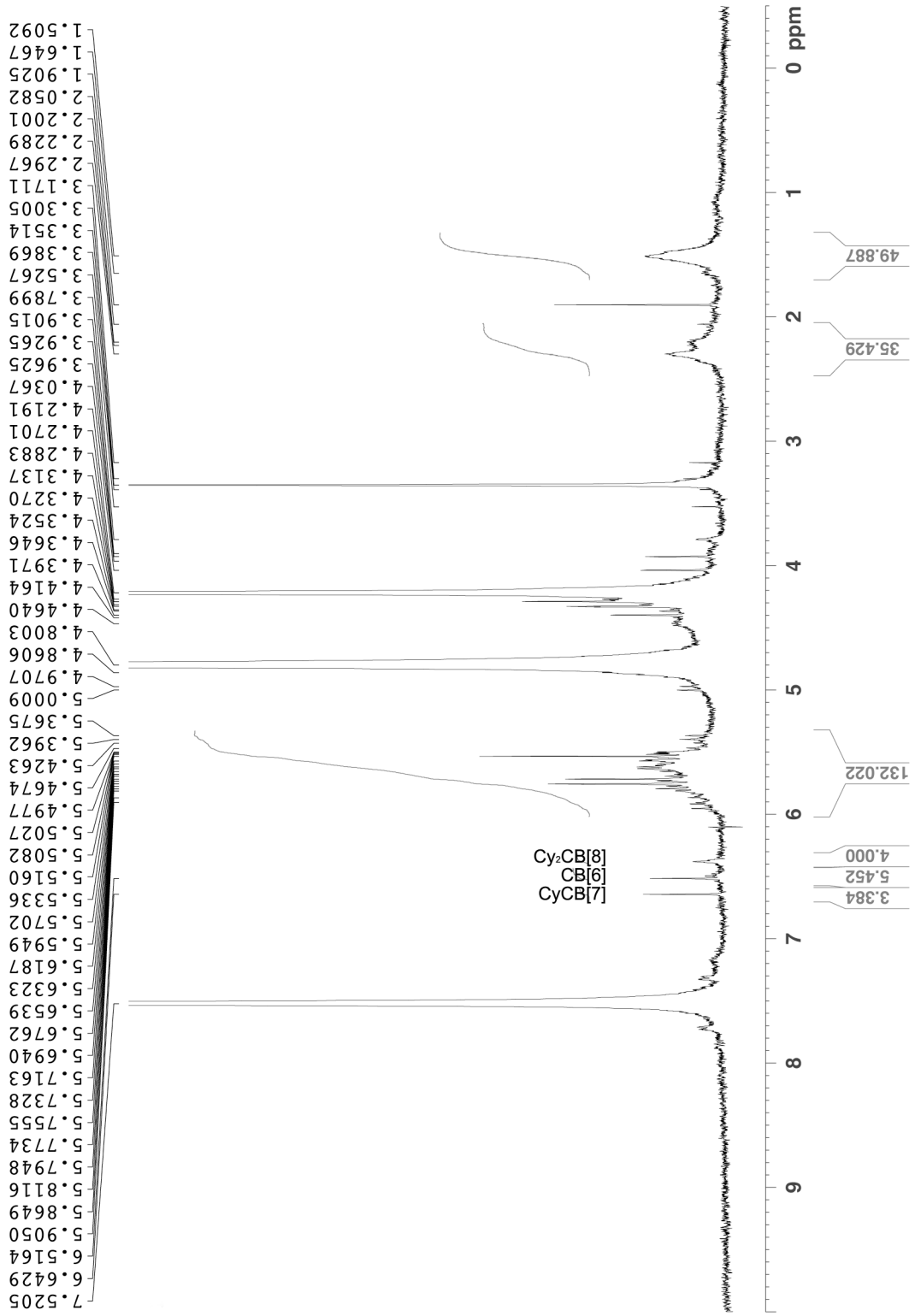

Figure III-S2. ^{1}H NMR spectrum recorded (400 MHz, D2O, RT) for the crude reaction mixture from the reaction between **III-1** and **III-2$_{Cy}$** in the presence of **III-3** as a probe. ^{1}H NMR integration of the **III-3** binding region (6-7 ppm) allows us to determine the contents of the crude mixture (26% CyCB[7], 42% CB[6], and 31% Cy_2CB[8]).

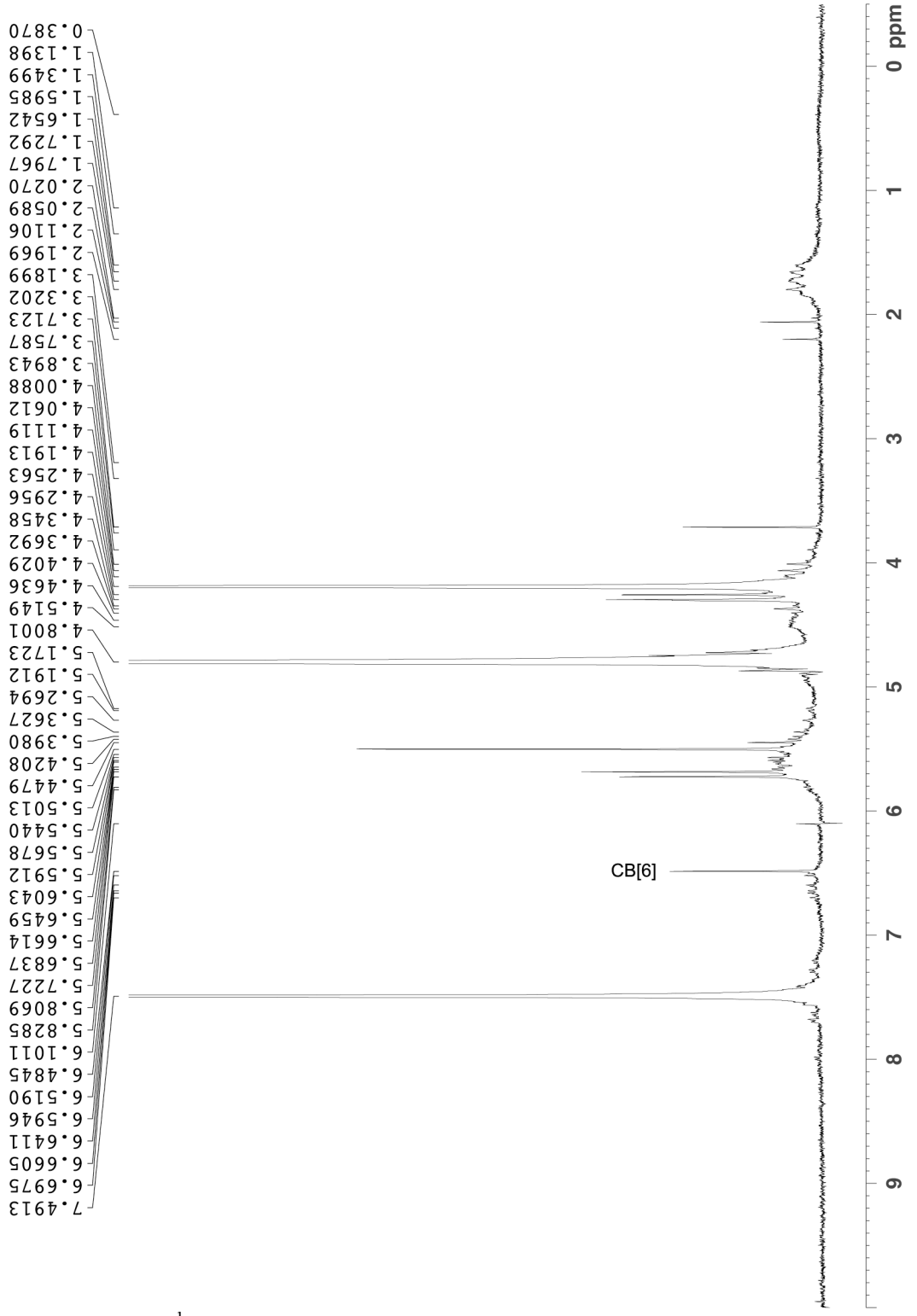

Figure III-S3. ^{1}H NMR spectrum recorded (400 MHz, D_2O, RT) for the crude reaction mixture from the attempted reaction between **III-1** and **III-11** in the presence of **III-3** as a probe. Observation of the **III-3** binding region (6-7 ppm) allows us to determine the contents of the crude mixture. This spectrum shows that no Me_4CB[8] formed under these conditions.

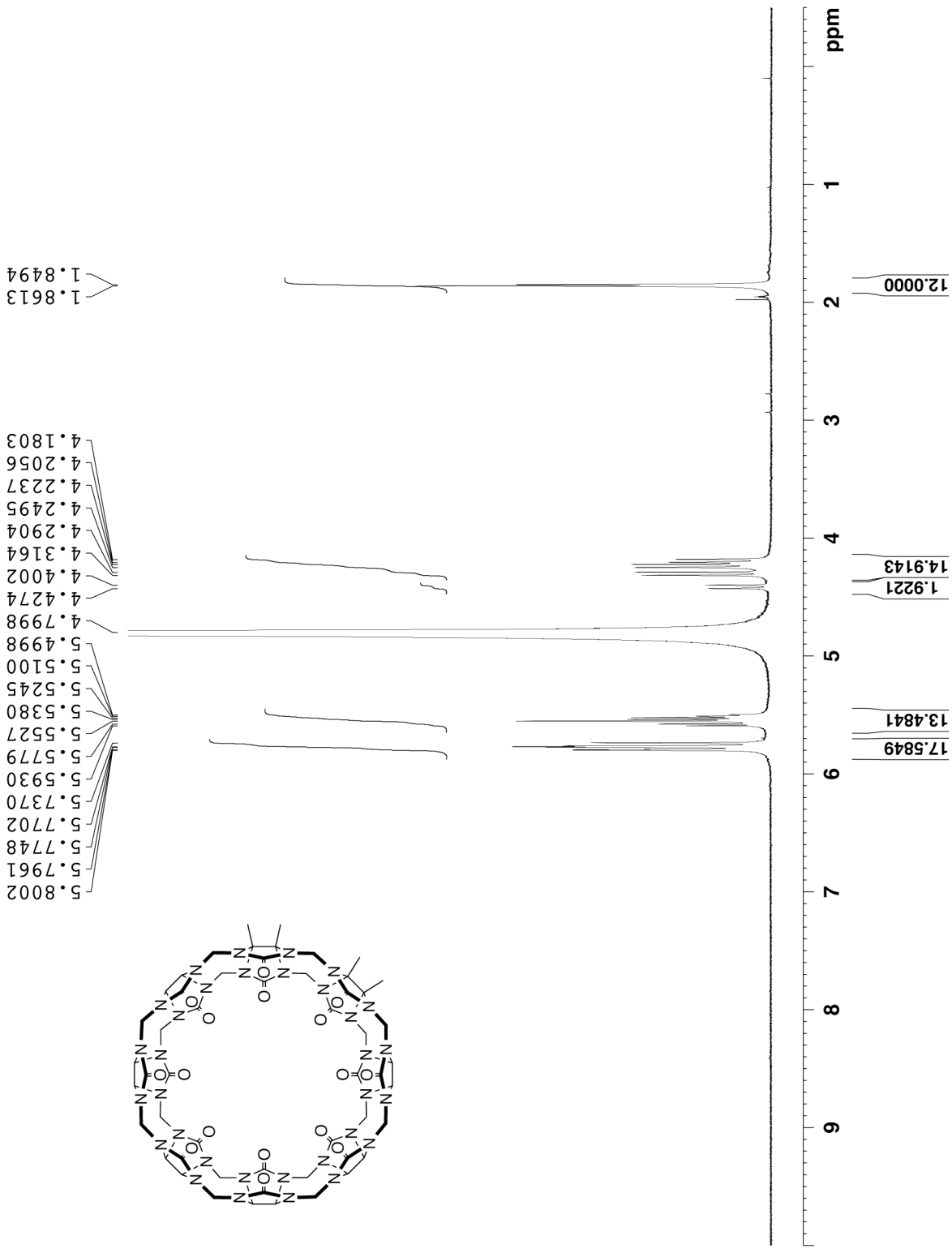

Figure III-S4. ^{1}H NMR spectrum (D_2O, 600 MHz, RT) recorded for free Me_4CB[8].

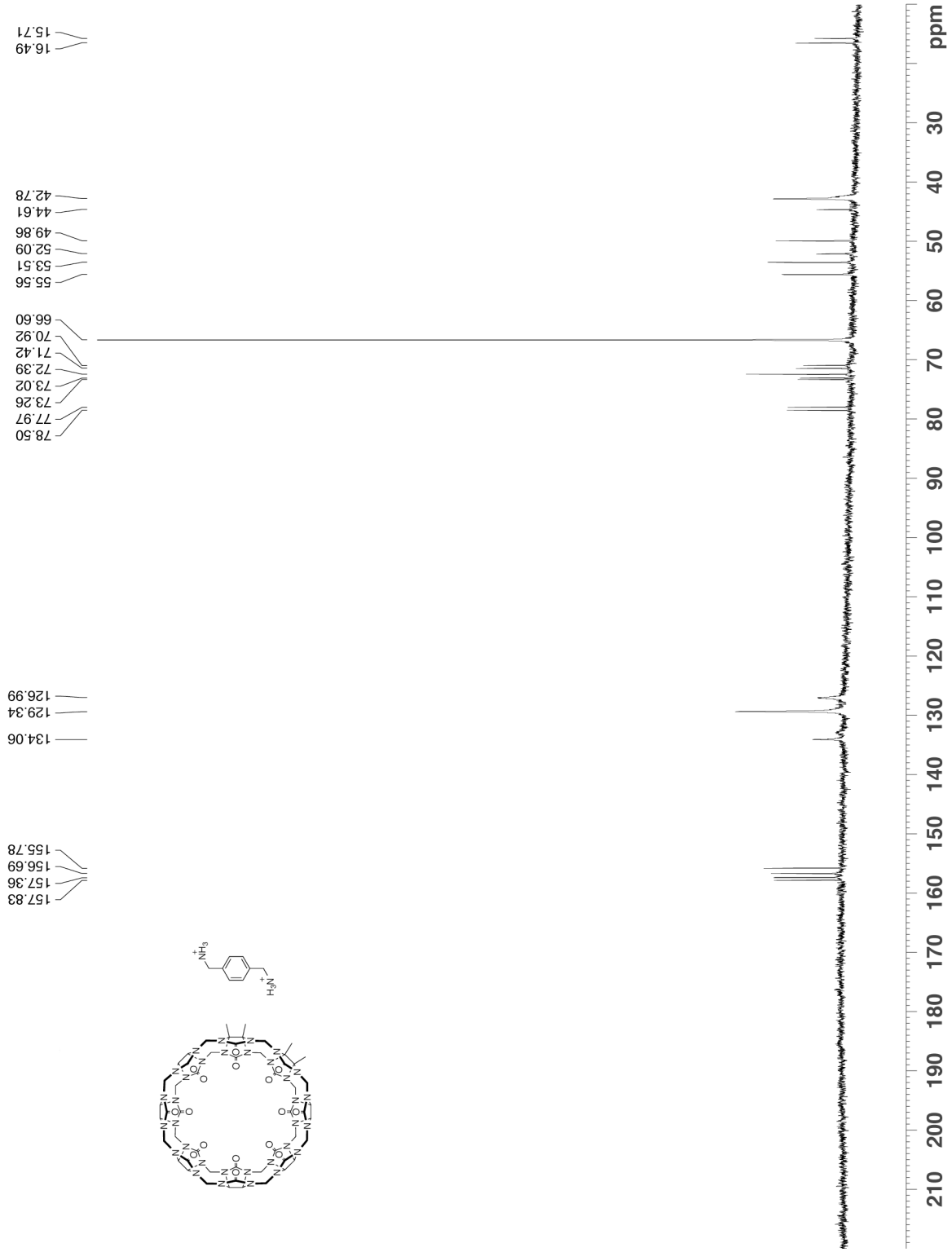

Figure III-S5. ^{13}C NMR spectrum (D_2O, 125 MHz, rt) recorded for Me_4CB[8]• **III-3**$_2$.

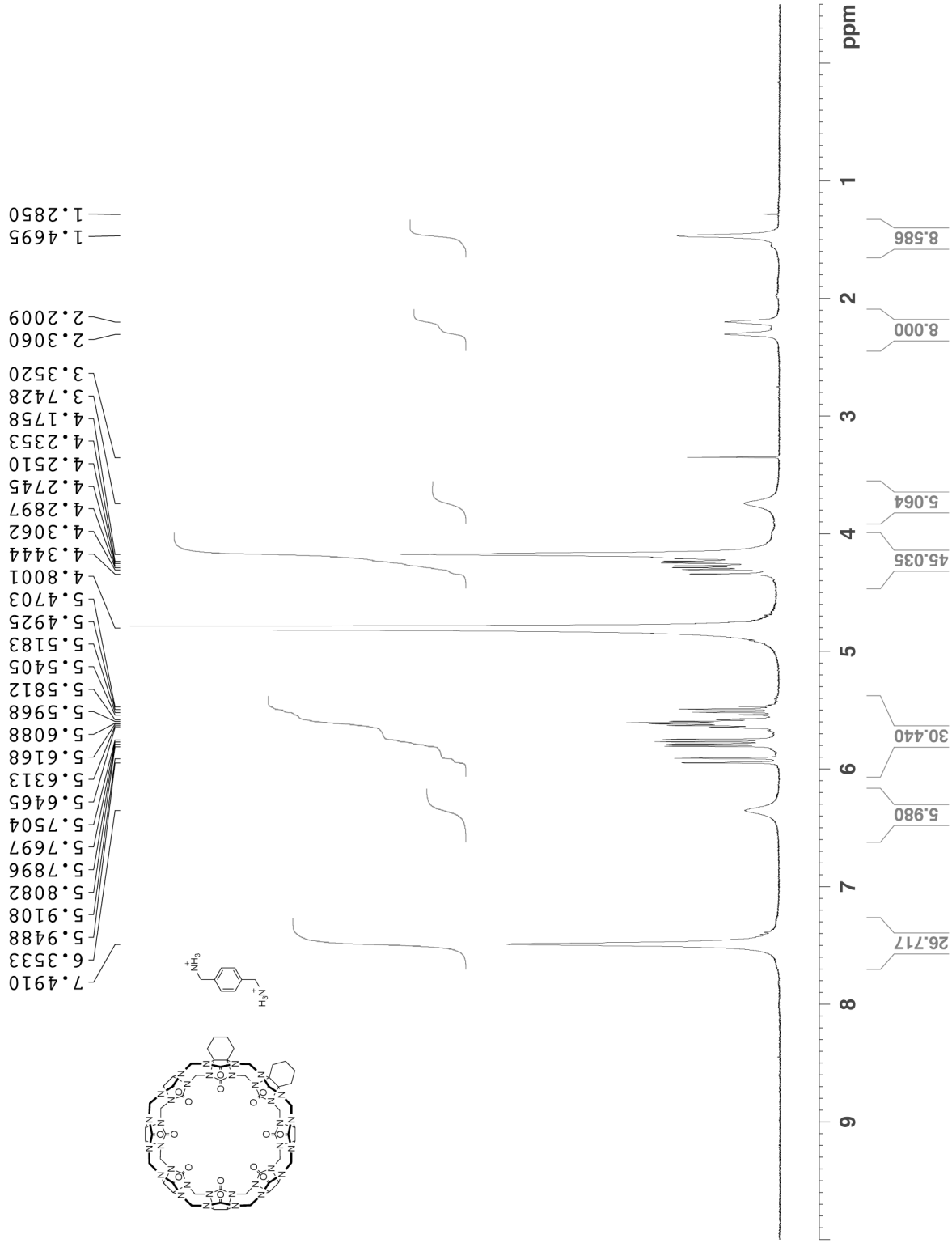

Figure III-S6. ^{1}H NMR (400 MHz, D_2O, RT) recorded for $Cy_2CB[8]$ in the presence of excess **III-3** as probe.

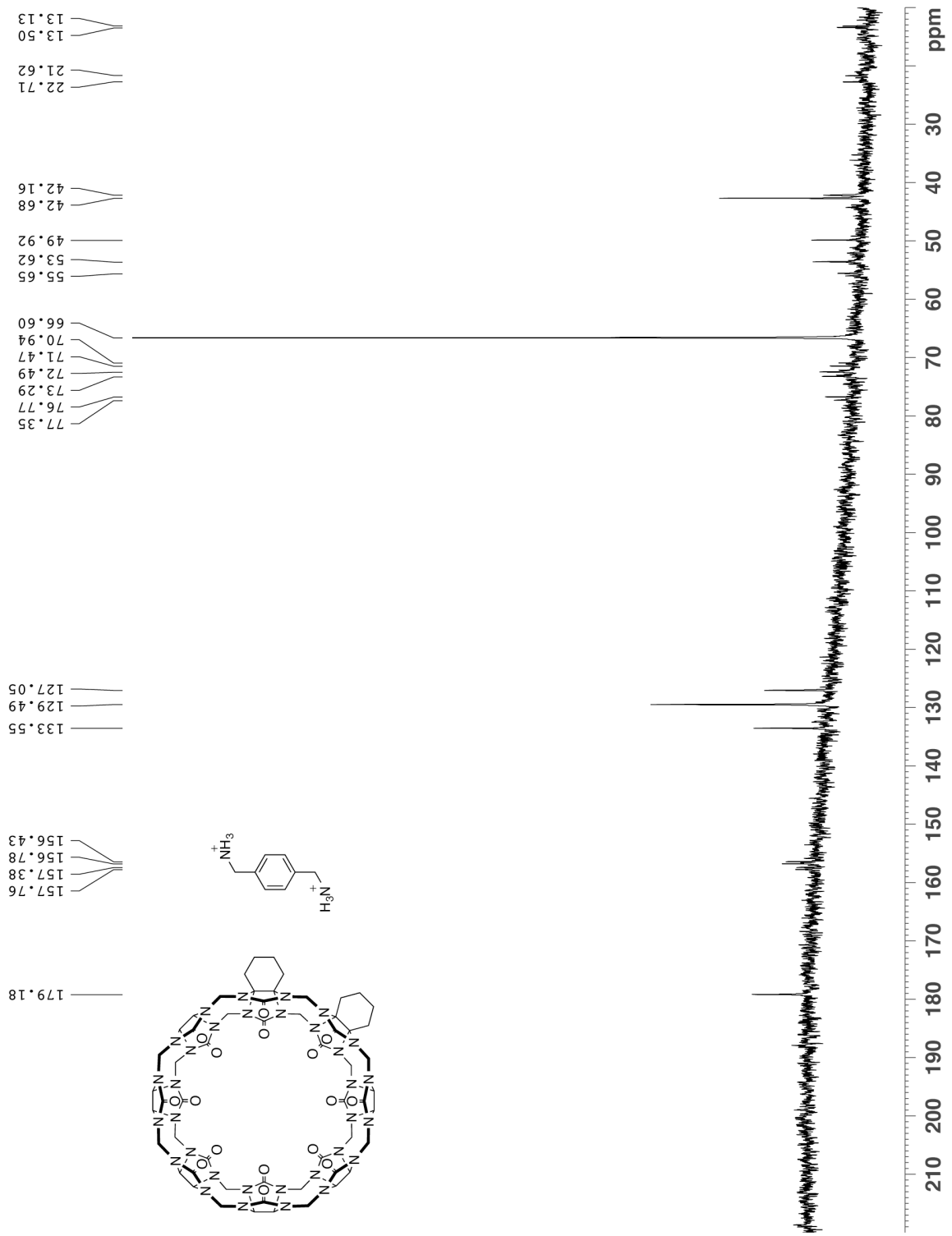

Figure III-S7. ^{13}C NMR (125 MHz, D_2O, RT) recorded for $Cy_2CB[8]$• **III-3** in the presence of 1,4-dioxane as internal standard.

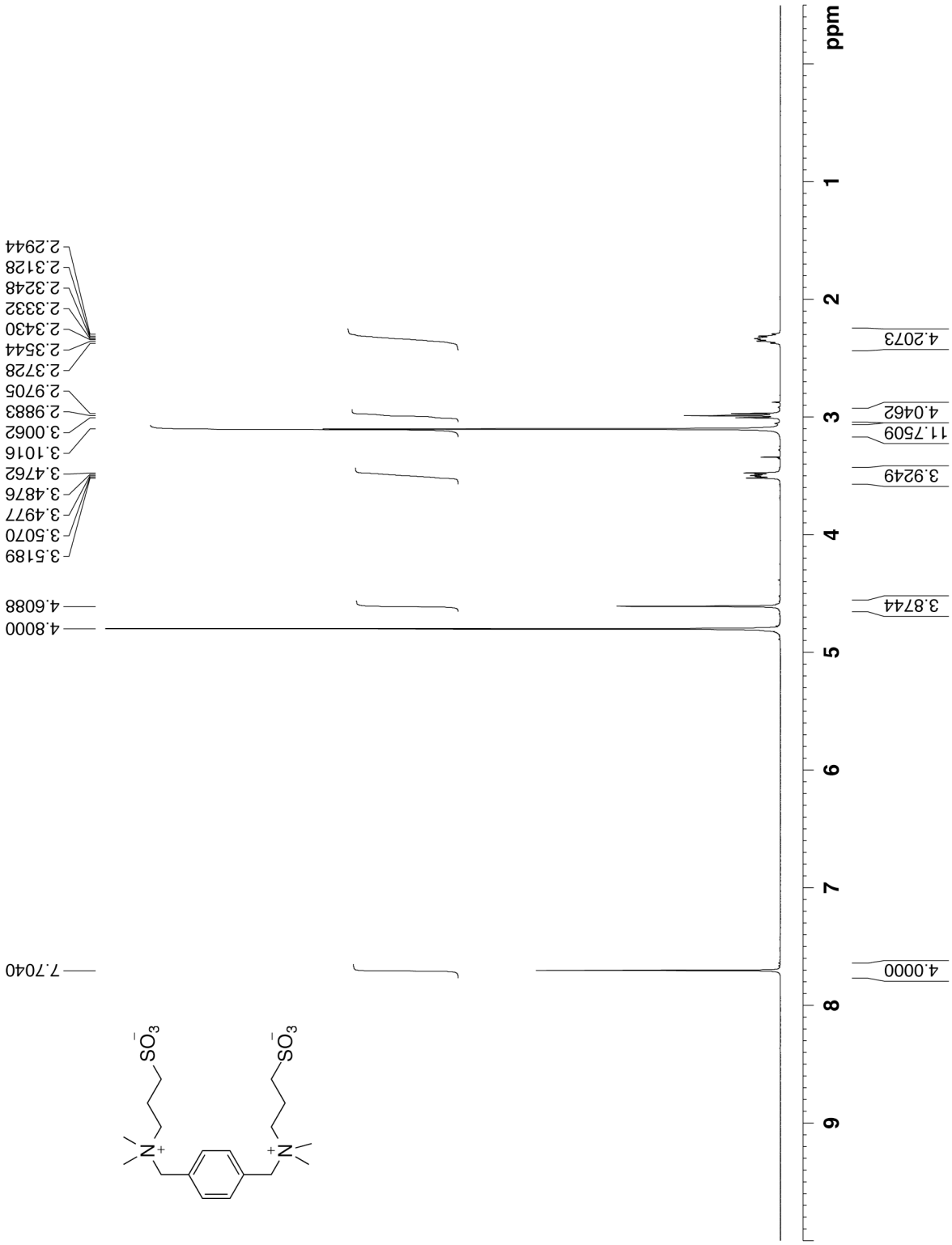

Figure III-S8. ^{1}H NMR (400 MHz, D_2O, RT) recorded for **III-4**.

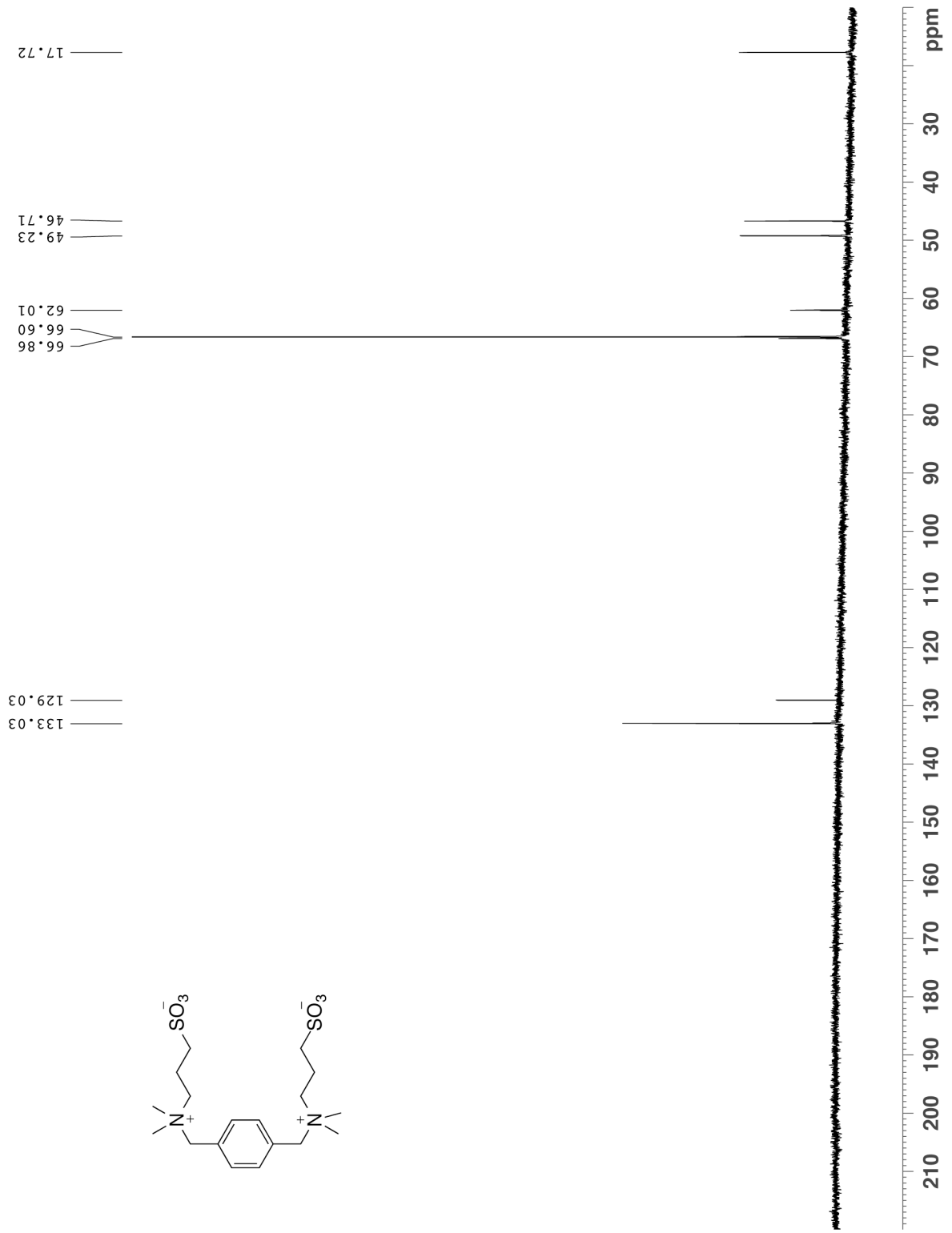

Figure III-S9. ^{13}C NMR (125 MHz, D_2O, RT) recorded for **III-4**.

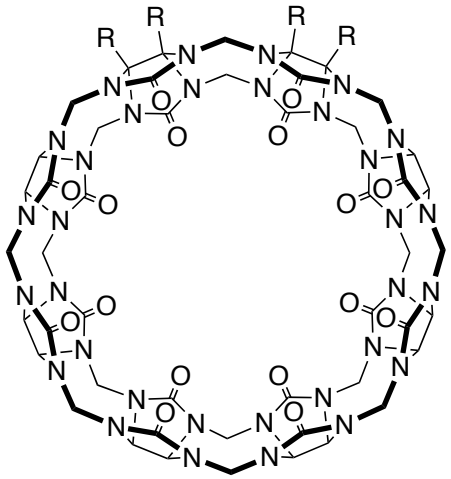

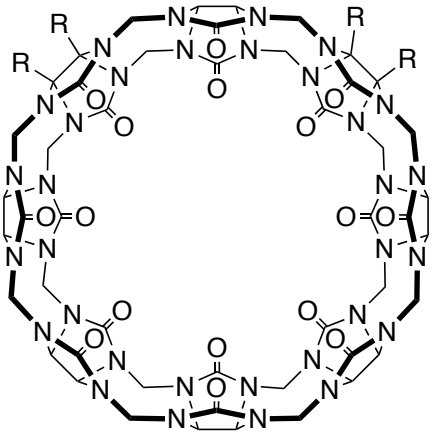

Symmetry:	C_{2v}	C_{2v}
^{13}C C=O resonances:	4 (2:2:2:2 ratio)	5 (1:2:2:2:1 ratio)
CH_2 resonances:	5 (1:2:2:2:1 ratio)	4 (2:2:2:2 ratio)

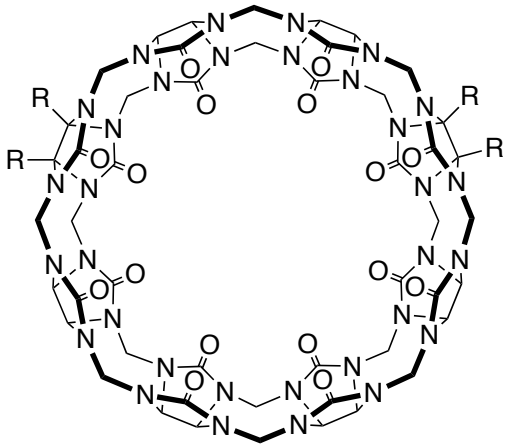

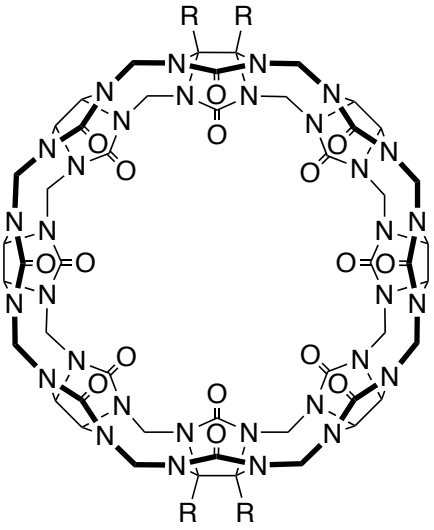

Symmetry:	C_{2v}	D_{2h}
^{13}C C=O resonances:	4 (2:2:2:2 ratio)	3 (2:4:2 ratio)
CH_2 resonances:	5 (1:2:2:2:1 ratio)	2 (4:4 ratio)

Figure III-S10. Enumeration of the structures of the four different $Me_4CB[8]$ isomers, their symmetry properties and the expected ^{13}C and ^{1}H resonance patterns.

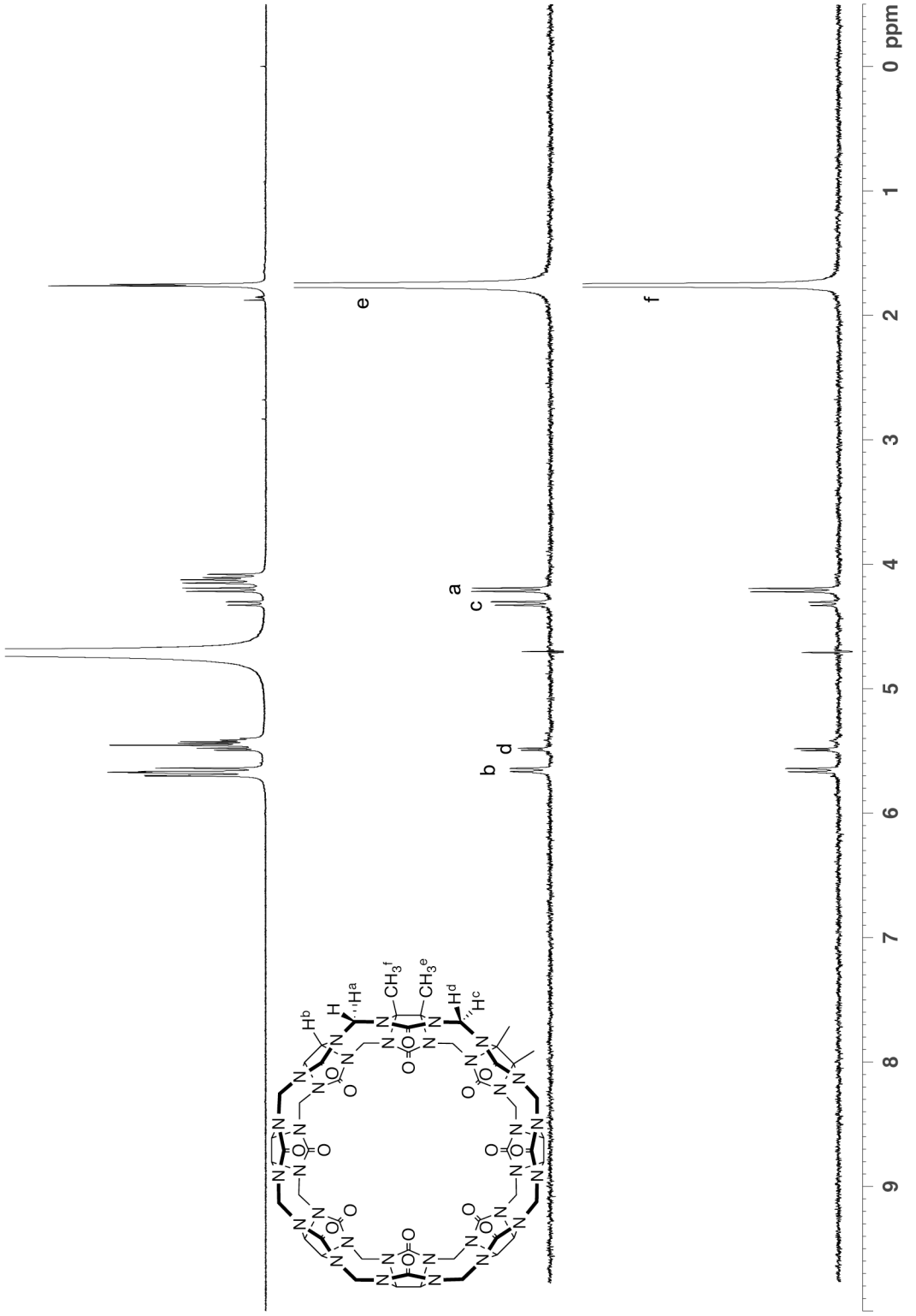

Figure III-S11. a) ^{1}H NMR (600 MHz, D_2O, RT) recorded for $Me_4CB[8]$. 1D selective nuclear Overhauser effect ^{1}H NMR spectrum recorded for $Me_4CB[8]$ irradiated at: b) 1057.40 Hz and c) 1050.07 Hz.

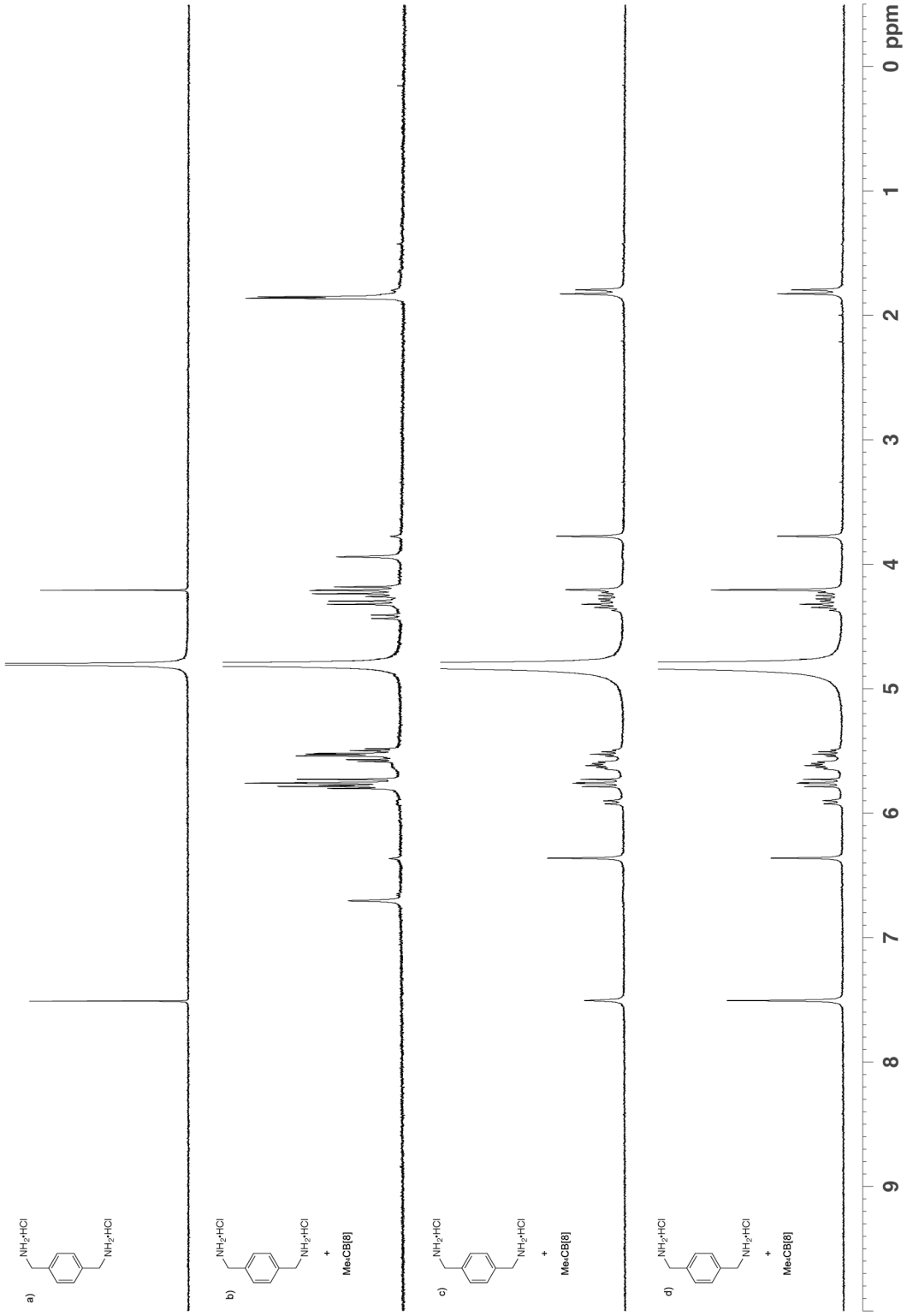

Figure III-S12. ^{1}H NMR spectra recorded (D_2O, 400 MHz, RT) for: a) **III-3** (0.3 mM), b) a 1:1 mixture of $Me_4CB[8]$ (0.3 mM) and **III-3** (0.3 mM), c) a 1:2 mixture of $Me_4CB[8]$ (0.3 mM) and **III-3** (0.6 mM), and d) a 1:3 mixture of $Me_4CB[8]$ (0.3 mM) and **III-3** (0.9 mM).

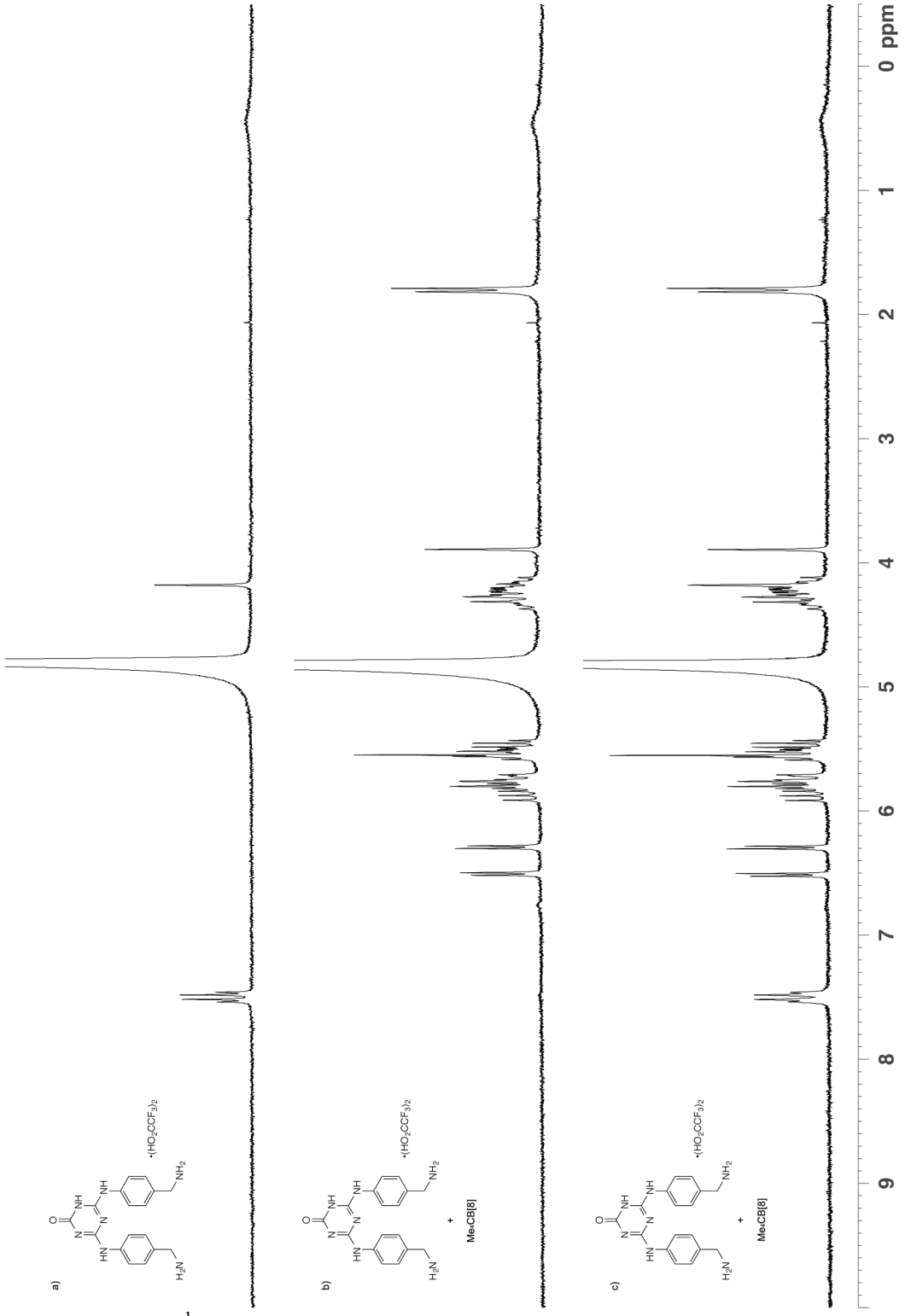

Figure III-S13. ^{1}H NMR spectra recorded (D_2O, 400 MHz, RT) for: a) **III-12** (0.3 mM), b) a 1:1 mixture of Me_4CB[8] (0.3 mM) and **III-12** (0.3 mM), and c) a 1:2 mixture of Me_4CB[8] (0.3 mM) and **III-12** (0.6 mM).

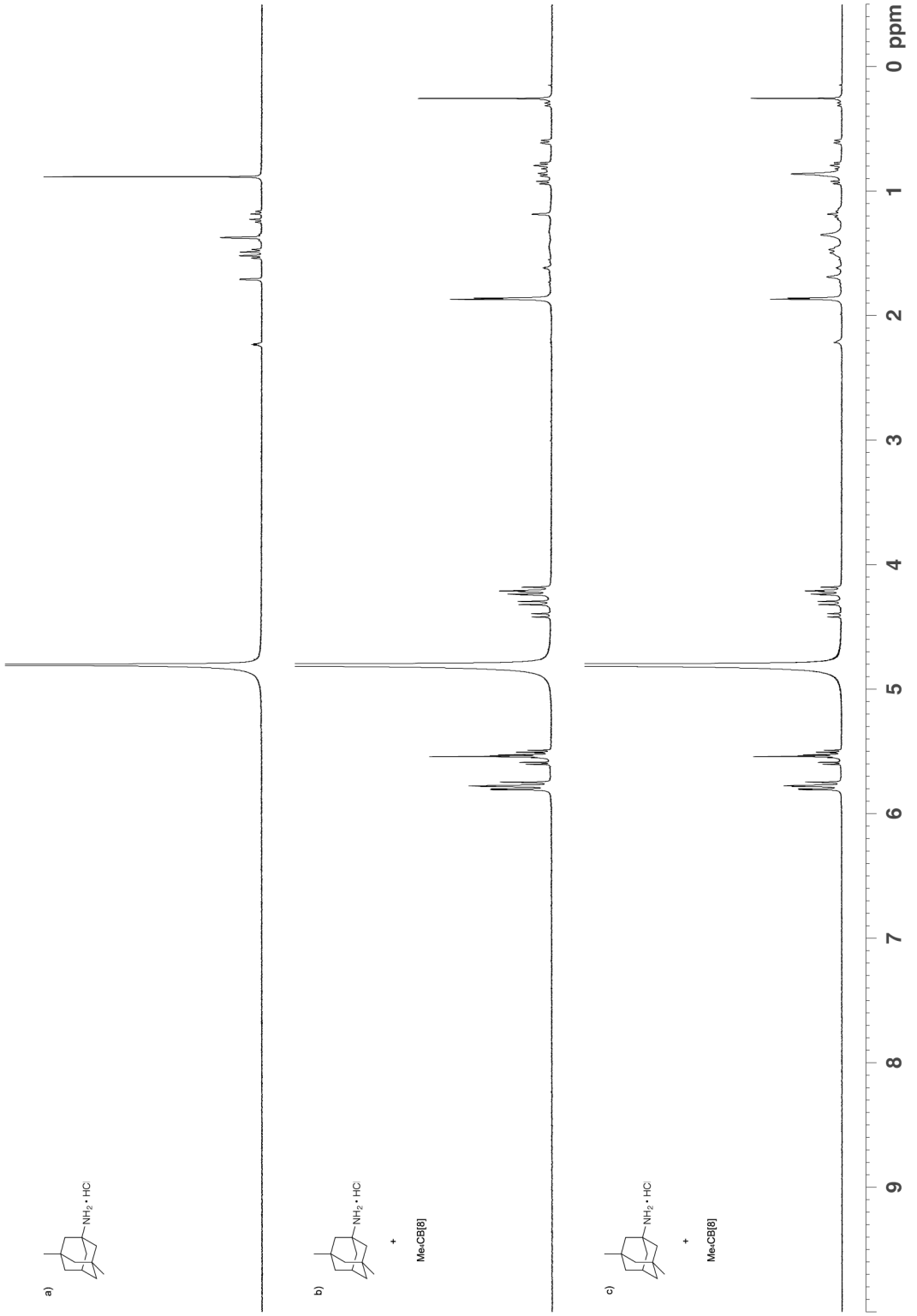

Figure III-S14. ^{1}H NMR spectra recorded (D_2O, 400 MHz, RT) for : a) **III-14** (0.3 mM), b) a 1:1 mixture of Me_4CB[8] (0.3 mM) and **III-14** (0.3 mM), and c) a 1:2 mixture of Me_4CB[8] (0.3 mM) and **III-14** (0.6 mM).

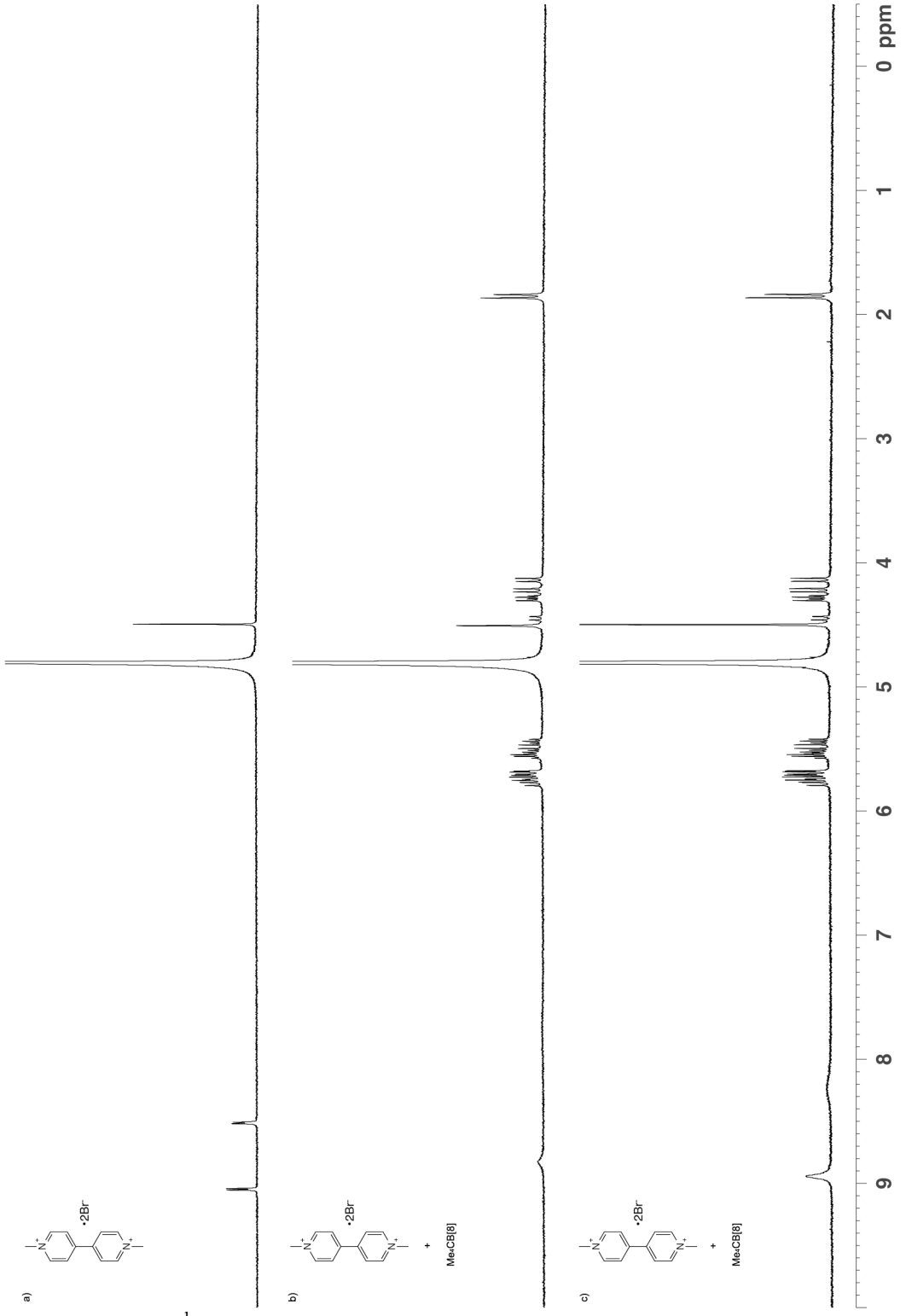

Figure III-S15. ^{1}H NMR spectra recorded (D_2O, 400 MHz, RT) for : a) **III-16** (0.3 mM), b) a 1:1 mixture of $Me_4CB[8]$ (0.3 mM) and **III-16** (0.3 mM), and c) a 1:2 mixture of $Me_4CB[8]$ (0.3 mM) and **III-16** (0.6 mM).

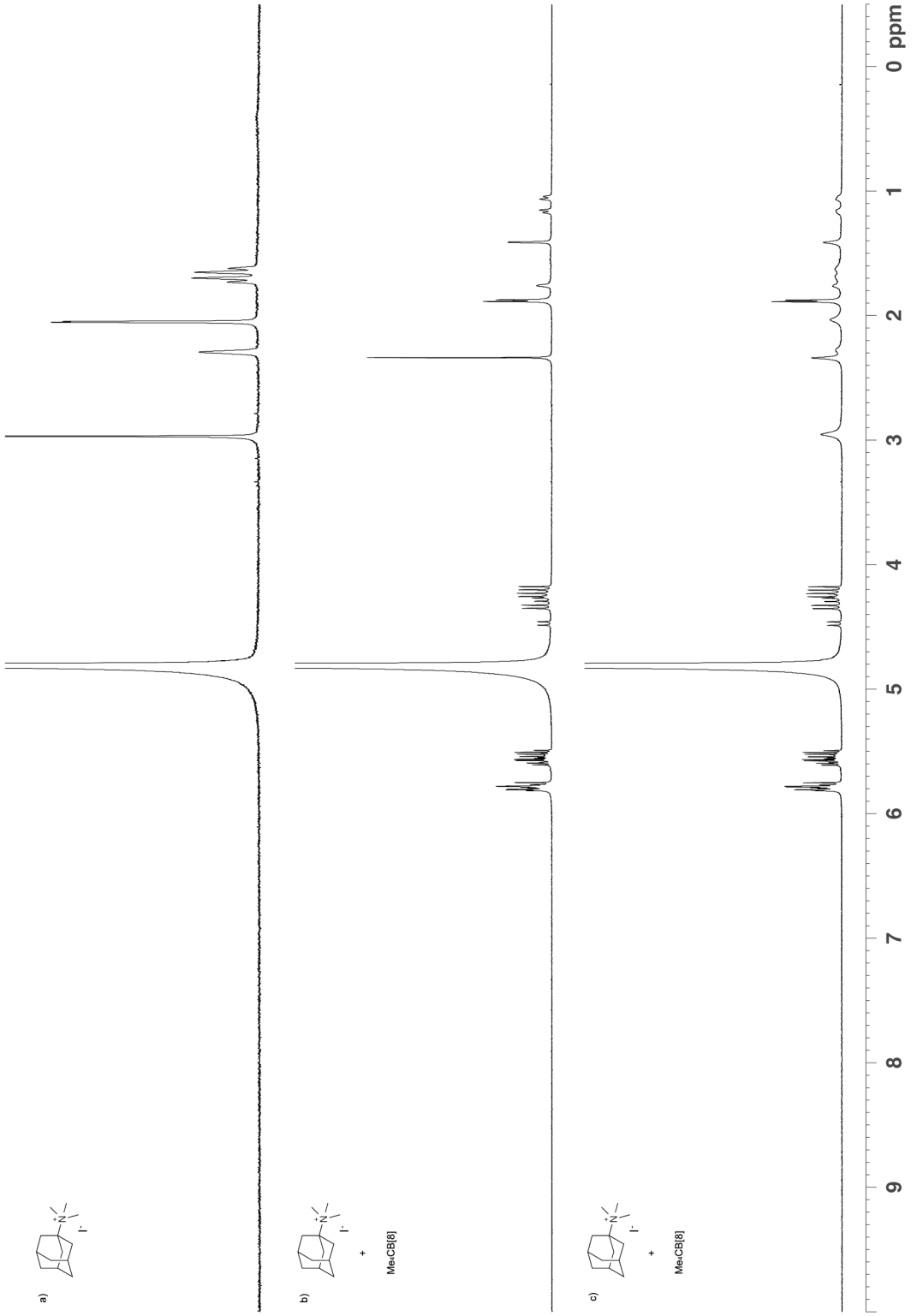

Figure III-S16. ^{1}H NMR spectra recorded (D_2O, 400 MHz, RT) for : a) **III-13** (0.3 mM), b) a 1:1 mixture of Me_4CB[8] (0.3 mM) and **III-13** (0.3 mM), and c) a 1:2 mixture of Me_4CB[8] (0.3 mM) and **III-13** (0.6 mM).

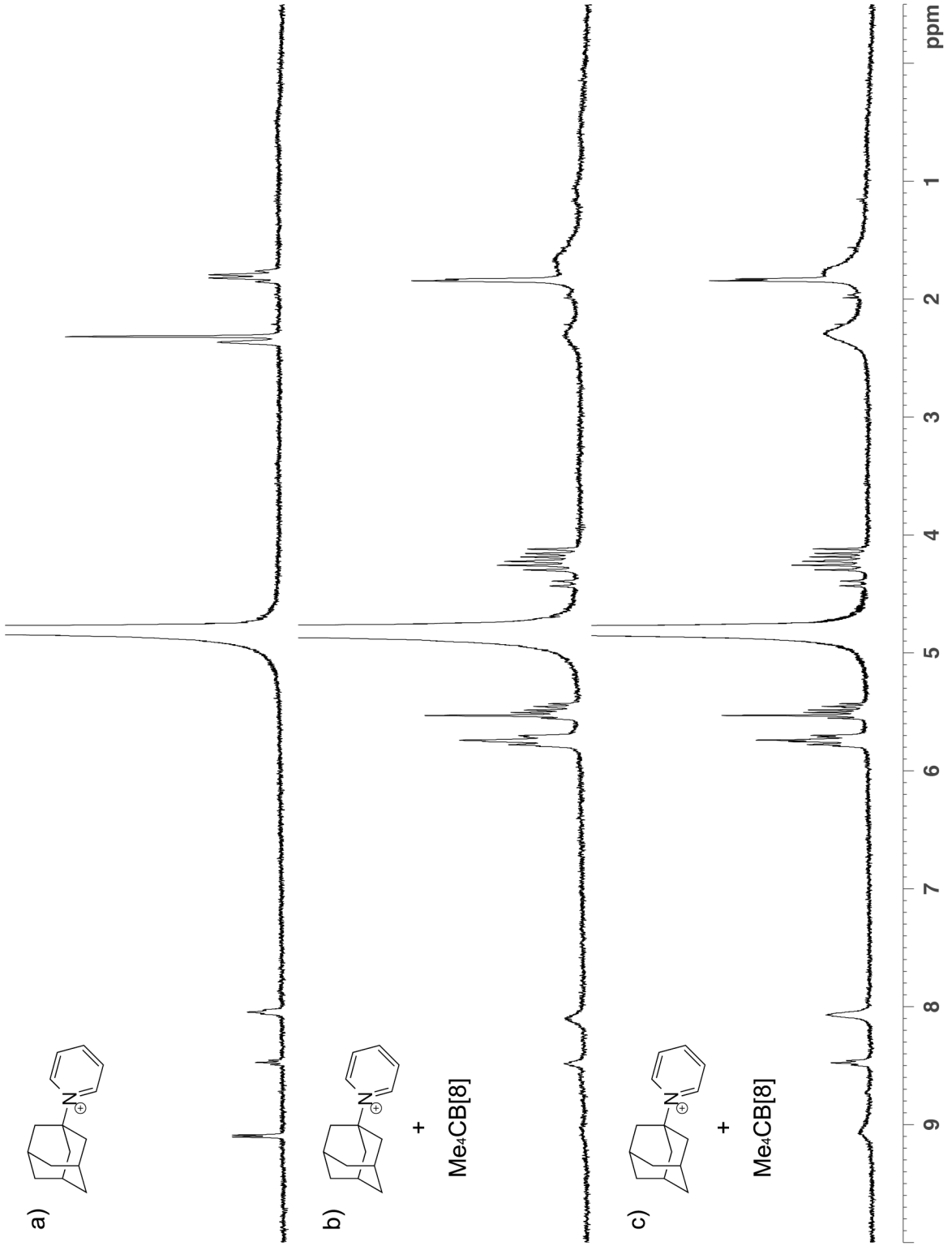

Figure III-S17. ^{1}H NMR spectra recorded (D_2O, 400 MHz, RT) for : a) **III-15** (0.3 mM), b) a 1:1 mixture of $Me_4CB[8]$ (0.3 mM) and **III-15** (0.3 mM), and c) a 1:2 mixture of $Me_4CB[8]$ (0.3 mM) and **III-15** (0.6 mM).

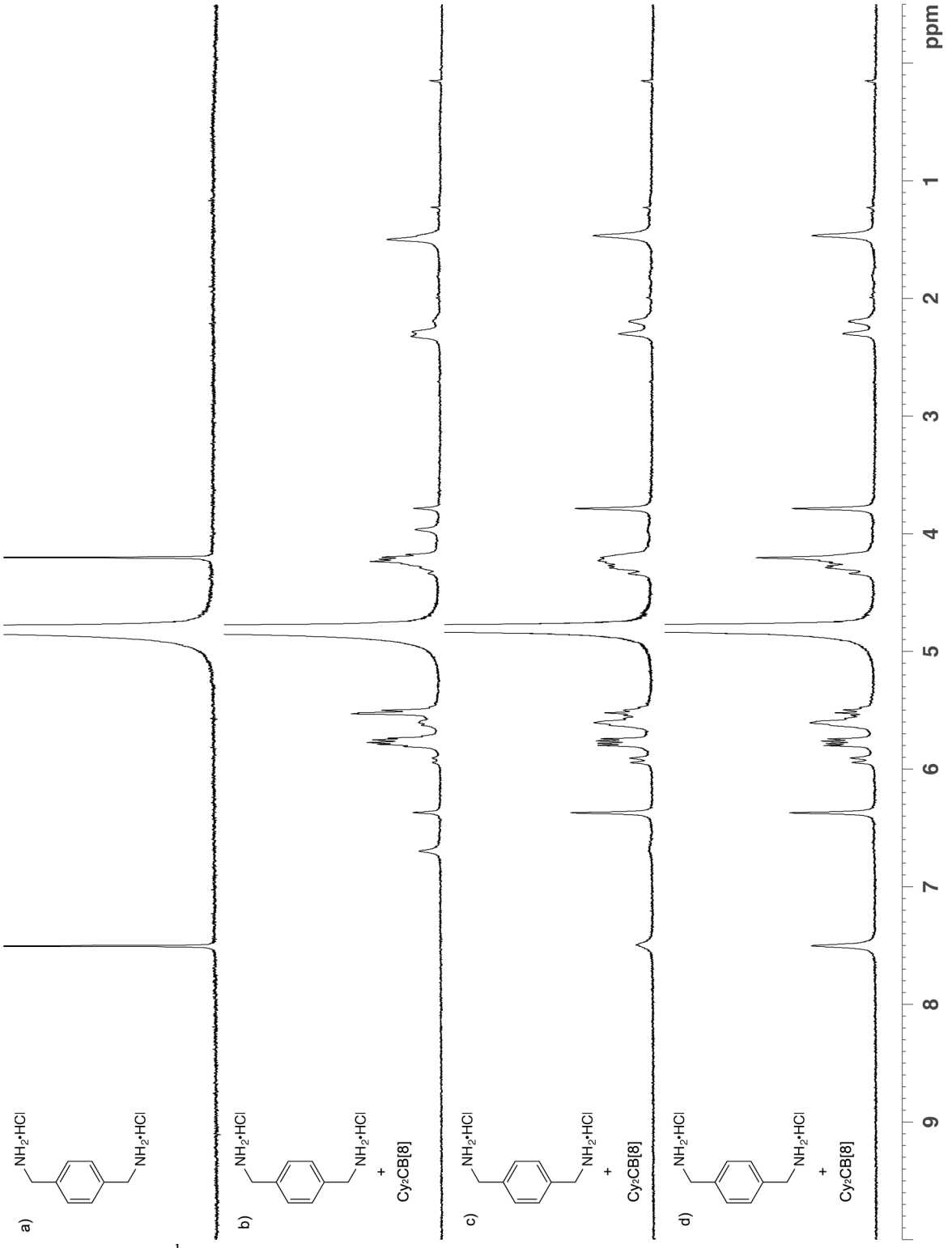

Figure III-S18. ^{1}H NMR spectra recorded (D_2O, 400 MHz, RT) for : a) **III-3** (0.3 mM), b) a 1:1 mixture of $Cy_2CB[8]$ (0.3 mM) and **III-3** (0.3 mM), c) a 1:2 mixture of $Cy_2CB[8]$ (0.3 mM) and **III-3** (0.6 mM), and d) a 1:3 mixture of $Cy_2CB[8]$ (0.3 mM) and **III-3** (0.9 mM).

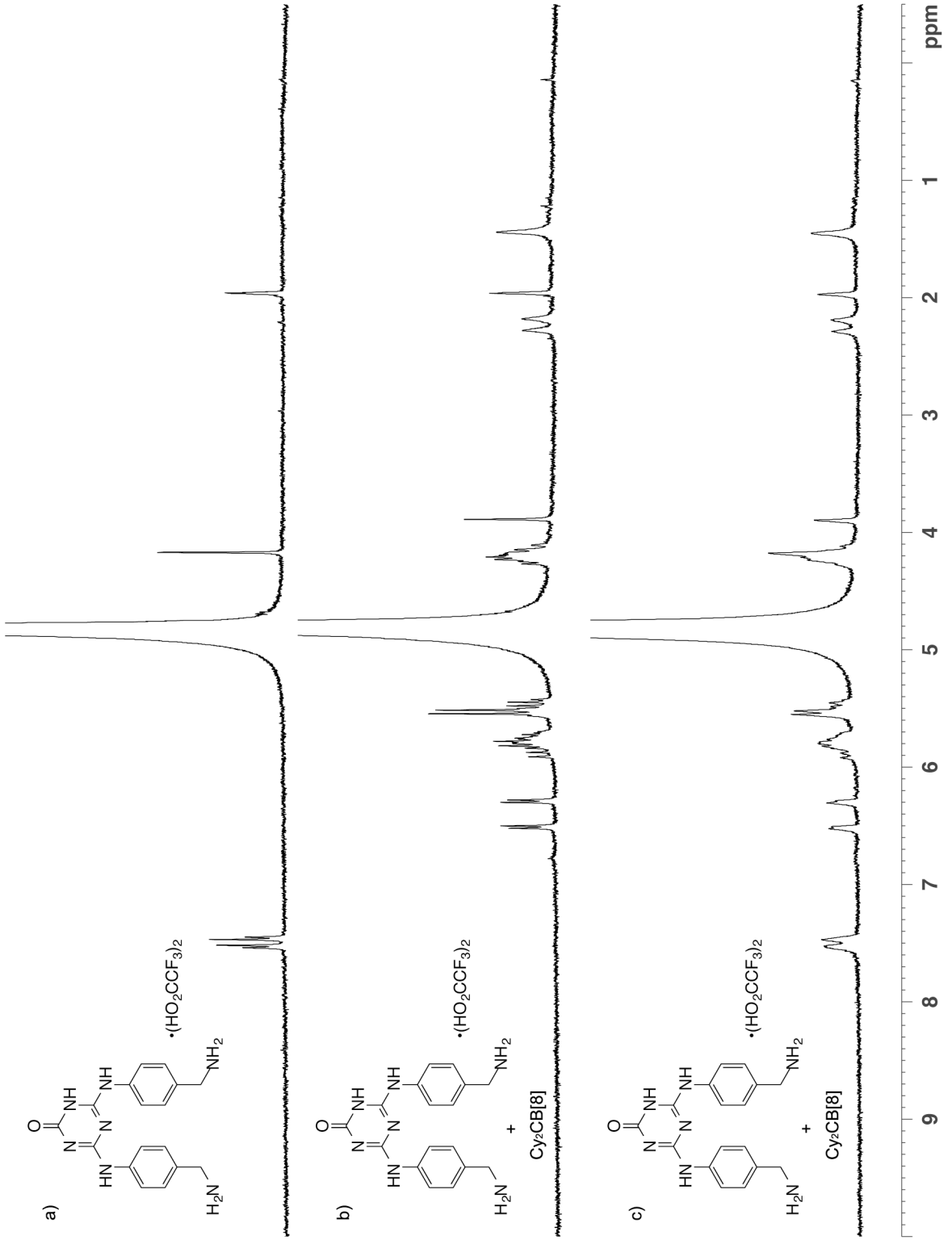

Figure III-S19. ^{1}H NMR spectra recorded (D_2O, 400 MHz, RT) for : a) **III-12** (0.3 mM), b) a 1:1 mixture of $Cy_2CB[8]$ (0.3 mM) and **III-12** (0.3 mM), and c) a 1:2 mixture of $Cy_2CB[8]$ (0.3 mM) and **III-12** (0.6 mM).

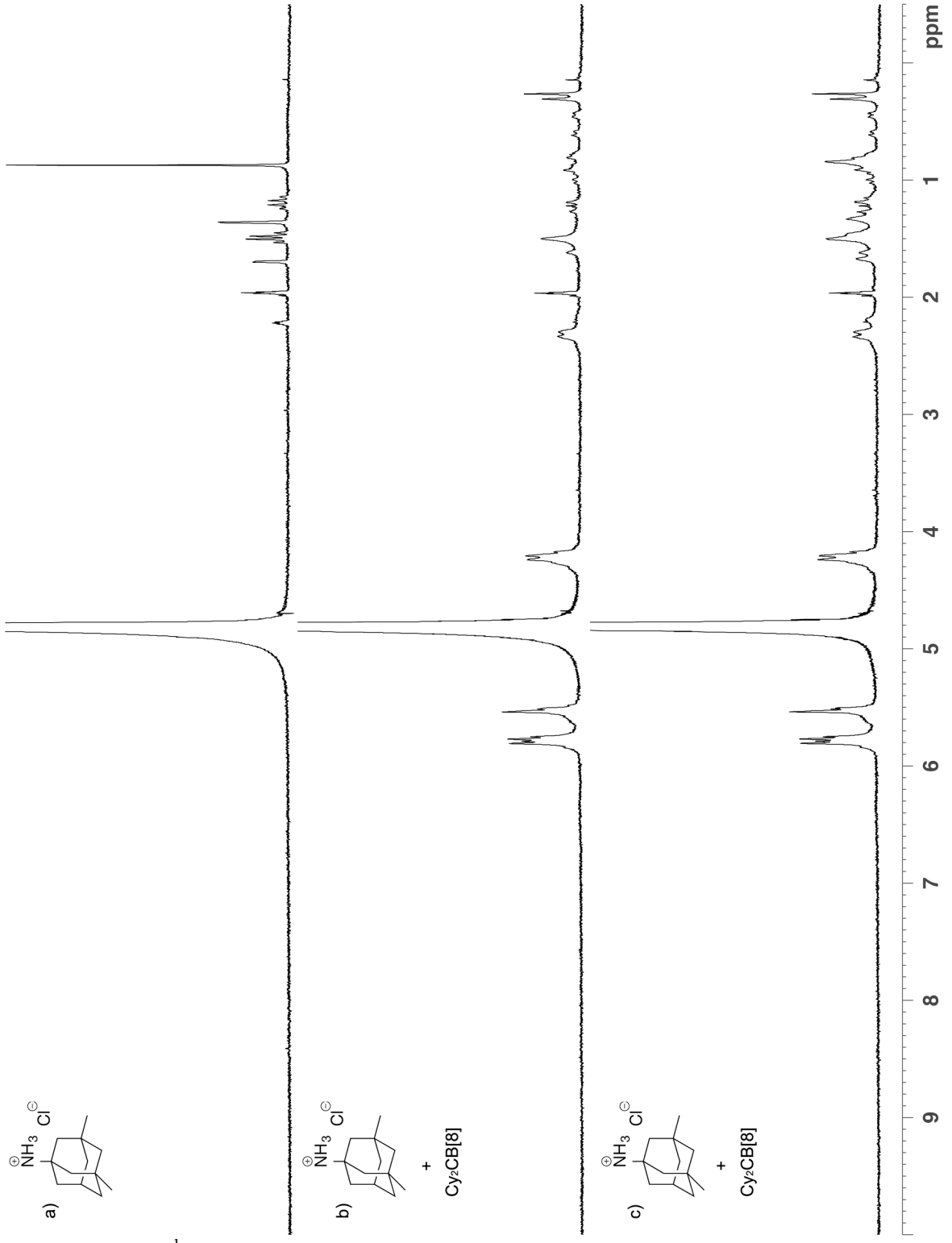

Figure III-S20. ^{1}H NMR spectra recorded (D_2O, 400 MHz, RT) for : a) **III-14** (0.3 mM), b) a 1:1 mixture of $Cy_2CB[8]$ (0.3 mM) and **III-14** (0.3 mM), and c) a 1:2 mixture of $Cy_2CB[8]$ (0.3 mM) and **III-14** (0.6 mM).

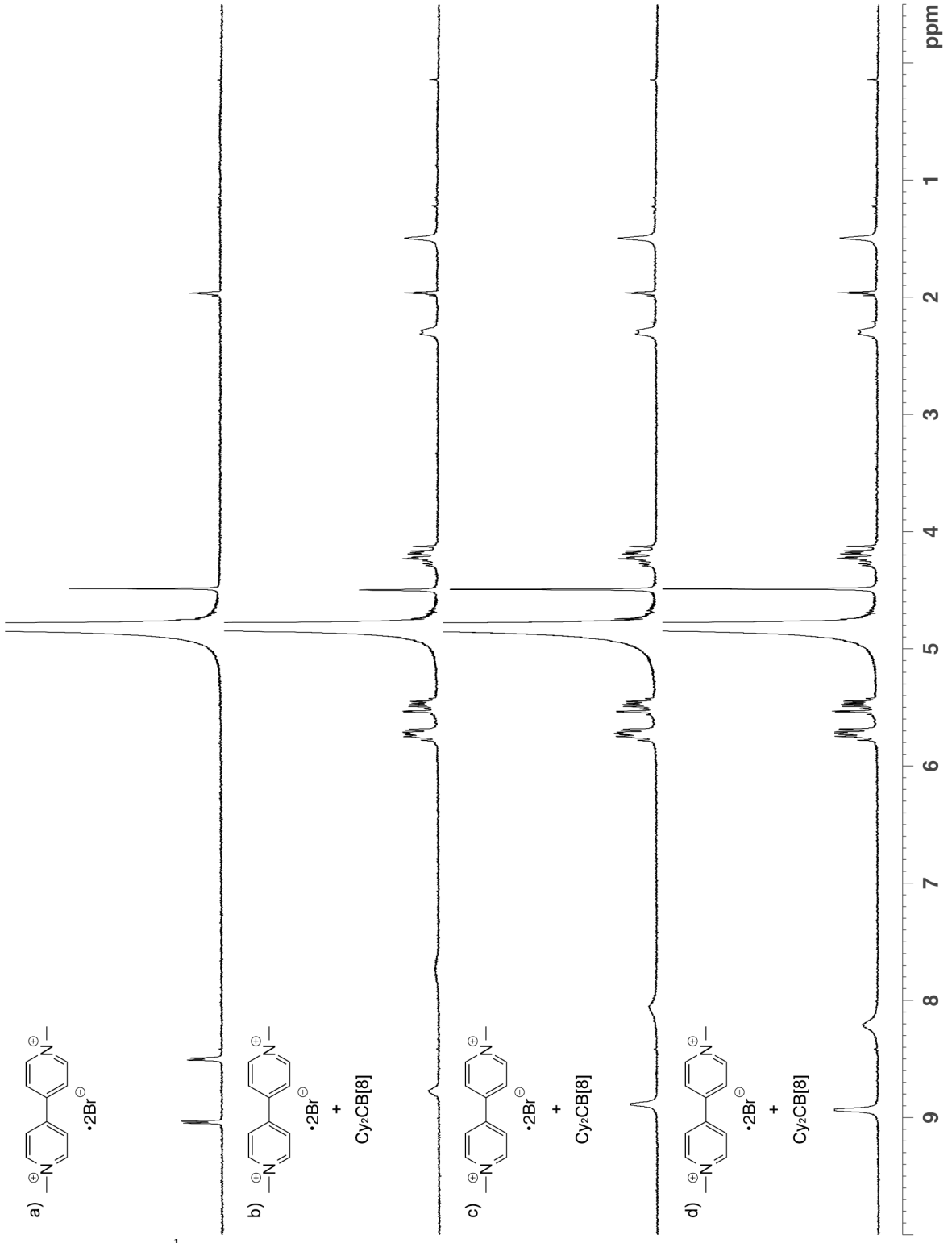

Figure III-S21. ^{1}H NMR spectra recorded (D_2O, 400 MHz, RT) for : a) **III-16** (0.3 mM), b) a 1:1 mixture of $Cy_2CB[8]$ (0.3 mM) and **III-16** (0.3 mM), c) a 1:2 mixture of $Cy_2CB[8]$ (0.3 mM) and **III-16** (0.6 mM), and d) a 1:3 mixture of $Cy_2CB[8]$ (0.3 mM) and **III-16** (0.9 mM).

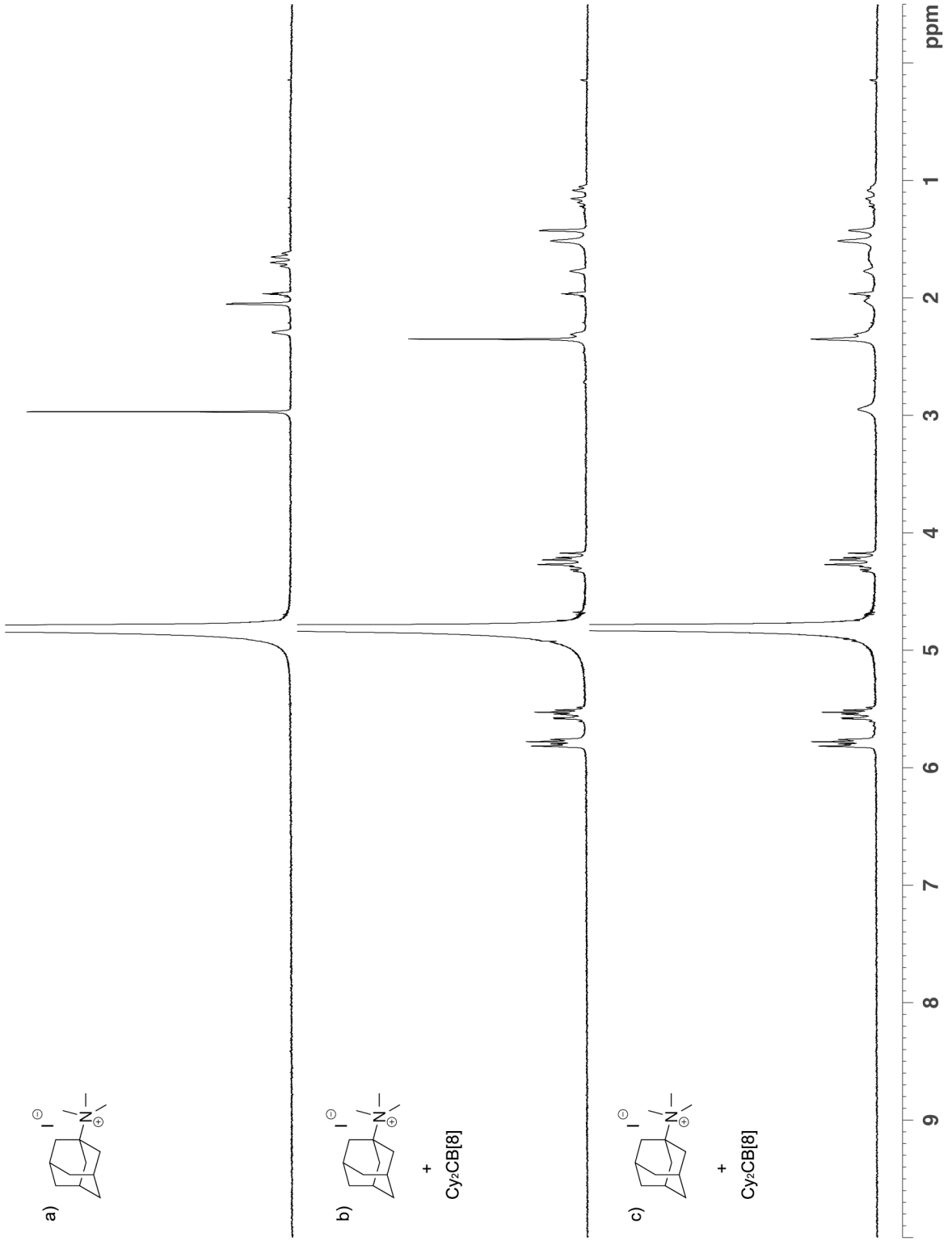

Figure III-S22. ^{1}H NMR spectra recorded (D_2O, 400 MHz, RT) for : a) **III-13** (0.3 mM), b) a 1:1 mixture of $Cy_2CB[8]$ (0.3 mM) and **III-13** (0.3 mM), and c) a 1:2 mixture of $Cy_2CB[8]$ (0.3 mM) and **III-13** (0.6 mM).

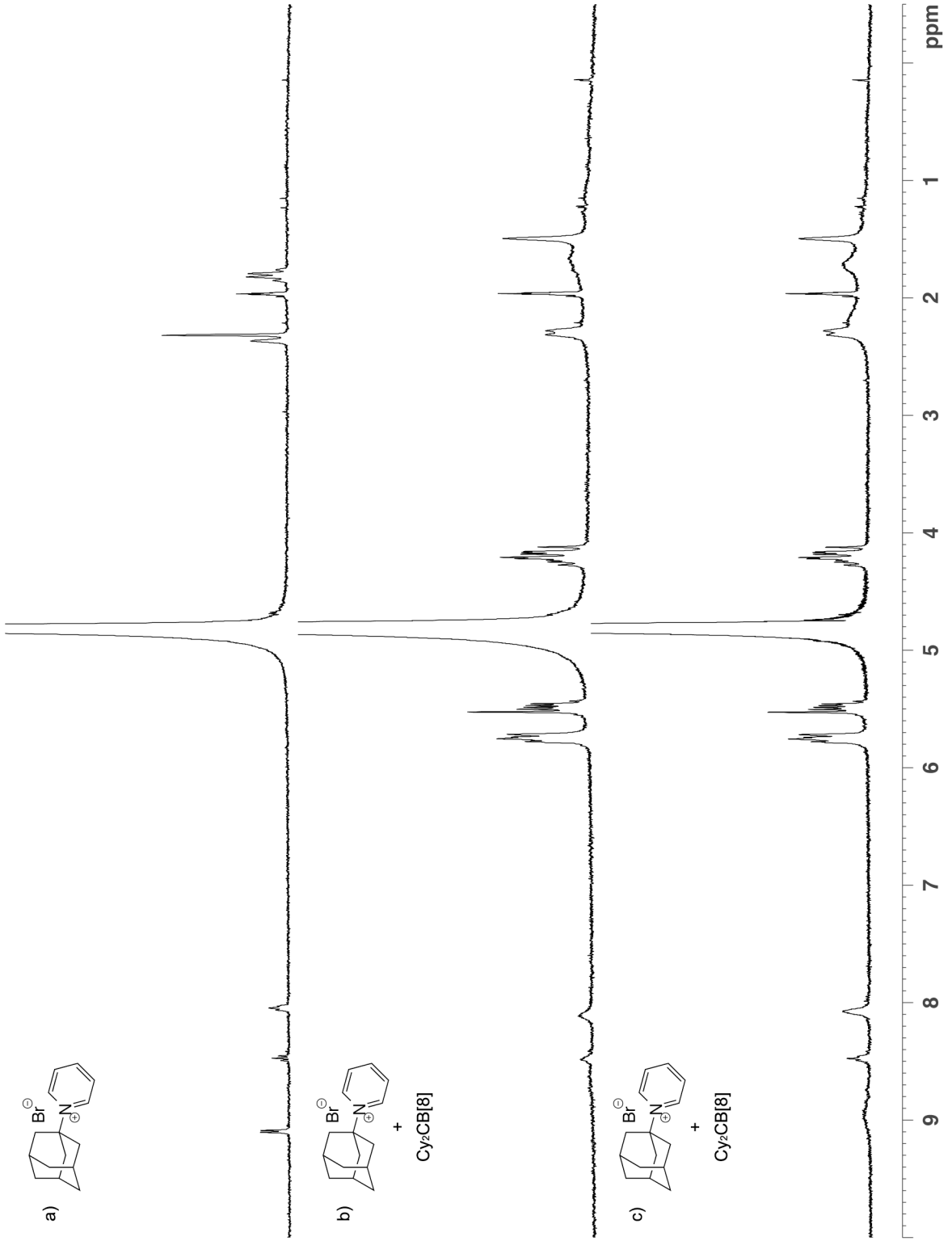

Figure III-S23. ^{1}H NMR spectra recorded (D_2O, 400 MHz, RT) for : a) **III-15** (0.3 mM), b) a 1:1 mixture of $Cy_2CB[8]$ (0.3 mM) and **III-15** (0.3 mM), and c) a 1:2 mixture of $Cy_2CB[8]$ (0.3 mM) and **III-15** (0.6 mM).

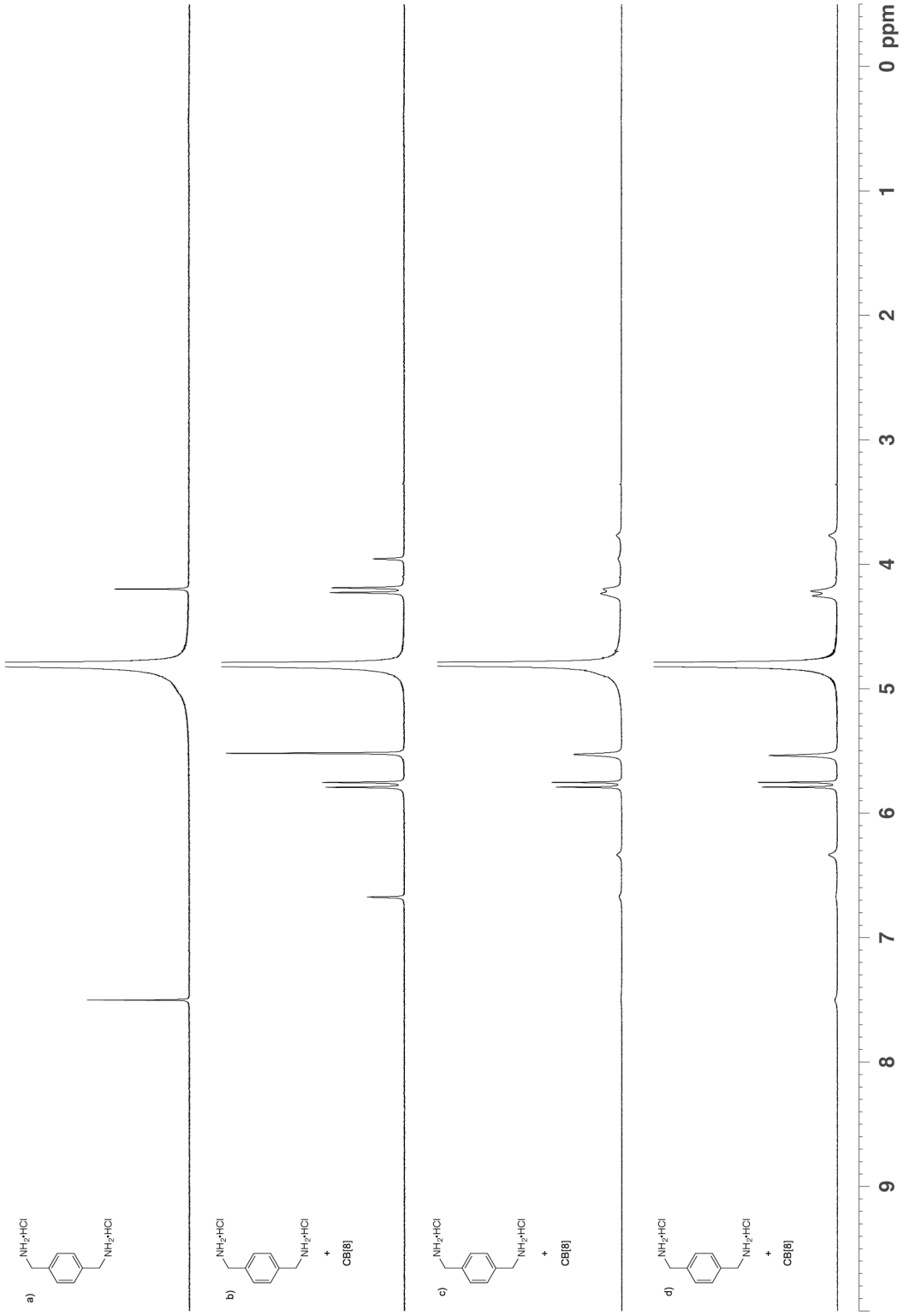

Figure III-S24. ^{1}H NMR spectra recorded (D_2O, 400 MHz, RT) for : a) **III-3** (0.3 mM), b) a 1:1 mixture of CB[8] (0.3 mM) and **III-3** (0.3 mM), c) a 1:2 mixture of CB[8] (0.3 mM) and **III-3** (0.6 mM), and d) a 1:3 mixture of CB[8] (0.3 mM) and **III-3** (0.9 mM).

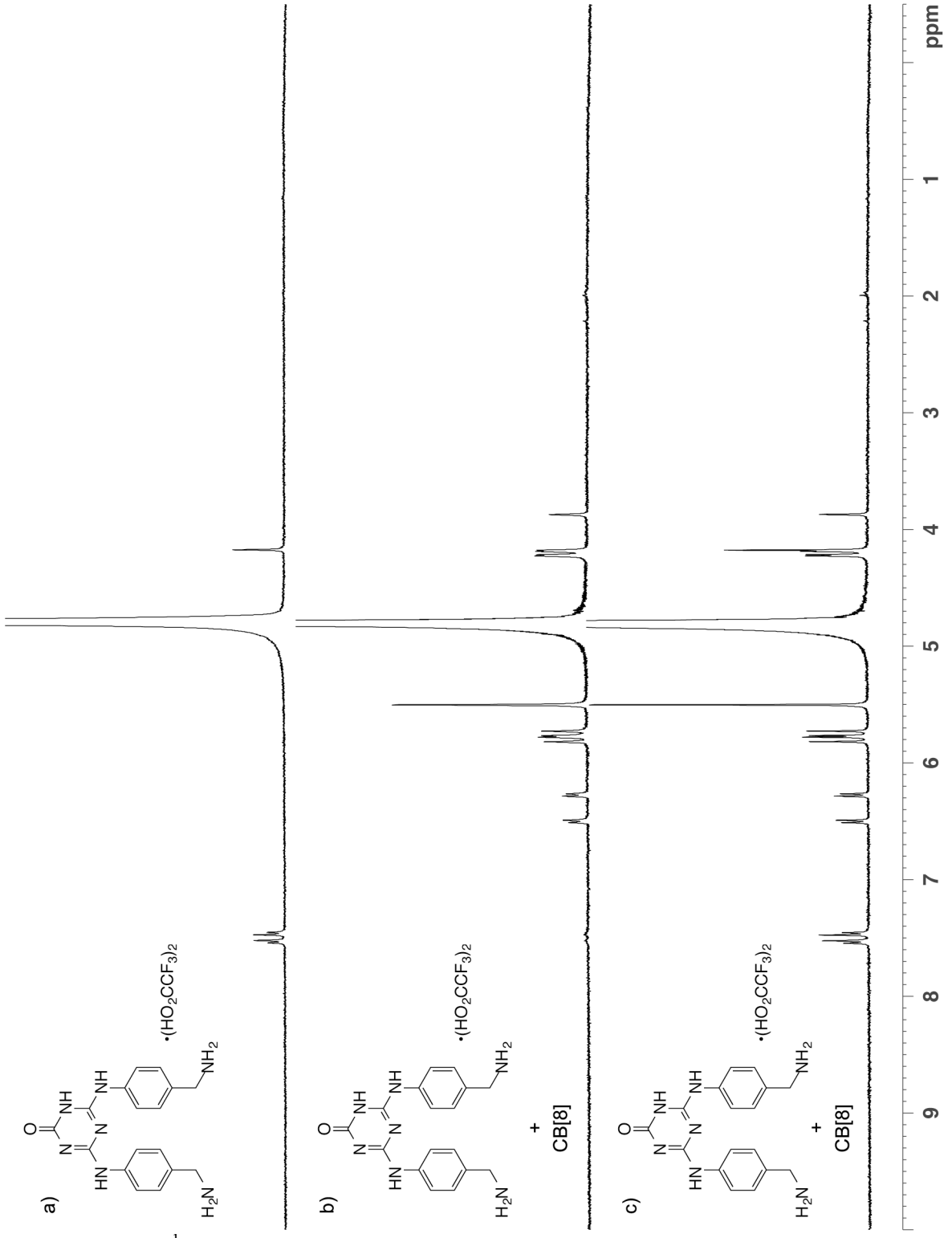

Figure III-S25. ^{1}H NMR spectra recorded (D_2O, 400 MHz, RT) for : a) **III-12** (0.3 mM), b) a 1:1 mixture of CB[8] (0.3 mM) and **III-12** (0.3 mM), and c) a 1:2 mixture of CB[8] (0.3 mM) and **III-12** (0.6 mM).

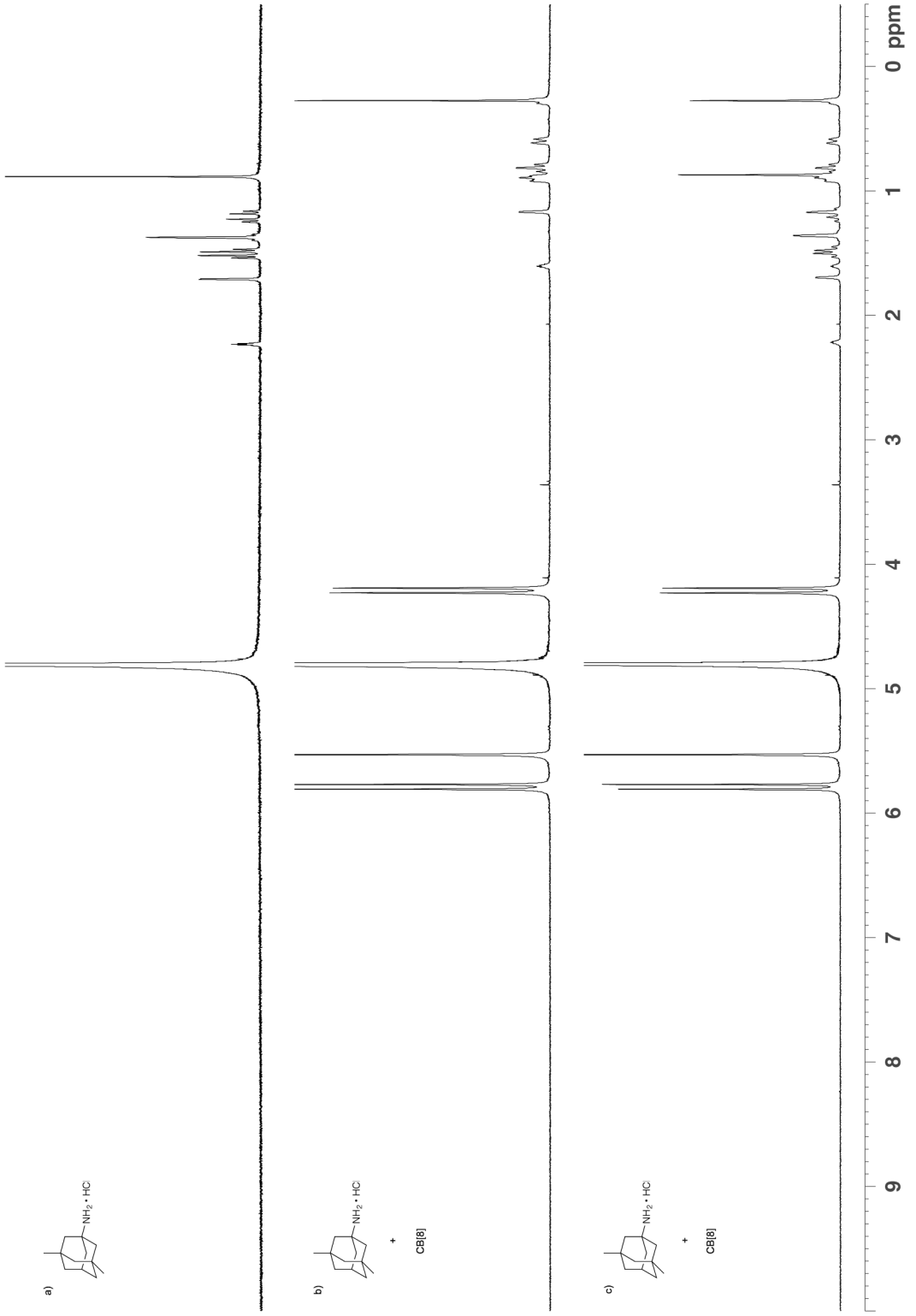

Figure III-S26. ^{1}H NMR spectra recorded (D_2O, 400 MHz, RT) for : a) **III-14** (0.3 mM), b) a 1:1 mixture of CB[8] (0.3 mM) and **III-14** (0.3 mM), and c) a 1:2 mixture of CB[8] (0.3 mM) and **III-14** (0.6 mM).

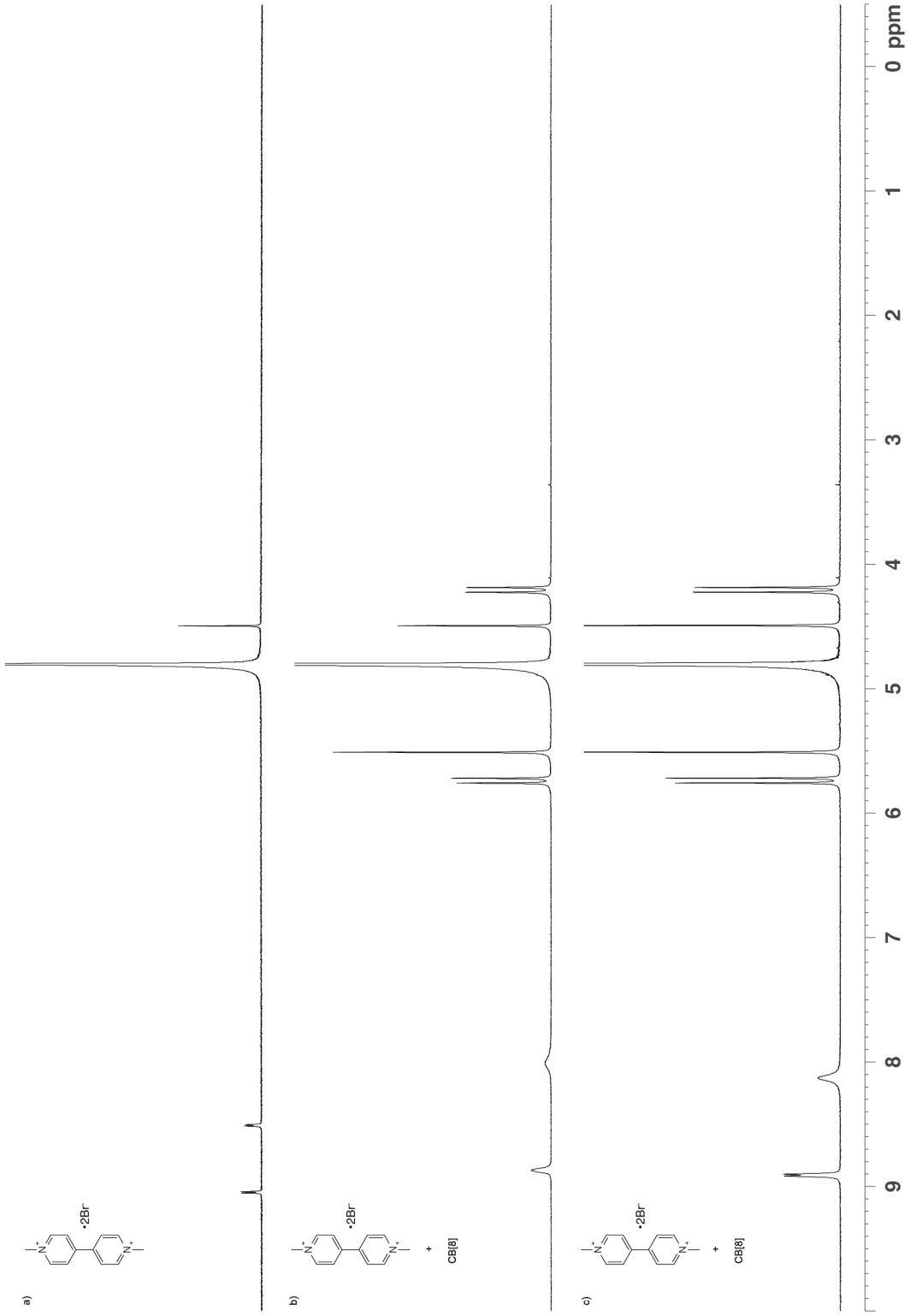

Figure III-S27. ^{1}H NMR spectra recorded (D_2O, 400 MHz, RT) for : a) **III-16** (0.3 mM), b) a 1:1 mixture of CB[8] (0.3 mM) and **III-16** (0.3 mM), and c) a 1:2 mixture of CB[8] (0.3 mM) and **III-16** (0.6 mM).

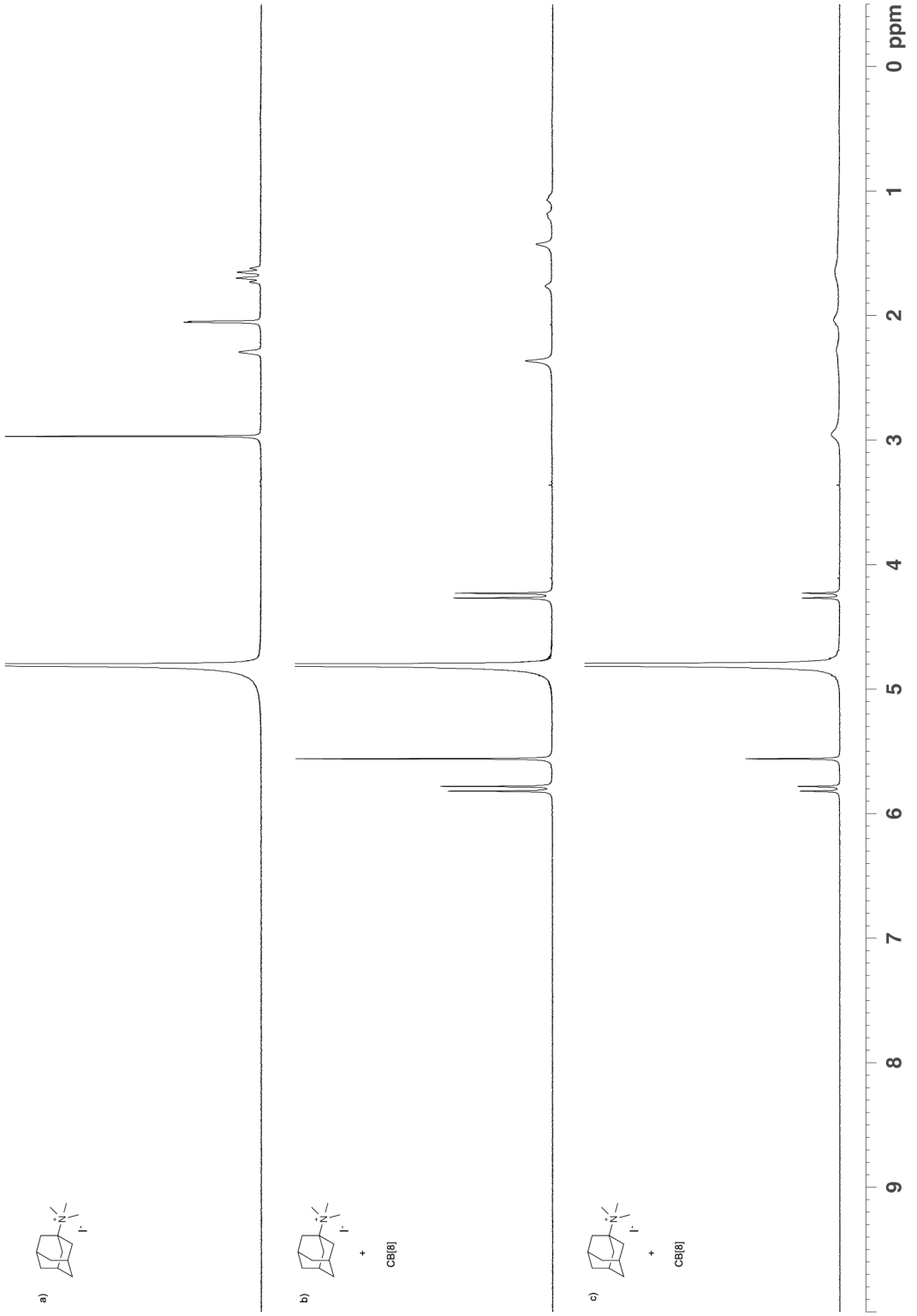

Figure III-S28. ^{1}H NMR spectra recorded (D_2O, 400 MHz, RT) for : a) **III-13** (0.3 mM), b) a 1:1 mixture of CB[8] (0.3 mM) and **III-13** (0.3 mM), and c) a 1:2 mixture of CB[8] (0.3 mM) and **III-13** (0.6 mM).

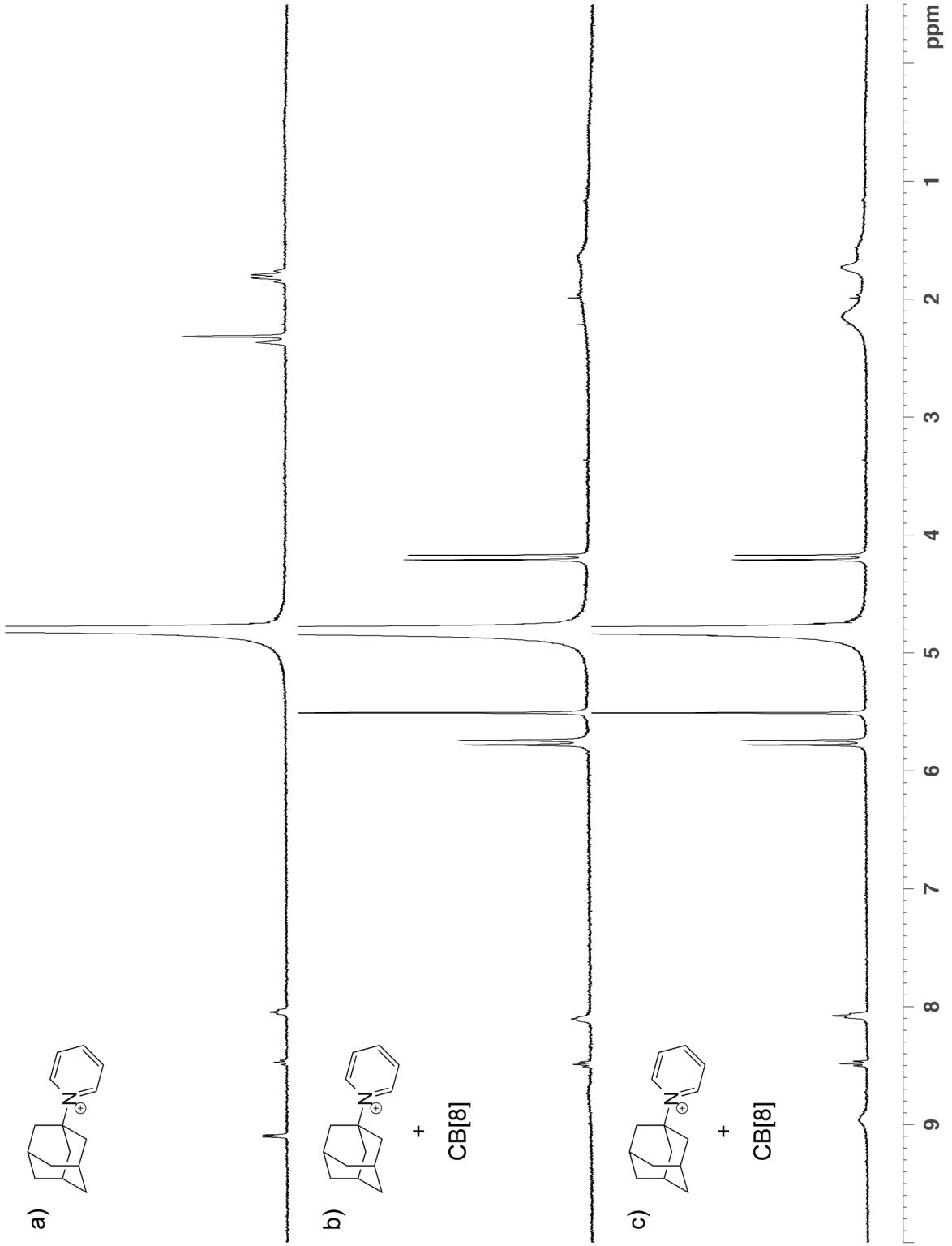

Figure III-S29. ^{1}H NMR spectra recorded (D_2O, 400 MHz, RT) for : a) **III-15** (0.3 mM), b) a 1:1 mixture of CB[8] (0.3 mM) and **III-15** (0.3 mM), and c) a 1:2 mixture of CB[8] (0.3 mM) and **III-15** (0.6 mM).

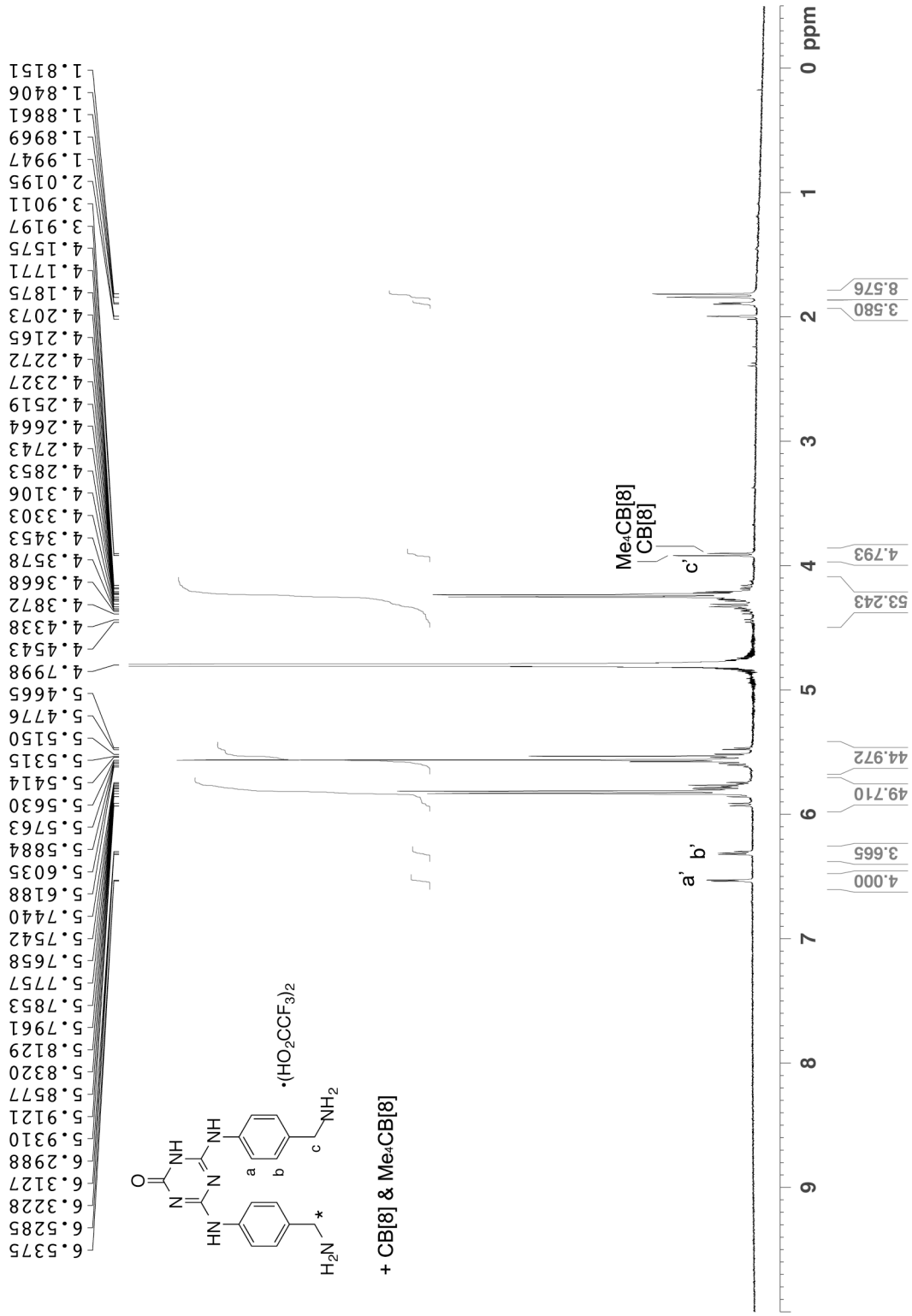

Figure III-S30. ^{1}H NMR collected (800 MHz, 50 mM sodium acetate buffered D_2O, RT) for the competition between Me_4CB[8] and CB[8] for **III-12**.

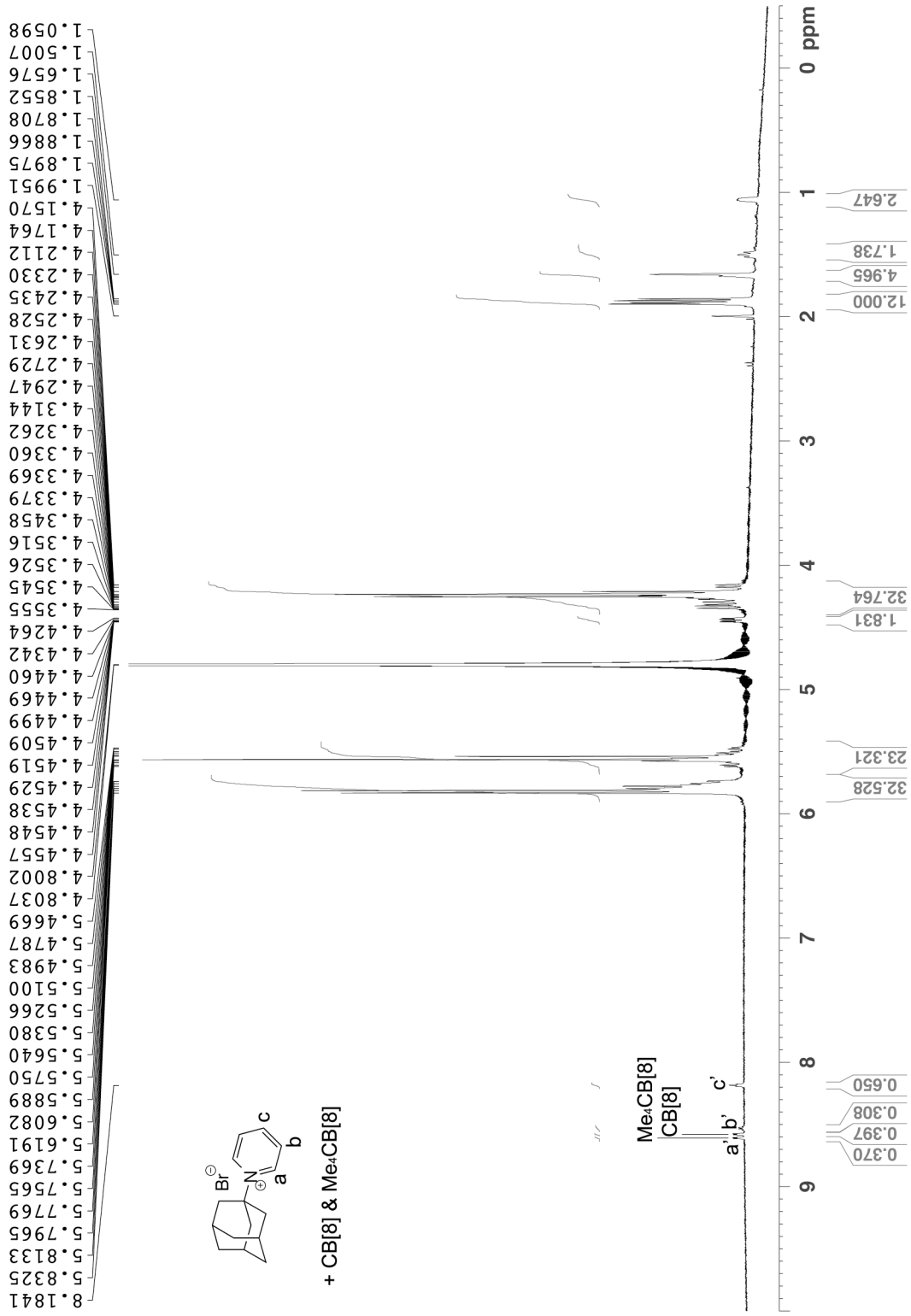

Figure III-S31. ^{1}H NMR collected (800 MHz, 50 mM sodium acetate buffered D_2O, RT) for the competition between Me_4CB[8] and CB[8] for **III-15**.

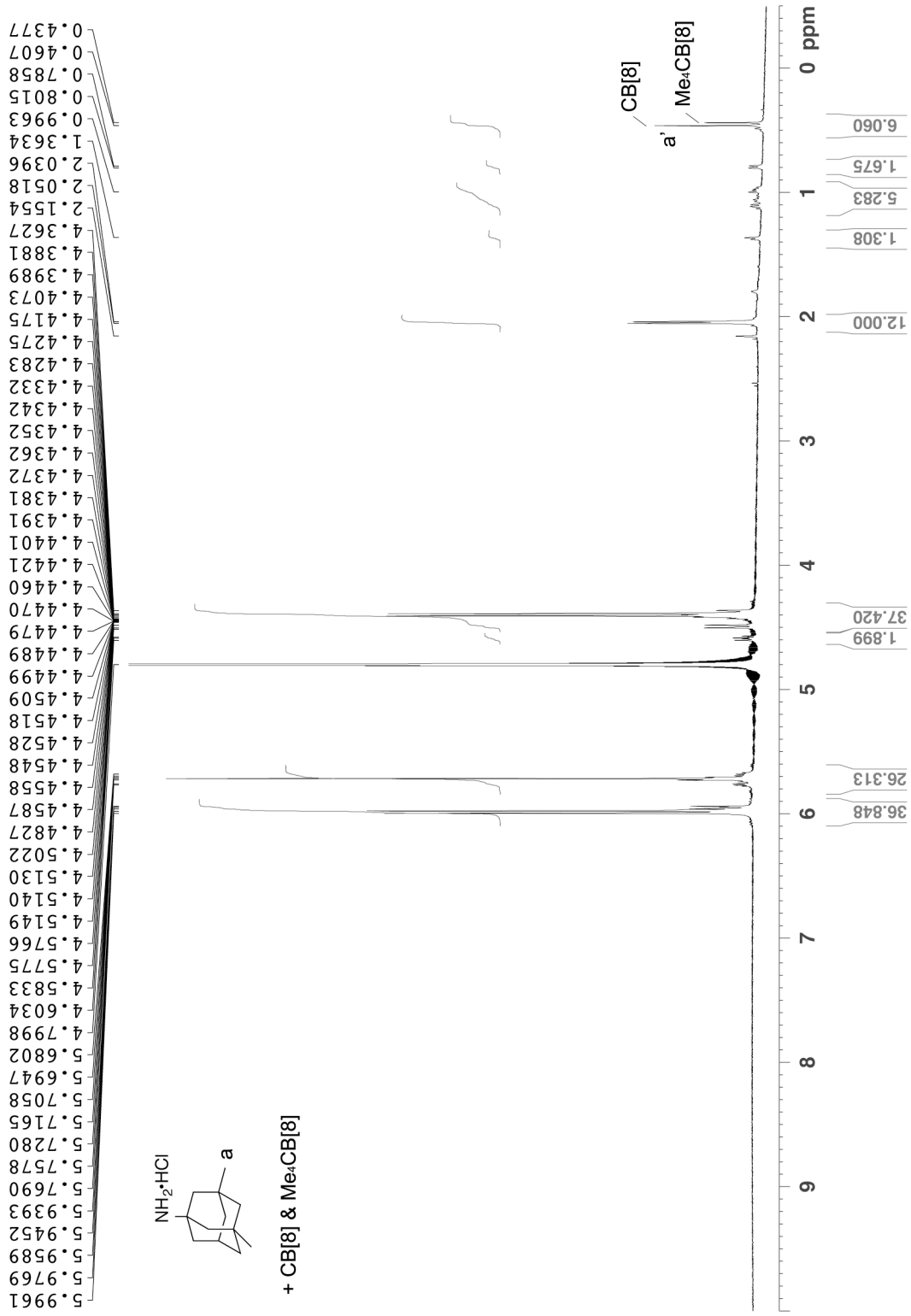

Figure III-S32. ^{1}H NMR collected (800 MHz, 50 mM sodium acetate buffered D_2O, RT) for the competition between Me_4CB[8] and CB[8] for **III-14**.

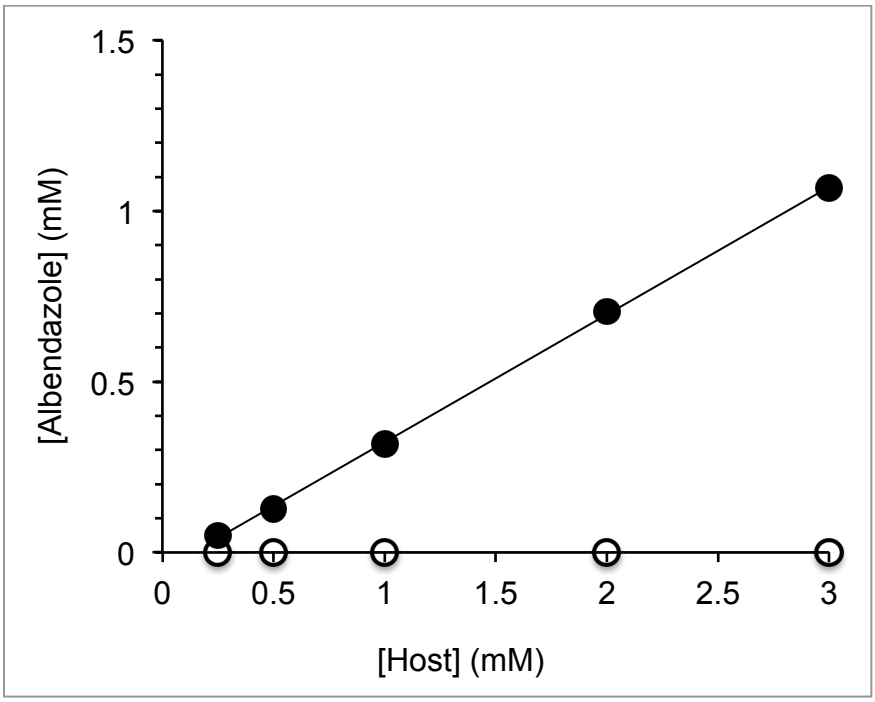

Figure III-S33. Phase solubility diagrams constructed for albendazole with Me_4CB[8] (•) and CB[8] (o). Conditions: 50 mM sodium acetate buffered D_2O (pH = 4.74, RT).

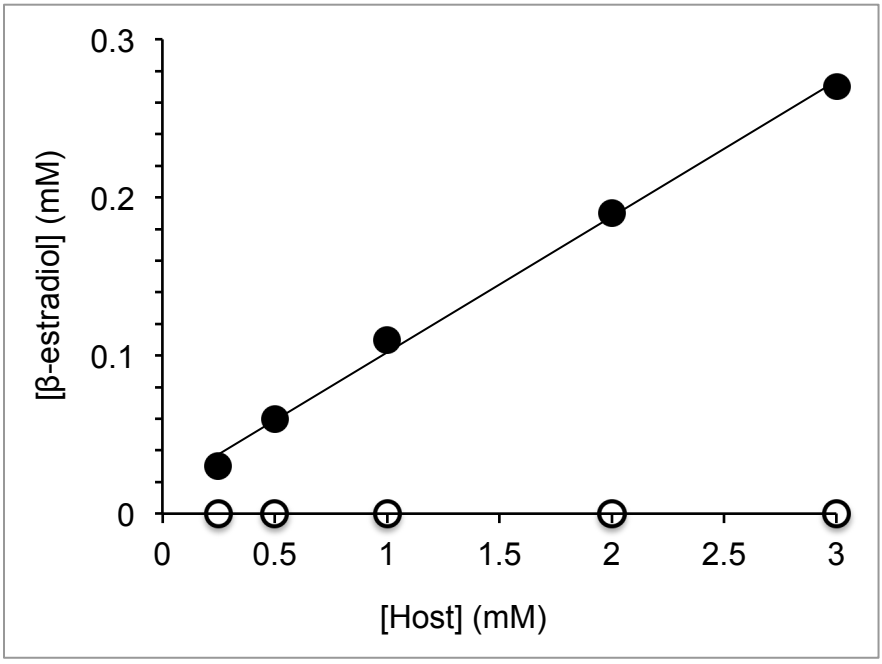

Figure III-S34. Phase solubility diagrams constructed for β-estradiol with Me_4CB[8] (•) and CB[8] (o). Conditions: 50 mM sodium phosphate buffered D_2O (pH = 7.4, RT).

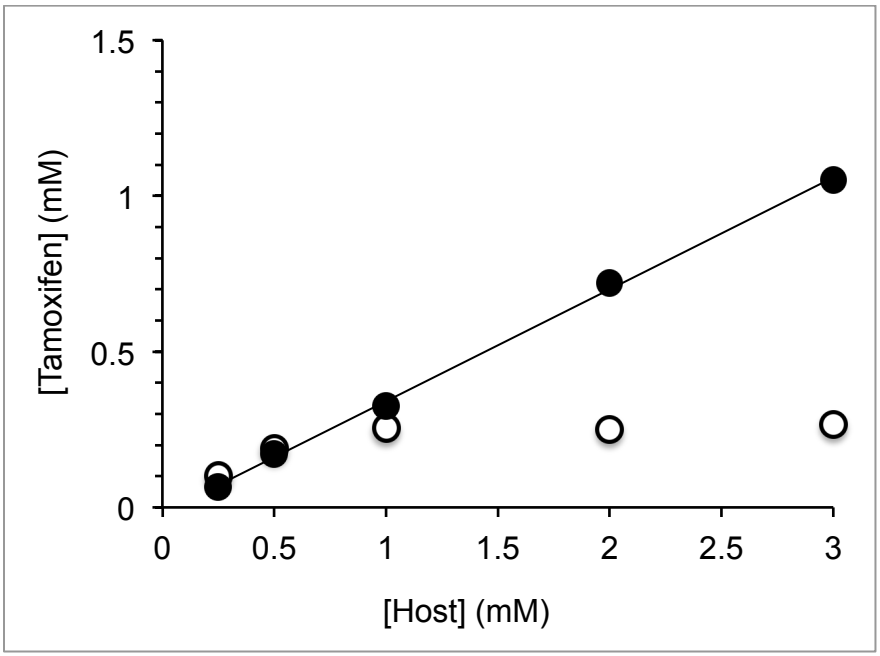

Figure III-S35. Phase solubility diagrams constructed for tamoxifen with Me_4CB[8] (•) and CB[8] (o). Conditions: 50 mM sodium phosphate buffered D_2O (pH = 7.4, RT).

Table III-S1. Values of slope and K_a (M^{-1}) derived from the PSDs for solubilization of four drugs with Me_4CB[8] or CB[8].

Drug	**Me_4CB[8] Slope**	**CB[8] Slope**
Amiodarone	0.44	0
Tamoxifen	0.36	0.36
β-estradiol	0.086	0
Albendazole	0.37	0

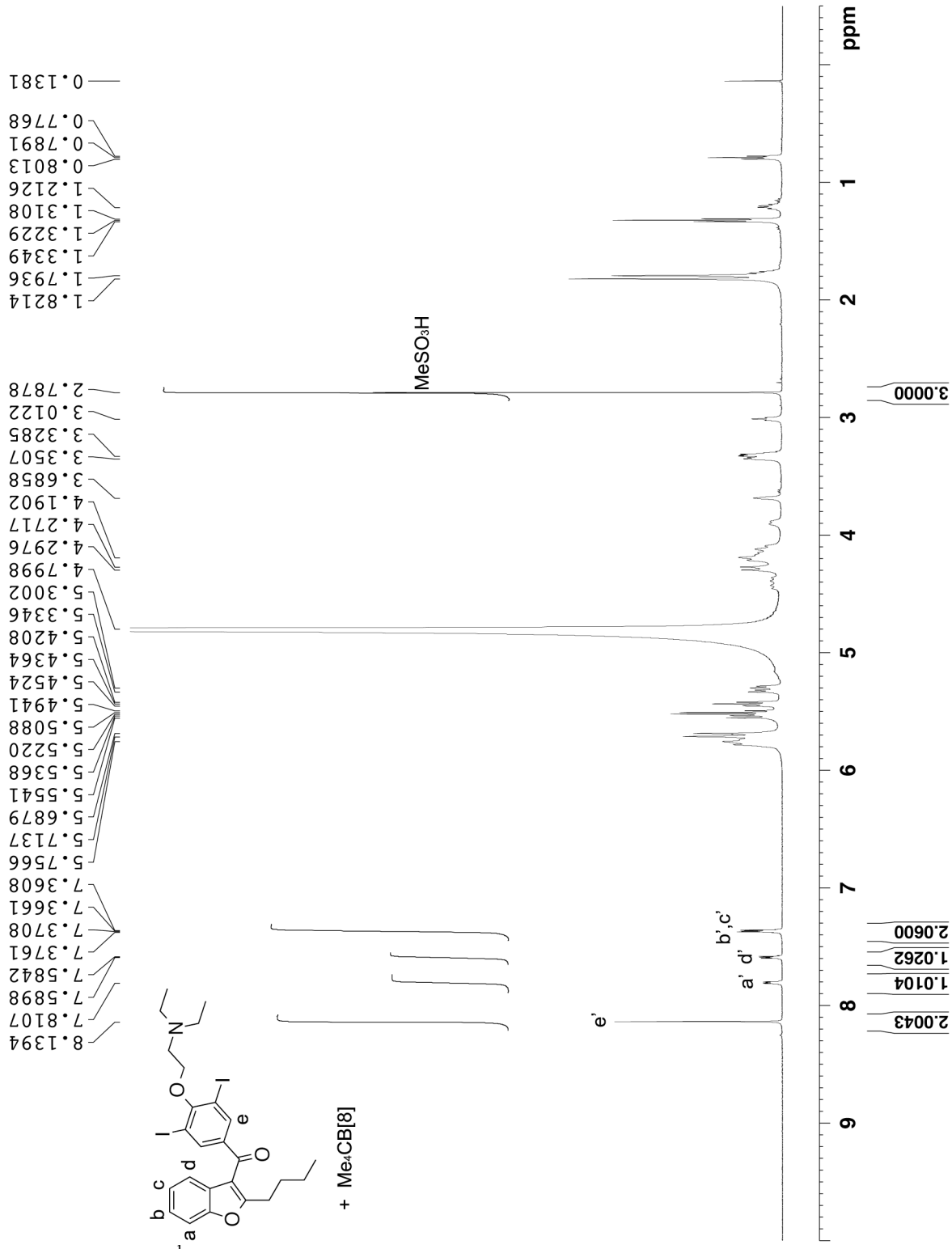

Figure III-S36. ^{1}H NMR (600 MHz, 50 mM sodium phosphate buffered D_2O (pH = 7.4), RT) recorded for 3 mM $Me_4CB[8]$ and solubilized amiodarone with $MeSO_3H$ as internal standard. Integration of the aromatic peaks a-e of amiodarone allowed us to calculate the amount of solubilized amiodarone.

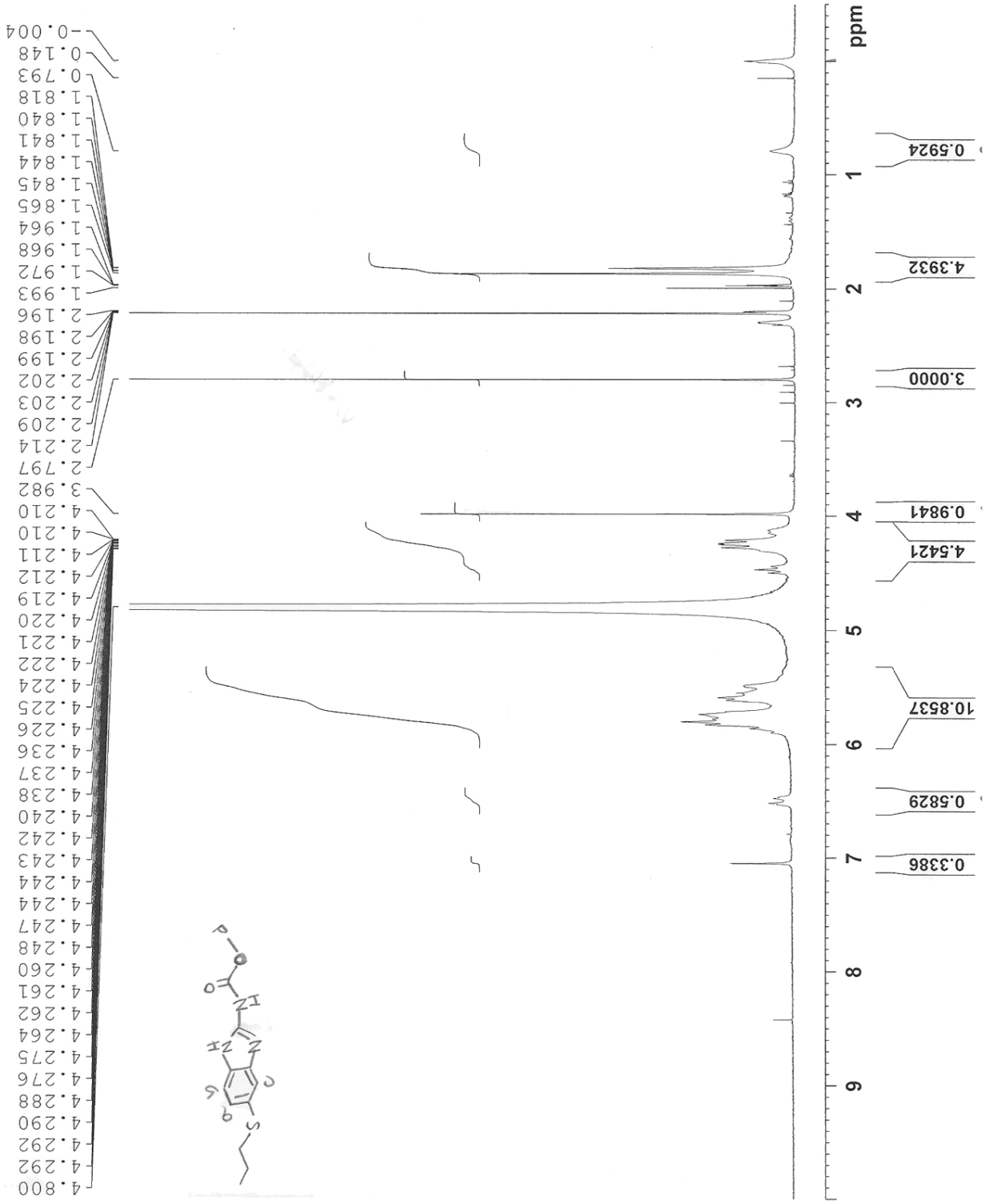

Figure III-S37. ^{1}H NMR (600 MHz, 50 mM sodium phosphate buffered D_2O (pH = 7.4), RT) recorded for 3 mM $Me_4CB[8]$ and solubilized albendazole with $MeSO_3H$ as internal standard.

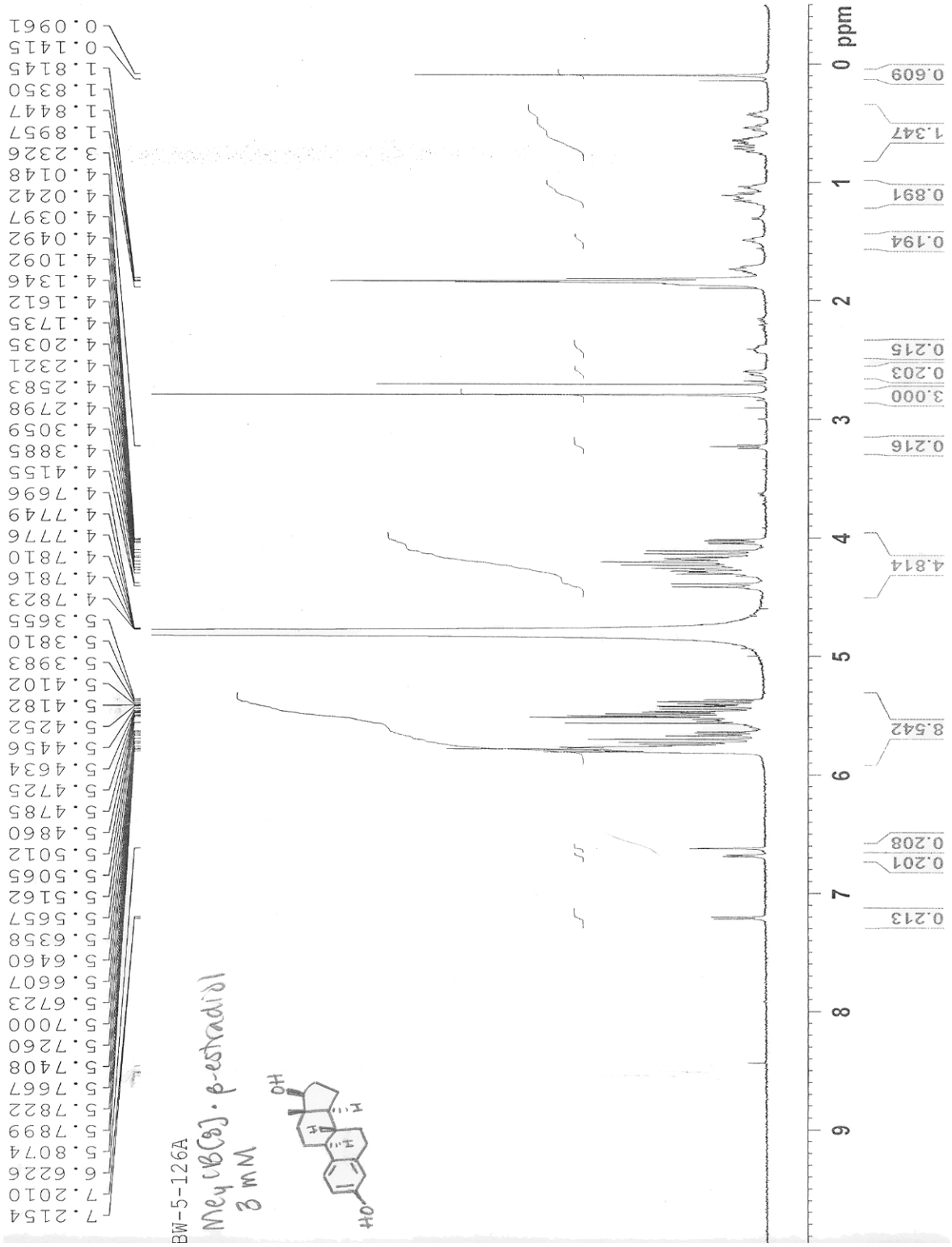

Figure III-S38. ^{1}H NMR (600 MHz, 50 mM sodium phosphate buffered D_2O (pH = 7.4), RT) recorded for 3 mM $Me_4CB[8]$ and solubilized estradiol with $MeSO_3H$ as internal standard.

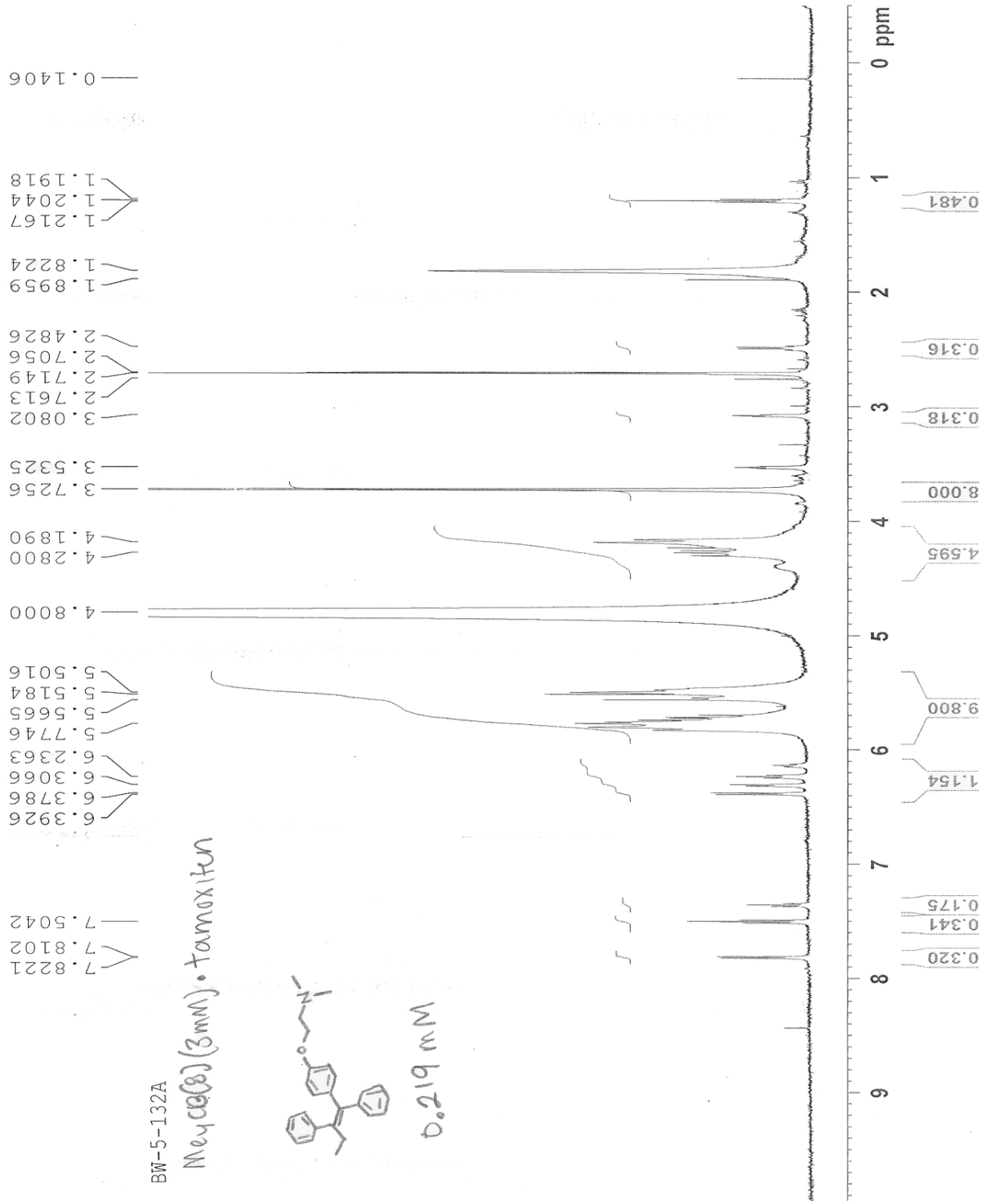

Figure III-S39. ^{1}H NMR (600 MHz, 50 mM sodium phosphate buffered D_2O (pH = 7.4), RT) recorded for 3 mM $Me_4CB[8]$ and solubilized tamoxifen with $MeSO_3H$ as internal standard.

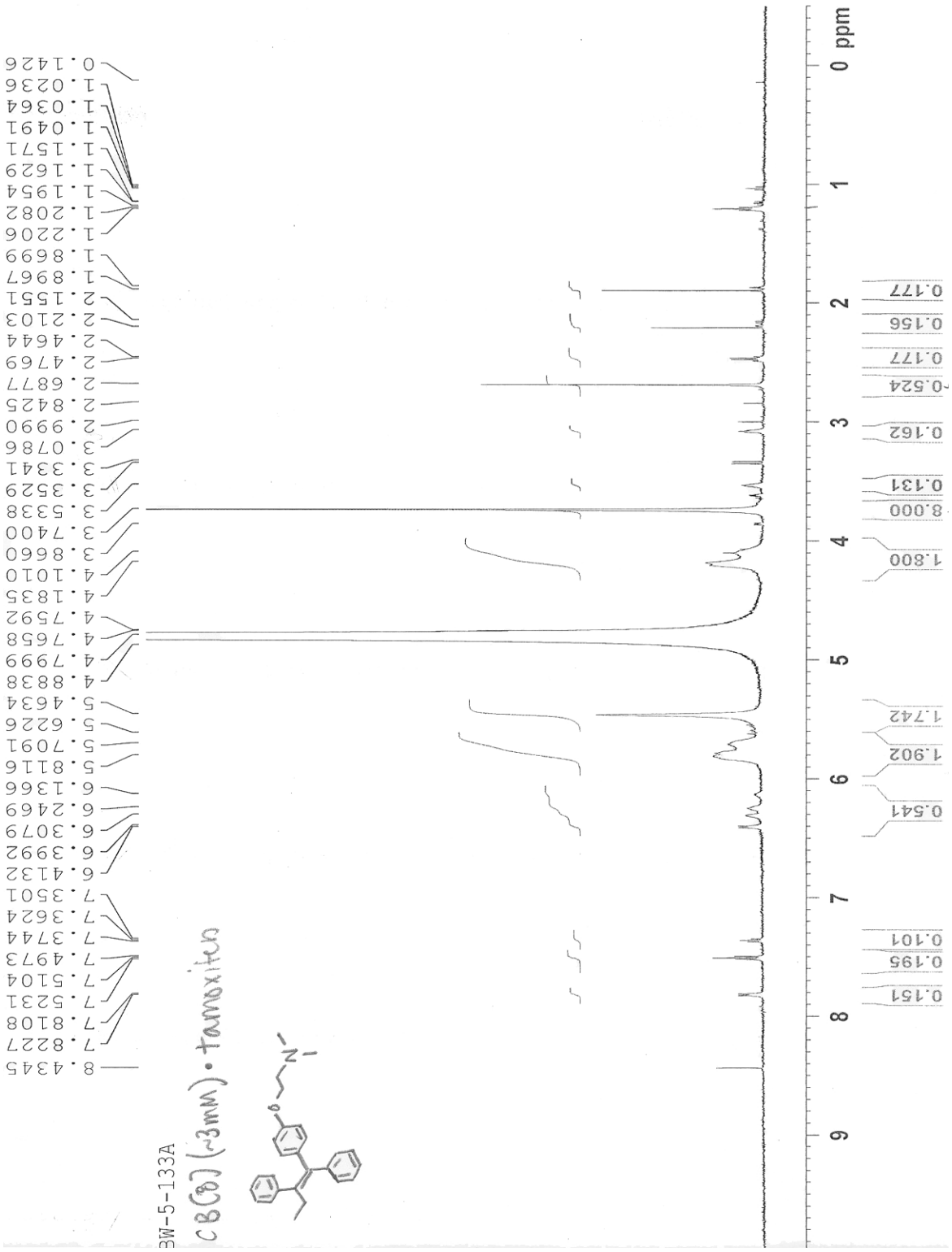

Figure III-S40. ^{1}H NMR (600 MHz, 50 mM sodium phosphate buffered D_2O (pH = 7.4), RT) recorded for 3 mM CB[8] and solubilized tamoxifen with dioxane as internal standard.

Details of the X-ray crystal structures. Crystals of the Me_4CB[8]•**3**, Me_4CB[8]•**5**, and Cy_2CB[8]•**3** were obtained by combining host with 1.5 equivalents of guest in a minimum volume of H_2O followed by the dropwise addition of KI (1 M) until the solution became cloudy. Enough H_2O was added to obtain a homogenous solution and then the solution was filtered through a 0.22 micron filter and transferred to a clean vial which was loosely capped. Crystals appeared after 2 – 5 days. We were unable to obtain crystals of the uncomplexed macrocycles from acidic water.

Details of the Crystal Structure of Me_4CB[8]•3_2. A colorless prism-like specimen of $C_{68}H_{126}I_4N_{36}O_{37}$, approximate dimensions 0.35 mm × 0.46 mm × 0.52 mm, was used for the X-ray crystallographic analysis. Instrument description The X-ray intensity data were measured on a Bruker APEX-II CCD system equipped with a graphite monochromator and a MoKα sealed tube (λ = 0.71073 Å). Data collection temperature was 100 K.

The total exposure time was 10.10 hours. The frames were integrated with the Bruker SAINT software package using a narrow-frame algorithm. The integration of the data using a monoclinic unit cell yielded a total of 40940 reflections to a maximum θ angle of 25.00° (0.84 Å resolution), of which 9169 were independent (average redundancy 4.465, completeness = 99.9%, R_{int} = 2.29%) and 8451 (92.17%) were greater than $2\sigma(F^2)$. The final cell constants of *a* = 13.8420(15) Å, *b* = 24.405(3) Å, *c* = 16.1065(18) Å, β = 106.6605(13)°, *V* = 5212.6(10) $Å^3$, are based upon the refinement of the XYZ-centroids of 9847 reflections above 20 σ(I) with 4.536° < 2θ < 55.52°. Scaling Data were corrected for absorption effects using the multi-scan method (SADABS). The calculated minimum and maximum transmission coefficients (based on crystal size) are 0.5350 and 0.6360.

The structure was solved and refined using the Bruker SHELXTL Software Package, using the space group $P2_1/n$, with Z = 2 for the formula unit, $C_{68}H_{126}I_4N_{36}O_{37}$. Structure refinement The final anisotropic full-matrix least-squares refinement on F^2 with 774 variables converged at R_1 = 7.86%, for the observed data and wR_2 = 17.71% for all data. The goodness-of-fit was 1.116. The largest peak in the final difference electron density synthesis was 0.826 $e^-/Å^3$ and the largest hole was -0.709 $e^-/Å^3$ with an RMS deviation of 0.120 $e^-/Å^3$. On the basis of the final model, the calculated density was 1.623 g/cm^3 and F(000), 2588 e^-.

Crystallographic References: Software APEX2 Version 2010.11-3 (Bruker AXS Inc.) SAINT Version 7.68A (Bruker AXS Inc., 2009) SADABS Version 2008/1 (G. M. Sheldrick, Bruker AXS Inc.) XPREP Version 2008/2 (G. M. Sheldrick, Bruker AXS Inc.) XS Version 2008/1 (G. M. Sheldrick, *Acta Cryst.* (2008). A**64**, 112-122) XL Version 2012/4 (G. M. Sheldrick, (2012) University of Gottingen, Germany) Platon (A. L. Spek, *Acta Cryst.* (1990). A**46**, C-34)

Table III-S2. Sample and crystal data for UM2644.

Identification code	2644
Chemical formula	$C_{68}H_{126}I_4N_{36}O_{37}$
Formula weight	2547.64
Temperature	100(2) K
Wavelength	0.71073 Å

Crystal size	0.35 × 0.46 × 0.52 mm	
Crystal habit	colorless prism	
Crystal system	monoclinic	
Space group	$P2_1/n$	
Unit cell dimensions	a = 13.8420(15) Å	α = 90°
	b = 24.405(3) Å	β = 106.6605(13)°
	c = 16.1065(18) Å	γ = 90°
Volume	5212.6(10) $Å^3$	
Z	2	
Density (calculated)	1.623 Mg/cm^3	
Absorption coefficient	1.293 mm^{-1}	
F(000)	2588	

Table III-S3. Data collection and structure refinement for UM2644.

Diffractometer	Bruker APEX-II CCD	
Radiation source	sealed tube, MoKα	
Theta range for data collection	2.13 to 25.00°	
Index ranges	$-16 \le h \le 16$, $-29 \le k \le 28$, $-19 \le l \le 19$	
Reflections collected	40940	
Independent reflections	9169 [R(int) = 0.0229]	
Coverage of independent reflections	99.9%	
Absorption correction	multi-scan	
Max. and min. transmission	0.6360 and 0.5350	
Structure solution technique	direct methods	
Structure solution program	ShelXS-97 (Sheldrick, 2008)	
Refinement method	Full-matrix least-squares on F^2	
Refinement program	ShelXL-2014 (Sheldrick, 2014)	
Function minimized	$\Sigma w(F_o^2 - F_c^2)^2$	
Data / restraints / parameters	9169 / 384 / 774	
Goodness-of-fit on F^2	1.116	
Final R indices	8451 data; I>2σ(I)	$R_1 = 0.0786$, $wR_2 = 0.1749$
	all data	$R_1 = 0.0828$, $wR_2 = 0.1771$
Weighting scheme	$w=1/[\sigma^2(F_o^2)+(0.0300P)^2+59.0000P]$, $P=(F_o^2+2F_c^2)/3$	
Largest diff. peak and hole	0.826 and -0.709 $eÅ^{-3}$	
R.M.S. deviation from mean	0.120 $eÅ^{-3}$	

$R_{int} = \Sigma|F_o^2 - F_o^2(\text{mean})| / \Sigma[F_o^2]$
$R_1 = \Sigma||F_o| - |F_c|| / \Sigma|F_o|$
$\text{GOOF} = S = \{\Sigma[w(F_o^2 - F_c^2)^2] / (n - p)\}^{1/2}$
$wR_2 = \{\Sigma[w(F_o^2 - F_c^2)^2] / \Sigma[w(F_o^2)^2]\}^{1/2}$

Details of the Crystallographic Structure of Me_4CB[8]•5. A colorless plate-like specimen of $C_{69}H_{109}I_3N_{39}O_{32.50}$, approximate dimensions 0.05 mm × 0.31 mm × 0.35 mm, was used for the X-ray crystallographic analysis. Instrument description The X-ray intensity data were measured on a Bruker APEX-II CCD system equipped with a graphite monochromator and a MoKα sealed tube (λ = 0.71073 Å). Data collection temperature was 150 K.

The total exposure time was 16.39 hours. The frames were integrated with the Bruker SAINT software package using a narrow-frame algorithm. The integration of the data using a monoclinic unit cell yielded a total of 101090 reflections to a maximum θ angle of 22.50° (0.93 Å resolution), of which 25025 were independent (average redundancy 4.040, completeness = 99.2%, R_{int} = 7.90%) and 15101 (60.34%) were greater than $2\sigma(F^2)$. The final cell constants of *a* = 14.6208(14) Å, *b* = 50.782(5) Å, *c* = 26.406(3) Å, β = 100.4681(11)°, *V* = 19279.(3) $Å^3$, are based upon the refinement of the XYZ-centroids of 9966 reflections above 20 σ(I) with 4.487° < 2θ < 39.84°. Scaling Data were corrected for absorption effects using the multi-scan method (SADABS). The calculated minimum and maximum transmission coefficients (based on crystal size) are 0.6890 and 0.9480.

The structure was solved and refined using the Bruker SHELXTL Software Package, using the space group $P2_1/c$, with Z = 8 for the formula unit, $C_{69}H_{109}I_3N_{39}O_{32.50}$. Structure refinement The final anisotropic full-matrix least-squares refinement on F^2 with 2453 variables converged at R_1 = 9.81%, for the observed data and wR_2 = 23.46% for all data. The goodness-of-fit was 1.207. The largest peak in the final difference electron density synthesis was 1.251 $e^-/Å^3$ and the largest hole was -1.267 $e^-/Å^3$ with an RMS deviation of 0.123 $e^-/Å^3$. On the basis of the final model, the calculated density was 1.644 g/cm^3 and F(000), 9720 e^-.

Crystallographic References: Software APEX2 Version 2010.11-3 (Bruker AXS Inc.) SAINT Version 7.68A (Bruker AXS Inc., 2009) SADABS Version 2008/1 (G. M. Sheldrick, Bruker AXS Inc.) XPREP Version 2008/2 (G. M. Sheldrick, Bruker AXS Inc.) XS Version 2008/1 (G. M. Sheldrick, *Acta Cryst.* (2008). A**64**, 112-122) XL Version 2012/4 (G. M. Sheldrick, (2012) University of Gottingen, Germany) Platon (A. L. Spek, *Acta Cryst.* (1990). A**46**, C-34)

Table III-S4. Sample and crystal data for UM2665.

Identification code	2665	
Chemical formula	$C_{69}H_{109}I_3N_{39}O_{32.50}$	
Formula weight	2385.65	
Temperature	150(2) K	
Wavelength	0.71073 Å	
Crystal size	0.05 × 0.31 × 0.35 mm	
Crystal habit	colorless plate	
Crystal system	monoclinic	
Space group	$P2_1/c$	
Unit cell dimensions	a = 14.6208(14) Å	α = 90°

	b = 50.782(5) Å	β = 100.4681(11)°
	c = 26.406(3) Å	γ = 90°
Volume	19279.(3) $Å^3$	
Z	8	
Density (calculated)	1.644 Mg/cm^3	
Absorption coefficient	1.074 mm^{-1}	
F(000)	9720	

Table III-S5. Data collection and structure refinement for UM2665.

Diffractometer	Bruker APEX-II CCD	
Radiation source	sealed tube, MoKα	
Theta range for data collection	1.60 to 22.50°	
Index ranges	$-15 \leq h \leq 15$, $-54 \leq k \leq 54$, $-28 \leq l \leq 28$	
Reflections collected	101090	
Independent reflections	25025 [R(int) = 0.0790]	
Coverage of independent reflections	99.2%	
Absorption correction	multi-scan	
Max. and min. transmission	0.9480 and 0.6890	
Structure solution technique	direct methods	
Structure solution program	XT-2014 (Sheldrick, 2014)	
Refinement method	Full-matrix least-squares on F^2	
Refinement program	ShelXL-2014 (Sheldrick, 2014)	
Function minimized	$\Sigma\, w(F_o^2 - F_c^2)^2$	
Data / restraints / parameters	25025 / 1579 / 2453	
Goodness-of-fit on F^2	1.207	
Δ/σ_{max}	0.001	
Final R indices	15101 data; I>2σ(I)	$R_1 = 0.0981$, $wR_2 = 0.2107$
	all data	$R_1 = 0.1549$, $wR_2 = 0.2346$
Weighting scheme	$w=1/[\sigma^2(F_o^2)+(0.0600P)^2+149.0000P]$, $P=(F_o^2+2F_c^2)/3$	
Largest diff. peak and hole	1.251 and -1.267 $eÅ^{-3}$	
R.M.S. deviation from mean	0.123 $eÅ^{-3}$	

$R_{int} = \Sigma|F_o^2 - F_o^2(\text{mean})| / \Sigma[F_o^2]$
$R_1 = \Sigma||F_o| - |F_c|| / \Sigma|F_o|$
$\text{GOOF} = S = \{\Sigma[w(F_o^2 - F_c^2)^2] / (n - p)\}^{1/2}$
$wR_2 = \{\Sigma[w(F_o^2 - F_c^2)^2] / \Sigma[w(F_o^2)^2]\}^{1/2}$

Details of the crystal structure of $Cy_2CB[8]•3_2$. A colorless plate-like specimen of $C_{72}H_{132}I_4N_{36}O_{38}$, approximate dimensions 0.14 mm × 0.16 mm × 0.26 mm, was used for the X-ray crystallographic analysis. Instrument description The X-ray intensity data were measured on a Bruker APEX-II CCD system equipped with a graphite monochromator and a MoKα sealed tube (λ = 0.71073 Å). Data collection temperature was 150 K.

The total exposure time was 19.79 hours. The frames were integrated with the Bruker SAINT software package using a narrow-frame algorithm. The integration of the data using a triclinic unit cell yielded a total of 18939 reflections to a maximum θ angle of 26.59° (0.79 Å resolution), of which 18939 were independent (average redundancy 1.000, completeness = 88.0%) and 14989 (79.14%) were greater than $2\sigma(F^2)$. The final cell constants of a = 14.877(2) Å, b = 16.089(3) Å, c = 24.245(4) Å, α = 80.894(2)°, β = 89.257(2)°, γ = 68.144(2)°, V = 5311.5(15) $Å^3$, are based upon the refinement of the XYZ-centroids of 3501 reflections above 20 σ(I) with 4.741° < 2θ < 49.58°. Scaling Data were corrected for absorption effects using the multi-scan method (SADABS). The calculated minimum and maximum transmission coefficients (based on crystal size) are 0.7140 and 0.8370.

The structure was solved and refined using the Bruker SHELXTL Software Package, using the space group P-1, with Z = 2 for the formula unit, $C_{72}H_{132}I_4N_{36}O_{38}$. Structure refinement The final anisotropic full-matrix least-squares refinement on F^2 with 1495 variables converged at R_1 = 7.09%, for the observed data and wR_2 = 17.40% for all data. The goodness-of-fit was 1.004. The largest peak in the final difference electron density synthesis was 2.999 $e^-/Å^3$ and the largest hole was -1.602 $e^-/Å^3$ with an RMS deviation of 0.144 $e^-/Å^3$. On the basis of the final model, the calculated density was 1.637 g/cm^3 and F(000), 2664 e^-.

Crystallographic References: Software APEX2 Version 2010.11-3 (Bruker AXS Inc.) SAINT Version 7.68A (Bruker AXS Inc., 2009) SADABS Version 2008/1 (G. M. Sheldrick, Bruker AXS Inc.) XPREP Version 2008/2 (G. M. Sheldrick, Bruker AXS Inc.) XS/XT Version 2014 (G. M. Sheldrick, (2014) University of Gottingen, Germany) XL Version 2014 (G. M. Sheldrick, (2014) University of Gottingen, Germany) Platon (A. L. Spek, *Acta Cryst.* (1990). A**46**, C-34)

Table III-S6. Sample and crystal data for UM2710.

Identification code	2710	
Chemical formula	$C_{72}H_{132}I_4N_{36}O_{38}$	
Formula weight	2617.73	
Temperature	150(2) K	
Wavelength	0.71073 Å	
Crystal size	0.14 × 0.16 × 0.26 mm	
Crystal habit	colorless plate	
Crystal system	triclinic	
Space group	P-1	
Unit cell dimensions	a = 14.877(2) Å	α = 80.894(2)°

	b = 16.089(3) Å	β = 89.257(2)°
	c = 24.245(4) Å	γ = 68.144(2)°
Volume	5311.5(15) $Å^3$	
Z	2	
Density (calculated)	1.637 Mg/cm^3	
Absorption coefficient	1.272 mm^{-1}	
F(000)	2664	

Table III-S7. Data collection and structure refinement for UM2710.

Diffractometer	Bruker APEX-II CCD	
Radiation source	sealed tube, MoKα	
Theta range for data collection	1.67 to 26.59°	
Reflections collected	18939	
Coverage of independent reflections	88.0%	
Absorption correction	multi-scan	
Max. and min. transmission	0.8370 and 0.7140	
Structure solution technique	direct methods	
Structure solution program	ShelXS-97 (Sheldrick, 2008)	
Refinement method	Full-matrix least-squares on F^2	
Refinement program	ShelXL-2014 (Sheldrick, 2014)	
Function minimized	$\Sigma w(F_o^2 - F_c^2)^2$	
Data / restraints / parameters	18939 / 676 / 1495	
Goodness-of-fit on F^2	1.004	
Final R indices	14989 data; I>2σ(I)	$R_1 = 0.0709$, $wR_2 = 0.1623$
	all data	$R_1 = 0.0887$, $wR_2 = 0.1740$
Weighting scheme	$w=1/[\sigma^2(F_o^2)+(0.0500P)^2+49.0000P]$, $P=(F_o^2+2F_c^2)/3$	
Largest diff. peak and hole	2.999 and -1.602 $eÅ^{-3}$	
R.M.S. deviation from mean	0.144 $eÅ^{-3}$	

$R_1 = \Sigma||F_o| - |F_c|| / \Sigma|F_o|$
$GOOF = S = \{\Sigma[w(F_o^2 - F_c^2)^2] / (n - p)\}^{1/2}$
$wR_2 = \{\Sigma[w(F_o^2 - F_c^2)^2] / \Sigma[w(F_o^2)^2]\}^{1/2}$

Crystallographic information files for Me_4CB[8]•**II-3**$_2$, Cy_2CB[8]•**II-3**$_2$, and Me_4CB[8]•**II-12** are available free of charge on ACS publication website at DOI: 10.1021/acs.orglett.5b02558.

Bibliography

1. Green, N. M. *Biochem. J.* **1963**, *89*, 585-591.
2. Green, N. M. *Biochem. J.* **1966**, *101*, 774.
3. (a) Kata, M.; Schauer, M. *Acta. Pharm. Hung.* **1991**, *61*, 23-31; (b) Saetern, A. M.; Nguyen, N. B.; Bauer-Brandl, A.; Brandl, M. *Int. J. Pharm.* **2004**, *284*, 61-68.
4. (a) Jung, H.; Park, K. M.; Yang, J.-A.; Oh, E. J.; Lee, D.-W.; Park, K.; Ryu, S. H.; Hahn, S. K.; Kim, K. *Biomaterials* **2011**, *32*, 7687-7694; (b) Duan, Q.; Cao, Y.; Li, Y.; Hu, X.; Xiao, T.; Lin, C.; Pan, Y.; Wang, L. *J. Am. Chem. Soc.* **2013**, *135*, 10542-10549.
5. (a) Bali, M. S.; Buck, D. P.; Coe, A. J.; Day, A. I.; Collins, J. G. *Dalton Trans.* **2006**, *45*, 5337-5344; (b) Kumar, V. P.; Reddy, V. P.; Sridhar, R.; Srinivas, B.; Narender, M.; Rao, K. R., *J. Org. Chem.* **2008,** *73*, 1646-1648.
6. Jun, S. I.; Lee, J. W.; Sakamoto, S.; Yamaguchi, K.; Kim, K. *Tetrahedron Lett.* **2000**, *41*, 471-475.
7. Ko, Y. H.; Kim, H.; Kim, Y.; Kim, K. *Angew. Chem., Int. Ed.* **2008**, *47*, 4106-4109.
8. Lee, J. W.; Choi, S.; Ko, Y. H.; Kim, S.-Y.; Kim, K. *Bull. Korean Chem. Soc.* **2002**, *23*, 1347-1350.
9. Minami, T.; Esipenko, N. A.; Zhang, B.; Kozelkova, M. E.; Issacs, L.; Nishiyabu, R.; Kubo, Y.; Anzenbacher, P. *J. Am. Chem. Soc.* **2012**, *134*, 20021-20024.
10. (a) Pederson, C. J. *J. Am. Chem. Soc.* **1967**, *89*, 2495-2496; (b) Pederson, C. J. *J. Am. Chem. Soc.* **1967**, *89*, 7017-7036.

11. Ogoshi, T.; Kanai, S.; Fujinami, S.; Yamagishi, T.-a.; Nakamoto, Y. *J. Am. Chem. Soc.* **2008**, *130*, 5022-5023.

12. Ogoshi, T.; Masaki, K.; Shiga, R.; Kitajima, K.; Yamagishi, T.-a. *Org. Lett.* **2011**, *13*, 1264-1266.

13. Ogoshi, T.; Harada, A. *Sensors* **2008**, *8*, 4961-4982.

14. (a) Bassini, V. L.; Krieger, D.; Duchene, D.; Wouessidjewe, D. *J. Inclusion Phenom. Mol. Recognit. Chem.* **1996**, *25*, 149-152; (b) Cheng, J.; Khin, K. T.; Davis, M. E. *Mol. Pharm.* **2004**, *1*, 183-193.

15. Behrend, R.; Meyer, E.; Rusche, F. *Liebigs Ann.* **1905**, *339*, 1-37.

16. Freeman, W. A.; Mock, W. L.; Shih, N. Y. *J. Am. Chem. Soc.* **1981**, *103*, 7367-7368.

17. (a) Mock, W. L.; Shih, N.-Y. *J. Org. Chem.* **1986**, *51*, 4440-4446; (b) Mock, W. L.; Shih, N.-Y. *J. Am. Chem. Soc.* **1988**, *110*, 4706-4710.

18. Day, A. I.; Arnold, A. P. Method for synthesis cucurbiturils. WO2000068232A1, 2000.

19. (a) Hoffmann, R.; Knoche, W.; Fenn, C.; Buschmann, H.-J. *J. Chem. Soc. Faraday Trans.* **1994**, *90*, 1507-1511; (b) Buschmann, H.-J.; Mutihac, L.; Jansen, K. *J. Inclusion Phenom. Macrocyclic Chem.* **2001**, *39*, 1-11.

20. Kim, J.; Jung, I.-S.; Kim, S.-Y.; Lee, E.; Kang, J.-K.; Sakamoto, S.; Yamaguchi, K.; Kim, K. *J. Am. Chem. Soc.* **2000**, *122*, 540-541.

21. Cheng, X.-J.; Liang, L.-L.; Chen, K.; Ji, N.-N.; Xiao, X.; Zhang, J.-X.; Zhang, Y.-Q.; Xue, S.-F.; Zhu, Q.-J.; Ni, X.-L.; Zhu, T. *Angew. Chem. Int. Ed.* **2013**, *52*, 7252-7255.

22. Liu, S.; Zavalij, P. Y.; Isaacs, L. *J. Am. Chem. Soc.* **2005**, *127*, 16798-16799.

23. Day, A.; Arnold, A. P.; Blanch, R. J.; Snushall, B. *J. Org. Chem.* **2001**, *66*, 8094-8100.

24. Nau, W. M.; Florea, M.; Assaf, K. I. *Isr. J. Chem.* **2011**, *51*, 559-577.

25. Cao, L.; Sekutor, M.; Zavalij, P. Y.; Mlinaric-Majerski, K.; Glaser, R.; Isaacs, L. *Angew. Chem. Int. Ed.* **2014**, *53*, 988-993.

26. Liu, S.; Ruspic, C.; Mukhopadhyay, P.; Chakrabarti, S.; Zavalij, P. Y.; Isaacs, L. *J. Am. Chem. Soc.* **2005**, *127*, 15959-15967.

27. Kim, H.-J.; Heo, J.; Jeon, W. S.; Lee, E.; Kim, J.; Sakamoto, S.; Yamaguchi, K.; Kim, K. *Angew. Chem., Int. Ed.* **2001**, *40*, 1526-1529.

28. Bardelang, D.; Udachin, K. A.; Leek, D. M.; Margeson, J. C.; Chan, G.; Ratcliffe, C. I.; Ripmeester, J. A. *Cryst. Growth Des.* **2011**, *11*, 5598-5614.

29. (a) Zhao, J.; Kim, H.-J.; Oh, J.; Kim, S.-Y.; Lee, J. W.; Sakamoto, S.; Yamaguchi, K.; Kim, K. *Angew. Chem., Int. Ed.* **2001**, *40*, 4233-4235; (b) Jon, S. Y.; Selvapalam, N.; Oh, D. H.; Kang, J.-K.; Kim, S.-Y.; Jeon, Y. J.; Lee, J. W.; Kim, K. *J. Am. Chem. Soc.* **2003**, *125*, 10186-10187.

30. Flinn, A.; Hough, G. C.; Stoddart, J. F.; Williams, D. J. *Angew. Chem.* **1992**, *104*, 1550-1551.

31. (a) Day, A. I.; Arnold, A. P.; Blanch, R. J. *Molecules* **2003**, *8*, 74-84; (b) Zhao, Y.; Xue, S.; Zhu, Q.; Tao, Z.; Zhang, J.; Wei, Z.; Long, L.; Hu, M.; Xiao, H.; Day, A. I. *Chin. Sci. Bull.* **2004**, *49*, 1111-1116.

32. Wu, F.; Wu, L.-H.; Xiao, X.; Zhang, Y.-Q.; Xue, S.-F.; Tao, Z.; Day, A. I. *J. Org. Chem.* **2012**, *77*, 606-611.

33. Ahn, Y.; Jang, Y.; Selvapalam, N.; Yun, G.; Kim, K. *Angew. Chem. Int. Ed.* **2013**, *52*, 3140-3144.

34. Zhao, N.; Lloyd, G. O.; Scherman, O. A. *Chem. Commun.* **2012**, *48*, 3070-3072.

35. Huang, W.-H.; Zavalij, P. Y.; Isaacs, L. *J. Am. Chem. Soc.* **2008**, *130*, 8446-8454.

36. Isaacs, L. D.; Briken, V.; Ma, D.; Hettiarachchi, G.; Nguyen, D. M. Preparation of acyclic cucurbit[n]uril-type molecular containers for use as drug delivery. WO2012051407A2, 2012.

37. (a) Hettiarachchi, G.; Nguyen, D.; Wu, J.; Lucas, D.; Ma, D.; Isaacs, L.; Briken, V. *PLoS One* **2010**, *5*, No pp. given.; (b) Ma, D.; Hettiarachchi, G.; Nguyen, D.; Zhang, B.; Wittenberg, J. B.; Zavalij, P. Y.; Briken, V.; Isaacs, L. *Nat. Chem.* **2012**, *4*, 503-510.

38. Isaacs, L. D.; Ma, D.; Eikermann, M. Preparation of acyclic cucurbit[n]uril-type molecular containers for reversal of drug-induced neuromuscular block. WO2012051413A1, 2012.

39. Huang, W.-H.; Zavalij, P. Y.; Isaacs, L. *Org. Lett.* **2008**, *10*, 2577-2580.

40. Lucas, D.; Minami, T.; Iannuzzi, G.; Cao, L.; Wittenberg, J. B.; Anzenbacher, P.; Isaacs, L. *J. Am. Chem. Soc.* **2011**, *133*, 17966-17976.

41. (a) Marquez, C.; Huang, F.; Nau, W. M. *IEEE Trans. Nanobiosci.* **2004**, *3*, 39-45; (b) Day, A. I.; Blanch, R. J.; Coe, A.; Arnold, A. P. *J. Inclusion Phenom. Macrocyclic Chem.* **2002**, *43*, 247-250.

42. Lucas, D.; Minami, T.; Iannuzzi, G.; Cao, L.; Wittenberg, J. B.; Anzenbacher, P. J.; Isaacs, L. *J. Am. Chem. Soc.* **2011**, *133*, 17966-17976.

43. Lee, J. W.; Samal, S.; Selvapalam, N.; Kim, H.-J.; Kim, K. *Acc. Chem. Res.* **2003**, *36*, 621-630.

44. (a) Stella, V. J.; Rajewski, R. A. *Pharm. Res.* **1997**, *14*, 556-567; (b) De Greef, T. F. A.; Smulders, M. M. J.; Wolffs, M.; Schenning, A. P. H. J.; Sijbesma, R. P.; Meijer, E. W., *Chem. Rev.* **2009,** *109*, 5687.

45. (a) Chakraborty, A.; Wu, A.; Witt, D.; Lagona, J.; Fettinger, J. C.; Isaacs, L. *J. Am. Chem. Soc.* **2002**, *124*, 8297-8306; (b) Wu, A.; Chakraborty, A.; Witt, D.; Lagona, J.; Damkaci, F.; Ofori, M. A.; Chiles, J. K.; Fettinger, J. C.; Isaacs, L. *J. Org. Chem.* **2002**, *67*, 5817-5830; (c) Witt, D.; Lagona, J.; Damkaci, F.; Fettinger, J. C.; Isaacs, L. *Org. Lett.* **2000**, *2*, 755-758.

46. Zhao, Y.; Xue, S.; Zhu, Q.; Tao, Z.; Zhang, J.; Wei, Z.; Long, L.; Hu, M.; Xiao, H.; Day, A. I. *Chin. Sci. Bull.* **2004**, *49*, 1111-1116.

47. Liu, S.; Ruspic, C.; Mukhopadhyay, P.; Chakrabarti, S.; Zavalij, P. Y.; Isaacs, L. *J. Am. Chem. Soc.* **2005**, *127*, 15959-15967.

48. Day, A. I.; Arnold, A. P.; Blanch, R. J.; Snushall, B. *J. Org. Chem.* **2001**, *66*, 8094-8100.

49. Kimpe, N. D.; D'Hondt, L.; Stanoeva, E., diimine. *Tetrahedron Lett.* **1991**, *32*, 3879-3882.

50. Kimpe, N. D.; Stevens, C., *Tetrahedron* **1995**, *51*, 2387-2402.

51. Ozcubukcu, S.; Okzal, E.; Jimeno, C.; Pericas, M. *Org. Lett.* **2009**, *11*, 6480-6483.

52. (a) Park, K.-M.; Kim, S.-Y.; Heo, J.; Whang, D.; Sakamoto, S.; Yamaguchi, K.; Kim, K. *J. Am. Chem. Soc.* **2002,** *124*, 2140-2147; (b) Ko, Y. H.; Kim, K.; Kang, J.-K.; Chun, H.; Lee, J. W.; Sakamoto, S.; Yamaguchi, K.; Fettinger, J. C.; Kim, K. *J. Am.*

Chem. Soc. **2004,** *126*, 1932-1933; (c) Da Silva, J. P.; Jayaraj, N.; Jockusch, S.; Turro, N.; Ramamurthy, V. *Org. Lett.* **2011**, *13*, 2410-2413.

53. Cohen, Y.; Avram, L.; Frisch, L. *Angew. Chem. Int. Ed.* **2005,** *44*, 520-554.
54. Jonas, U.; Cardullo, F.; Belik, P.; Diederich, F.; Guegel, A.; Harth, E.; Herrmann, A.; Isaacs, L.; Muellen, K.; et. al. *Eur. J. Chem.* **1995**, *1,* 243-51.
55. Ayhan, M. M.; Karoui, H.; Hardy, M.; Rockenbauer, A.; Charles, L.; Rosas, R.; Udachin, K.; Tordo, P.; Bardelang, D.; Ouari, O. *J. Am. Chem. Soc.* **2015**, *137*, 10238-10245.
56. Robinson, E. L.; Zavalij, P. Y.; Isaacs, L., *Supramol. Chem.* **2015,** *27*, 288-297.
57. (a) Zhou, J.-J.; Yu, X.; Zhao, Y.-C.; Xiao, X.; Zhang, Y.-Q.; Zhu, Q.-J.; Xue, S.-F.; Zhang, Q.-J.; Liu, J.-X.; Tao, Z. *Tetrahedron* **2014**, *70*, 800-804; (b) Gilberg, L.; Zhang, B.; Zavalij, P. Y.; Sindelar, V.; Isaacs, L. *Org. Biomol. Chem.* **2015**, *13*, 4041-4050.
58. Cao, L.; Isaacs, L., Sampl 4. *Supramol. Chem.* **2014**, *26*, 251-258.
59. (a) Zhang, B.; Isaacs, L. *J. Med. Chem.* **2015**, *57*, 9554-9563; (b) Higuchi, T.; Connors, K. A. *Adv. Anal. Chem. Inst.* **1965**, *4*, 117-212; (c) Connors, K. A., *Binding Constants*. John Wiley & Sons: New York, 1987.